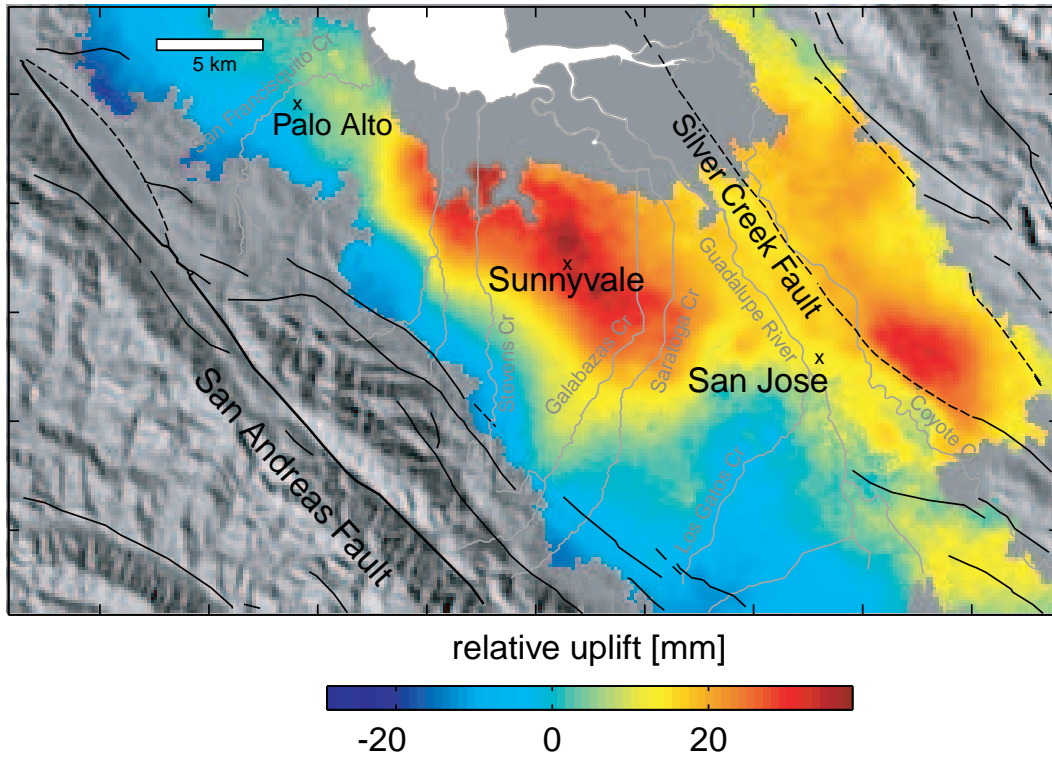


# Berkeley Seismological Laboratory

Land Uplift in the Santa Clara Valley, 1992-1998



Annual Report  
July 2001 - June 2002

# Contents

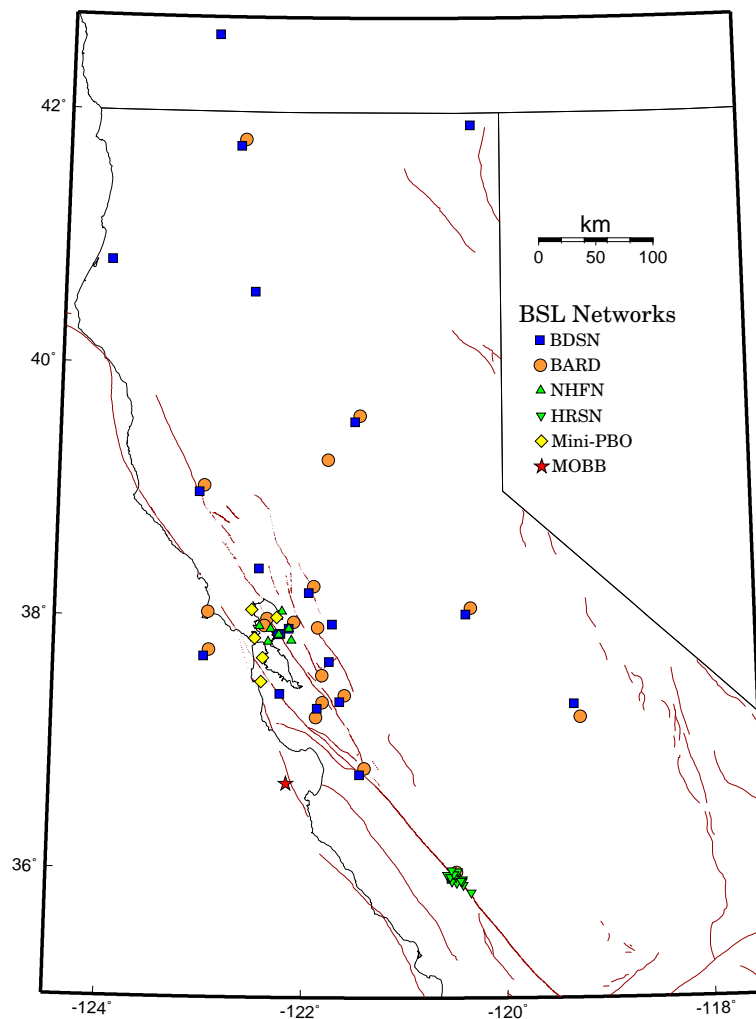
<b>I</b>	<b>Introduction</b>	<b>4</b>
<b>1</b>	<b>Director's Report</b>	<b>5</b>
1.	Background and Facilities . . . . .	5
2.	Highlights of 2001-2002 . . . . .	6
3.	Acknowledgements . . . . .	8
4.	Glossary of Common Acronyms . . . . .	10
<b>2</b>	<b>In Memoriam - Thomas V. McEvelly</b>	<b>12</b>
1.	Introduction . . . . .	13
2.	McEvelly Graduate Student Fellowship in Seismology . . . . .	13
3.	A Celebration Of Tom McEvelly's Life . . . . .	13
4.	References . . . . .	15
<b>II</b>	<b>Operations</b>	<b>16</b>
<b>3</b>	<b>California Integrated Seismic Network</b>	<b>17</b>
1.	Introduction . . . . .	17
2.	CISN Background . . . . .	17
3.	2001-2002 Activities . . . . .	18
4.	Acknowledgements . . . . .	23
<b>4</b>	<b>Berkeley Digital Seismic Network</b>	<b>24</b>
1.	Introduction . . . . .	24
2.	BDSN Overview . . . . .	24
3.	2001-2002 Activities . . . . .	27
4.	Acknowledgements . . . . .	32
5.	References . . . . .	32
<b>5</b>	<b>Northern Hayward Fault Network</b>	<b>33</b>
1.	Introduction . . . . .	33
2.	NHFN Overview . . . . .	33
3.	2001-2002 Activities . . . . .	35
4.	Acknowledgements . . . . .	40
5.	References . . . . .	40
<b>6</b>	<b>Parkfield Borehole Network</b>	<b>42</b>
1.	Introduction . . . . .	42
2.	HRSN Overview . . . . .	42
3.	2001-2002 Activities . . . . .	44
4.	Examples of Data . . . . .	49
5.	Future Directions . . . . .	51
6.	Acknowledgements . . . . .	51
7.	References . . . . .	51

<b>7</b>	<b>Parkfield-Hollister Electromagnetic Monitoring Array</b>	<b>53</b>
1.	Introduction . . . . .	53
2.	MT Overview . . . . .	53
3.	Activities in 2001-2002 . . . . .	54
4.	Data Processing . . . . .	54
5.	Acknowledgements . . . . .	57
6.	References . . . . .	57
<b>8</b>	<b>Bay Area Regional Deformation Network</b>	<b>58</b>
1.	Introduction . . . . .	58
2.	BARD Stations . . . . .	61
3.	2001-2002 Activities . . . . .	62
4.	Data Analysis and Results . . . . .	64
5.	Real-Time Processing . . . . .	66
6.	Acknowledgements . . . . .	66
7.	References . . . . .	66
<b>9</b>	<b>Plate Boundary Deformation Project</b>	<b>67</b>
1.	Introduction . . . . .	67
2.	New Site Installations . . . . .	68
3.	Strainmeter Data . . . . .	71
4.	Acknowledgements . . . . .	71
<b>10</b>	<b>Ocean Floor Broadband Station in Monterey Bay</b>	<b>73</b>
1.	Introduction . . . . .	73
2.	Instrumentation . . . . .	73
3.	Deployment . . . . .	74
4.	Examples of data . . . . .	75
5.	Acknowledgements . . . . .	76
6.	References . . . . .	76
<b>11</b>	<b>Data Acquisition and Quality Control</b>	<b>78</b>
1.	Introduction . . . . .	78
2.	McCone Hall Facilities . . . . .	78
3.	Data acquisition . . . . .	79
4.	Seismic Noise Analysis . . . . .	79
5.	Sensor Testing Facility . . . . .	81
6.	Sensor testing in 2001-2002 . . . . .	85
7.	UrEDAS Project . . . . .	88
8.	Acknowledgements . . . . .	91
9.	References . . . . .	91
<b>12</b>	<b>Northern California Earthquake Monitoring</b>	<b>93</b>
1.	Introduction . . . . .	93
2.	Joint Notification System Overview . . . . .	93
3.	2001-2002 Activities . . . . .	99
4.	Routine Earthquake Analysis . . . . .	100
5.	Acknowledgements . . . . .	100
6.	References . . . . .	103
<b>13</b>	<b>Northern California Earthquake Data Center</b>	<b>104</b>
1.	Introduction . . . . .	104
2.	NCEDC Overview . . . . .	104
3.	2001-2002 Activities . . . . .	104
4.	Data Collections . . . . .	105
5.	Data Quality Control . . . . .	109

6.	Database Development . . . . .	110
7.	Data Access & Distribution . . . . .	110
8.	Acknowledgements . . . . .	111
<b>14</b>	<b>Outreach and Educational Activities</b>	<b>112</b>
1.	Introduction . . . . .	112
2.	Outreach Overview . . . . .	112
3.	2000-2001 Activities . . . . .	112
4.	Acknowledgements . . . . .	113
<b>III</b>	<b>Ongoing Research Projects</b>	<b>114</b>
<b>15</b>	<b>Source and Geodetic Studies</b>	<b>115</b>
1.	Parkfield Research . . . . .	116
2.	Deep Fault Slip Kinematics from Characteristic Microearthquakes . . . . .	122
3.	Time-dependent depth distribution of aftershocks: Implications for fault mechanics and crustal rheology	129
4.	Moment-Length Scaling of Large Strike-Slip Earthquakes and the Strength of Faults . . . . .	132
5.	Historical Earthquake Re-analysis Project . . . . .	134
6.	Northern California Seismicity Project . . . . .	138
7.	Accelerated Stress Buildup on the Southern San Andreas Fault and Surrounding Regions Caused by Mojave Desert Earthquakes . . . . .	140
8.	Land Uplift and Subsidence in the Santa Clara Valley . . . . .	141
9.	Application of Point Measurements from InSAR to Study Slow Earthquakes on the Central San Andreas Fault . . . . .	144
10.	Crustal Deformation Along the Northern San Andreas Fault System . . . . .	146
11.	Urban Geodesy: Monitoring Active Deformation near the Hayward fault . . . . .	148
12.	Active Tectonics of the Adriatic Region (Central Mediterranean) . . . . .	150
13.	Fluid Influenced Faulting in Long Valley Caldera . . . . .	153
14.	Finite Fault Inversion of the September 25, 1999 ( $M_w=6.4$ ) Taiwan Earthquake . . . . .	154
15.	Automated Moment Tensor Software for Monitoring the Comprehensive Test Ban Treaty . . . . .	156
<b>16</b>	<b>Regional and Global Structure Studies</b>	<b>159</b>
1.	Waveform Constrained Seismic Velocity Structure in Northern California . . . . .	160
2.	Detection and Location of Potential Sources of Background Low Frequency Surface Wave Energy . . . . .	162
3.	Global Anisotropy beneath Continental Roots . . . . .	164
4.	Superplumes from the core-mantle boundary to the base of the lithosphere: evidence from Q tomography	166
5.	Progress in modeling deep mantle isotropic shear and compressional velocity structure using waveform inversion . . . . .	168
6.	Investigating Mantle's density resolution using the Neighborhood Algorithm . . . . .	170
7.	Towards Forward Modeling of 3D Heterogeneity at the Base of the Mantle . . . . .	173
8.	Using the Coupled Method of Spectral Elements and Modal Solution to study the D" layer. . . . .	175
9.	Short scale heterogeneity in the lowermost mantle: insights from PcP-P and ScS-S data . . . . .	177
<b>IV</b>	<b>Appendices</b>	<b>180</b>

# Part I

## Introduction



# Chapter 1

## Director's Report

### 1. Background and Facilities

The Berkeley Seismological Laboratory (BSL), formerly the Berkeley Seismographic Station (BSS), is the oldest Organized Research Unit (ORU) on the U. C. Berkeley campus. Its mission is unique in that, in addition to research and education in seismology and earthquake-related science, it is responsible for providing timely information on earthquakes (particularly those that occur in northern and central California) to the U.C. Berkeley constituency, the general public, and various local and state government and private organizations. The BSL is therefore both a research center and a facility/data resource, which sets it apart from most other ORUs. A major component of our activities is focused on developing and maintaining several regional observational networks, and participating, along with other agencies, in various aspects of the collection, analysis, archival and distribution of data pertaining to earthquakes, while maintaining a vigorous research program on earthquake processes and Earth structure. In addition, the BSL staff spends considerable time with public relations activities, including tours, talks to public groups, responding to public enquiries about earthquakes and, more recently, World-Wide-Web presence (<http://www.seismo.berkeley.edu/seismo/>).

U.C. Berkeley installed the first seismograph in the Western Hemisphere at Mount Hamilton (MHC) in 1887. Since then, it has played a leading role in the operation of state-of-the-art seismic instruments and in the development of advanced methods for seismic data analysis and interpretation. Notably, the installation, starting in 1927, of Wood-Anderson seismographs at 4 locations in northern California (BKS, ARC, MIN and MHC) allowed the accurate determination of local earthquake magnitude ( $M_L$ ) from which a unique historical catalog of regional earthquakes has been maintained to this day, providing crucial input to earthquake probabilities studies.

Over the years, the BSS continued to keep apace of technological improvements. The first centrally telemetered network using phone lines in an active seismic region was installed by BSS in 1960. The BSS was the

first institution in California to operate a 3-component "broadband" system (1963). Notably, the BSS played a major role in the early characterization of earthquake sources using "moment tensors" and source-time functions, and made important contributions to the early definitions of detection/discrimination of underground nuclear tests and to earthquake hazards work, jointly with UCB Engineering. Starting in 1986, the BSS acquired 4 state-of-the-art broadband instruments (STS-1), while simultaneously developing PC-based digital telemetry, albeit with limited resources. As the telecommunication and computer technology made rapid progress, in parallel with broadband instrument development, paper record reading could be completely abandoned in favor of largely automated digital data analysis.

The current modern facilities of BSL have been progressively built over the last 12 years, initiated by significant "upgrade" funding from U.C. Berkeley in 1991-1995. The BSL currently operates and acquires data, continuously and in real-time, from over 40 regional digital seismic stations, including 20 located in boreholes, 21 permanent GPS stations of the BARD network, and 2 electromagnetic stations. The seismic data are fed into the BSL real-time processing and analysis system and are used in conjunction with data from the USGS NCSN network in the joint earthquake notification program for northern California, started in 1996. This program capitalizes on the complementary capabilities of the networks operated by each institution to provide rapid and reliable information on the location, size and other relevant source parameters of regional earthquakes. In recent years, a major emphasis in BSL instrumentation has been in densifying the state-of-the-art seismic and geodetic networks, while a major on-going emphasis in research has been the development of robust methods for quasi-real time automatic determination of earthquake source parameters and predicted strong ground motion, using a sparse network combining broadband and strong motion seismic sensors, as well as permanent geodetic GPS receivers.

The backbone of the BSL operations is a regional network of 20+ digital broadband and strong motion seismic stations, the Berkeley Digital Seismic Network (BDSN),

with continuous telemetry to UC Berkeley. This network provides the basic regional data for the real-time estimation of location, size and rupture parameters for earthquakes of M 3 and larger in central and northern California, within our Rapid Earthquake Data Integration (REDI) program. It also provides a fundamental database for the investigation of three-dimensional crustal structure and its effects on regional seismic wave propagation, ultimately crucial for estimating ground shaking for future earthquakes. Most stations also record auxiliary temperature/pressure channels, valuable in particular for background noise quality control. Complementing this network is a 20+ station "high-resolution" network of borehole seismic sensors along the Hayward Fault (HFN), operated jointly with the USGS/Menlo Park and linked to the Bridge Safety Project of the California Department of Transportation, which has made possible the installation of sensor packages at 15 bedrock boreholes at 5 east-bay bridges in collaboration with LLNL. A major science goal of this network is to collect high signal-to-noise data for microearthquakes along the Hayward Fault to gain insight into the physics that govern fault rupture and its nucleation. The BSL is also involved in the operation and maintenance of the Parkfield borehole seismic array (HRSN), which is yielding enlightening results on quasi-periodic behavior of microearthquake clusters and important new constraints on earthquake scaling laws and is currently playing an important role in the characterization of the site for the future San Andreas Fault Observatory at Depth (SAFOD). Since April 2002, the BSL is also involved in the operation of a permanent broadband ocean bottom station, MOBB, in collaboration with MBARI (Monterey Bay Aquarium Research Institute).

In addition to the seismic networks, the BSL is involved in data archival and distribution for the permanent geodetic BARD (Bay Area Regional Deformation) Network as well as the operation and maintenance, and data processing of 21 out of its 70+ sites. Whenever possible, BARD sites are collocated with BDSN sites in order to minimize telemetry costs. In particular, the development of analysis methods combining the seismic and geodetic data for the rapid estimation of source parameters of significant earthquakes has been one focus of BSL research.

Finally, two of the BDSN stations also share data acquisition and telemetry with 5-component electromagnetic sensors installed with the goal of investigating the possibility of detection of tectonic signals.

Archival and distribution of data from these and other regional networks is performed at the Northern California Earthquake Data Center (NCEDC), operated at the BSL in collaboration with USGS/Menlo Park. The data reside on a mass-storage device (2.5 Terabyte capacity), and are accessible "on-line" over the Internet

(<http://www.quake.geo.berkeley.edu>). Among others, data from the USGS Northern California Seismic Network (NCSN), are archived and distributed through the NCEDC. The NCEDC also maintains, archives and distributes the ANSS/CNSS earthquake catalog.

Core University funding to our ORU provides salary support for 3 field engineers, one computer expert, 2 data analysts, 1 staff scientist and 2 administrative staff. This covers the basic needs of the operations of the BDSN and seed funding for our other activities. All other programs are supported through extra-mural grants primarily from the USGS and NSF, and in the past year, the Office of Emergency Services (OES). We acknowledge valuable recent contributions from other sources such as Caltrans, the CLC program, PEER, as well as our Earthquake Research Affiliates.

## 2. Highlights of 2001-2002

### 2.1 Infrastructure and Earthquake Notification

Three major projects of the BSL deserve attention in 2001-2002: CISN, "Mini-PBO", and the ocean bottom observatory MOBB.

A focus of the past year has been the planning and initial implementation of the BSL component of the CISN (California Integrated Seismic Network), with support in FY'02 (received in April 2002) from the State of California through the Office of Emergency Services (OES) (Chapter 3).

A major goal of the CISN is to ensure a more uniform system for earthquake monitoring in California, through the improvement of seismic infrastructure in northern California and continued maintenance of the TriNet system in southern California. Another major goal is to integrate the earthquake monitoring and reporting efforts in the State, using compatible software and creating a single catalog. A present focus is to improve the robustness of statewide rapid notification and work with the California OES and other emergency responders to maximize the use and benefit of this real time seismic information.

In anticipation of the pending funding, BSL staff conducted searches and surveys to identify potential sites for new broadband stations, two of which have been selected and permitted, and will be installed as soon as the equipment becomes available. With very little time to spend the funds from OES in FY'02 (3 months), the BSL purchased equipment for 5 BDSN sites, and focused efforts on the development of software to re-design the USGS/UCB joint earthquake notification system and move towards merging the systems now in operation at each of the two institutions. Initial steps have been taken towards exchanging data in real-time with southern California, involving 10 stations in each sub-region.

BSL staff have spent considerable efforts in organizational activities for CISN, notably by participating in the CISN Project Management Group (Gee) and the Standards Committee (Neuhauser-chair, Gee, Lombard). Romanowicz rotated off as chair of the CISN Steering Committee, but still remains involved. The CISN also represents California as a designated region of ANSS (Advanced National Seismic System) and the BSL is actively involved in planning activities for the ANSS.

This past year has been marked by a climax in the installation efforts towards the "Mini-PBO" project (Chapter 9), a project supported partly by a grant from the NSF/MRI program, in collaboration with CIW, UCSD and USGS/Menlo Park, with matching from UCB and these other institutions as well as Caltrans ([http://www.seismo.berkeley.edu/seismo/bdsn/mpbo\\_overview.html](http://www.seismo.berkeley.edu/seismo/bdsn/mpbo_overview.html)). This project's focus is the installation of a network of multi-parameter stations in the San Francisco Bay Area to monitor the evolution of tectonic strain in time and space - a pilot project for the Plate Boundary Observatory (PBO) currently being planned in the framework of an NSF/MRE proposal. "Mini-PBO" instrumentation comprises 3 component borehole strainmeters and seismometers, GPS receivers and auxiliary sensors (such as pore pressure, temperature, and tilt). The data are telemetered to UC Berkeley and distributed through the NCEDC. The first two holes were drilled in early summer 2001 and instrumented in 2002. Three additional holes were drilled in the summer of 2002, with considerable involvement of BSL staff (Murray, Basset, W. Johnson, Karavas) and are currently in various stages of instrument installation. The initial goal of 10 stations has been reduced to 6 due to budgetary constraints related to considerable cost-overruns in drilling. The plan is for the 6th and last hole to be drilled with Caltrans's help in the Fall of 2002.

The MOBB (Monterey Ocean bottom Broad Band observatory) is a collaborative project between the BSL and MBARI and builds upon the experience gained in 1997 through the MOISE project, which involved the temporary deployment of a broadband ocean bottom system in Monterey Bay. MOBB is now a permanent installation and comprises a broadband seismic package (Guralp CMG-1), a battery and recording package, as well as auxiliary sensors: a current-meter and a DPG (differential Pressure Gauge). The system was assembled and tested at BSL in early 2002, and successfully deployed in April 2002 (Chapter 10). In particular, extensive testing and seismometer insulation procedures were developed at Byerly Vault on the UCB campus prior to deployment (Chapter 11).

In the past year, the BSL has been closely involved in the coordination of site characterization for the SAFOD drilling project in the Parkfield area (Chapter 6). In particular, data from the new HRSN borehole site at CCRB,

located 2 km south of the target drilling site, is recording signals from the pilot drilling project which may prove crucial for guiding drilling of the SAFOD hole. The new earthquake triggering scheme for the HRSN network has also been finalized, with the goal of reducing the bandwidth necessary for data telemetry to BSL.

Other accomplishments in the past year include the deployment of a new BDSN station (HUMO - Chapter 4) in southern Oregon, in collaboration with USGS/NSN and IRIS programs, and a new BARD station at OHLN (Ohlone Park), the first GPS station to be mounted on top of a Mini-PBO borehole (Chapter 8). A single frequency (L1) GPS receiver profile has been installed across the Hayward Fault, with assistance from UNAVCO engineers, to investigate the resolution power of this cost-effective way to monitor creep on the fault.

The NHFN network project has seen the upgrade of the infrastructure of 7 stations on the Bay Bridge (Chapter 5), in anticipation of the deployment of the Quanterra recording systems and the development of an algorithm to identify highly similar microearthquakes on the Hayward Fault based on complex spectral phase coherency.

On the NCEDC front (Chapter 13), we continue archiving and distribution on-line of data from expanding BDSN, NHFN, HRSN, BARD, Mini-PBO, and other networks and data collections in northern California. A notable addition is the continuous acquisition and archiving of broadband data from 4 stations operated by the University of Nevada, Reno, and 7 stations operated by the USGS Menlo Park. The USGS "low frequency" geophysical time series data collection (strain, creep, magnetic field, water level, etc.) is now accessible in standard MiniSEED format and instrument responses are available for over 90% of the archived channels. The NCEDC also started to archive and make publically available the state-of-health channels for the BDSN/NHFN/MPBO stations. The NCEDC is participating in the UNAVCO-sponsored GPS Seamless Archive Centers (GSAC) initiative, which is developing common protocols and interfaces for the exchange and distribution of continuous and survey-mode GPS data, and is now both a primary provider for BARD/BSL data, a wholesale collection point for other northern California GPS data, and a retail center for all GSAC data.

The BSL continues to collaborate with the USGS/Menlo Park in the generation of ShakeMap for northern California and has been developing and implementing successive upgrades to this system, integrated within the REDI environment (Chapter 12). ShakeMap is calculated routinely for magnitude 3.5 and larger events in northern California. Any magnitude 5.0 or larger will now also trigger the finite-fault processing.

Finally, the BSL has taken steps to use automatically produced moment magnitude ( $M_w$ ), when available, to supplement estimates of local magnitude ( $M_L$ ), which is

particularly useful in the case of significant earthquakes.  $M_w$  has been routinely produced within the REDI system for many years, but, until now, not broadcast as the "official magnitude", due in part to questions about the reliability of the automatic solutions. In the past year, the robustness of the moment tensor codes has been improved, facilitating the transition to official broadcasting.

## 2.2 Research Accomplishments

Chapter 15 documents the main research contributions of the last year. Research at the BSL spans a broad range of topics, from the study of microseismicity at the local scale to global deep earth structure, and includes seismological, geodetic and remote sensing (InSAR) techniques.

In this past year, Nadeau and collaborators have continued investigation of fault zone characteristics from the analysis of microearthquakes at Parkfield, and extended their scaling of recurrence times and moments of microearthquakes over 15 orders of magnitude in seismic moment (15.1). They have also been involved in determining the detailed seismic structure around the future site of the SAFOD. These microseismicity techniques are now also being extended to the study of faults in the San Francisco Bay Area (15.2) and to the investigation of the brittle-ductile transition zone and its rheological properties (Rolandone et al.; (15.3). At a very different, global scale, Romanowicz and Ruff re-examined the scaling of moment to length of large strike-slip earthquakes and found that the data fall into two distinct classes indicative of stronger (mostly oceanic) or weaker (mostly continental) faults (15.4).

For the second year, Uhrhammer has been engaged in a major effort to transcribe Berkeley historical earthquake data dating back to 1910, and stored on cards or paper records, to computer readable format, with the goal of obtaining more complete seismicity catalogs and better characterize the evolution of seismicity with time and space. An initial focus on the San Francisco Bay Area (15.5) is being extended to northern California (15.6). Five undergraduate students have been involved in this project.

A study by Freed has investigated earthquake triggering of other earthquakes on the San Andreas Fault in southern California (15.7).

In a novel application, Schmidt and Bürgmann have used InSar data to study land uplift and subsidence in the Santa Clara Valley, highlighting the spatial complexity of the aquifer system (15.8), while Johanson and Bürgmann are using InSar to detect slow earthquakes on the creeping sections of the San Andreas Fault system (15.9). Murray is engaged in resurveying 40 GPS monuments that were last surveyed in 1993-95 to further characterize crustal deformation in the northern San Andreas Fault system (15.10) and D'Alessio and collaborators are using GPS in survey mode to monitor motion

on the Hayward Fault (15.11), and obtain a creep rate of 4.2 mm/year at the Berkeley Memorial Stadium. The BSL has also shared its expertise by collaborating in the deployment of a new regional continuous GPS network in northern Italy, around the epicenter of the damaging 1976 Friuli earthquake (15.12).

Several studies of earthquakes at the regional scale are reported: an investigation of the influence of fluids on faulting at Long Valley Caldera by Templeton and Dreger (15.13); a study of the mechanisms of major aftershocks of the 1999 Chi-Chi earthquake in Taiwan by Chi and Dreger (15.14); adaptation of the BSL real time moment tensor techniques to the monitoring of nuclear explosions in the framework of the International Monitoring System (Hellweg et al., 15.15); and the on-going development of a method to locate the sources of continuous low-frequency background Earth oscillations (Rhie and Romanowicz, 15.16).

In a transition to studies of Earth structure, Rhie and Dreger (15.17) report on their waveform modeling of the seismic velocity structure in Northern California. At the global scale, we report progress in global anelastic tomography, resulting in a new model of attenuation in the upper-mantle, which has revealed the connection of low-ermost mantle "superplumes" with upwelling regions in the upper mantle and hotspots (Gung and Romanowicz, 15.17); with Gung and Panning, we have started to investigate radial anisotropy at the global scale (15.18), and have found that discrepancies in different global tomographic models of the upper mantle can be reconciled if anisotropy beneath lithospheric roots (depth range 250-400km) is considered; we have also started investigating anisotropy at greater depths in the mantle and extended our S modeling techniques to include inversion for P velocity (Panning and Romanowicz, 15.19). Rousset and Romanowicz are developing a method based on a neighbourhood algorithm to investigate the range of plausible models for degree 2 heterogeneity in density in the mantle (15.20); with Toh and Capdeville, we are making progress in exploiting the rich capabilities of the coupled mode-spectral element method to study complex 3D structure at the base of the mantle (15.21;15.22); finally, with Tkalcic, we documented sharp, uncorrelated, lateral variations in P and S velocities at the base of the mantle(15.23).

## 3. Acknowledgements

I wish to thank our technical and administrative staff, scientists and students for their contributions to this annual report. Individual contributions to activities and report preparation are mentioned in the corresponding sections, except for the Appendix section, prepared by Christina Jordan and Eleanor Blair.

Starting July 1st, 2002, Professor Douglas Dreger has

been appointed Associate Director of the BSL. In particular, Doug has assumed overall responsibility, with help from Bob Nadeau, for the HRSN and NHFN programs, following Professor McEvelly's death.

I also wish to specially thank the individuals who regularly contribute to the smooth operation of the BSL facilities: André Basset, Sierra Boyd, Rich Clymer, Doug Dreger, John Friday, Lind Gee, Wade Johnson, Bill Karavas, Pete Lombard, Rick McKenzie, Mark Murray, Bob Nadeau, Doug Neuhauser, Charley Paffenbarger, David Rapkin, Cathy Thomas, Bob Uhrhammer, and Stephane Zuzlewski.

Eleanor Blair, Heather Read and Christina Jordan continue to provide valuable support to the administration of our lab, with help from Patricia Villa. The BSL administrative office has continued to assist the EPS department administrative personnel, in a continued period of transition in that office. We are also grateful to Ruth Saha, who helped out during a period of high demand.

In 2001-2002, there have been some changes in BSL personnel. Dr Fumiko Tajima left in May 2002 to become a professor at Hiroshima University in Japan. Hrvoje Tkalčić also left in May for a post-doctoral position in sunny San Diego. Steve Chu graduated in December 2001 and left in May to work for a start-up company. We also experienced some turnover in the Administrative office, with the departure of Keia Shipp and Aric Mayer.

We welcome three new post-docs at the BSL: Maurizio Battaglia, Andy Freed, and Frederique Rolandone. We also welcome four new staff members: Heather Read and Patricia Villa joined the administrative office, Cathy Thomas became part of the field engineering team, and Jim Yan joined the BSL as a programmer. Unfortunately, because of the temporal limitations of CISN funding, Jim Yan left at the end of June.

I also wish to thank our undergraduate assistants S. Chu, J. Epstein, T. Fournier, L. Krain, K. Spiller, G. Treves, and M. Wilmarth for their contributions to our research and operational activities. I am particularly thankful to Lind Gee and Christina Jordan for their help in putting together this Annual Report.

Lane Johnson retired in June 2002 from his teaching position in the Department of Earth and Planetary Science. He will continue research activities at LBNL. I wish to thank him in particular for his role as Acting Director of the BSL during my sabbatical in the spring of 2002 and wish him well in his retirement.

Finally, I wish to express my deep sorrow upon Professor Tom McEvelly's death (Chapter 2). Professor McEvelly passed away on 02/22/2002 after a courageous fight with cancer. Tom's death is a considerable loss for the BSL. We miss his leadership in research, in recent years focused on the Parkfield program, and his cheerful and energizing presence.

The Annual Report of the Berkeley Seismological

Laboratory is available on the WWW at [http://www.seismo.berkeley.edu/seismo/annual\\_report/](http://www.seismo.berkeley.edu/seismo/annual_report/).

Barbara Romanowicz  
Sept 10, 2002

## 4. Glossary of Common Acronyms

Table 1.1: Standard abbreviations used in this report.

Acronym	Definition
AGU	American Geophysical Union
ANSS	Advanced National Seismic System
BARD	Bay Area Regional Deformation
BDSN	Berkeley Digital Seismic Network
BSL	Berkeley Seismological Laboratory
BSS	Berkeley Seismographic Station
CISN	California Integrated Seismic Network
CGS	California Geological Survey
CLC	Campus Laboratory Collaboration
CNSS	Council of the National Seismic System
EM	Electromagnetic
EPRI	Electric Power Research Institute
FBA	Force Balance Accelerometer
FIR	Finite Impulse Response
FRAD	Frame Relay Access Device
GPS	Global Positioning System
HFN	Hayward Fault Network
HRSN	High Resolution Seismic Network
IGS	International Geodetic Service
IMS	International Monitoring System
InSAR	Interferometric Synthetic Aperture Radar
IRIS	Incorporated Research Institutions for Seismology
ISC	International Seismological Center
ISTAT	Integrating Science, Teaching, and Technology
JPL	Jet Propulsion Laboratory
LBNL	Lawrence Berkeley National Laboratory
LLNL	Lawrence Livermore National Laboratory
MBARI	Monterey Bay Aquarium Research Institute
MHH	Murdoch, Hutt, and Halbert
MOBB	Monterey Ocean bottom BroadBand observatory
MOISE	Monterey Bay Ocean Bottom International Seismic Experiment
MPBO	Mini-Plate Boundary Observatory
MRI	Major Research Initiative
MRE	Major Research Equipment
MT	Magnetotelluric
NCEDC	Northern California Earthquake Data Center
NCSN	Northern California Seismic Network
NEHRP	National Earthquake Hazards Reduction Program
NEIC	National Earthquake Information Center
NHFN	Northern Hayward Fault Network
NGS	National Geodetic Survey
NSF	National Science Foundation
NSN	National Seismic Network
OES	Office of Emergency Services
ORU	Organized Research Unit
PBO	Plate Boundary Observatory
PEER	Pacific Earthquake Engineering Center
PH	Pilot Hole
PPE	Parkfield Prediction Experiment

*continued on next page*

Table 1.1: *continued*

Acronym	Definition
PSD	Power Spectral Density
REDI	Rapid Earthquake Data Integration
SAF	San Andreas Fault
SAFOD	San Andreas Fault Observatory at Depth
SAR	Synthetic Aperture Radar
SCEC	Southern California Earthquake Center
SCEDC	Southern California Earthquake Data Center
SCIGN	Southern California Integrated GPS Network
SEED	Standard for the Exchange of Earthquake Data
SHFN	Southern Hayward Fault Network
SIO	Scripps Institutions of Oceanography
SNCL	Station Network Channel Location
SSA	Seismological Society of America
STP	Seismogram Transfer Program
UCB	University of California at Berkeley
UNAVCO	University NAVSTAR Consortium
UrEDAS	Urgent Earthquake Detection and Alarm System
USGS	United States Geological Survey

## Chapter 2

# In Memoriam - Thomas V. McEvelly



Figure 2.1: Tom McEvelly (1934-2002). Photograph courtesy of Lawrence Berkeley National Laboratory.

## 1. Introduction

Thomas Vincent McEvelly died on February 22, 2002. Tom was a valuable member of the Berkeley Seismological Laboratory and the Department of Earth and Planetary Science.

Tom contributed to the BSL in many ways - through important seismological research, through the development of several seismological networks and observational practices, and through service as Assistant Director from 1968 to 1989 and several stints as Acting Director (most recently from February 1 to May 31, 2001). His leadership in the development of the Parkfield High Resolution Seismic Network, the Hayward Fault Network, and Mini-Plate Boundary Observatory was critical to the success of these projects and his influence continues in these efforts today.

Tom's many achievements have been remembered in obituaries written by Lane Johnson for the *Seismological Society of America* (Johnson, 2002) and Bruce Bolt for the *American Geophysical Union* (Bolt, 2002).

A Web site has been established where photographs, press releases, and testimonials are available at [http://www.seismo.berkeley.edu/seismo/news/tom\\_mcevelly.html](http://www.seismo.berkeley.edu/seismo/news/tom_mcevelly.html).

## 2. McEvelly Graduate Student Fellowship in Seismology

To preserve his memory, Tom's family has requested that the Department of Earth and Planetary Science establish the McEvelly Graduate Student Fellowship in Seismology. Contributions toward the McEvelly Graduate Student Fellowship should be made out to "The Regents of the University of California" and addressed to Susan Torrano, Department of Earth and Planetary Science, 307 McCone Hall, University of California, Berkeley, CA, 94720-4767.

## 3. A Celebration Of Tom McEvelly's Life

Tom's contributions to the BSL, the Department, to seismology, and to his friends and family were celebrated in a memorial service at UC Berkeley on April 22 in the Faculty Club. Ian Carmichael, Barbara Romanowicz, Ernie Majer, Jim Hannon, and Steve McEvelly offered remembrances during the ceremony. Many members of the community shared stories and memories.

The following is a transcript of the address given by Barbara Romanowicz during the service.

### 3.1 Tom McEvelly's career as a seismologist

It is rather hard to summarize in a few minutes Tom's lifetime contributions to Seismology, especially as I was only entering high school and had no clue that there was such a field as Seismology, when Tom was joining the ranks of Ph.D.'s at St Louis University.

So, I decided to give it a personal perspective, and I would like his numerous students and collaborators who are here today to excuse me if I omit some important aspect of Tom's work.

I first became aware of Tom's scientific existence around 1981-82, when, as a post-doc, I was studying surface wave dispersion across Tibet, to remotely unravel the crust and lithospheric structure of that unique area of the world. Tom's early work, indeed his Ph.D. topic, was on the study of crustal structure through the inversion of Love and Rayleigh wave phase velocities under the central US. In this work, which he published in BSSA at the end of 1964, he found that, in this region, he couldn't fit Love and Rayleigh waves with a unique model, implying the existence of anisotropy in the upper mantle under the continent. Well, these were the pioneering days of such studies, but they remain quite current even as I speak. For me this was particularly striking at the time (that is in the early 1980's), as, for whatever it is worth now, I was able to find a single model to fit Love and Rayleigh wave dispersion data across Tibet.

After he came to Berkeley, Tom's work naturally turned to the regional earthquake problem, progressively adding and I will say lots more about that, but since I mentioned my work on Tibet, published in 1982 - it turns out Tom also got interested in Tibet structure as seen by surface waves at about the same time as I did, and with student Kin-Yip Chun proposed, in addition to the very unusual 70 km thick crust, the existence of a mid-crustal low velocity zone in Tibet, an intriguing result from the point of view of rheology and dynamics. Because this work was done in parallel with mine, and I was in France at that time, somehow I only became aware of it much later on, when I came to work at Berkeley.

I first met Tom in person when he became the first president of the IRIS Consortium in 1984. I may have met him earlier, but that's the time I really first paid attention. I still remember having been struck by his cheerful style presiding the IRIS meeting at the Fall San Francisco AGU that year.

So, anyway, back to Tom's career at UC Berkeley since the mid-60's. Several main themes prevail: an interest in seismic instrumentation, which dates back to his involvement with the seismic instrument manufacturer Sprengnether, amplified by his participation in regional network issues at the Berkeley Seismographic Station. Tom turned into one of the best experts in seismic instrumentation in the country - in 1982, as a member of

the NAS Committee on Seismology, he chaired an NRC panel and report on seismic networks which resulted in his involvement in the IRIS program from its very beginning. I emphasize this here, because circumstances have it that almost 20 years later, we are holding today and tomorrow, a session of the Executive Committee of IRIS here at Berkeley, and I have asked Dave Simpson, the IRIS president, to later comment specifically on Tom's contribution through IRIS to the seismological community.

For those of you who are not familiar with this program, IRIS stands for Incorporated Research Institutions for Seismology, and is an NSF funded consortium devoted to the development of infrastructure for seismology. Its main 3 components are the Global Seismic Network, a network of 120 seismic stations distributed globally contributing data for the study of the deep structure of the Earth at the global scale, the PASSCAL program, a pool of portable seismic instruments for regional deployments, and a Data Management System to collect, archive and distribute the IRIS data.

The second theme of Tom's research career, has to do with various aspects of applied seismology: involvement in CTBT related research, monitoring of the Geysers geothermal area, and various other studies which he conducted in collaboration with colleagues at Lawrence Berkeley National Laboratory. I will let Ernie Majer comment on those contributions.

The third theme, and one on which I would like to now expand on, is the study of earthquake processes based on observations on the San Andreas system in California. It doesn't take much to figure out that this main direction of Tom's research was profoundly influenced by the 1966 Parkfield earthquake, which occurred shortly after Tom first came to Berkeley. Parkfield is a very small town (population about 20-some the last time I checked) about half way between San Francisco and Los Angeles, on the San Andreas Fault, which has become the focus of intense seismological interest after this 1966 earthquake, because it appeared to be the site of periodically recurring earthquakes of about magnitude 6, every 22 years on average, the 1966 being the last one of a series of 5 documented events. Parkfield also lies right at the boundary between a "locked zone" on the SAF, to the south, which last broke in the 1857 great Los Angeles (Fort Tejon) earthquake, and a "creeping zone" to the north, which slips steadily and may not have ever experienced a large earthquake.

Shortly after 1968, with students Bill Bakun and John Filson, Tom studied the 1966 Parkfield sequence, using surface wave data, which he was an expert on and later went on to study earthquake source processes with a variety of techniques, in particular near field recordings in the 1980's with Keith McLaughlin and Lane Johnson.

Perhaps more significantly, Tom was involved from

the very beginning in the Parkfield earthquake prediction experiment which got off the ground in the early 1970's. Notable early contributions are a paper with Lane Johnson in *Science* in 1973 on the "dilatancy" issue (the change in the ratio of shear to compressional velocities before earthquakes), and his work using the synthetic VIBROSEIS source of shear wave vibrations, with which he produced a large dataset of consistent waveforms to study temporal changes in crustal properties in the vicinity of the San Andreas Fault, as they might relate to earthquakes - a topic which is still generating publications, most recently with Valeri Korneev at LBL and Eleni Karageorgi, now back in Greece. Tom also was an important mover in several other data acquisition programs using artificial sources to study crustal structure, such as CALCRUST in the 1980's, and more recently the BASIX experiment (1993) in the San Francisco Bay Area.

The real highlight of his career, however, emerged from his investment in the deployment of a then highly unique 10 station borehole seismic network at Parkfield, which started producing data in 1987. The idea was to install seismometers several hundred meters under the Earth's surface, to get away from the noise-generating near-surface weathered layers of rocks, and pick-up clear signals from tiny microearthquakes (down to magnitude  $M -1$ ) that illuminate the fault zone and might reveal something on how the fault works at the microscopic scale. This proved worthwhile. The strong heterogeneity of structure in and around the fault zone turned out to be an issue: it blurred the view and preventing the earthquakes from being accurately located. With students Alberto Michellini and Bill Foxall, Tom first concentrated on resolving this complex structure through joint hypocentral and velocity inversions, unravelling strikingly organized heterogeneity in the fault zone. The discovery of repeating earthquakes, clusters of tightly localized tiny earthquakes producing identical seismic waveforms and their systematic exploitation, through the development of an appropriate data mining methodology, with Bill Foxall and then graduate student Bob Nadeau, led to a series of papers of fundamental significance for earthquake physics. Based on 10 years of data from the borehole Parkfield network, Nadeau and McEvilly documented the quasi-periodic occurrence of micro-earthquakes within well identified clusters, and more recently showed the passage of a stress wave across the Parkfield area in the time period 1988-1995. As shown by Nadeau and Johnson (1998), the characteristics of the micro earthquake clusters has consequences on the distribution of strength and stress, as well as heat generation on the fault. Tom's illness caught him in the middle of finalizing most recent work, in which Nadeau and he documented intriguing pulses in slip rate on the San Andreas fault over distances of tens of kilometers.

To the very end, Tom kept a hands-on approach and wanted to have a chance to "look" at data and process them himself. Bob Nadeau specially travelled to Saint Louis to bring him his Sun workstation so he could work whenever he felt better. It is really too bad that Tom won't be around to glean all the fruits of his hard work at Parkfield, which are only starting to ripen.

Let me finally mention that the Parkfield borehole network has played and is still playing a critical role in the definition of the SAFOD experiment, the San Andreas Fault Observatory at Depth, which is part of the NSF Earthscope Major Research Equipment initiatives hopefully soon to be funded. Tom played a very active role in SAFOD and his absence will be felt.

Closer to home, I would like to finish on a more personal note: Tom's visits (he travelled a lot in recent years) were always like a ray of sunshine at the Berkeley Seismological Laboratory. He was very supportive of our efforts, and I particularly appreciated his advice on delicate diplomatic issues - with him, there was always an easy way out, he had the charm to always turn a confrontational issue into an easy solution - even though he would drive Eleanor, our MSO, crazy with his imaginative solutions to bureaucratic problems - I have lost one of a handful of friends that I could always rely on in my professional life.

## 4. References

Johnson, L., Thomas V. McEvelly, *Seism. Res. Lett.*, 73. 455-456, 2002.

Bolt, B., Thomas Vincent McEvelly, *EOS, Trans. AGU*, 83. 311, 2002.

## Part II Operations



# Chapter 3

## California Integrated Seismic Network

### 1. Introduction

Advances in technology have made it possible to integrate separate earthquake monitoring networks into a single seismic system as well as to unify earthquake monitoring instrumentation. In California, this effort was initiated under the TriNet Project in southern California, where Caltech, the then California Division of Mines and Geology, and the USGS combined their efforts to create a unified seismic system for southern California. With major funding provided by FEMA, OES, and the USGS, the TriNet project provided the opportunity to upgrade and expand the monitoring infrastructure, combining resources in federal, state, university partnership. More recently, the California Geological Survey, Caltech Seismological Laboratory, Berkeley Seismological Laboratory, USGS Menlo Park, and the USGS Pasadena have agreed to cooperate on a statewide basis, because of the obvious benefit to the state.

In the 2000-2001 Annual Report, we described the efforts to create this collaboration through the establishment of a memorandum of agreement and the development of the CISN strategic and implementation plans. In the last year, efforts to form the California Integrated Seismic Network (CISN) took a great leap forward.

### 2. CISN Background

#### 2.1 Organization

The core CISN institutions (California Geological Survey, Berkeley Seismological Laboratory, Caltech, USGS Menlo Park, USGS Pasadena) and OES have signed a MOA (included in the 2000-2001 Annual Report) that describes the CISN organizational goals, products, management, and responsibilities of member organizations. To facilitate coordination of activities among institutions, the CISN has formed three management centers:

- Southern California Management Center: Caltech/USGS Pasadena
- Northern California Management Center: UC Berkeley/USGS Menlo Park

- Engineering Management Center: California Geological Survey/USGS National Strong Motion Program

A goal of the CISN is for the Northern and Southern California Management Centers operate as twin earthquake processing centers. The Engineering Management Center has the lead responsibility for producing engineering data products.

The Steering Committee oversees CISN projects and is comprised of two representatives from each core institution and a representative from OES. Barbara Romanowicz was elected the first chair of the Steering Committee, and was succeeded in December 2001 by Lucy Jones of USGS Pasadena.

An external Advisory Committee, representing the interests of structural engineers, seismologists, emergency managers, industry, government, and utilities, has been formed for review and oversight. The Advisory Committee is chaired by Bruce Clark of the California Seismic Safety Commission. The Advisory Committee has held meetings in July 2001 and 2002.

The Steering Committee has formed other committees, including a Program Management Group to address planning and coordination, a Strong Motion Working Group to focus on issues related to strong-motion data, and a Standards Committee to resolve technical design and implementation issues.

In addition to the core members, several organizations contribute data that enhances the capabilities of the CISN. Contributing members of the CISN include: University of California, Santa Barbara; University of California, San Diego; University of Nevada, Reno; University of Washington; California Department of Water Resources; Lawrence Livermore National Lab; and Pacific Gas and Electric.

#### 2.2 CISN and ANSS

The Advanced National Seismic System (ANSS) is being developed along a regionalized model. 8 regions have been organized and the CISN represents the "California

region". Over the last 3 years, ANSS funding in California has primarily been directed to the USGS Menlo Park to expand the strong-motion instrumentation in the San Francisco Bay Area. As a result, instruments at over 100 sites have been installed or upgraded, significantly improving the data available for ShakeMaps.

The CISN is currently developing plans for the FY 02-03 ANSS program.

### 2.3 CISN and OES

The California Governor's Office of Emergency Services has had a long-term interest in coordinated earthquake monitoring. The historical separation between northern and southern California and between strong-motion and weak-motion networks resulted in a complicated situation for earthquake response.

OES has been an advocate of increased coordination and collaboration in California earthquake monitoring and encouraged the development of the CISN Strategic and Implementation Plans. In FY 2001/2002, Governor Gray Davis requested support for the CISN, to be administered through OES. Funding for the California Geological Survey, Caltech and UC Berkeley was made available in spring 2002, officially launching the statewide coordination efforts.

The CISN/OES program was publically announced on April 15, 2002, during a press conference held at the new headquarters of OES in Sacramento. Invited speakers included Dallas Jones, Director of OES; Darryl Young, Director of the Department of Conservation; Jim Davis, California State Geologist; and Lind Gee from the BSL.

## 3. 2001-2002 Activities

The CISN funding from OES facilitated a number of activities at the BSL during the past year.

### 3.1 Expanded Instrumentation

As part of the CISN/OES project, the BSL purchased equipment for 5 BDSN stations, including STS-2 seismometers, Episensors, and Q4120 data loggers. During 2001-2002, BSL staff initiated efforts to identify potential sites, considering such factors as the current distribution of stations, private versus public property, location of power and telecommunications, and geologic materials.

Two new sites north of the San Francisco Bay were located and permitted for development as broadband observatories. In Lake County, the BSL will build an observatory on the property of the Homestake Mining Company's McLaughlin Mine. Further north, the BSL will build an observatory at the Alder Springs Conservation Camp in the Mendocino National Forest. The status of permitting and site preparation is more fully described in Chapter 4.

Other areas under consideration for future installations include the Pt. Reyes area, the Santa Cruz Mountains (in collaboration with UC Santa Cruz), Pacheco Peak (in collaboration with the California Division of Forestry), Hat Creek (in collaboration with UC Berkeley Department of Astronomy), and Carmel Valley (UC Berkeley Hastings Preserve).

### 3.2 Network Operations and Maintenance

As part of the CISN project, the BSL purchased a number of upgrade kits for their Q4120 data loggers with the goal of improving remote diagnostic capabilities. Three different kits were purchased – power board only, calibration board only, and combined power and calibration boards – in order to ensure that every Q4120 has a power board and that every 8-channel Q4120 also has a calibration board. The power boards provide the capability to monitor battery voltage, allowing staff to discriminate between power and telemetry problems remotely. The calibration boards provide the capability to monitor mass position as well as allow remote calibration of the seismic sensors. Both boards also record data logger temperature.

The boards have not yet been received at the BSL. Prior to widespread upgrades, BSL staff will need to establish procedures for installing and testing these upgrades and then develop a plan for systematic deployment. One of the advantages of this upgrade is that the 21 Q4120 8-channel data loggers maintained by the BSL will be fully interchangeable, as will the 9 4-channel systems. This ability to swap data loggers will facilitate maintenance in the future.

### 3.3 Statewide Communications

One of the major accomplishments of the past year was the design and initial implementation of a CISN communications infrastructure. Doug Neuhauser of the BSL took the lead in investigating options and the CISN partners decided to establish a "ring" of T1 communication links (Figure 3.1) with dual routers at each node. As of June 30, 3 of the 5 links have been ordered and installed (2 of which were ordered by the BSL). Caltech placed the orders for the remaining 2 links in July and installation is expected in September. Orders were also placed for 8 of the 10 routers needed to connect the CISN centers, as the BSL agreed to purchase the routers for the USGS Menlo Park, OES, and CGS, in addition to their own. Caltech's order for 2 routers were placed after July 1 - and delivery is expected in September.

When fully implemented, the CISN ring will have full T1 capacity between adjacent nodes with rapid fallover to secure Internet tunnels among the sites. The network will be able to survive the loss of a single node, T1 cir-



Figure 3.1: Map showing the geographical distribution of the CISN partners and centers. The communications "ring" is shown schematically with installed links (solid lines) and ordered links (dotted lines).

cuits, or router at any site. The routers will be configured to gracefully fail if one or both links at a node fail.

### 3.4 Northern California Management Center

As part of this effort within the CISON, the BSL and the USGS Menlo Park have begun to plan for the next generation of the northern California joint notification system. Chapter 12 describes the operations of the existing Management Center and reports on design discussions.

#### Communications Infrastructure

In order to migrate to a design such as Figure 12.5, the BSL and the USGS Menlo Park need to enhance the communications infrastructure between their sites. Presently, data and information are shared on a dedicated frame-relay connection, with fallback to the Internet.

With OES funding, the BSL commissioned Telecommunications Design Services, Inc. to perform a feasibility study for a microwave communication link between Berkeley and Menlo Park. This study was conducted in June 2002 and a report delivered to the BSL, with copies given to the USGS Menlo Park.

The goal of the study was to evaluate options for a microwave communication link between the BSL and USGS elements of the Northern California Management Center. The report concludes that a repeater site will be required, given the length of the path and the obstructions (buildings, bridges, etc.). According to the report, the Space Sciences Laboratory at UC Berkeley will be a good site for the repeater.

The results of this study are under discussion between the BSL and the USGS. Further discussion is required before moving forward with issues of permission and purchase of hardware.

#### Computing Upgrade

The current data acquisition and processing computers used as part of the Northern California Management Center at the BSL are nearly 4 years old. As part of the OES project, the BSL purchased computers to replace these aging systems.

The BSL purchased five Sun 280R computers. Two of these will be used to immediately replace the current data acquisition and processing computers. One will be used to establish a second ShakeMap installation for northern California. (We currently have a "development" installation of ShakeMap operating at the BSL, which uses input from the finite-fault processing to predict ground motions in areas without stations. The new ShakeMap installation will completely parallel the installation in Menlo Park for redundancy.) The remaining two new computers will be used to set up a pilot system for statewide

earthquake processing. In addition to the 280R computers, the BSL purchased two Sun StorEdge RAID disk systems. The additional disk systems are required by the expanded waveform exchange among the centers.

The new computer systems were delivered on June 30th. The systems will be deployed in racks in the BSL computer server room and will be configured during the next quarter.

### 3.5 Statewide Integration

In January, the BSL hosted a meeting of the CISON Standards Committee. This meeting was focused on issues related to establishing a statewide earthquake processing system. The Standards Committee defined and prioritized projects necessary to develop a prototype system and established working groups to address them (see the minutes from the meeting at <http://www.cison.org/standards/meetings.html>).

The working groups include members from all CISON institutions. Since the January meeting, the Standards Committee has held conference calls approximately every 2-4 weeks to review progress on these issues. The CISON Standards Committee plans to have meetings at least twice a year.

### 3.6 Software Calibration

The CISON partners are working together on the problem of software calibration, particularly as it pertains to automated earthquake processing. Currently, the software implemented in the Southern California Management Center is very different from the software implemented in the Northern California Management Center. Eventually, there may be standardization of software across the management centers, but in the short term, the focus is on calibrating the software to produce the same answers, given the same input data.

In the last year, effort was focused on phase pickers, the association algorithm (binder), the location algorithm (hypoinverse), and magnitude estimation (various). The USGS Menlo Park has taken the lead in testing configurations for a statewide version of the associator and for developing a version of hypoinverse that accounts for velocity models statewide.

The BSL has implemented the Earthworm picker, which is used at Caltech and the USGS Menlo Park, on the data from the Berkeley Digital Seismic Network. All three CISON centers are now running the same picking algorithm, although small differences in configuration exist. We spent some time experimenting with a configuration suitable for its broadband network, as the preliminary configuration produced very few picks. Additional effort is needed to improve the performance of the picker with broadband data.

A test of the association algorithm is underway at the USGS Menlo Park. A preliminary assessment showed

that the Northern and Southern California centers use slightly different configurations of the associator and that these different configurations produce different results. A prototype statewide configuration has been developed and is being tested in Menlo Park and Pasadena.

Staff at the USGS Menlo Park are also working to establish a configuration of the location program for a statewide system. This problem is better defined, as the program can be structured to use different velocity models and station delays.

On the magnitude front, issues of calibration have been complicated by differences between the northern and southern California networks. In southern California, the TriNet upgrade has created a mostly digital seismic network. In northern California, the networks are dominated by analog instrumentation. This means that different magnitude methods are used by each center. A Standards Committee Working Group was tasked to look at the issues presented by this difference in infrastructure.

As part of this effort, the BSL has been looking at some of the software developed under the TriNet project with the goal of adapting it for northern California. Of particular interest are the codes which continuously process waveform data to create timeseries of pre-computed amplitudes (*Kanamori et al., 1999*) such as MI100 (local magnitude computed for a fixed distance of 100 km), Me100 (energy magnitude computed for a fixed distance of 100 km), peak ground acceleration, peak ground velocity, and spectral acceleration at 3, 1, and 0.3 seconds. The continuous processing of the amplitudes is advantageous in providing a steady computing load (as opposed to "peaking" during an earthquake) and rapid access to the data of interest.

Caltech has shared this software with the BSL. Unfortunately, the package could not be installed "as is" and modifications were required. In particular, changes were required to support network and location codes (the SNCL problem). Considerable time was spent in tracking timing discrepancies between the TriNet software and BSL codes for handling waveforms and a small bug in the TriNet codes was found.

As of June 30th, the BSL has adapted versions of the programs which place waveform data in a "common data area (cda)", extract data from the cda, process waveform data to produce reduced amplitude timeseries and write them an "amplitude data area (ada)", and read amplitudes from the ada.

The BSL plans to bring up these codes on the Sun Fire 280r computers as soon as the new computers are configured. This will allow the Northern and Southern California Management Centers to begin exchanging the reduced amplitude time series.

Beyond establishing the amplitude exchange between the centers, the next step for the NC center to modify the existing software to make use of these pre-computed am-

plitudes. This requires changes to several modules in the REDI system. BSL staff are considering several possible approaches. This aspect of the implementation is complicated by the fact that the original TriNet programs use commercial software to perform some functions.

Once the software is operational within the REDI system, the question of magnitude corrections will need to be addressed. Historically, Caltech and the BSL have held different views about the calibration of Wood-Anderson seismometers. As a result, the amplitudes computed from the TriNet software uses a different gain than that used in equivalent BSL processing. This difference will merit careful review in order to avoid introducing problems with the historical catalog.

### 3.7 Data Exchange

Pick exchange was initiated between the Northern and Southern California Management Centers during the previous quarter. With the implementation of the Earthworm picker at the BSL, picks from the BSL have been added to those from the USGS Menlo Park and Caltech.

In the spring, a CISN Standards WG proposed a model for exchanging the reduced amplitude timeseries. During this quarter, BSL staff developed software to use this model for exchange: `ada2ring` (which reads the amplitudes from an `ada` and writes them to an Earthworm ring) and `ring2ada` (which reads the amplitudes from an Earthworm ring and writes them to an `ada`). These programs will allow the CISN to begin exchanging the pre-computed amplitudes using existing Earthworm import/export software. The software developed at the BSL has been tested locally, and a copy given to Caltech so that the center-center feed may be tested. Full exchange will be implemented when the BSL has the new Sun Fire 280r computers configured.

Also during this year, Caltech and the BSL identified 20 stations (10 each) which will be configured to send data to both the Northern and Southern California Data Centers (Figure 3.2). Caltech and the BSL both ordered the DLCIs (data link connection identifier) which will allow the 2nd center to establish a PVC (permanent virtual circuit) to each station using the frame-relay network.

Doug Neuhauser began working on the necessary configuration changes to the Quanterra data loggers. The new Quanterra configuration will allow for 4 telemetry links at each data logger: 1 primary and 1 secondary link to the BSL, 1 link to Caltech, and 1 additional link.

BSL staff participated in a working group to define a new format for exchanging ground motion amplitudes. The purpose of this format is to insure all information necessary for building ShakeMaps and constructing Internet Quick Reports is available.

### Dual data feeds

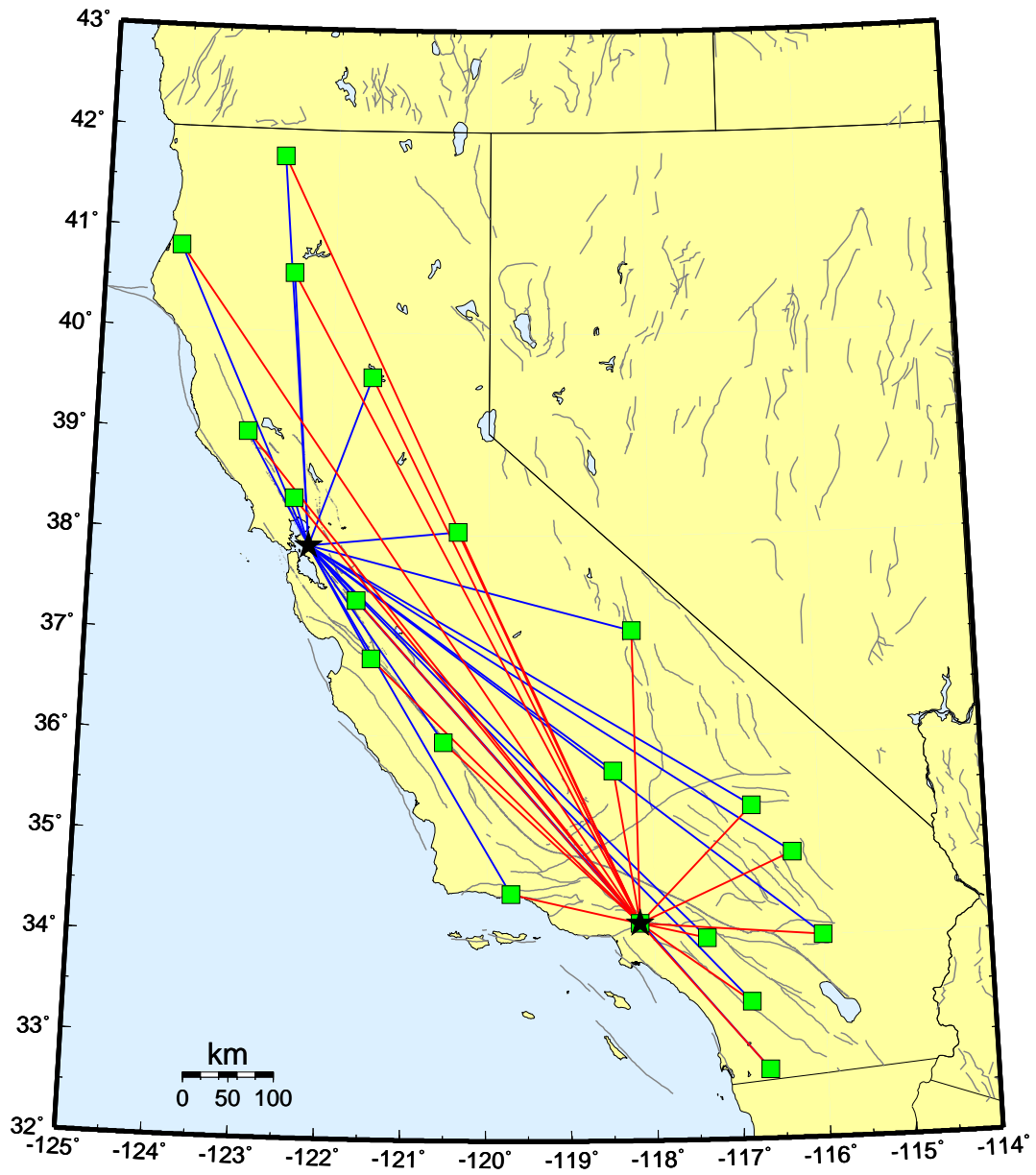


Figure 3.2: Map showing the 20 stations selected to send data directly to the northern and southern California processing centers.

### 3.8 Statewide Earthquake processing

To establish a testbed for statewide processing, several elements must be in place;

- a) full pick exchange
- b) statewide association algorithm
- c) statewide location algorithm
- d) waveform or amplitude time series exchange
- e) standardized magnitude estimation
- f) calibration of station corrections for magnitude

At this point in time (a) is largely complete. Items (b) and (c) are underway. Additional work is required for items (d-f) at this time.

## 4. Acknowledgements

CISN activities at the BSL are supported by funding from the Governor's Office of Emergency Services.

Barbara Romanowicz and Lind Gee are members of the CISN Steering Committee. Lind Gee is a member of the CISN Program Management Committee and she leads the CISN project at the BSL. Doug Neuhauser is chair of the CISN Standards Committee, which includes Lind Gee and Pete Lombard as members.

Because of the breadth of the CISN project, many BSL staff have been involved including: John Friday, Lind Gee, Bill Karavas, Pete Lombard, Doug Neuhauser, Charley Paffenbarger, Dave Rapkin, Cathy Thomas, and Jim Yan.

Lind Gee, Pete Lombard, and Doug Neuhauser contributed to this chapter.

# Chapter 4

## Berkeley Digital Seismic Network

### 1. Introduction

The Berkeley Digital Seismic Network (BDSN) is a regional network of very broadband and strong motion seismic stations spanning northern California and linked to UC Berkeley through continuous telemetry (Figure 4.1 and Table 4.1). This network is designed to monitor regional seismic activity at the magnitude 3+ level as well as to provide high quality data for research projects in regional and global broadband seismology.

The network upgrade and expansion initiated in 1991 has continued, and it has grown from the original 3 broadband stations installed in 1986-87 (BKS, SAO, MHC) to 23 stations in 2002. One station was added in the past year (HUMO).

We take particular pride in high quality installations, which involves often lengthy searches for appropriate sites away from sources of low-frequency noise as well as continuous improvements in installation procedures and careful monitoring of noise conditions at existing stations.

Future expansion of our network is contingent on the availability of funding and coordination with other institutions for the development of a denser state-of-the-art strong motion/broadband seismic network and joint earthquake notification system in this seismically hazardous region.

### 2. BDSN Overview

Twenty-one of the BDSN sites are equipped with 3 component broadband seismometers and strong-motion accelerometers, and a 24-bit digital data acquisition system or data logger. Two additional sites (RFSB and SCCB) consist of a strong-motion accelerometer and a 24-bit digital data logger. Data from all BDSN stations are transmitted to UC Berkeley using continuous telemetry. In order to insure against data loss during utility disruptions, each site has a 3-day supply of battery power and is accessible via a dialup phone line. The combination of high-dynamic range sensors and digital data loggers ensures that the BDSN has the capability to record

the full range of earthquake motion for source and structure studies. Table 4.2 lists the instrumentation at each site.

Most BDSN stations have Streckeisen three-component broadband sensors (*Wielandt and Streckeisen, 1982; Wielandt and Steim, 1986*). Guralp CMG-3T downhole broadband sensors contributed by LLNL are deployed in post-hole installations at BRIB and FARB. The strong-motion instruments are Kinometrics FBA-23 or FBA-EST with  $\pm 2$  g dynamic range. The recording systems at all sites are either Q730, Q680, Q980 or Q4120 Quanterra data loggers, with 3, 6, 8, or 9 channel systems. The Quanterra data loggers employ FIR filters to extract data streams at a variety of sampling rates and these have been implemented as acausal filters in the BDSN. In general, the BDSN stations record continuous data at .01, 0.1, 1.0, and 20.0 samples per second and triggered data at either 80 or 100 samples per second using the Murdock, Hutt, and Halbert event detection algorithm (*Murdock and Hutt, 1983*) (Table 4.3). In addition to the 6-channels of seismic data, signals from thermometers and barometers are recorded at nearly every site (Figure 4.2).

In parallel with the upgrade of the broadband network, a grant from the CalREN (California Research and Education Network) Foundation enabled the BSL to convert data telemetry from analog leased lines to digital frame-relay connections. The frame-relay network uses digital phone circuits that can support 56 Kbit/s to 1.5 Mbit/s throughput. Since frame-relay is a packet-switched network, a site may use a single physical circuit to communicate with multiple remote sites through the use of "permanent virtual circuits". Frame Relay Access Devices (FRADs), which replace modems in a frame-relay network, can simultaneously support multiple interfaces such as RS-232 async ports, synchronous V.35 ports, and ethernet connections. In practical terms, the upgrade to frame relay communication provides faster data telemetry between the remote sites and the BSL, remote console control of the data loggers, additional services such as ftp and telnet to the data loggers, data transmission to multiple sites, and the ability to communicate and transmit

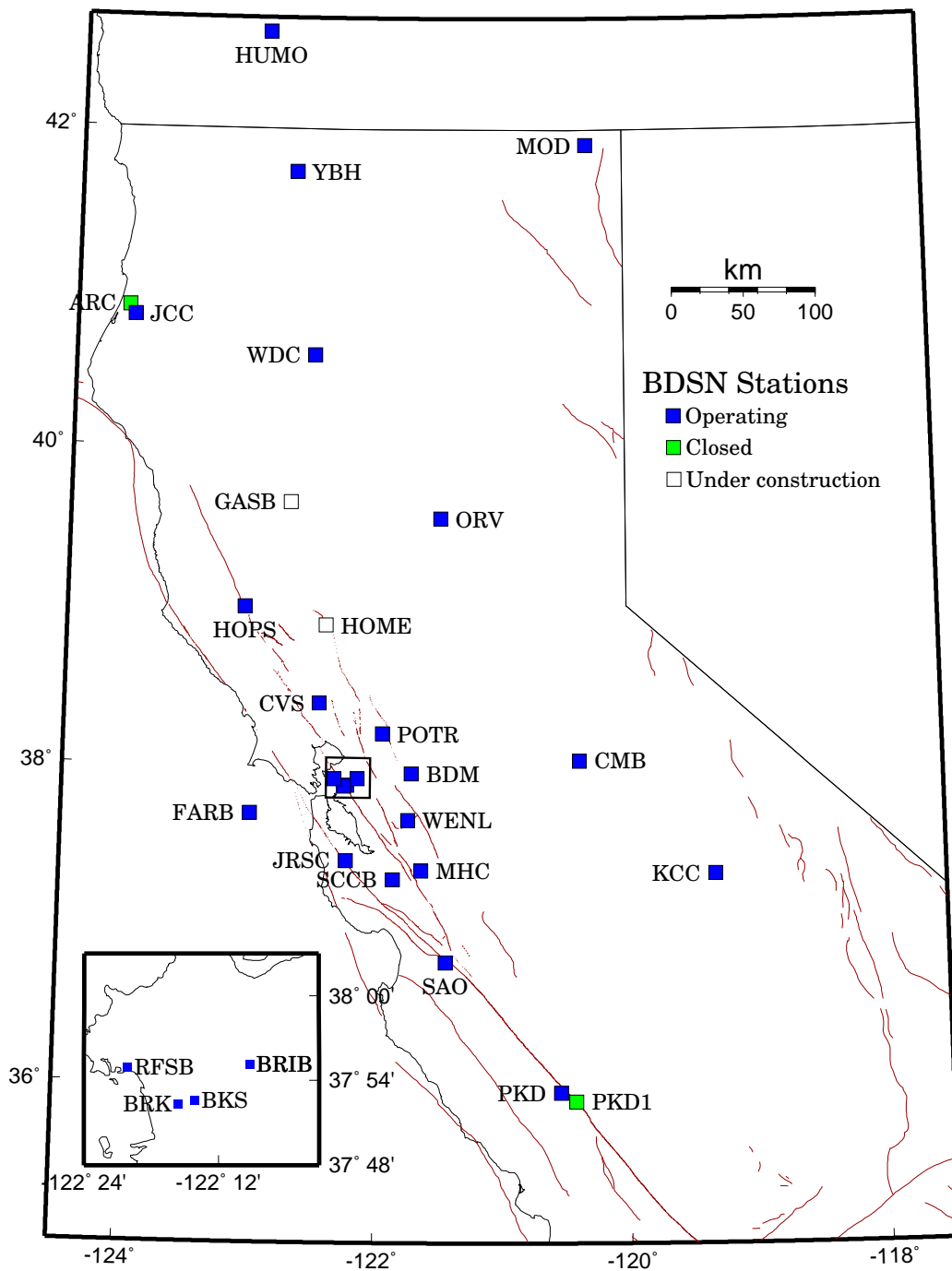


Figure 4.1: Map illustrating the distribution of operational (filled squares), planned (open squares), and closed (grey squares) BDSN stations in northern and central California.



data from multiple instruments such as GPS receivers and/or multiple data loggers at a single site. Today, 20 of the BDSN sites use frame-relay telemetry for all or part of their communications system.

As described in Chapter 11, data from the BDSN are acquired centrally at the BSL. These data are used in the Rapid Earthquake Data Integration System as well as in routine earthquake analysis (Chapter 12). As part of routine quality control (Chapter 11), power spectral density analyses are performed weekly and Figure 4.3 shows a summary of the results for 2001-2002. The occurrence of a significant teleseism also provides the opportunity to review station health and calibration and Figure 4.4 displays the response of the BDSN to a  $M_w$  7.3 earthquake in Russia-China border region.

BDSN data are archived at the Northern California Earthquake Data Center and this is described in detail in Chapter 13.

Sensor	Channel	Rate (sps)	Mode	FIR
Broadband	UH?	0.01	C	Ac
Broadband	VH?	0.1	C	Ac
Broadband	LH?	1.0	C	Ac
Broadband	BH?	20.0	C	Ac
Broadband	HH?	80.0/100.0	T	Ac
Strong-motion	LL?	1.0	C	Ac
Strong-motion	BL?	20.0	C	Ac
Strong-motion	HL?	80.0/100.0	C	Ac
Thermometer	LKS	1.0	C	Ac
Barometer	LDS	1.0	C	Ac

Table 4.3: Typical data streams acquired at BDSN stations, with channel name, sampling rate, sampling mode, and the FIR filter type. C indicates continuous; T triggered; Ac acausal. The LL and BL strong-motion channels are not transmitted over the continuous telemetry but are available on the Quanterra disk system if needed.

### 3. 2001-2002 Activities

#### 3.1 Station Maintenance

Given the remoteness of the off-campus stations, BDSN data acquisition equipment and systems have been designed, configured, and installed for both cost effectiveness and reliability. As a result, the need for regular station visits has been reduced. Most station visits are necessitated by some catastrophic failure. The 2001-2002 fiscal year was no exception.

#### Vandalism

At station JCC, vandals broke into the steel and concrete vault, cut the instrument power cables, and stole the station batteries. Data acquisition was interrupted

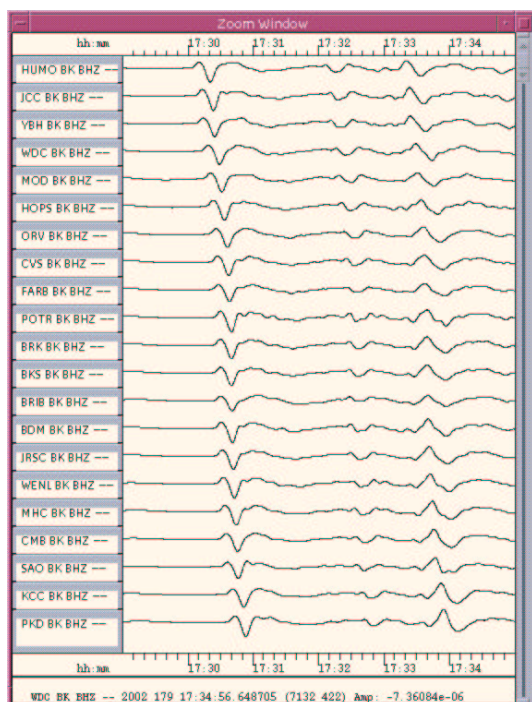


Figure 4.4: BDSN Z-component broadband recording of the P, pP and sP recorded waveforms from a large deep focus teleseism the occurred in the Russia-northeast China border region ( $M_w$  7.3; 2002.179,17:19; depth 566 km; 75 deg NW of Berkeley). The waveforms have been bandpass filtered (0.01-0.1 Hz), deconvolved to absolute ground displacement, and ordered by distance from the epicenter. The similarity of the waveforms in the BDSN broadband records implies that the vertical components are responding normally and that the instrument responses are correct.

## BDSN PSD Low Noise Synopsis (2001–2002)

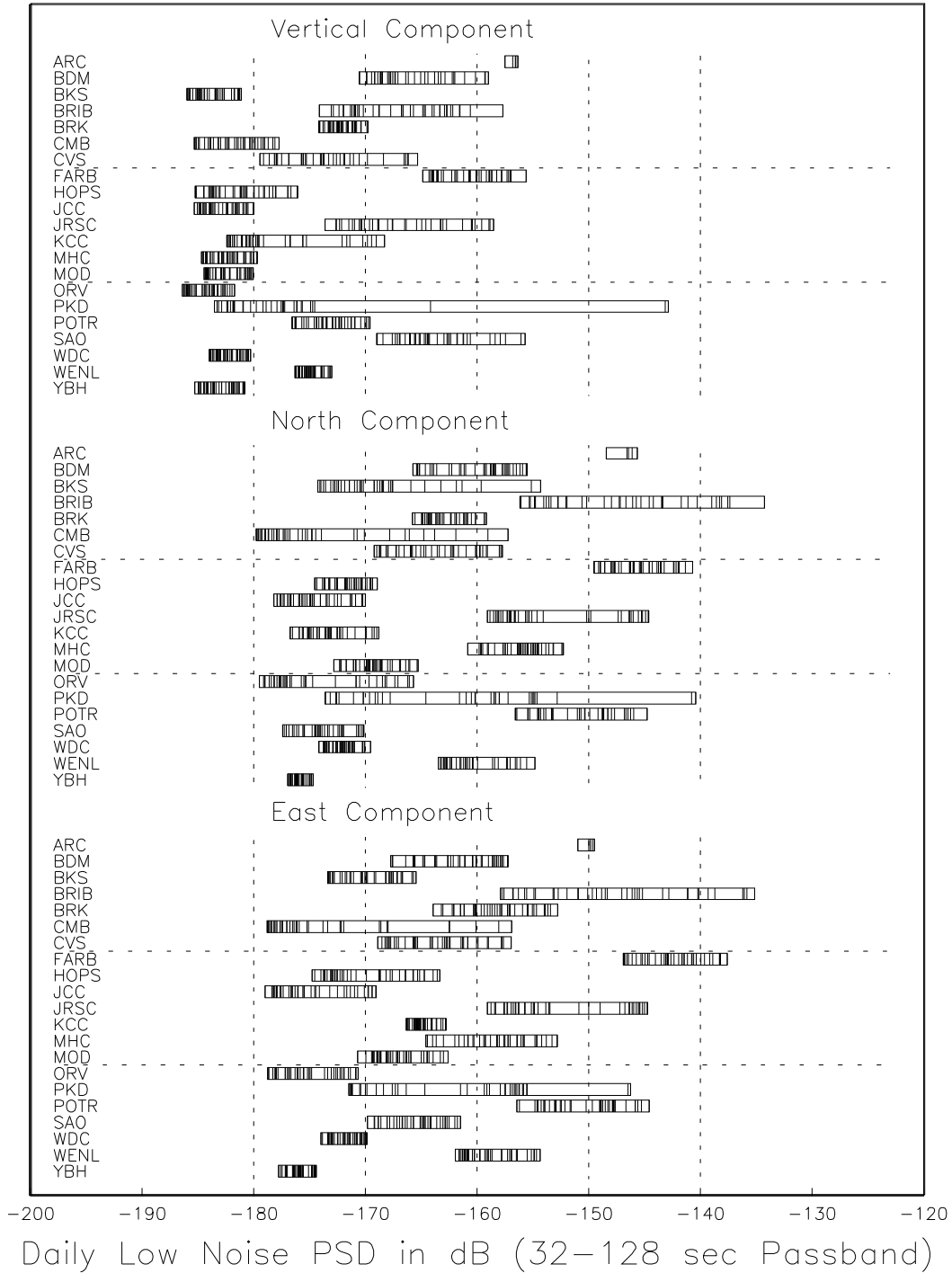


Figure 4.3: PSD noise analysis for BDSN stations, by channel, in the period range from 32-128 sec. PKD stands out in terms of its high noise level variation, which was caused by a problem in the sensor. FARB, sited on the Farallon Islands, stands out as the station with the highest average background noise level. BRIB, sited in a shallow borehole on a hillside prone to seasonal tilting, is also relatively noisy. YBH, sited in a remote and abandoned hard rock mining drift, stands out as exceptionally quiet site. The newest BDSN station, JCC, is also among the quietest of the BDSN stations.

Code	Net	Latitude	Longitude	Elev (m)	Over (m)	Date	Location
ARC	BK	40.87772	-124.07738	30.1	0	1992/05 - 2001/07	HSU, Arcata
BDM	BK	37.95397	-121.86554	219.8	34.7	1998/11 -	Black Diamond Mines, Antioch
BKS	BK	37.87622	-122.23558	243.9	25.6	1988/01 -	Byerly Vault, Berkeley
BRIB	BK	37.91886	-122.15179	219.7	2.5	1995/06 -	Briones Reservation, Orinda
BRK	BK	37.87352	-122.26099	49.4	2.7	1994/03 -	Haviland Hall, Berkeley
CMB	BK	38.03455	-120.38651	697.0	2	1986/10 -	Columbia College, Columbia
CVS	BK	38.34526	-122.45840	295.1	23.2	1997/10 -	Carmenet Vineyard, Sonoma
FARB	BK	37.69782	-123.00110	-18.5	0	1997/03 -	Farallon Island
HOPS	BK	38.99349	-123.07234	299.1	3	1994/10 -	Hopland Field Stat., Hopland
HUMO	BK	42.60710	-122.95669	554.9	TBD	2002/06 -	Hull Mountain, Oregon
JCC	BK	40.81745	-124.02955	27.2	0	2001/04 -	Jacoby Creek
JRSC	BK	37.40373	-122.23868	70.5	0	1994/07 -	Jasper Ridge, Stanford
KCC	BK	37.32363	-119.31870	888.1	87.3	1995/11 -	Kaiser Creek
MHC	BK	37.34164	-121.64257	1250.4	0	1987/10 -	Lick Obs., Mt. Hamilton
MOD	BK	41.90246	-120.30295	1554.5	5	1999/10 -	Modoc Plateau
ORV	BK	39.55451	-121.50036	334.7	0	1992/07 -	Oroville
PKD	BK	35.94517	-120.54160	583.0	3	1996/08 -	Bear Valley Ranch, Parkfield
PKD1	BK	35.88940	-120.42611	431.6	0	1991/10 - 2000/09	Haliburton House, Parkfield
POTR	BK	38.20263	-121.93535	20.0	6.5	1998/02 -	Potrero Hill, Fairfield
RFSB	BK	37.91608	-122.33607	-26.7	0	2001/02 -	RFS, Richmond
SAO	BK	36.76403	-121.44722	317.2	3	1988/01 -	San Andreas Obs., Hollister
SCCB	BK	37.28773	-121.86584	101.6	0	2000/04 -	SCC Comm., Santa Clara
WDC	BK	40.57988	-122.54113	268.3	75	1992/07 -	Whiskeytown
WENL	BK	37.62211	-121.75697	138.9	30.3	1997/06 -	Wente Vineyards, Livermore
YBH	BK	41.73204	-122.71039	1059.7	60.4	1993/07 -	Yreka Blue Horn Mine, Yreka

Table 4.1: Stations of the Berkeley Digital Seismic Network. Each BDSN station is listed with its station code, network id, location, operational dates, and site description. The latitude and longitude (in degrees) are given in the WGS84 reference frame and the elevation (in meters) is relative to the WGS84 reference ellipsoid. The elevation is either the elevation of the pier (for stations sited on the surface or in mining drifts) or the elevation of the well head (for stations sited in boreholes). The overburden is given in meters. The date indicates either the upgrade or installation time.

while the batteries were replaced and multiple steel locking mechanisms were installed to prevent future vandalism. Local police were notified.

Local police were also notified when vandals broke into the instrument enclosure and stole the GPS receiver at SAO. Engineers from the BSL rebuilt the enclosure building and instrument mounting in a manner to minimize the likelihood of future problems, although the proximity of this site to areas of public access remains a concern.

### BDM Power system

We experienced problems at BDM (Black Diamond Mine) this year, with the data logger and telemetry subsystem rebooting periodically. The cause of the reboots was found to be the interaction among a power supply of marginal size, a low voltage cut-off device, and battery with an internally shorted cell. When the line power to the data acquisition system was turned off, the system batteries would power the system until the battery voltage was sufficiently reduced to cause the low voltage

device to turn off all power to the system. When the line power was restored, the power supply was inadequately sized to raise the voltage of the internally shorted battery high enough that the system could reboot while pulling the battery voltage lower to the point of the low voltage device turning the system off again. The cycle would thus repeat indefinitely. BSL engineers replaced all the station batteries and installed a larger power supply.

### PKD

At station PKD, data are telemetered via spread spectrum radios from the vault to Carr Hill, where a frame-relay connection carries the data to Berkeley. During the past year, as additional groups have added experiments and additional radios, the radio throughput became unacceptably low. After multiple trips and collaboration with USGS and other technicians, BSL engineers were able to improve the data rate by raising the height of the antenna and changing polarization of the transceiver antennas. However, data throughput could diminish fur-

Code	Broadband	Strong-motion	Data logger	T/B	GPS	Other	Telemetry	Dial-up link
ARC	STS-2	FBA-23	Q980				FR	X
BDM	STS-2	FBA-23	Q4120	X			FR	
BKS	STS-1	FBA-23	Q980	X		Baseplates	FR	X
BRIB	CMG-3T	FBA-23	Q980		X	Vol. Strain	FR	X
BRK	STS-2	FBA-23	Q680				POTS	
CMB	STS-1	FBA-23	Q980	X	X	Baseplates	FR/NSN	X
CVS	STS-2	FBA-23	Q4120	X			FR	
FARB	CMG-3T	FBA-23	Q4120	X	X		R-FR/R	
HOPS	STS-1	FBA-23	Q980	X	X	Baseplates	FR	X
HUMO	STS-2	FBA-ES-T	Q4120	X			NSN	X
JCC	STS-2	FBA-23	Q980	X			FR	X
JRSC	STS-2	FBA-23	Q680				FR	X
KCC	STS-1	FBA-23	Q980	X		Baseplates	R-Mi-FR	X
MHC	STS-1	FBA-23	Q980	X	X		FR	X
MOD	STS-1	FBA-ES-T	Q980	X	X	Baseplates	NSN	X
ORV	STS-1	FBA-23	Q980	X	X	Baseplates	FR	X
PKD	STS-2	FBA-23	Q980	X	X	EM	R-FR	X
PKD1		FBA-23	Q980				FR	X
POTR	STS-2	FBA-ES-T	Q4120	X	X		FR	X
RFSB		FBA-ES-T	Q730				FR	
SAO	STS-1	FBA-23	Q980	X	X	Baseplates, EM	FR/NSN	X
SCCB		FBA-ES-T	Q730		X		FR	
WDC	STS-2	FBA-23	Q980	X			FR/NSN	X
WENL	STS-2	FBA-23	Q4120	X			FR	
YBH	STS-1	FBA-23	Q980	X	X	Baseplates	FR	X

Table 4.2: Instrumentation of the BDSN as of 06/30/2002. Every BDSN station consists of collocated broadband and strong-motion sensors, with the exception of PKD1, RFSB and SCCB which are strong-motion only, with a 24-bit Quanterra data logger and GPS timing. Additional columns indicate the installation of a thermometer/barometer package (T/B), collocated GPS receiver as part of the BARD network (GPS), and additional equipment (Other) such as warpless baseplates or electromagnetic sensors (EM). The main and alternate telemetry paths are summarized for each station. FR - frame relay circuit, R - radio, Mi - microwave, POTS - plain old telephone line, NSN - USGS NSN satellite link. An entry like R-Mi-FR indicates multiple telemetry links, in this case, radio to microwave to frame relay.

ther if additional transmitters are added near Parkfield.

Also during 2001-2002, the STS-2 sensor at PKD was replaced. Routine PSD analysis indicated an increase in the noise level.

### YBH Upgrades

Station YBH was previously chosen as an alternative monitoring station by both IMS and DTRA. In collaboration with the IMS, BSL installed a VSAT data link, long-period microbarograph, and separate battery backup. We also installed an IMS-supplied, stand-alone data validation computer and door switch. To observe long periods on the microbarograph, the sensor was installed in a copper pipe anchored to the rock wall of the adit. Foam insulation was applied to the outside of the copper pipe to further dampen the temperature fluctuations of the sensor. Additionally, a second pier was constructed at YBH for installation of an STS-2 seismometer in 2002-

2003. The STS-2 will be deployed in parallel with the existing STS-1 seismometers, bringing YBH into compliance as an auxillary station of the IMS.

### CMB Trailer

After many years of service, the portable trailer at CMB was retired. This structure housed the data logger and other electronics. Prior to its deployment at CMB, the trailer was in service at the Jamestown station for nearly twenty years. The combination of the structural failure, the pooling of rainwater on the roof, and the collapse of the floor led to the purchase and installation of a steel shipping container in 2001-2002. Special attention was paid to insulating, and grounding the the container prior to installation of the data acquisition and telemetry equipment.

## STS-1 hinges

In November of 2001, Bob Uhrhammer reported observations of 1-sided steps on the STS-1 North component at station BKS. In January and early February of 2002, BSL staff replaced the electronics box and tested the baseplates, and concluded that rust on the sensor hinge was the source of the noise. Small rust spots were observed on another STS-1 sensor (both sensors had not been evacuated in their early history).

Since replacement hinges are not available from Streckheisen - and since as many as 20 BDSN sensors could develop this problem, BSL staff began efforts to manufacture replacement hinges. During a visit in February, Erhard Wielandt recommended replacing all 4 hinges simultaneously, using material similar to the original. BSL staff spent time developing a reproducible recipe for the hinges, including laser cutting the edges for smoothness. The first set of replacement hinges is being tested now.

## 3.2 New Installations

### Hull Mountain, Oregon (HUMO)

In the fall of 2000, we began a search for a site to extend BDSN north of the California/Oregon border, as part of a collaboration with the USGS National Seismic Network and the Global Seismic Network of IRIS, to be located north of the midpoint between the existing sites at MOD and YBH. This station will be one of the sites of the 100 station NSN/GSN "backbone" in the U.S. Our experience shows that sites which are located on hard granite have less ground tilt and are quieter in the long period, so the first step in locating the new site was to consult a geological map of the area.

In the Medford, Oregon area, we contacted officials at six ranger offices within two National Forests, and the Bureau of Land Management in hopes of finding an abandoned mining adit similar to YBH and MOD. This area was historically an active mining region with many possible sites. Several of the possible adit sites were flooded, several more were located but had collapsed since mining ending, and others were deemed too far from utilities. A suitable adit was located north of Medford, 12 kilometers west of Shady Cove, and this site was permitted with the US Bureau of Land Management. By placing the seismographic equipment on public lands as opposed to private lands, the longevity of the site is assured.

Although instruments located underground clearly exhibit better signal to noise characteristics, technical challenges to securing the site, power, telemetry, and external clock present themselves as a result of this type of installation.

As found, the front of the adit was largely blocked by a small landslide. The entrance was excavated and a steel culvert placed to line the weathered rock near the entrance, prevent collapse, and to provide an anchor point

for a lockable grate steel grate. Commercial power and phone lines were trenched and placed below the steel culvert. At this location, at the request of the BLM biologist, a solid door was not used in order that bats may enter and hibernate during winter months. All instrumentation -data logger, seismometers, battery back up, barometer, thermistor and telemetry equipment, is located 110 meters inside of the adit. To achieve external GPS clock signal, a high gain antenna was placed outside the adit. Low attenuation coaxial cable connects the antenna and the data logger clock.

At this time, connection to the National Seismic Network VSAT is being established. Because the equipment is underground and the site is located within a mature forest, it was necessary to locate the VSAT dish approximately 300 meters away from the data logger in a location with a view of the southern sky (where the NSN satellite is located). To achieve digital telemetry over this distance, a fiber optic link will connect the data logger with the VSAT hardware. Again, all data and power lines will be trenched and buried.

While the VSAT system is being completed, the station is accessible via a dial-up phone line. Preliminary data analysis indicates that the background noise level at HUMO is lower than that observed at WDC. Figure 4.5 shows raw P waveforms at HUMO and WDC from a recent teleseism.

In this collaborative effort, the USGS/NSN provided the STS-2 seismometer, the BSL supplied the Episensors and the Quanterra data logger, and IRIS provided support for the installation expenses.

## 3.3 New Site Development

In the past year, two new sites north of the San Francisco Bay were located and permitted for development as broadband observatories. In Lake County, the BSL will build an observatory on the property of the Homestake Mining Company's McLaughlin Mine. Further north, the BSL will build an observatory at the Alder Springs Conservation Camp in the Mendocino National Forest.

### McLaughlin Mine

The McLaughlin Mine site is on property owned and formerly operated by Homestake Mining Company as a surface gold mine. Although local geological maps indicate the area to be volcanic in origin, the mining operation revealed the geology to be extremely varied and complex. With the conclusion of mining operations, the property will be managed as a UC-Davis reserve for research. The seismographic vault will be one of the first research projects on the new reserve. The site will be located approximately 20 kilometers east of the town of Lower Lake, California. The area where the vault will be constructed consists largely of Franciscan sandstone. At this time, a contractor has been hired to excavate and

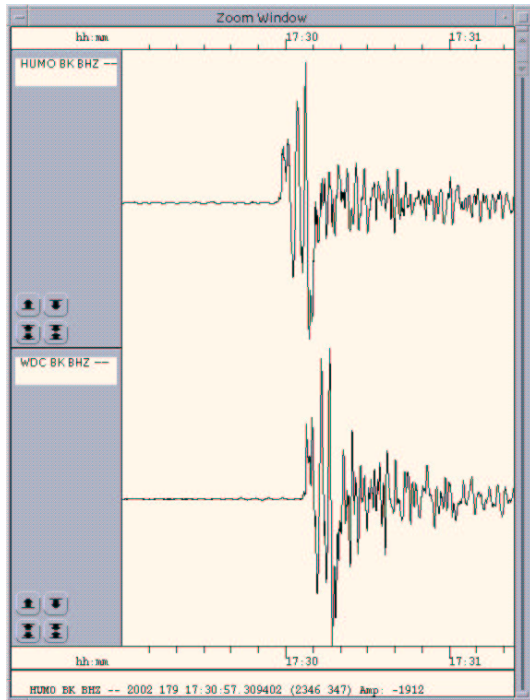


Figure 4.5: A comparison of the raw P-wave Z-component waveform recorded by the STS-2 broadband seismometer sited at the newest BDSN station at Hull Mountain, OR (HUMO) with the corresponding waveform recorded by the STS-2 broadband seismometer sited at Whiskeytown Dam, CA (WDC) 228 km S of HUMO. The P-waves were generated by a large deep-focus teleseism that occurred in the Russia-northeast China border region ( $M_w$  7.3; 2002.179,17:19; depth 566 km; 72 degrees NW of HUMO). Both stations are sited in remote abandoned hard rock mining drifts. The highly similar first  $\sim$ 15 seconds of the P-wave waveforms shows that the two stations are responding nearly identically to the teleseismic signal and the differences later in the P-wave coda are due primarily to differences in the crustal structure at the two sites.

construct a vault from a steel container similar to those found at stations JCC, PKD, and HOPS. The BSL has registered the name HOME for this site.

### Alder Springs

Located approximately 35 kilometers west of the central valley town of Williams, at the Alder Springs site a short period observatory is operated by the California Department of Water Resources. Rocks are mostly serpentine in nature. Again, a seismographic vault similar to those at JCC, PKD, and HOPS will be built. The BSL vault will house the Department of Water Resources equipment presently installed in a fiberglass enclosure. This site has been named GASB by the BSL.

## 4. Acknowledgements

Under Barbara Romanowicz's general supervision, Lind Gee and Doug Neuhauser oversee the BDSN data acquisition operations and Bill Karavas is head of the field engineering team. John Friday, Dave Rapkin, Cathy Thomas, and Bob Uhrhammer contribute to the operation of the BDSN. Bill Karavas, Bob Uhrhammer, and Lind Gee contributed to the preparation of this chapter.

Support for the installation of HUMO was provided by the USGS/NSN and IRIS. The California Governor's Office of Emergency Services provided funding toward the development of sites HOME and GASB as part of the CISN.

## 5. References

- Murdock, J., and C. Hutt, A new event detector designed for the Seismic Research Observatories, *USGS Open-File-Report 83-0785*, 39 pp., 1983.
- Wielandt, E., and J. Steim, A digital very broad band seismograph, *Ann. Geophys.*, 4, 227-232, 1986.
- Wielandt, E., and G. Streckeisen, The leaf spring seismometer: design and performance, *Bull. Seis. Soc. Am.*, 72, 2349-2367, 1982.

# Chapter 5

## Northern Hayward Fault Network

### 1. Introduction

Complementary to the regional broadband network, a deployment of borehole-installed, wide-dynamic range seismographic stations is being established along the Hayward Fault and throughout the San Francisco Bay toll bridges network. This project is a cooperative development of the BSL and the USGS, with support from USGS, Caltrans, EPRI, the University of California Campus/Laboratory Collaboration (CLC) program, LLNL, and LBNL (Figure 5.1 and Table 5.1).

The purpose of the network is twofold: to lower substantially the threshold of microearthquake detection and increase the recorded bandwidth for events along the Hayward fault; and to obtain bedrock ground motion signals at the bridges from small earthquakes for investigating bridge responses to stronger ground motions. A lower detection threshold will increase the resolution of fault-zone structural features and define spatio-temporal characteristics in the seismicity at  $M \sim > -1.0$ , where occurrence rates are dramatically higher than those captured by the surface sites of the NCSN. This new data collection will contribute to improved working models for the Hayward fault. The bedrock ground motion recordings are being used to provide input for estimating the likely responses of the bridges to large, potentially damaging earthquakes. Combined with the improved Hayward fault models, source-specific response calculations can be made.

The Hayward Fault Network (HFN) consists of two parts. The Northern Hayward Fault Network (NHFN) is operated by the BSL and currently consists of 20 stations, including those located on the Bay bridges. This network is considered part of the BDSN and uses the network code BK. The Southern Hayward Fault Network (SHFN) is operated by the USGS and currently consists of 5 stations. This network is considered part of the NCSN and uses the network code NC. This chapter is primarily focused on the NHFN and activities associated with the BSL operations.

### 2. NHFN Overview

All sites of the HFN have six-component borehole sensor packages which were designed and fabricated at LBNL's Geophysical Measurement Facility by Don Lippert and Ray Solbau, with the exception of site SFAB. Three channels of acceleration are provided by Wilcoxon 731A piezoelectric accelerometers and three channels of velocity are provided by Oyo HS-1 4.5 Hz geophones (Table 5.2). Sensors are installed at depths of 100-300 m and provide signals to the on-site data loggers (Quanterra Q4120 and Q730, Nanometrics HRD24, or RefTek 72A-07 systems).

The 0.1-400 Hz Wilcoxon accelerometers have lower self-noise than the geophones above about 25-30 Hz, and remain on scale and linear to 0.5 g. In tests performed in the Byerly vault at UC Berkeley, the Wilcoxon is considerably quieter than the FBA-23 at all periods, and is almost as quiet as the STS-2 between 1 and 50 Hz.

Eight of the NHFN sites have Quanterra data loggers with continuous telemetry to the BSL. Similar to BDSN sites, these stations are capable of on-site recording and local storage of all data for more than one day and have batteries to provide backup power. Signals from these stations are digitized at a variety of data rates up to 500 Hz at 24-bit resolution (Table 5.3). In contrast to the BDSN implementation, the NHFN data loggers employ causal FIR filters at high data rates and acausal FIR filters at lower data rates. Because of limitations in telemetry bandwidth and disk storage, these 7 sites transmit triggered data at 500 sps, using the Murdock, Hutt, and Halbert (MHH) event detection algorithm (*Murdock and Hutt*, 1983), and continuous data at reduced rates (100, 20 and 1 sps) to the BSL.

The remaining 12 sites of the NHFN have in the past recorded data using RefTek data loggers. These sites do not have continuous telemetry for acquisition and require visits from BSL staff for data recovery. Seven of these sites located on the Bay Bridge are scheduled to be upgraded with Quanterra data loggers and continuous telemetry in the fall of 2002 (see Figure 11.2 in Chapter 11). The Bay Bridge component of the NHFN has been

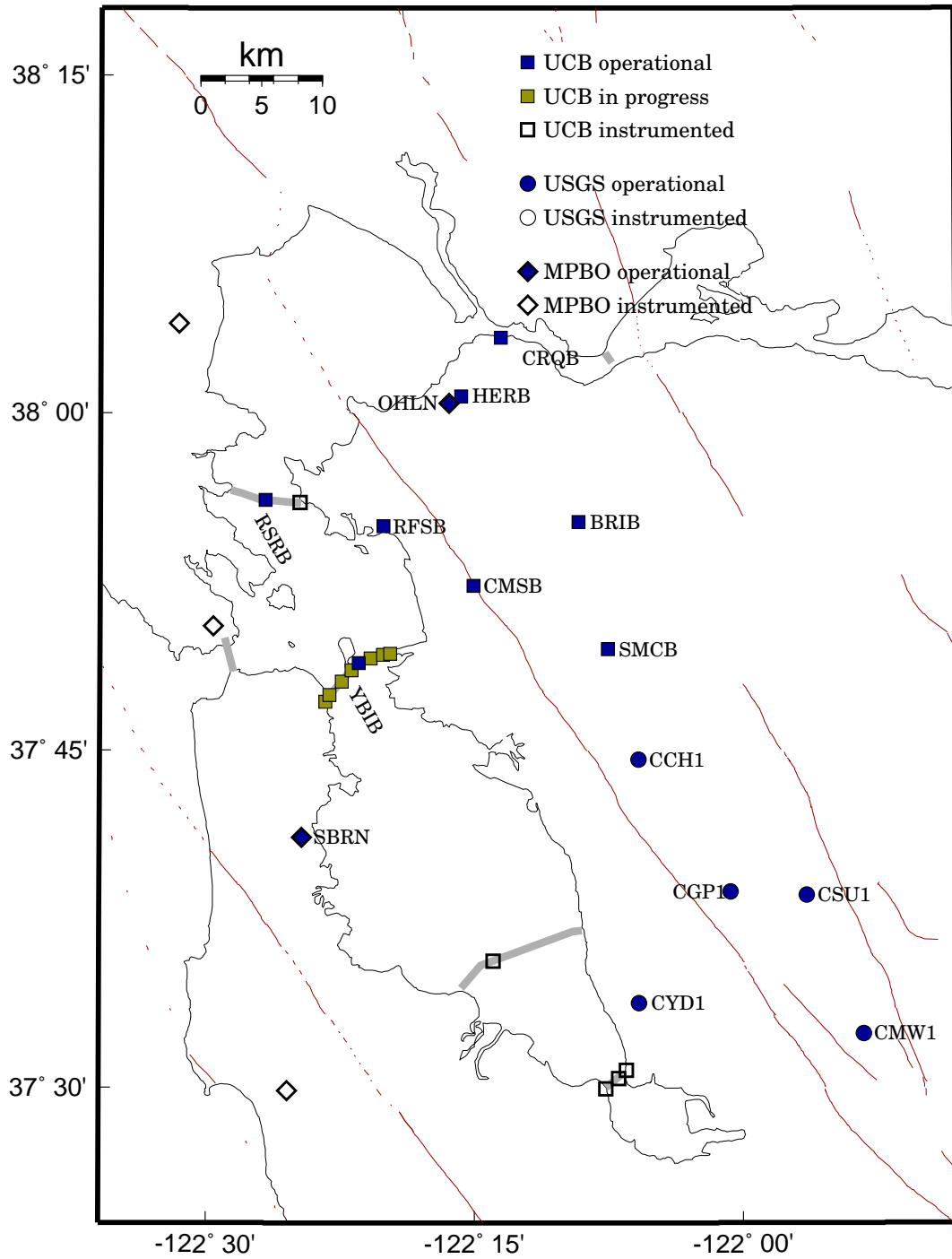


Figure 5.1: Map showing the locations of the HFN stations operated by the BSL (NHFN - squares) and the USGS (SHFN - circles) and Mini-PBO stations (diamonds) in the San Francisco Bay Area. Operational sites are filled, while sites in progress are grey. Other instrumented boreholes are indicated as open symbols.

delayed during the past year, primarily due to the major effort required to upgrade the HRSN (Chapter 6).

Signals from the 5 SHFN stations are digitized by Nanometrics data loggers at 200 sps and transmit continuous data to Menlo Park by radio. The digital data streams are processed by the Earthworm system with the NCSN data and waveforms are saved when the Earthworm detects an event.

As part of the USGS and BSL collaboration on the HFN, data from the NHFN and SHFN sites with continuous telemetry are shared in near real-time. NHFN data are transmitted to the USGS and SHFN data are transmitted to the BSL.

Experience has shown that the MHH detector does not provide uniform triggering across the NHFN on the smallest events of interest. In order to insure the recovery of 500 sps data for these earthquakes, a central-site controller has recently been implemented at the BSL using the 500 sps vertical component geophone data for event detection. Originally the 100 sps vertical component geophone data was used for event detection but the bandwidth proved to be inadequate for detection of the smaller events where most of the seismic wave energy was at frequencies above 40 Hz. Triggers from this controller will be used to recover the 500 sps data from the NHFN data loggers.

Data from the NHFN and SHFN are archived at the NCEDC. At this time, the tools are not in place to archive the Hayward fault data together. The NHFN data are archived with the BDSN data, while the SHFN are archived with the NCSN data (Chapter 13). However, the new central-site controller will provide the capability to both include SHFN data in the event detection and extract SHFN waveforms for these events in the future.

As originally planned, the Hayward Fault Network was to consist of 24 to 30 stations, 12-15 each north and south of San Leandro, managed respectively by UCB and USGS. This is not happening quickly, although west of the fault, Caltrans has provided sites along the Bay bridges. This important contribution to the Hayward Fault Network has doubled the number of sites with instrumentation. At times, Caltrans provides holes of opportunity away from the bridges (e.g., HERB), so we have plans for additional stations that will bring the network geometry to a more effective state for imaging and real-time monitoring of the fault.

As a check on the calibration and an example of the capabilities of a borehole installed network, we compare the bandpass filtered (0.3-2 Hz) ground displacements, as inferred from the vertical component accelerometer and from the vertical component geophone data streams recorded at BRIB, CMSB, CRQB, HERB, OHLN, SBRN (the newest MPBO station, sited on San Bruno Mtn, San Francisco Peninsula), and RFSB, for a M 7.7 deep focus earthquake that occurred in the Fiji Islands at a depth

Sensor	Channel	Rate (sps)	Mode	FIR
Accelerometer	CL?	500.0	T	Ca
Accelerometer	HL?	100.0	C	Ca
Accelerometer	BL?	20.0	C	Ac
Accelerometer	LL?	1.0	C	Ac
Geophone	DP?	500.0	T	Ca
Geophone	EP?	100.0	C	Ca
Geophone	BP?	20.0	C	Ac
Geophone	LP?	1.0	C	Ac

Table 5.3: Typical data streams acquired at each NHFN site, with channel name, sampling rate, sampling mode and FIR filter type. C indicates continuous; T triggered; Ca causal; and Ac acausal. The 100 sps channels (EP & HL) are only archived when the 500 sps channels are not available.

of 580 km. in Figure 5.2.

### 3. 2001-2002 Activities

During this year, two stations of the NHFN continued to be not operational. YBIB was shut down when power was cut off in August 2000 and RSRB was taken offline in April 2001 during the retrofit project on the Richmond-San Rafael Bridge. YBIB is anticipated to return after solar panels are installed in late 2002/early 2003. No estimate of the return of RSRB is currently available.

#### 3.1 Station Maintenance

The most pervasive problem at NHFN stations equipped with Q4120 data loggers is power line noise (60 Hz and its harmonics at 120, 180, and 240 Hz). This noise reduces the sensitivity of the MHH detectors.

Whenever a NHFN station is visited, the engineer at the site and a seismologist at the BSL work together to expedite the testing process, especially when attempting to identify and correct ground-loop faults which generally induce significant 60, 120, 180, and 240 Hz seismic signal contamination due to stray power line signal pickup, generally inductively coupled and aggravated by the presence of ground loops.

#### CMSB

Replaced batteries. Repaired signal cable where it was chewed by rodents. Q4120 is drawing 2.9 amps. The preamp draws about 200 ma which is correct. This indicates higher than normal current (Q4120 current should be ~2.3 amps) into the Q4120 and gradual failure of one of the circuits.

Code	Net	Latitude	Longitude	Elev (m)	Over (m)	Date	Location
BRIB	BK	37.91886	-122.15179	219.7	108.8	1995/07 - current	BR, Orinda
CMSB	BK	37.87195	-122.25168	94.7	167.6	1994/12 - current	CMS, Berkeley
CRQB	BK	38.05578	-122.22487	-25.0	38.4	1996/07 - current	CB
HERB	BK	38.01250	-122.26222	-25.0	217.9	2000/05 - current	Hercules
RFSB	BK	37.91608	-122.33610	-27.3	91.4	1996/01 - current	RFS, Richmond
RSRB	BK	37.93575	-122.44648	-48.0	109	1997/06 - current *	RSRB, Pier 34
SMCB	BK	37.83881	-122.11159	180.9	3.4	1997/12 - current	SMC, Moraga
YBIB	BK	37.81420	-122.35923	-27.0	61	1997/12 - current *	BB, Pier E2
OHLN	BK	38.00742	-122.27371			2001/07 - current	MPBO, Ohlone Park
SBRN	BK	37.68562	-122.41127			2001/08 - current	MPBO, San Bruno Mtn.
SFAB	BK	37.78610	-122.3893		0.0	1998/06 - current	BB, SF Anchorage
W02B	BK	37.79120	-122.38525		57.6	1996/04 - current	BB, Pier W2
W05B	BK	37.80100	-122.37370		36.3	1997/10 - current	BB, Pier W5
YBAB	BK	37.80940	-122.36450		3.0	1998/06 - current	BB, YB Anchorage
E07B	BK	37.81847	-122.34688		134.0	1996/02 - current	BB, Pier E7
E17B	BK	37.82086	-122.33534		160.0	1995/08 - current	BB, Pier E17
BBEB	BK	37.82167	-122.32867		150	1994/03 - 1995/10	BB, Pier E23
DB1B	BK	37.49947	-122.12755		0.0	1994/07 - 1994/09	DB, Pier 1
					1.5	1994/09 - 1994/09	
					71.6	1994/09 - 1994/09	
					228.0	1993/08 - current	
DB2B	BK	37.50687	-122.11566			1994/07 - current	DB, Pier 27
					189.2	1992/07 - 1992/11	
DB3B	BK	37.51295	-122.10857		1.5	1994/09 - 1994/11	DB, Pier 44
					62.5	1994/09 - 1994/09	
					157.9	1994/07 - current	
SM1B	BK	37.59403	-122.23242		298.0	not recorded	SMB, Pier 343
RB2B	BK	37.93372	-122.41313		44	1997/06 - current	RSRB, Pier 58
CCH1	NC	37.7432	-122.0967	226		1995/05 - current	Chabot
CGP1	NC	37.6454	-122.0114	340		1995/03 - current	Garin Park
CMW1	NC	37.5403	-121.8876	343		1995/06 - current	Mill Creek
CSU1	NC	37.6430	-121.9402	499		1995/10 - current	Sunol
CYD1	NC	37.5629	-122.0967	-23		2002/09 - current	Coyote

Table 5.1: Stations of the Hayward Fault Network. Each HFN station is listed with its station code, network id, location, operational dates, and site description. The latitude and longitude (in degrees) are given in the WGS84 reference frame. The elevation of the well head (in meters) is relative to the WGS84 reference ellipsoid. The overburden is given in meters. The date indicates either the upgrade or installation time. The abbreviations are: BB - Bay Bridge; BR - Briones Reserve; CMS - Cal Memorial Stadium; CB - Carquinez Bridge; DB - Dumbarton Bridge; MPBO - mini-Plate Boundary Observatory RFS - Richmond Field Station; RSRB - Richmond-San Rafael Bridge; SF - San Francisco; SMB - San Mateo Bridge; SMC - St. Mary's College; and, YB - Yerba Buena. The \* for YBIB and RSRB indicates that the stations are not currently operational at this time. RSRB is shut down while Caltrans is retrofitting the Richmond-San Rafael bridge (as of April 19, 2001) and YBIB has been off-line since August 24, 2000 when power cables to the site were shut down. The table also includes 2 MPBO stations which became operational in the last year.

Site	Geophone	Accelerometer	Z	H1	H2	Data logger	Notes	Telemetry
BRIB	Oyo HS-1	Wilcoxon 731A	-90	79	349	Q4120	Acc. failed, Dilat.	FR
CMSB	Oyo HS-1	Wilcoxon 731A	-90	19	109	Q4120		FR
CRQB	Oyo HS-1	Wilcoxon 731A	-90	251	341	Q4120		FR
HERB	Oyo HS-1	Wilcoxon 731A	-90	TBD	TBD	Q4120		FR
RFSB	Oyo HS-1	Wilcoxon 731A	-90	256	346	Q4120		FR
RSRB	Oyo HS-1	Wilcoxon 731A	-90	50	140	Q4120	2 acc. failed	FR
SMCB	Oyo HS-1	Wilcoxon 731A	-90	76	166	Q4120	Posthole	FR
YBIB	Oyo HS-1	Wilcoxon 731A	-90	257	347	Q4120	Z geop. failed	Radio
OHLN	Mark L-22		-90	TBD	TBD	Q4120	Tensor.	FR
SBRN	Mark L-22		-90	TBD	TBD	Q4120	Tensor.	FR
SFAB	None	LLNL S-6000	TBD	TBD	TBD	RefTek 72A-07	Posthole	
W02B	Oyo HS-1	Wilcoxon 731A	-90	TBD	TBD	RefTek 72A-07		
W05B	Oyo HS-1	Wilcoxon 731A	-90	TBD	TBD	RefTek 72A-07		
YBAB	Oyo HS-1	Wilcoxon 731A	-90	TBD	TBD	RefTek 72A-07		
E07B	Oyo HS-1	Wilcoxon 731A	-90	TBD	TBD	RefTek 72A-07		
E17B	Oyo HS-1	Wilcoxon 731A	-90	TBD	TBD	RefTek 72A-07		
BBEB	Oyo HS-1	Wilcoxon 731A	-90	TBD	TBD	None at present	Acc. failed	
DB1B	Oyo HS-1	Wilcoxon 731A	-90	TBD	TBD	RefTek 72A-07	Acc. failed	
DB2B	Oyo HS-1	Wilcoxon 731A	-90	TBD	TBD	RefTek 72A-07		
DB3B	Oyo HS-1	Wilcoxon 731A	-90	TBD	TBD	RefTek 72A-07	Acc. failed	
SM1B	Oyo HS-1	Wilcoxon 731A	-90	TBD	TBD	None at present		
RB2B	Oyo HS-1	Wilcoxon 731A	-90	TBD	TBD	RefTek 72A-07		
CCH1	Oyo HS-1	Wilcoxon 731A	-90	TBD	TBD	Nanometrics HRD24	Dilat.	Radio
CGP1	Oyo HS-1	Wilcoxon 731A	-90	TBD	TBD	Nanometrics HRD24	Dilat.	Radio
CMW1	Oyo HS-1	Wilcoxon 731A	-90	TBD	TBD	Nanometrics HRD24	Dilat.	Radio
CSU1	Oyo HS-1	Wilcoxon 731A	-90	TBD	TBD	Nanometrics HRD24	Dilat.	Radio
CYD1	Oyo HS-1	Wilcoxon 731A	-90	TBD	TBD	Nanometrics HRD24	Dilat.	Radio

Table 5.2: Instrumentation of the HFN as of 06/30/2002. Every HFN downhole package consists of co-located geophones and accelerometers, with the exception of OHLN and SFAB. 6 HFN sites also have dilatometers (Dilat.) and the 2 MPBO sites have tensor strainmeters (Tensor.) 7 NHFN sites have Quanterra data loggers with continuous telemetry to the BSL. The remaining sites use RefTek data loggers for on-site recording. The 5 SHFN sites have Nanometrics data loggers with radio telemetry to the USGS. The orientation of the sensors (vertical - Z, horizontals - H1 and H2) are indicated where known or identified as "to be determined" (TBD).

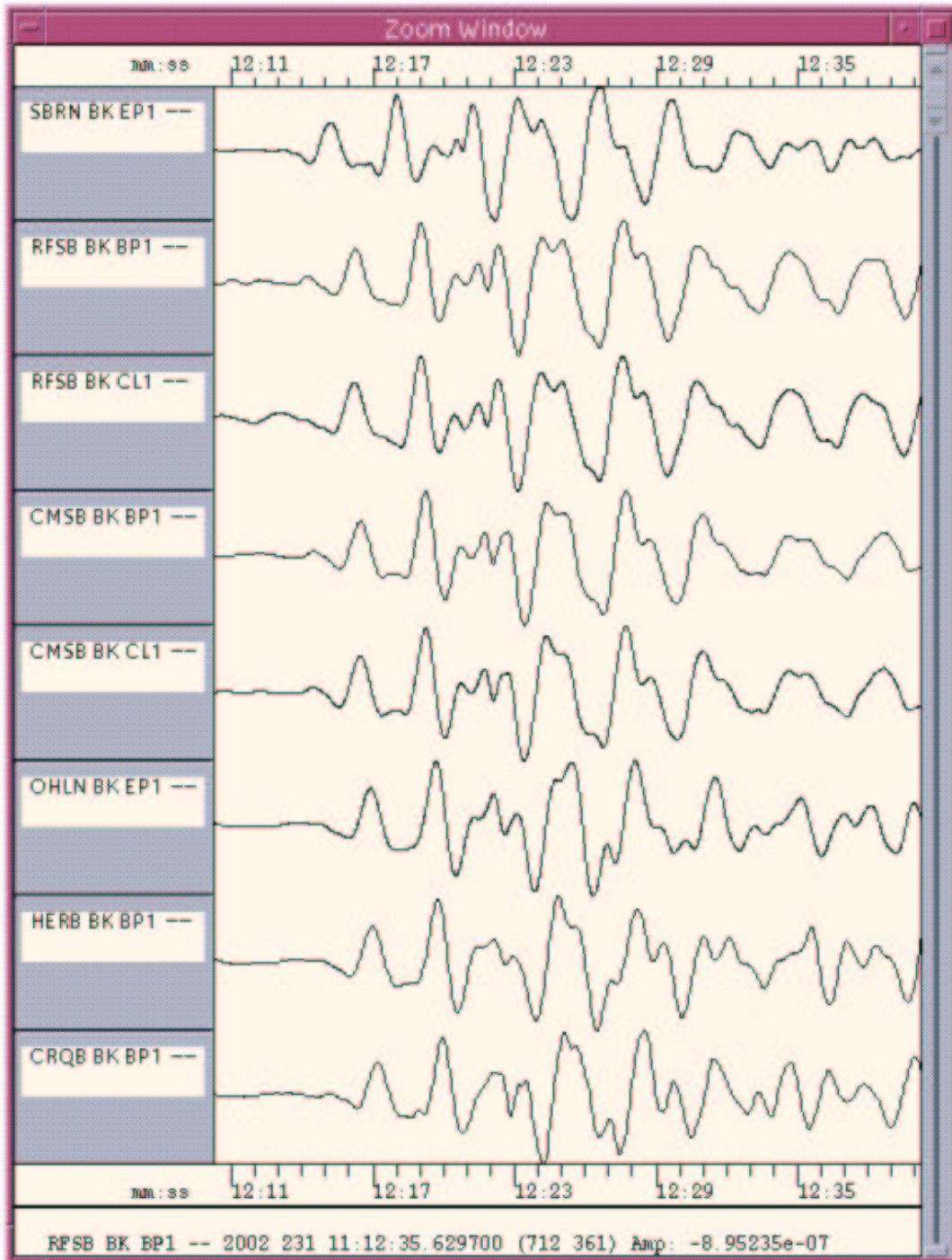


Figure 5.2: Ground displacement waveforms, inferred from accelerometer and velocity sensors at six borehole stations (4 NHFN and 2 MPBO) for the 19 August 2002 deep focus Fiji Islands teleseism (11:01 UT, -21.70, -179.51, 580 km deep, M 7.7). The waveforms have been 0.3-2 Hz bandpass filtered and deconvolved to ground displacement and ordered by epicentral distance for comparison. The highly similar waveforms indicate that the instruments are operating normally and that the transfer functions are correct.

## HERB

Q4120 installed on 18 September, 2001. Geophone channel experiencing large 60 Hz and harmonics signals apparently due to the presence of ground loops. Investigation of this signal contamination continues.

## RFSB

The Q4120 serial ports failed due to faulty capacitors.

## SMCB

Experienced numerous intermittent telemetry problems during year. Rebuilt power system and installed new FRAD, power supply and batteries in a second Hoffman box. Q4120 failed due to a blown hard wired fuse on circuit board. Replaced fuse and reinstalled Q4120.

## 3.2 Event Detection

As noted in the Introduction, one of the purposes of the HFN is to lower the threshold of microearthquake detection. Towards this goal, we have been developing four new algorithms: a pattern recognition approach to identify small events; a phase onset time detector with sub-sample timing resolution, and; a phase coherency method for single component identification of highly similar events, and; a spectrogram method for characterizing the frequency-time power distribution of the observed seismic waveforms.

### Pattern Recognition

In order to improve the detection and analysis of small events (down to  $M_L \sim -1.0$ ) some specialized algorithms are being developed. The Murdock-Hutt detection algorithms used by MultiSHEAR, which basically flags an event whenever the short-term average exceeds a longer-term average by some threshold ratio, is neither appropriate for nor capable of detecting the smallest seismic events. One solution is to use a pattern recognition approach to identify small events associated with the occurrence of an event which was flagged by the REDI system. Tests have indicated that the pattern recognition detection threshold is  $M_L \sim -1.0$  for events occurring within  $\sim 10$  km of a NHFN station. The basic idea is to use a quarter second of the initial P-wave waveform, say, as a master pattern to search for similar patterns that occur within  $\pm$  one day, say, of the master event. Experimentally, up to six small CMSB recorded events, at the  $M_L \sim -1.0$  threshold and occurring within  $\pm$  one day of a master pattern, have been identified.

The pattern recognition method is CPU intensive, however, and it will require a dedicated computer to handle the pattern recognition tasks. To expedite the auto-correlation processing of the master pattern, an integer arithmetic cross-correlation algorithm has been de-

veloped which speeds up the requisite processing by an order of magnitude.

### Phase Onset Time Detection

The phase onset time detector makes use of the concept that the complex spectral phase data, over the bandwidth of interest (ie, where the SNR is sufficiently high), will sum to a minimum at the onset of an impulsive P-wave. The algorithm searches for the minimum phase time via phase shifting in the complex frequency domain over the bandwidth where the SNR is above 30 dB, say, to identify the onset time of the seismic phase. The algorithm requires that the recorded waveforms be deconvolved to absolute ground displacement. This implicitly requires that any acausality in the anti-aliasing filtration chain, such as the FIR filters used in the BDSN Quanterra data loggers, be removed. The algorithm typically resolves P-wave onset times to one-fiftieth of the sample interval or better.

### Phase Coherency

The spectral phase coherency algorithm was developed to facilitate high resolution quantification of the similarities and differences between highly similar Hayward fault events which occur months to years apart. Figure 5.3 shows an example of three highly similar  $M_L \sim 1.3$  events. The 0.997 complex spectral phase coherency between the waveforms for events a (1998.202.132956) and c (2000.170.171607) implies that the centroids of these two events are not more than  $\sim 20$  cm apart spatially. Extrapolation of magnitude versus fault rupture area, empirically derived using  $M \sim 4-7$  earthquakes, yields an expected rupture radius of  $\sim 20$  m for a  $M 1.3$  event. However, the 0.997 phase coherency implies that the source rupture time histories can not differ by more than  $\sim 6 \mu\text{sec}$  which, in turn, implies that either the rupture spatial-temporal histories of the two sources are virtually identical over a radius of  $\sim 20$  m or that the sources have a high stress drop and a rupture radius of order a few meters at most. Of these two possibilities, the latter is considered the most likely.

The resolution of the complex spectral phase coherency methodology is an order of magnitude better than the cross correlation method which is commonly used to identify highly similar events with resolution of order a few meters.

### Spectrogram Analysis

Figure 5.4 shows an example of a spectrogram derived from the CMSB Z-component ground acceleration recording of a  $M 1.3$  local earthquake (1998.202.132956). Most of the power is in the first few seconds and coincides with the P-wave and S-wave arrivals and their immediate coda. There is little energy above  $\sim 110$  Hz and after

~5 seconds for this M 1.3 event and ~10 km propagation path. Spectrograms can be used as a tool to help in the characterization of seismic sources and propagation paths.

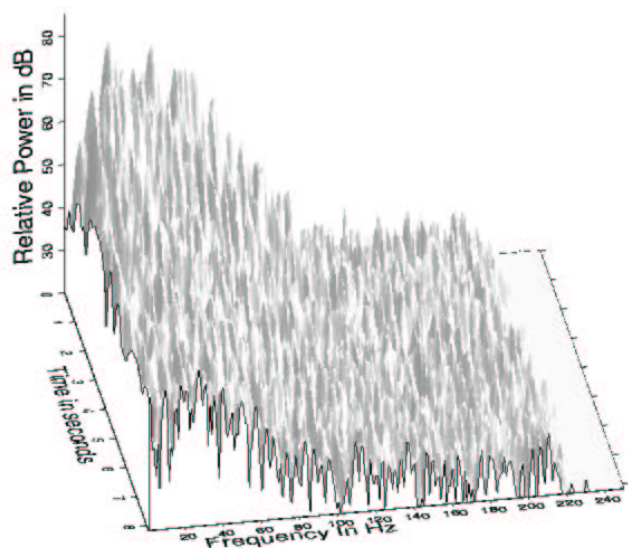


Figure 5.4: Spectrogram of the CMSB Z-component ground accelerations for the M 1.3 earthquake (Inset (a) in Figure 5.3). Plotted is relative power (dB) as a function of time and frequency.

### 3.3 New Installations

#### San Francisco-Oakland Bay Bridge Stations

The infrastructure at seven stations along the San Francisco-Oakland Bay Bridge (SFAB, W02B, W05B, YBAB, E07B, E17B, and BBEB) was upgraded with the installation of weatherproof boxes, power, and telemetry in anticipation of installing Q730 data loggers and telemetering the data back to Berkeley in the fall of 2002.

#### Mini-PBO

The stations of the Mini-PBO project (Chapter 9) are equipped with borehole seismometers. As these stations have become operational, they augment HFN coverage (Figure 5.1). In the last year, OHLN at Ohlone Park, Hercules, has added to the coverage in the vicinity of San Pablo Bay and provides an interesting comparison with the NHFN station HERB.

## 4. Acknowledgements

Thomas V. McEvilly passed away in February 2002 (Chapter 2). Tom was instrumental in developing the Hayward Fault Network, and without his dedication and

hard work the creation and continued operation of the NHFN would not have been possible.

Under Bob Nadeau's and Doug Dreger's general supervision, Rich Clymer, Wade Johnson, Doug Neuhauser, Bob Uhrhammer, Bill Karavas, John Friday, and Dave Rapkin all contribute to the operation of the NHFN. Bob Uhrhammer and Lind Gee contributed to the preparation of this chapter.

Partial support for the NHFN is provided by the USGS through the NEHRP external grant program. Expansion of the NHFN has been made possible through generous funding from Caltrans, with the assistance of Pat Hipley. Larry Hutchings of LLNL has been an important collaborator on the project.

## 5. References

Murdock, J., and C. Hutt, A new event detector designed for the Seismic Research Observatories, *USGS Open-File-Report 83-0785*, 39 pp., 1983.

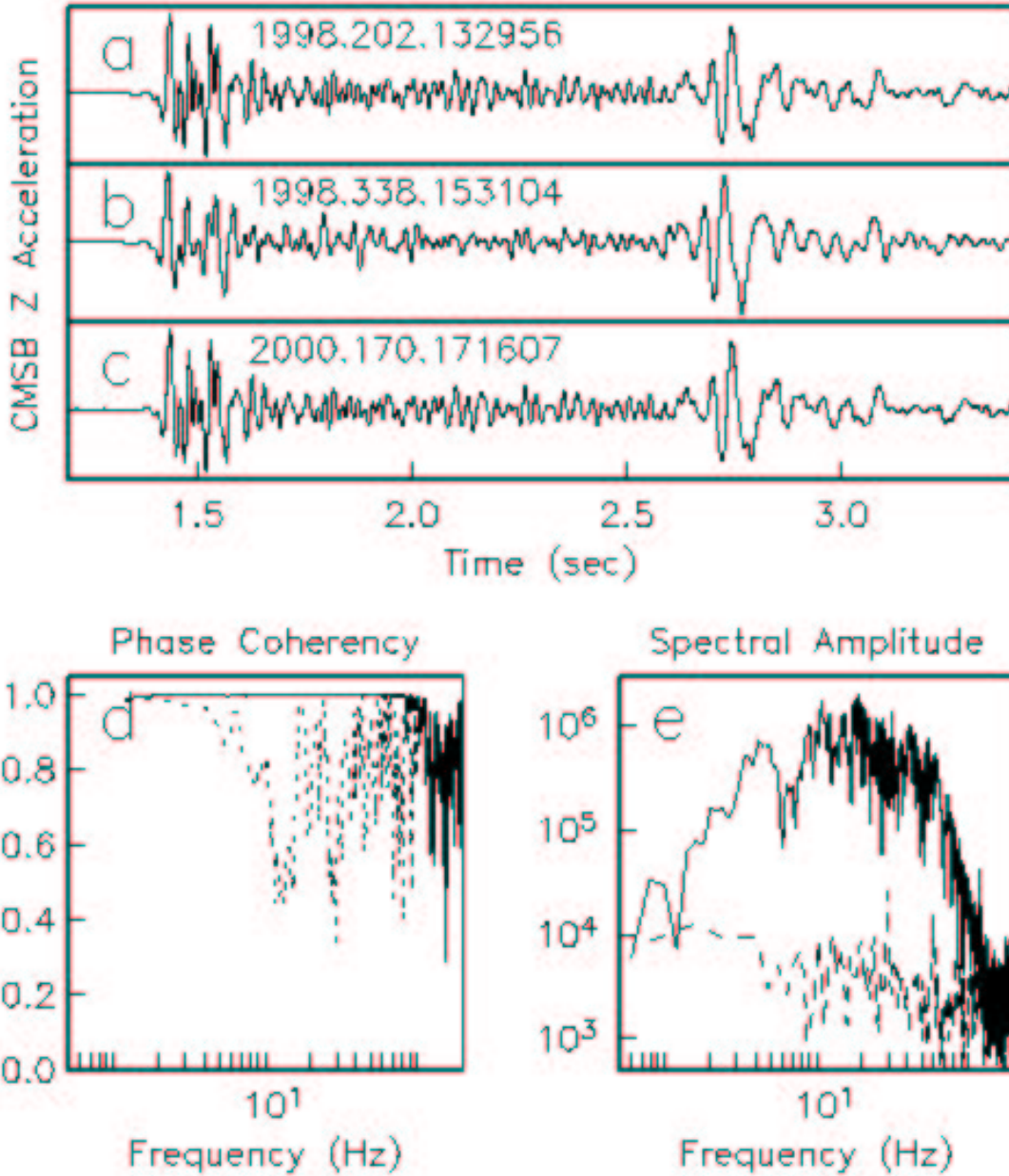


Figure 5.3: Example of using complex spectral phase coherency as a discriminant for analyzing a trio of highly similar earthquakes which occurred on the Hayward fault approximately 6 km northwest of Berkeley. The borehole station CMSB (197 m depth) raw Z-component acceleration data for the three earthquakes are shown in parts (a), (b) and (c). Note that the M 1.3 waveforms in (a) and (c) are visually virtually identical while the M 1.7 waveforms in (b) differs in detail and it has a 11 msec shorter S-P interval than either (a) or (c). The Phase coherency between (a) and (c), shown as the solid line in (d) (calculated using 10 seconds of the Z-component waveforms starting  $\sim 1.38$  seconds prior to the P-wave onset, i. e. using the entire waveform including through the S-wave coda), is 0.997 in the 2-80 Hz frequency band. The inference is that the (a) and (c) centroid locations differ by not more than 20 cm (assuming that the near source scatterers are isotropically distributed). The dashed line in (d) is the phase coherency between the (b) and (c) waveforms and the dips in the coherency at  $\sim 15$  Hz and  $\sim 30$  Hz can be interpreted as destructive interference caused by differences in their centroid locations of order 100 m (compatible with the  $\sim 60$  m along ray path differences in their S-P times). The solid and dashed lines in (e) are the (c) waveform signal and noise amplitude spectra, respectively. The SNR is 40+ dB in the  $\sim 10$ -70 Hz band and above unity in the  $\sim 1.5$ -110 Hz band and the change in slope above  $\sim 65$  Hz is interpreted as the corner frequency of the M 1.3 earthquake source.

# Chapter 6

## Parkfield Borehole Network

### 1. Introduction

The operation of the High Resolution Seismic Network (HRSN) at Parkfield, California began in 1987, as part of the U.S. Geological Survey initiative known as the Parkfield Prediction Experiment (PPE) (*Bakun and Lindh, 1985*).

Figure 6.1 shows the location of the network, its relationship to the San Andreas fault, sites of significance to previous and ongoing research using the HRSN, relocated earthquake locations, and the epicenter of the 1966 M6 earthquake that motivated the PPE. The HRSN records exceptionally high-quality data, owing to its 13 closely spaced three-component borehole sensors, its very wide bandwidth high frequency recordings (0-125 Hz), and its sensitivity (recording events below magnitude -1.0) due to the extremely low attenuation and background noise levels at the 200-300 m sensor depths (*Karageorgi et al., 1992*).

Several aspects of the Parkfield region make it ideal for the study of small earthquakes and their relationship to tectonic processes. These include the fact that the network spans the expected nucleation region of a repeating magnitude 6 event and the transition from locked to creeping behavior on the San Andreas fault, the availability of three-dimensional P and S velocity models, a very complete seismicity catalogue, a well-defined and simple fault segment, a homogeneous mode of seismic energy release as indicated by the earthquake source mechanisms (over 90% right-lateral strike-slip), and the planned drilling zone and penetration and instrumentation site of the San Andreas Fault deep observatory at depth (SAFOD) installation (see: <http://www.icdp-online.de/html/sites/sanandreas/objectives/proposal.html>).

In a series of journal articles and Ph.D. theses, we have presented the cumulative, often unexpected, results of this effort. They trace the evolution of a new and exciting picture of the San Andreas fault zone responding to its plate-boundary loading, and they are forcing new thinking on the dynamic processes and conditions within the fault zone at the sites of recurring small earthquakes. Recent results are described in Chapter 15.

### 2. HRSN Overview

#### 2.1 1986 - 1998

The HRSN was installed in deep (200-300m) boreholes beginning in 1986. Sensors are 3-component geophones in a mutually orthogonal gimbaled package. This ensures that the sensor corresponding to channel DP1 is aligned vertically and that the others are aligned horizontally. In November 1987, the Varian well vertical array was installed and the first VSP survey was conducted, revealing clear S-wave anisotropy in the fault zone. During 1988, the original network was completed to a ten station 3-component 500 sps set of stations telemetered into a central detection/recording system operating in triggered mode and incorporating a deep (572 m) sensor in the Varian well string into the network. The Varian system was slaved in 1988, for about two years, to the Vibroseis control signals, allowing simultaneous recording of vibrator signals on both systems. In 1991, low-gain event recorders (from PASSCAL) were installed to extend the dynamic range to  $M_L$  about 4.5. The data acquisition system operated quite reliably until late 1996, when periods of unacceptably high down time developed, with as many as 7 of the remote, solar-powered telemetered stations down due to marginal solar generation capacity and old batteries, and recording system outages of a week or more became common. In July of 1998 it failed permanently. The original acquisition system that failed was a modified VSP recorder acquired from LBNL, based on a 1980- vintage LSI-11 cpu and a 5 MByte removable Bernoulli system disk with a 9-track tape drive, configured to record both triggered microearthquake and Vibroseis (discontinued in 1997) data. The system was remote and completely autonomous - tapes were mailed to Berkeley. The old system had one-sample timing uncertainty, and record length limitation because the tape write system recovery after event detection was longer than the length of the record, leaving the system off-line after record termination and until write recovery had completed.

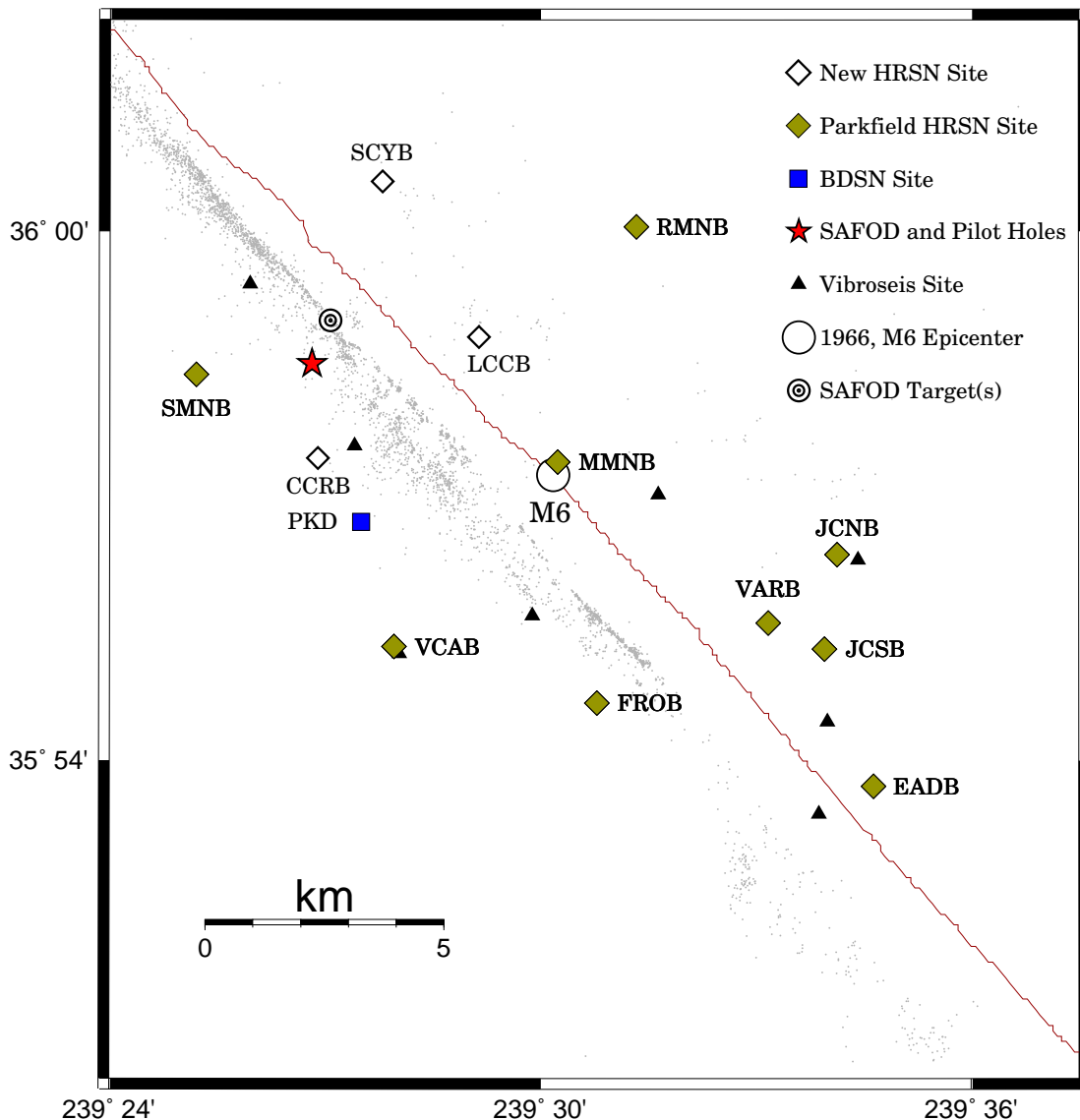


Figure 6.1: Map showing the San Andreas Fault trace, the location of the original 10 Parkfield HRSN stations (filled diamonds) and the 3 new sites (open diamonds), along with the BDSN station PKD (filled square). The locations of the 8 source points for the Vibroseis wave propagation monitoring experiment are represented by small black triangles. The epicenter of the 1966 M6 Parkfield main shock is located at the large open circle. The location of the pilot hole and proposed SAFOD drill site is shown by the filled star, and the location of the 2 alternative M2 repeating earthquake targets (70 meters apart) are shown as concentric circles. Seismicity relocated using an advanced 3-D double-differencing algorithm applied to a cubic splines interpolated 3-D velocity model (*Michelini and McEvilly, 1991*) is also shown (grey points). Station GHIB (Gold Hill, not shown) is located on the San Andreas Fault about 8 km to the Southeast of station EADB.

## 2.2 1998 - 1999

In fall 1998, the original HRSN acquisition system was replaced by 10 PASSCAL RefTek systems with continuous recording. This required the development of a major data handling procedure, in order to capture microearthquakes as small as  $M = -1.0$ , not seen on surface stations, since continuous telemetry to the BSL was not an option at that time.

In July, 1999 we had to reduce the network to four RefTeks at critical sites that would ensure continuity in the archive of characteristic events and temporal variations in recurrence. Properties of the 10 original sites are summarized in Table 6.2.

## 2.3 Upgrade and SAFOD Expansion

Thanks to emergency funding from the USGS NEHRP, we have replaced the original 10-station system with a modern 24-bit acquisition system (Quanterra 730 4-channel digitizers, advanced software using flash disk technology, spread-spectrum telemetry, Sun Ultra 10/440 central processor at the in-field collection point, with 56K frame-relay connectivity to Berkeley). The new system is now online and recording data continuously at a central site located on the California Department of Forestry (CDF) fire station in Parkfield.

We have also added three new borehole stations at the NW end of the network as part of the deep fault-zone drilling (San Andreas Fault Observatory at Depth - SAFOD) project, with NSF support, to improve resolution at the planned drilling target on the fault. Figure 6.1 illustrates the location of the proposed drill site (star) and the new borehole sites.

These three new stations use similar hardware to the main network, with the addition of an extra channel for electrical signals. Station descriptions and instrument properties are summarized in Tables 6.1 and 6.2. All HRSN Q730 data loggers employ FIR filters to extract data at 250 and 20 Hz (Table 6.3).

The remoteness of the drill site and new stations required the intermediate data collection point at Gastro Peak, with a microwave link to the CDF facility. We are sharing this link with the PASSCAL broadband array deployed around the drill site by the University of Wisconsin and the Rensselaer Polytechnic Institute. We are using the HRSN triggering algorithm in a joint triggering scheme which will allow the 60-station array to identify events on the lower noise, greater sensitivity of the borehole network. This has significantly increased event detection and reduced false triggers for the 60-station network data.

Figure 6.2 shows the telemetry system for the upgraded HRSN. The HRSN stations use SLIP to transmit TCP and UDP data packets over bidirectional spread-spectrum radio links between the on-site data acquisition systems and the central recording system at the CDF. Six

of the sites transmit directly to a router at the central recording site. The other seven sites transmit to a router at Gastro Peak, where the data are aggregated and transmitted to the central site over a 4 MBit/second digital 5.4 GHz microwave link. The microwave link was installed to support the current IRIS PASSCAL broadband array deployment in Parkfield, and is shared by the HRSN and PASSCAL. All HRSN data are recorded to disk at the CDF site. A modified version of the REDI real-time system detects events from the HRSN data, creates event files with waveforms from the HRSN and PASSCAL networks, and sends the event data in near real-time to UC Berkeley.

The upgraded system is compatible with the data flow and archiving common to all the elements of the BDSN/NHFN and the NCEDC, and is providing remote access and control of the system. It is also providing data with better timing accuracy and longer records which are to eventually flow seamlessly into NCEDC. The new system solves the problems of timing resolution, dynamic range, and missed detections, in addition to providing the added advantage of conventional data flow (the old system recorded SEGY format).

## 3. 2001-2002 Activities

Significant efforts were made to identify and reduce noise and telemetry problems arising from the new recording, telemetry and site design this year. Detection, monitoring, and high-resolution recording of earthquakes down to the smallest possible magnitudes with the highest possible signal-to-noise (especially in the region of the proposed SAFOD drilling) is a major objective of the HRSN data collection. Consequently, elimination of all sources of unnaturally occurring noise is a primary goal. The minimization of data loss due to station outages and data-dropouts is also critical to this objective, since reduced station coverage degrades the sensitivity of network triggering.

### 3.1 Noise Reduction

The sophisticated HRSN data acquisition involves integration of a number of distinct components at each station (i.e., sensor, preamp, solar panels, solar regulator, batteries, Freewave radio, antenna, lightening arresters, and associated cabling, connectors and grounds).

This complex integration of station and communication components combined with a variety of associated concerns (e.g., ground loops, cable resistances, radio interference at stations and between stations, atmospheric effects on telemetry and power, the integration of older (pre-upgrade) hardware components with new upgraded components, failure of older components, and malfunctioning and unexpected performance characteristics of newer components) makes identification of specific causes

Site	Net	Latitude	Longitude	Surf. (m)	Depth (m)	Date	Location
EADB	BP	35.89525	-120.42286	499	245	01/1988 -	Eade Ranch
FROB	BP	35.91078	-120.48722	542	284	01/1988 -	Froelich Ranch
GHIB	BP	35.83236	-120.34774	433	63	01/1988 -	Gold Hill
JCNB	BP	35.93911	-120.43083	559	224	01/1988 -	Joaquin Canyon North
JCSB	BP	35.92120	-120.43408	487	155	01/1988 -	Joaquin Canyon South
MMNB	BP	35.95654	-120.49586	731	221	01/1988 -	Middle Mountain
RMNB	BP	36.00086	-120.47772	1198	73	01/1988 -	Gastro Peak
SMNB	BP	35.97292	-120.58009	732	282	01/1988 -	Stockdale Mountain
VARB	BP	35.92614	-120.44707	511	572	01/1988 -	Varian Well
VCAB	BP	35.92177	-120.53424	790	200	01/1988 -	Vineyard Canyon
CCRB	BP	35.95716	-120.55161	601	251	05/2001 -	Cholame Creek
LCCB	BP	35.98006	-120.51423	637	252	08/2001 -	Little Cholame Creek
SCYB	BP	36.00942	-120.53661	947	252	08/2001 -	Stone Canyon

Table 6.1: Stations of the Parkfield HRSN. Each HRSN station is listed with its station code, network id, location, date of initial operation, and site description. The latitude and longitude (in degrees) are given in the WGS84 reference frame, the surface elevation (in meters) is relative to mean sea level, and the depth to the sensor (in meters) below the surface. Coordinates and station names for the 3 new sites are given at the bottom.

Site	Sensor	Z	H1	H2	RefTek 24	RefTek 72-06	Quanterra 730
EADB	Mark Products L22	-90	170	260	01/1988 - 12/1998	12/1998 - 07/1999	03/2001 -
FROB	Mark Products L22	-90	338	248	01/1988 - 12/1998	12/1998 - 07/1999	03/2001 -
GHIB	Mark Products L22	90	failed	unk	01/1988 - 12/1998	12/1998 - 07/1999	03/2001 -
JCNB	Mark Products L22	-90	0	270	01/1988 - 12/1998	12/1998 - 06/2001	03/2001 -
JCSB	Geospace HS1	90	300	210	01/1988 - 12/1998	12/1998 - 07/1999	03/2001 -
MMNB	Mark Products L22	-90	175	265	01/1988 - 12/1998	12/1998 - 06/2001	03/2001 -
RMNB	Mark Products L22	-90	310	40	01/1988 - 12/1998	12/1998 - 07/1999	03/2001 -
SMNB	Mark Products L22	-90	120	210	01/1988 - 12/1998	12/1998 - 06/2001	03/2001 -
VARB	Litton 1023	90	15	285	01/1988 - 12/1998	12/1998 - 07/1999	03/2001 -
VCAB	Mark Products L22	-90	200	290	01/1988 - 12/1998	12/1998 - 06/2001	03/2001 -
CCRB	Mark Products L22	-90	N45W	N45E	-	-	05/2001 -
LCCB	Mark Products L22	-90	N45W	N45E	-	-	08/2001 -
SCYB	Mark Products L22	-90	N45W	N45E	-	-	08/2001 -

Table 6.2: Instrumentation of the Parkfield HRSN. Most HRSN sites have L22 sensors and were originally digitized with a RefTek 24 system. After the failure of the WESCOMP recording system, PASSCAL RefTek recorders were installed. In July of 1999, 6 of the PASSCAL systems were returned to IRIS and 4 were left at critical sites. The upgraded network uses a Quanterra 730 4-channel system. For the three new stations (bottom) horizontal orientations are approximate (N45W and N45E) and will be determined more accurately in the near future.

## Parkfield HRSN + PASSCAL Configuration

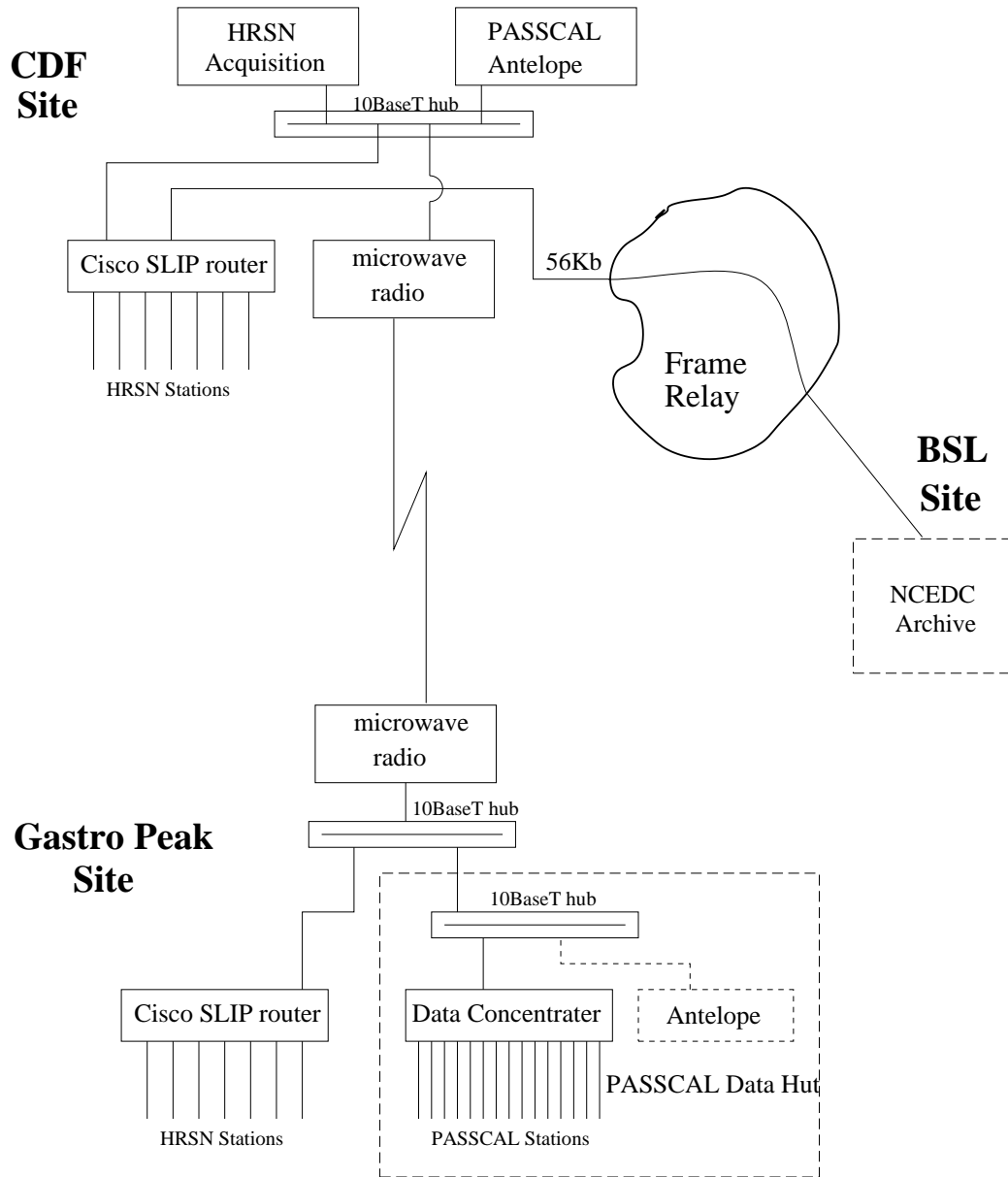


Figure 6.2: HRSN data flow is illustrated in this figure. 6 stations are acquired directly at the CDF facility while the other 7 send data to a router at Gastro Peak. These data are aggregated and transmitted to the CDF site over a microwave radio link. The HRSN computer system runs a modified version of the REDI software and event files with waveforms are created and transmitted to the BSL over the frame-relay link.

of network generated (i.e. artificial) noise difficult to identify.

Over the past year, our exhaustive iterative testing of HRSN performance has identified three primary causes for the observed artificial noise. We have designed and have implemented or are in the process of implementing fixes.

### Power separation

Persistent 50 and 100 Hz noise sources affecting nearly all stations to varying degrees has been found to result from the interaction of the preamp and Quanterra systems through their common connection to a single power supply system. As a fix, we have separated preamp solar and battery power from the power provided to the rest of the data acquisition system at each station.

### Solar regulators

Regularly occurring spikes occurring during the daylight hours were observed in the continuous data streams and found to be due to the solar regulators. We have purchased and tested new solar regulators and are installing them at all the sites.

### Preamp Noise

A significant contribution source of artificial noise is the preamp amplification levels. In the upgraded system, preamps from the older network were used. During integration of the older preamps with the increased dynamic range capabilities of the 24-bit Quanterra system, gain settings of the preamps were reduced from  $\times 10000$  to  $\times 80$  in order to match signal sensitivity of the new system with the older one. While these lower preamp gain levels are still within the operational design of the preamps, they are no longer in their optimal range which enhances the contribution of preamp generated noise. Initially, this was not expected to be a significant problem. However, we have subsequently found that even the small increase in preamp noise that results from the preamp gain reduction can significantly impact the sensitivity of the network for detecting and recording the very smallest events.

Figure 6.3 shows the preamp noise effect from a test done at station EADB using background noise on day 134 of year 2002. Considerable signal hash is seen at gain levels of  $\times 80$  (top 3-component waveforms), and significantly reduced when gains are increased to  $\times 1000$  (lower waveforms). Since we are also interested in recording on-scale as large events as possible on the unique borehole, high-frequency broadband width HRSN, simply increasing gain levels on all stations is not an option. Doing so would cause the recording system to saturate at lower magnitudes. Our plan is to redesign the preamp opera-

tion characteristics so that their operation at gain levels of  $\times 80$  is optimal.

A prototype preamp has been designed and built which is to be installed on an HRSN station for testing in the near future. If testing proves successful, installation of the redesigned preamps at all 13 stations is planned.

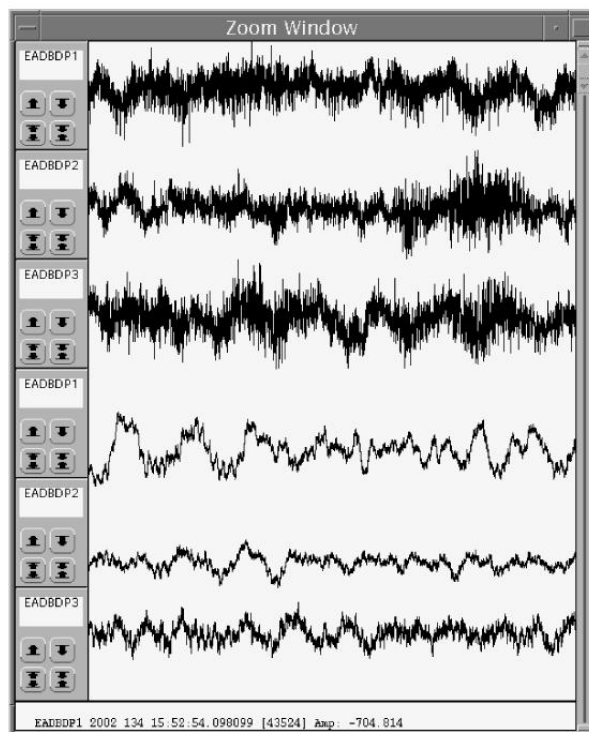


Figure 6.3: Preamp noise reduction test. Shown are 30 seconds of 3-component background signal recorded at station EADB on day 134 of 2002 at 1520 UTC (top 3) and 1550 UTC, when gain levels were set to  $\times 80$  and  $\times 1000$  respectively. Note the substantial reduction in preamp generated noise at high the higher gain. Network operation currently continues at  $\times 80$  gain despite the preamp noise, in order to optimize the dynamic range capabilities. A prototype redesign of the preamp with optimized operational characteristics at  $\times 80$  gain has been built and is to be field tested shortly.

## 3.2 Telemetry Dropouts

The cause of data dropouts at one of the new SAFOD critical stations (CCRB) was particularly difficult to determine. This problem did not appear during the early operation of CCRB, but became intermittent and then rather severe during the winter season. The majority of the time the transfer of data packets from CCRB to the central data collection site were satisfactory. However, a strong positive correlation of the times of dropouts with the occurrence of earthquakes was observed (defi-

nately not a desirable situation). It was eventually determined that the dropout problem was the result of an interplay involving data compression, station buffer size and marginal radio connectivity. For low amplitude background signals, the compression of data packets before telemetry was sufficient to prevent exceedence of the Quanterra buffer storage between periods of radio connectivity dropouts. However, during earthquakes, data compression is lower due to the higher amplitude signals of the quakes. This resulted in exceedence of the CCRB buffer storage capacity and data loss during earthquakes. Figure 6.4 shows an example of the dropout problem at an intermediate stage of its severity.

In an initial attempt to improve radio connectivity, installation of a large antenna dish was tried, but found to be an inadequate fix. A relay of the CCRB-Gastro Peak telemetry through a new repeater site was eventually required.

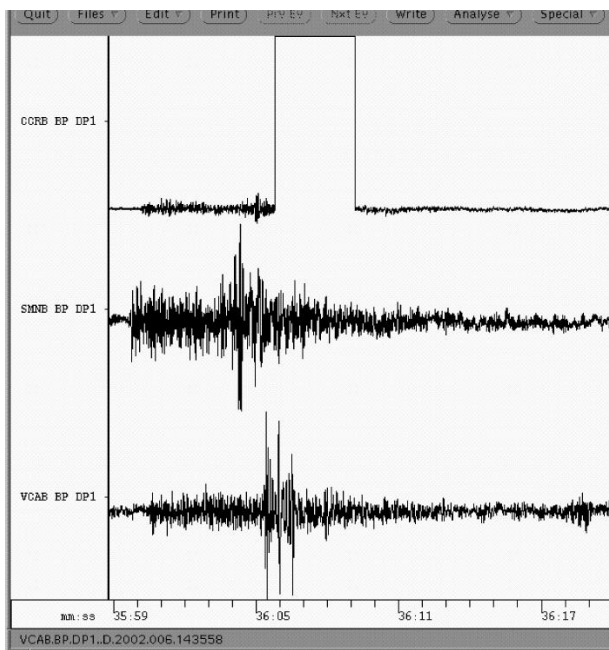


Figure 6.4: Data dropout example at station CCRB. Shown are 21 seconds of vertical component (DP1) waveform data from HRSN stations CCRB (top), SMNB (middle) and VCAB (bottom). Exceedence of local buffer capacity at CCRB caused data loss at about 5.5 seconds into the earthquake first arrival due to marginal radio telemetry and the reduced data compression possible for large amplitude (i.e. earthquake) signals.

### 3.3 SAFOD Pilot Hole Drilling

In June of 2002, drilling began on the SAFOD Pilot Hole (PH). The Pilot Hole was drilled to a depth of approximately 2 km (drilling was completed in late July).

Noise from the drilling was clearly visible at station CCRB, which may prove crucial for guiding SAFOD drilling in the future. Figure 6.5 shows the signal spectra below 65 Hz for 30 minutes of data recorded on the DP1 (vertical) channel at 250 sps generated by the SAFOD PH drilling on June 24 of 2002. The data are high-pass filtered at 0.5 Hz. The pilot hole was drilled within several 10's of meters from the planned SAFOD scientific hole and about 2 km due north of CCRB. Significant low frequency energy above background levels are seen below about 10 Hz.

Several significant spectral peaks can also be seen at about 1.5, 4.5, 6.5, and 10 Hz. The drill-bit spectra drops off sharply above 10 Hz. Comparable spectral amplitudes and character are observed on the DP1 and DP2 horizontal channels (not shown). The horizontal orientations (N45W and N45E) are bisected by the north-south oriented path from CCRB to the Pilot Hole. The frequency band and spectral character was also observed to change over longer time periods. We infer these changes to reflect either changes of the lithology being penetrated by the drill-bit or changes in the type of drill-bit or rotary speed. These changes further demonstrate the sensitivity of the borehole sensors for imaging bit generated noise.

With the completion of the pilot hole and the deployment of the downhole sensor strings, discussions are underway between the BSL and the USGS Menlo Park regarding use of the PH data within the HRSN system for enhanced triggering capability (see the "Future Directions" section).

### 3.4 Data Archive

At this time, continuous data streams on all 39 components are being recorded at 20 and 250 sps on the local HRSN computer at the CDF facility and archived on DLT tape. The 20 sps data are transmitted continuously to the BSL over the frame-relay linked and archived at the NCEDC. In addition, the 13 vertical component channels at 250 sps are also transmitted continuously to the BSL over the frame relay-circuit for purposes of fine tuning the triggering algorithm for detection at smallest possible magnitude levels.

An ongoing effort has been the development of a new earthquake triggering scheme, with the goal of replacing the continuous archive with triggered event gathers. A first cut version of the new scheme has been implemented and is already detecting earthquakes at an increased rate—about 3 times the number of earthquakes detected before the upgrade.

In order to facilitate the archive of the HRSN events, BSL staff are developing a Graphical User Interface

Sensor	Channel	Rate (sps)	Mode	FIR
Geophone	DP?	250.0	T	Ca
Geophone	BP?	20.0	C	Ac

Table 6.3: Data streams currently being acquired at each HRSN site. Sensor type, channel name, sampling rate, sampling mode, and type of FIR filter are given. C indicates continuous; T triggered; Ac acausal; Ca causal. "??" indicates orthogonal vertical and 2 horizontal components.

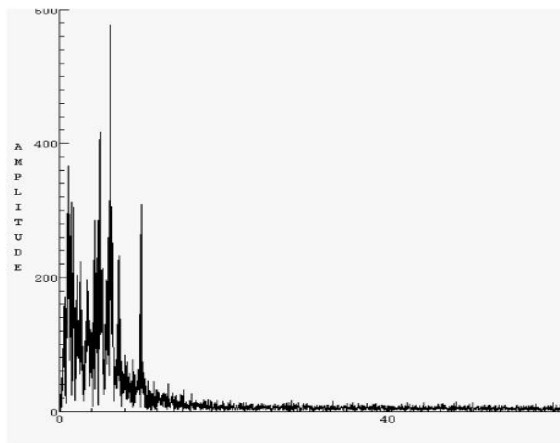


Figure 6.5: Signal spectra from SAFOD pilot hole drilling. Shown is the spectral amplitude below 65 Hz of 30 minutes of vertical component (DP1) data recorded by CCRB at 250 sps and high-pass filtered at 0.5 Hz. There is a marked absence of bit noise above 10 Hz, and distinct high amplitude spikes at about 1.5, 4.5, 6.5, and 10 Hz.

(GUI). The GUI will allow review of every trigger and either schedule the event to be archived or deleted (if it is noise, rather than an earthquake). The GUI will also allow the analysts to log problems, such as the noise spikes, and to characterize events based on S-P time.

## 4. Examples of Data

The upgrade of the HRSN system from a 16- to 24-bit system has greatly improved its ability to record earthquakes over a wider magnitude range. Previously, clipping of waveforms would take place around magnitude 1.5. With the new system, earthquake with magnitudes between 4 and 5 are expected to be recorded on scale.

As an example of the HRSN waveform data quality at larger magnitudes, Figure 6.6 shows waveforms from the Sept. 6, 2002 magnitude 3.9 earthquake near Parkfield, CA. As expected the signal-to-noise (S/N) is excellent at all the borehole stations. Clipping of seismograms is absent, even at station EADB located only 3 km away from the epicenter. Figure 6.6 also includes seismograms from two PH sensors (PL11, at surface, and PL21, at 1.85 km depth).

Figure 6.6 illustrates the power of three-component recordings in borehole installations, as the the horizontal records give much better definition of the S-arrival than the vertical component alone. Vertical and horizontal components recored at the station closest to the M3.9 (EADB) and at the new station closest to the SAFOD drill site (CCRB) are shown. The apparent S-phase as seen on the vertical components arrives noticeably later ( 0.1 sec.) than the S-phase arrival seen on the horizontal components. S-arrival time differences of this magnitude can lead to location errors on the order a km or more The later arriving apparent S in the vertical records could be attributed to near surface forward scattered energy or possibly to Fault Zone Guided Wave arrivals, known to exist at Parkfield, rather than to the true S-phase.

Although the PH sensors are currently only recording vertical motion, the recordings of the deep sensors (1.85 km) should significantly aid in the detection of the very smallest events in the penetration zone. A significant delay in the P-arrival time of the M3.9 event at PL11

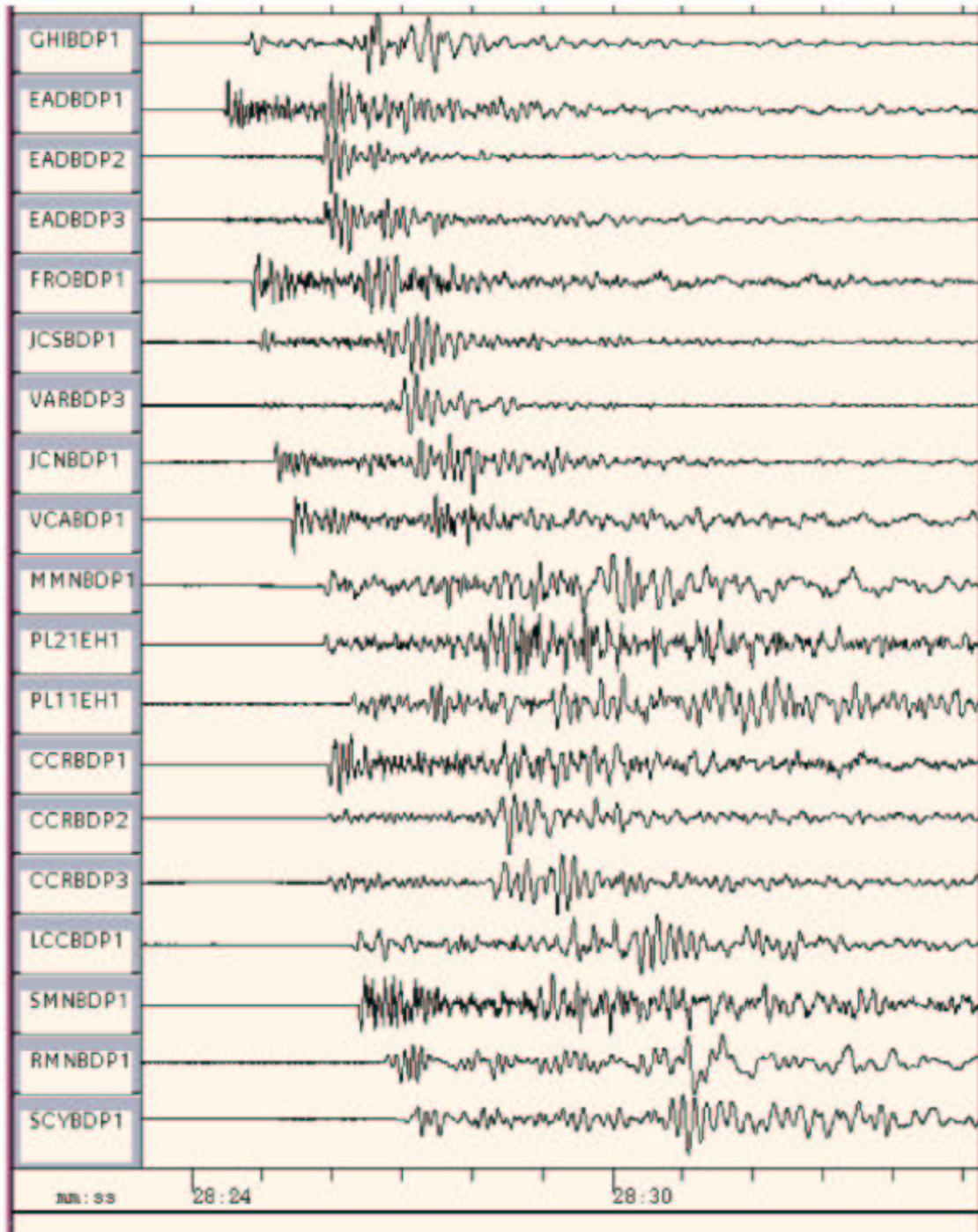


Figure 6.6: Sample HRSN and SAFOD Pilot Hole (PL11 and PL21) waveforms from the Sept. 6, 2002 magnitude 3.9 earthquake occurring some 3-4 km southeast of Parkfield, CA, at a depth of about 9.5 km. Station GHIB is located southeast of the event by about 5 km (top waveform). All other stations locate northwest of the event and are ordered according to their progressively increasing P arrival times. In general only the vertical components of the 3 component sensors are shown. Exceptionally, all three components of the station closest to the event (EADB) and the station closest to planned SAFOD drill site (CCRB) are shown. Horizontal component DP3 has been substituted for the vertical component at VARB due to a recording failure on the VARB vertical for this event. Seismograms are unfiltered and without corrections for sensor response or polarity. PH sensor PL21 is particularly deep ( 1.85 km below surface). The P arrival time of PH sensor PL11 (located at the surface) is approximately 0.39 sec. after that of PL21, so the PL11 waveform has been plotted out of arrival time order to facilitate comparison with PL21.

relative to that at PL21 ( 0.39 sec) can be seen. This indicates that the average P-wave velocity in the top 1.85 km of the crust at the PH site is on the order of 4.7 km/sec which is in general agreement with that observed in tomographic inversion of seismic and active source experiments in the area and with velocities expected for the Salinian composition of the crust penetrated by the PH. The PL21 record also shows some slight clipping. Events in the SAFOD penetration zone are much closer to PL21 than the M3.9 event, but are in general much smaller. However, the ultimate target of the SAFOD drilling is penetration of a site of repeating M2 earthquakes. It is not expected that a M2 close-in to PL21 will also cause it to clip, but an outside possibility for such clipping to occur does exist.

Figure 6.7 illustrates the performance of the HRSN borehole stations for recording teleseismic earthquakes. Shown are records of the August 19, 2002 magnitude 7.7 Fiji Is. deep focus earthquake occurring over 8900 km away from Parkfield. The signal-to-noise in the 0.3-2 Hz band shown is very good, allowing for a variety of waveform analyses for deformation of source characteristics and whole earth structure.

Note the contrast in waveform shape in this frequency band, particularly in the coda, of the MMNB recording. Station MMNB is located directly on the surface trace of the SAF and is known to record Fault Zone Guided Waves for local events. Information on the details of the local deep fault zone structure are also contained in the wave fields of energy generated by distant teleseismic events.

## 5. Future Directions

We are continuing to work at reducing magnitude threshold levels and improving data completeness across the network. Initiation of an automated state-of-health monitoring routine is planned soon and a semi-automated waveform and trigger review scheme (GUI based) is currently under development. These improvements will allow for rapid identification of network outages and problems with station/component specific waveform recording.

Additional efforts underway to increase event detection sensitivity include: 1) refinement of a station specific filtering scheme, 2) refinement of subnet triggering scheme to allow for 2 (instead of 3) station triggering criteria to provide detection of even smaller local earthquakes, 3) incorporation of the pilot hole array into the network triggering scheme to capture the smallest events in the SAFOD drilling area. 4) continue assessment of waveform/spectral character to search for further artificial noise sources at finer scales, and consideration and development for associated fixes.

Monitoring of the systematics of microseismic charac-

teristics, particularly in the SAFOD drilling and target zone, is a primary objective of the HRSN data collection effort. Continued analysis of these data for detailed seismic structure, for similar and characteristic microearthquake systematics, for slip rate evolution, and for determining the source patch size and other characteristics of the SAFOD target(s) and associated earthquakes is also a primary focus that is being pursued in our ongoing research (Chapter 15).

## 6. Acknowledgements

Thomas V. McEvelly passed away in February 2002 (Chapter 2). Tom was the PI on the HRSN project for many years, and without his dedication and hard work the creation and continued operation of the HRSN would not have been possible. His contributions continue to be appreciated in the extreme and the fruits of his labor many-fold.

This chapter was compiled by Bob Nadeau. Under Bob Nadeau's and Doug Dreger's general supervision, Rich Clymer, Wade Johnson, Doug Neuhauser, Bob Uhrhammer, John Friday, Pete Lombard, and Lane Johnson all contribute to the operation of the HRSN.

The upgrade and operation of the HRSN is partially supported by the USGS, through the NEHRP External Grants Program (01HQG00057 and 01HQGR0067). NSF provided support for the expansion of the HRSN near the SAFOD drill site (EAR-9814605).

## 7. References

- Bakun, W. H., and A. G. Lindh, The Parkfield, California, prediction experiment, *Earthq. Predict. Res.*, 3, 285-304, 1985.
- Karageorgi, E., R. Clymer and T.V. McEvelly, Seismological studies at Parkfield. II. Search for temporal variations in wave propagation using Vibroseis, *Bull. Seismol. Soc. Am.*, 82, 1388-1415, 1992.
- Michelini, A. and T.V. McEvelly, Seismological studies at Parkfield: I. Simultaneous inversion for velocity structure and hypocenters using B-splines parameterization, *Bull. Seismol. Soc. Am.*, 81, 524-552, 1991.

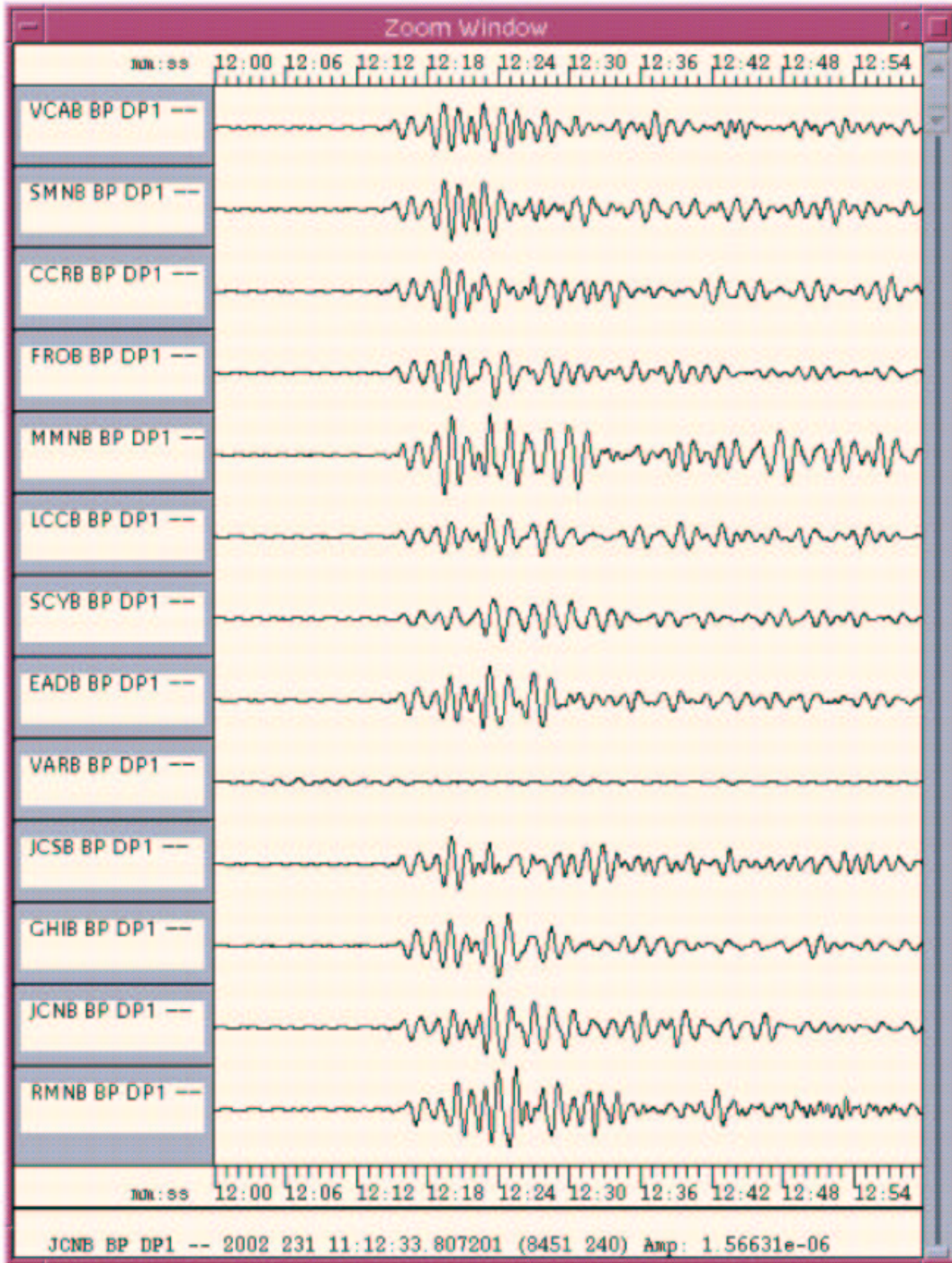


Figure 6.7: Sample 1 minute length seismograms for the 19 August 2002 deep focus Fiji Islands teleseism (11:01 UT, -21.70, -179.51, 580 km deep, M 7.7). Vertical components for the 13, 3-component HRSN borehole stations are shown. The waveforms have been deconvolved to ground velocity, and 0.3-2 Hz bandpass filtered, and plotted using an absolute scale. Station VARB vertical experienced a recording failure during this event. A similar plot for the same earthquake, recorded on the Northern Hayward Fault Network, is show in Figure 5.2.

# Chapter 7

## Parkfield-Hollister Electromagnetic Monitoring Array

### 1. Introduction

There are many reports of anomalous electric and magnetic fields, at frequencies from quasi DC to several 10's of Hertz, and changes in ground resistivity prior to earthquakes. Most reports are devoted to one or another of these phenomena using a variety of measurement configurations and data processing techniques. No such studies are reported using instrumentation capable of measuring all these properties simultaneously at a network of sites. It is the objective of this study to determine whether significant changes in resistivity, quasi DC electric fields, or ULF electric and magnetic fields occur before earthquakes in California. In 1995 we installed two well-characterized electric and magnetic field measuring systems at two sites along the San Andreas Fault which are part of the Berkeley Digital Seismic Network. Since then, magnetotelluric (MT) data have been continuously recorded at 40 Hz and 1 Hz and archived at the NCEDC (Table 7.1 and 7.2). At least one set of orthogonal electric dipoles measures the vector horizontal electric field,  $E$ , and three orthogonal magnetic sensors measure the vector magnetic field,  $B$ . These reference sites, now referred to as electromagnetic (em) observatories, are collocated with seismographic sites so that the field data share the same time base, data acquisition, telemetry and archiving system as the seismometer outputs. Using a robust multiple station MT processing algorithm (Egbert, 1997), we have examined the long term stability of single site and interstation transfer functions. Using a precise transfer function obtained from long runs of the array data, we can effectively predict the fields at one site from those measured at another site. Subtracting the predicted fields from the measured fields at a site yields residuals which are more sensitive to anomalous signals local to the site. Residual analysis in both time and frequency is the primary goal of this project.

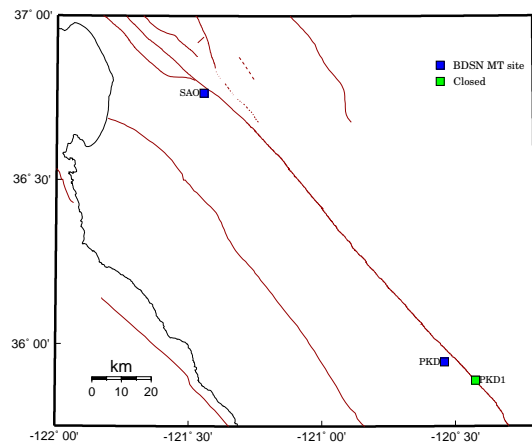


Figure 7.1: Map illustrating the location of operational (filled squares) and closed (grey squares) MT sites in central California.

### 2. MT Overview

The MT observatories are located at Parkfield (PKD1, PKD) 300 km south of the San Francisco Bay Area and Hollister (SAO), halfway between San Francisco and Parkfield (Figure 7.1). In 1995, initial sites were established at PKD1 and SAO, separated by a distance of 150 km, and equipped with three induction coils and two 100 m electric dipoles. PKD1 was established as a temporary seismic site, and when a permanent site (PKD) was found, a third MT observatory was installed in 1999 with three induction coils, two 100 m electric dipoles, and two 200 m electric dipoles. PKD and PKD1 ran in parallel for one month in 1999, and then the MT observatory at PKD1 was closed.

Data at the MT sites are fed to Quanterra data loggers, shared with the collocated BDSN stations, synchronized in time by GPS and sent to the BSL via dedicated communication links.

### 3. Activities in 2001-2002

In the past year, significant energy was directed toward the maintenance of the MT network and toward the establishment of routine data processing.

#### 3.1 Station Maintenance

##### SAO

SAO experienced problems with the power supplies for the B-field and E-field equipment. The B-field coils and the EFSC box were removed, calibrated, and returned. The voltage regulator circuit of the B-field power supply was replaced.

##### PKD

The site at Parkfield continued to have problems with electrodes drying out. Sierra Boyd visited the site several times to "water" the holes and experimented with using bentonite to help retain moisture. The electrodes were pulled in March and the copper-sulfate solution was replaced. In parallel, lead-lead-chloride electrodes were provided by John Booker of the University of Washington. It is hoped that the lead-lead-chloride electrodes will be less sensitive to the lack of moisture in the holes.

#### Instrument Responses

As part of the station maintenance, calibrations have been performed on various components of the MT systems. Sierra Boyd is working to ensure that the transfer function information at the NCEDC is correct and current.

#### 3.2 Data quality control

During this year, BSL staff worked in collaboration with Gary Egbert to install software developed by him for automated data processing. The software, which is described more fully below, provides the capability of identifying problems and alerting staff.

### 4. Data Processing

A major part of the recent effort at Oregon State University has been to develop user friendly computer codes for routine processing of data from the UCB MT sites. The processing system is based on a graphical user interface, written in MATLAB, which allows the user to download MT data from the NCEDC and complete all routine processing steps (including the multi-site). The program also can be used to plot processing results, multi-channel time series and various simple diagnostics of data quality. Results (including daily estimates of MT impedances, inter-station transfer functions, estimates of noise amplitudes, and summaries of frequency and time domain residual amplitudes) are then automatically archived for

statistical analysis and correlation in space and time with cluster events at Parkfield. There is now a daily printout of the signal to noise ratios (SNR) in dB for each channel of the array, Table 7.3. Currently, SNR's below 10 dB are flagged for inspection or repair by the array operators.

Any data in the NCEDC archive can be downloaded, but by default the program gets and processes the most recent unprocessed data. These codes will thus enable more-or-less automatic monitoring of system functionality, and make it easier to maintain a high rate of quality data return. The streamlined processing codes will also make it easier to reprocess existing data with any new schemes that will be implemented in the future. We are presently using the new system to process the backlog of data from the array, and to update analyses of residuals, and of MT impedance stability.

Several procedures for the residual analysis (the goal of the em array) have been developed: one uses a simple time-domain regression operator to estimate residuals in a moving time window. This algorithm is fast and provides a rapid method to scan incoming data for anomalies. We have tested this process on selected segments of data. No anomalous signals were detected, but there were no earthquakes during this interval.

Another approach is a frequency domain analysis using multiple station techniques (*Egbert, 1977*) which makes optimal use of data from all sites to estimate stable and reliable transfer functions. The multi-site analysis has also proven to be very useful for better understanding of signal and noise, and for separating coherent signals of differing spatial scales (Figure 7.2). For example, *Egbert et al. (2000)* used a multiple station analysis to show that the transfer function between SAO and PKD1 is systematically affected by both the DC train system in the Bay Area (BART) and by the non-uniformity of the natural fields in the Pc3 band (Figure 7.3). These results demonstrated that cultural noise sources can extend their effect over surprisingly large areas, and that at the same time natural ionospheric sources may exhibit significant spatial complexity. Because of this added spatial complexity, multiple sites are required for complete cancellation of the background (non-tectonic) em noise. Ideally three stations should be used to avoid bias errors in the transfer function estimates and to maintain better control over cultural noise.

Predictions based on data from at least three sites will significantly improve our ability to detect anomalous signals. Source complications, as well as local incoherent noise sources, are highly variable in time (e.g., Figure 7.3), making it a challenging task to verify that apparently anomalous signals truly originate in the earth. Thorough calibration and understanding of both local and distant noise sources is essential. This critical step has now been accomplished for the UCB array (*Egbert et al., 2000; Eisel and Egbert, 2001*). When a major Park-

field event does occur we will be in a very good position to detect and identify anomalous em emissions (if there are any) and to avoid the ambiguity of interpretation that has plagued much of the past search for em precursors.

So far we have focused on the frequency domain approach to study residuals. This analysis has revealed significant diurnal variations in the residual distributions. With a two site array, residuals are smallest between the hours of 0-4 am, making this a particularly good time to look for anomalous signals. Comparison of the temporal distribution of unusually large magnetic residuals to local earthquake catalogs has so far revealed no clear associations, but there have been few earthquakes of significant magnitude in the time period studied. *Karakelian et al.* (2000) analyzed data from some of their sites and ours and suggest that there was anomalous activity before the San Juan Bautista earthquake, but we have not been able to verify this.

The MT stations at PKD and SAO can also be used to monitor resistivity changes prior to earthquakes. Unlike the UC Riverside telluric array, the MT impedance can yield depth information because the depth of penetration of the em waves increases with period. Seasonal changes caused by precipitation would presumably be shallow and affect primarily the shorter periods, while deeper changes would be seen also at longer periods. The amplitude of the MT impedance may fluctuate at all periods in response to shallow changes (the so-called "static" shift problem), but the phase of the response is set by more regional structure at longer periods. Thus, variations in phase should be a sensitive indicator of resistivity variations at seismogenic depths (~10 km). *Eisel and Egbert* (2001) made a study of the stability of the MT impedances at PKD1. Typical deviations of estimates based on a single day of data differed from the long term average transfer function by 2-3% for T < 300s and increasing to about 10% for T=2000s. Variations between contiguous days were nearly random, so significantly smaller variability can be obtained by longer averaging times. There is some evidence from this analysis for a slow variation of about 1% in impedance amplitude when an 11 day average is applied. Relative resistivity variations are nearly frequency independent, appear anti-correlated between the x-y and y-x modes, and are larger than variations in phase. These features together are suggestive of temporal variations in near-surface static distortion. Although it is difficult to make a definitive statement on the basis of the data analyzed so far, there does not appear to be any seasonal component to these variations, as might be expected if they were due to near surface hydrology.

Sensor	Channel	Rate (sps)	Mode	FIR
Magnetic	VT?	0.1	C	Ac
Magnetic	LT?	1.0	C	Ac
Magnetic	BT?	40.0	C	Ac
Electric	VQ?	0.1	C	Ac
Electric	LQ?	1.0	C	Ac
Electric	BQ?	40.0	C	Ac

Table 7.2: Typical data streams acquired at each MT site, with channel name, sampling rate, sampling mode, and FIR filter type. C indicates continuous; T triggered; Ac acausal.

Station	Channel	T=30S	T=100S	T=300S
PKD	Hx	26	25	26
PKD	Hy	23	22	24
PKD	Hx	18	17	15
PKD	Ex1	16	16	18
PKD*	Ey1	9	10	11
PKD	Ex2	23	23	26
PKD	Ey2	21	23	25
SAO	Hx	21	21	23
SAO	Hy	21	20	24
SAO	Hx	15	12	12
SAO	Ex	22	21	22
SAO	Ey	21	21	20

Table 7.3: SNR at selected periods (dB): Bad channels indicated \*

Site	Net	Latitude	Longitude	Elev (m)	Date	Location
PKD	BK	35.945171	-120.541603	583	1999/02/05 -	Bear Valley Ranch, Parkfield
PKD1	BK	35.8894	-120.426109	431.6	1995/06/06 - 1999/03/08	Haliburton House, Parkfield
SAO	BK	36.76403	-121.44722	317.2	1995/08/15 -	San Andreas Obs., Hollister

Table 7.1: Sites of MT observatories

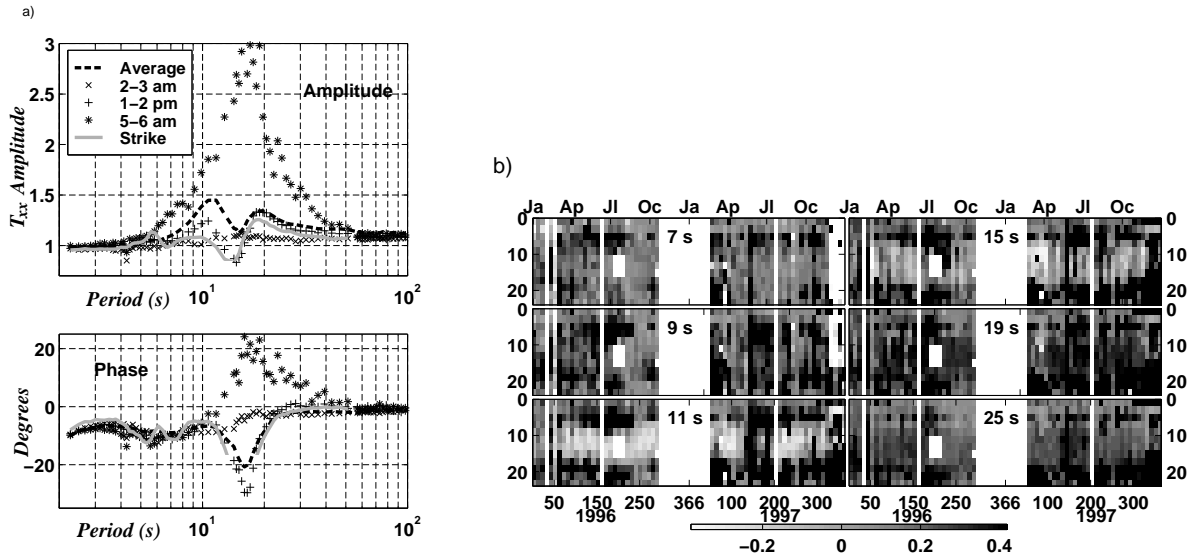


Figure 7.3: (a) Amplitude and phase of the Hx/Hx transfer function (TF) between PKD1 and SAO. Curves marked by symbols correspond to TFs estimated for different local times, as indicated in the legend. The heavy dashed line is the TF computed from all data (days 140-199, 1997), and the heavy grey solid line is the TF computed from the data collected during a strike by BART workers (days 150-156, 1997; see *Egbert et al. (2000)*). For periods outside of the band plotted, TFs computed for different data subsets are in close agreement. (b) Variations in the real part of the Hx/Hx TF as a function of local time and time of year, for data grouped into 10 day-long 2 hour bands.

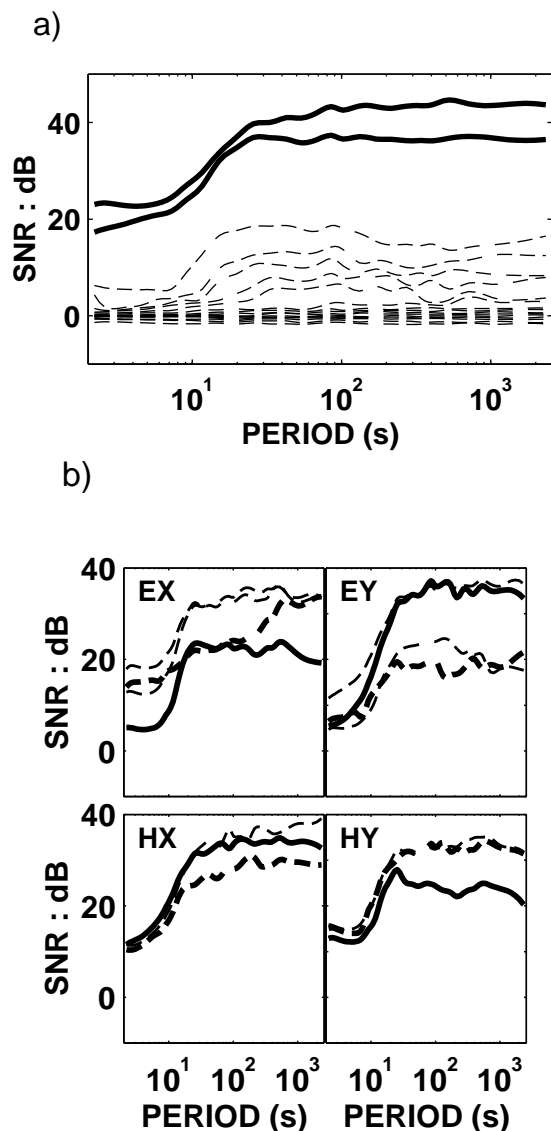


Figure 7.2: (a) Eigenvalues of the scaled Spectral Density Matrix (SDM) for the three site PKD1/PKD/SAO array, computed following the methods described in *Egbert* (1997). Briefly, cross-products of Fourier coefficients computed from short time segments of all 17 data channels are averaged for the 30 days. (b) The magnitude of incoherent noise power is estimated for each data channel, and these are used to non-dimensionalize the SDM. Eigenvalues of the 17x17 scaled SDM then given signal-to-noise (power) ratios of independent coherent EM sources. For idealized quasi-uniform MT sources, there should be only two eigenvalues significantly above the 0 dB noise level. Additional large eigenvalues, as seen here from 10-300 s, are a clear indication of "coherent noise", or temporally varying complications in source geometry. For the two dominant eigenvectors, the horizontal magnetic components are roughly uniform across the array, consistent with the usual MT assumptions. Eigenvectors three and four are dominated by gradients in the EM fields.

## 5. Acknowledgements

Frank Morrison directs the MT program, and collaborates closely with Gary Egbert of Oregon State University and Steve Park of UC Riverside. During Frank's sabbatical last year, Gary Egbert worked extensively with Sierra Boyd on aspects of the data processing. John Friday, Lind Gee, and Doug Neuhauser also contribute to the operation of the MT observatories. Sierra Boyd, Lind Gee, and Gary Egbert contributed to the preparation of this chapter.

Support for the MT array is provided by the USGS through the NEHRP external grants program and by the Plato Malozemoff Chair in Mineral Engineering held by Frank Morrison.

## 6. References

- Egbert, G.D., M. Eisel, O.S. Boyd and H.F. Morrison, DC trains and Pc3s: Source effects in mid-latitude geomagnetic transfer functions, *Geophys. Res. Lett.*, *27*, 25-28, 2000.
- Egbert, G.D., Robust Multiple-Station Magnetotelluric Data Processing, *Geoph. J. Int.*, *130*, 475-496, 1997.
- Eisel, M., and G.D. Egbert, On the stability of magnetotelluric transfer function estimates and the reliability of their variances, *Geophys. J. Int.*, *144*, 65-82, 2001.
- Karakelian, D., S.L. Klemperer, G.A. Thompson, and A.C. Fraser-Smith, Results from electromagnetic monitoring of the  $M_w$  5.1 San Juan Bautista, California earthquake of 12 August 1998, *Proc. of the 3rd Conference on Tectonics Problems of the San Andreas Fault System*, Eds. G. Bokelmann and R.L. Kovach, Stanford University Publication, Geological Sciences, Vol. XXI, 2000.

## Chapter 8

# Bay Area Regional Deformation Network

### 1. Introduction

The Bay Area Regional Deformation (BARD) network of continuously operating Global Positioning System (GPS) receivers monitors crustal deformation in the San Francisco Bay area (“Bay Area”) and northern California (*Murray et al.*, 1998a). It is a cooperative effort of the BSL, the USGS, and several other academic, commercial, and governmental institutions. Started by the USGS in 1991 with 2 stations spanning the Hayward fault (*King et al.*, 1995), BARD now includes 67 permanent stations (Figure 8.1) and will expand to about  $\sim 75$  stations by July 2003. The principal goals of the BARD network are: 1) to determine the distribution of deformation in northern California across the wide Pacific–North America plate boundary from the Sierras to the Farallon Islands; 2) to estimate three-dimensional interseismic strain accumulation along the San Andreas fault (SAF) system in the Bay Area to assess seismic hazards; 3) to monitor hazardous faults and volcanoes for emergency response management; and 4) to provide infrastructure for geodetic data management and processing in northern California in support of related efforts within the BARD Consortium and with surveying, meteorological, and other interested communities.

BARD currently includes 67 continuously operating stations, 34 in the Bay Area and northern California (Table 8.1), 15 near Parkfield, along the central San Andreas fault, and 18 near the Long Valley caldera near Mammoth (Table 8.2). The BSL maintains 21 stations (including 2 with equipment provided by Lawrence Livermore National Laboratory (LLNL) and UC Santa Cruz). Other stations are maintained by the USGS (Menlo Park and Cascade Volcano Observatory), LLNL, Stanford University, UC Davis, UC Santa Cruz, and East Bay Municipal Utilities District, the City of Modesto, the National Geodetic Survey, and the Jet Propulsion Laboratory. Many of these stations are part of larger networks devoted to real-time navigation, orbit determination, and crustal deformation.

Between 1993 and 1996, the BSL acquired 5 Ashtech Z-12 receivers from UC Berkeley and private (EPRI) fund-

ing, which together with 2 USGS receivers, formed the nucleus of the initial BARD network. Since 1996, the BSL has acquired additional Ashtech Z-12 receivers with Dorne-Margolin design choke ring antennas: 13 in 1996 from a combination of federal (NSF), state (CLC), and private (EPRI) funding, 4 in 2000 from USGS funding, and 7 in 2001 from NSF funding. Most of these receivers have been installed to enhance continuous strain measurements in the Bay Area and to consolidate the regional geodetic network. The network includes several profiles between the Farallon Islands and the Sierra Nevada in order to better characterize the larger scale deformation field in northern California (Figure 8.1). Six more of the BSL receivers will be installed next year, 2 along the southern Hayward fault, and 4 as part of the NSF-funded mini-PBO project establishing collocated GPS/seismometer/borehole strainmeter observatories in the Bay Area (see Chapter 9).

In 1996, researchers from the BSL, the USGS, Stanford University, LLNL, UC Davis, and UC Santa Cruz formed a consortium of institutions studying tectonic deformation in the San Francisco Bay area and northern California. Members of the BARD consortium agreed to pool existing resources and coordinate development of new ones in order to advance an integrated strategy for improving the temporal and spatial resolution of the strain field. This strategy includes the continued development of the network of continuous GPS receivers, the development and maintenance of a pool of GPS receivers for survey-mode operations that may be deployed in semi-permanent mode in the Bay Area when not otherwise in use, archiving of all data at the NCEDC, and development of a coordinated data analysis facility that will process permanent, semi-permanent, and survey data.

Today, raw and Rinex data files from the BSL stations and the other stations run by BARD collaborators are archived at the BSL/USGS Northern California Earthquake Data Center data archive maintained at the BSL (*Romanowicz et al.*, 1994). The data are checked to verify their integrity, quality, completeness, and conformance to the RINEX standard, and are then made accessible, usually within 2 hours of collection, to all BARD participants

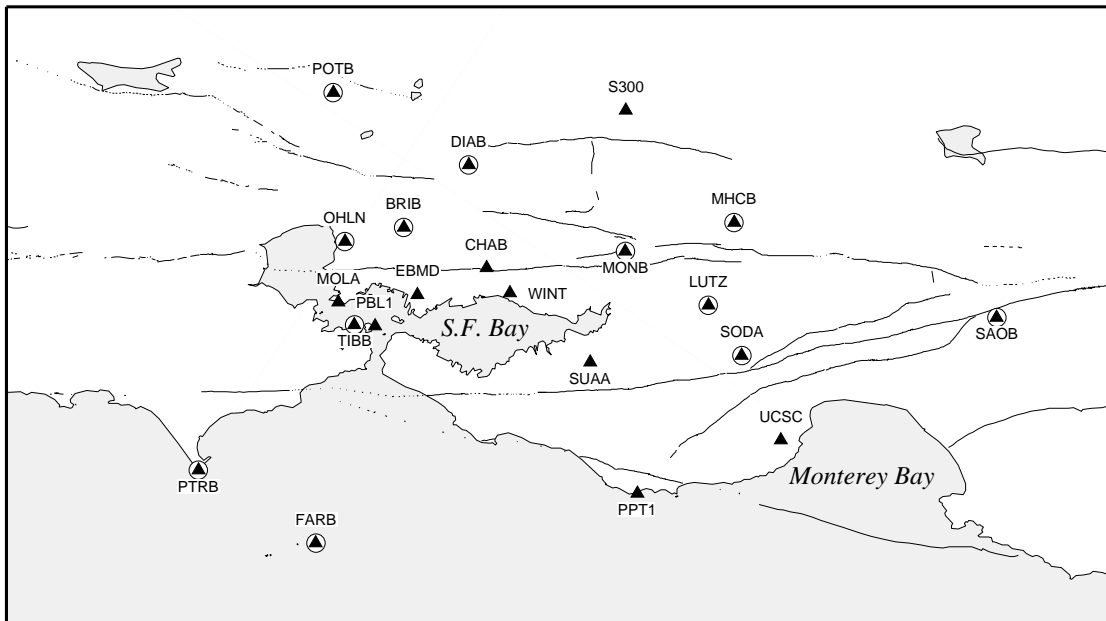
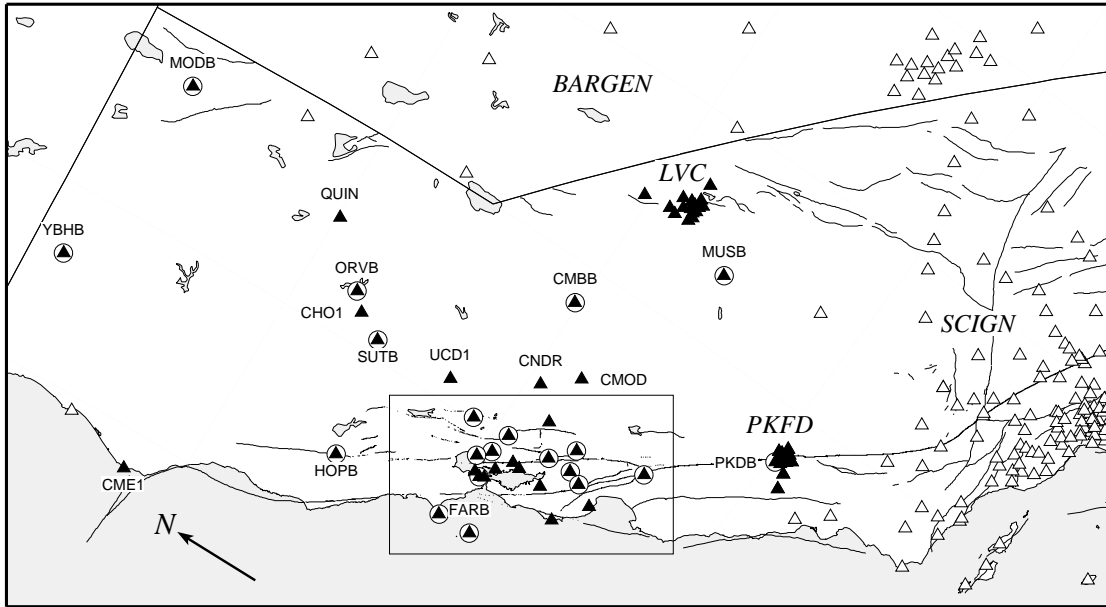


Figure 8.1: Operational BARD stations (solid triangles) in northern California (top) and in the San Francisco Bay area (bottom). The oblique Mercator projection is about the NUVEL-1 Pacific-North America Euler pole so that expected relative plate motion is parallel to the horizontal. Circled stations use continuous telemetry. The 18 station Long Valley Caldera (LVC) network and 15 station Parkfield (PKFD) networks are also part of BARD. Other nearby networks (open triangles) include: Basin and Range (BARGEN), and Southern California Integrated GPS Network (SCIGN).

Code	Latitude	Longitude	Start	Receiver	Maint.	Telem.	Location
BRIB	37.91940	-122.15255	1993.58	A-Z12	BSL	FR	Briones Reservation, Orinda
CMBB	38.03418	-120.38604	1993.92	A-Z12	BSL	FR	Columbia College, Columbia
DIAB	37.87858	-121.91563	1998.33	A-Z12	BSL	FR	Mt. Diablo
FARB	37.69721	-123.00076	1994.00	A-Z12	BSL	R-FR/R	Farallon Island
HOPB	38.99518	-123.07472	1995.58	A-Z12	BSL	FR	Hopland Field Stat., Hopland
LUTZ	37.28685	-121.86522	1996.33	A-Z12	BSL	FR	SCC Comm., Santa Clara
MHCB	37.34153	-121.64258	1996.33	A-Z12	BSL	FR	Lick Obs., Mt. Hamilton
MODB	41.90233	-120.30283	1999.83	A-Z12	BSL	NSN	Modoc Plateau
MOLA	37.94657	-122.41992	1993.75	T-SSE	BSL		Pt. Molate, Richmond
MONB	37.49892	-121.87131	1998.50	A-Z12	BSL	FR	Monument Peak, Milpitas
MUSB	37.16994	-119.30935	1997.83	A-Z12	BSL	R-Mi-FR	Musick Mt.
OHLN	38.00742	-122.27371	2001.83	A-Z12	BSL	FR	Ohlone Park, Hercules
ORVB	39.55463	-121.50029	1996.83	A-Z12	BSL	FR	Oroville
PKDB	35.94524	-120.54155	1996.67	A-Z12	BSL	FR	Bear Valley Ranch, Parkfield
POTB	38.20258	-121.95560	1998.92	A-Z12	BSL	FR	Potrero Hill, Fairfield
PTRB	37.99640	-123.01490	1998.58	A-Z12	BSL	R-FR	Point Reyes Lighthouse
SAOB	36.76530	-121.44718	1997.58	A-Z12	BSL	FR	San Andreas Obs., Hollister
SODB	37.16640	-121.92552	1996.33	A-Z12	BSL	R-FR	Soda Springs, Los Gatos
SUTB	39.20584	-121.82060	1997.33	A-Z12	BSL	R-FR	Sutter Buttes
TIBB	37.89087	-122.44760	1994.42	A-Z12	BSL	R	Tiburon
YBHB	41.73166	-122.71073	1996.75	A-Z12	BSL	FR	Yreka Blue Horn Mine, Yreka
CHAB	37.72412	-122.11931	1992.00	A-Z12	USGS		Chabot, San Leandro
WINT	37.65264	-122.14056	1992.00	A-Z12	USGS		Winton, Hayward
EBMD	37.81501	-122.28380	1999.18	T-SSi	EBMUD		EBMUD, Oakland
QUIN	39.97455	-120.94443	1992.68	Rogue	JPL		Quincy
S300	37.66642	-121.55815	1998.48	T-SSi	LLNL		Site 300, Livermore
CHO1	39.43264	-121.66496	1999.50	A-Z12	NGS		Chico
CME1	40.44177	-124.39633	1995.74	A-Z12	NGS		Cape Mendocino
CMOD	37.64130	-121.99997	2000.76	T-SSi	City		Modesto
CNDR	37.89641	-121.27849	1999.27	A-Z12	NGS		Condor, Stockton
PBL1	37.85306	-122.41944	1995.50	A-Z12	NGS		Point Blunt, Angel Island
PPT1	37.18167	-122.39333	1996.00	A-Z12	NGS		Pigeon Point
SUAA	37.42691	-122.17328	1994.30	A-Z12	SU		Stanford University
UCD1	38.53624	-121.75123	1996.38	T-SSi	UCD		UC Davis
UCSC	36.99279	-122.05219	2000.31	T-SSi	UCSC		UC Santa Cruz

Table 8.1: Currently operating stations of the BARD GPS network maintained by the BSL or by other agencies except in the Parkfield and Long Valley caldera regions. Other agencies include: EBMUD = East Bay Mun. Util. Dist., UCD = UC Davis, SU = Stanford Univ., UCSC = UC Santa Cruz, City = City of Modesto (see also Table 1.1). Receivers: A = Ashtech, T = Trimble. See Table 4.2 for telemetry codes and for BSL sites collocated with seismic stations. Data from other agencies retrieved or pushed by ftp or from the web.

and other members of the GPS community through Internet, both by anonymous ftp and by the World Wide Web (<http://quake.geo.berkeley.edu/bard/>).

Data and ancillary information about BARD stations are also made compatible with standards set by the International GPS Service (IGS), which administers the global tracking network used to estimate precise orbits and has been instrumental in coordinating the efforts of other regional tracking networks. The NCEDC also retrieves data from other GPS archives, such as at SIO, JPL, and NGS, in order to provide a complete archive

of all high-precision continuous GPS measurements collected in northern California.

Many of the BARD sites are classified as CORS stations by the NGS, which are used as reference stations by the surveying community. All continuous stations operating in July 1998 and May 2000 were included in a statewide adjustments of WGS84 coordinates for this purpose. Members of the BARD project regularly discuss these and other common issues with the surveying community at meetings of the Northern California GPS Users Group and the California Spatial Reference Center.

Code	Latitude	Longitude	Start	Receiver	Maint.	Location
CAND	35.93935	-120.43370	1999.33	A-Z12	USGS	Cann, Parkfield
CARH	35.88838	-120.43082	2001.58	A-Z12	USGS	Carr Hill 2, Parkfield
CARR	35.88835	-120.43084	1989.00	A-Z12	JPL	Carr Hill, Parkfield
CRBT	35.79161	-120.75075	2001.67	A-Z12	USGS	Camp Roberts, Parkfield
HOGS	35.86671	-120.47949	2001.50	A-Z12	USGS	Hogs, Parkfield
HUNT	35.88081	-120.40238	2001.58	A-Z12	USGS	Hunt, Parkfield
LAND	35.89979	-120.47328	1999.33	A-Z12	USGS	Lang, Parkfield
LOWS	35.82871	-120.59428	2001.58	A-Z12	USGS	Loves, Parkfield
MASW	35.83260	-120.44306	2001.58	A-Z12	USGS	Mason West, Parkfield
MIDA	35.92191	-120.45883	1999.75	A-Z12	USGS	Mida, Parkfield
MNMC	35.96947	-120.43405	2001.58	A-Z12	USGS	Mine Mt., Parkfield
POMM	35.91991	-120.47843	1999.75	A-Z12	USGS	Pomm, Parkfield
RNCH	35.89999	-120.52482	2001.58	A-Z12	USGS	Ranchita, Parkfield
TBLP	35.91741	-120.36034	2001.67	A-Z12	USGS	Table, Parkfield
BALD	37.78330	-118.90130	1999.67	A-ZFX	CVO	Bald Mt., LVC
CA99	37.64460	-118.89670	1999.67	A-ZFX	CVO	Casa 1999, LVC
CASA	37.64464	-118.89666	1993.00	Rogue	JPL	Casa Diablo, LVC
DDMN	37.74430	-118.98120	1999.67	A-ZFX	CVO	Deadman Creek, LVC
DECH	38.05150	-119.09060	2001.58	A-ZFX	CVO	Dechambeau Ranch, LVC
HOTK	37.65860	-118.82130	2001.67	A-Z12	CVO	Hot Creek, LVC
JNPR	37.77170	-119.08470	1997.81	A-Z12	USGS	Juniper, LVC
KNOL	37.65912	-118.97917	1998.58	A-ZFX	CVO	Knolls, LVC
KRAC	37.71330	-118.88050	2001.67	A-Z12	CVO	Krakatoa-USGS, LVC
KRAK	37.71313	-118.88114	1994.73	Rogue	JPL	Krakatoa, LVC
LINC	37.63719	-119.01729	1998.67	A-Z12	CVO	Lincoln, LVC
MINS	37.65376	-119.06090	1995.92	A-Z12	USGS	Minaret Summit, LVC
MWTP	37.64052	-118.94473	1998.58	A-ZFX	CVO	Mammoth Water Treat Plant, LVC
PMTN	37.83130	-119.05690	1999.67	A-Z12	CVO	Panorama Mt., LVC
RDOM	37.67707	-118.89794	1998.58	A-ZFX	CVO	Resurgent Dome, LVC
SAWC	37.68990	-118.95310	2000.65	A-ZFX	CVO	Saw, LVC
TILC	37.61890	-118.86280	2000.65	A-Z12	CVO	Tilla, LVC
WATC	37.66440	-118.65390	2001.67	A-Z12	CVO	Waterson, LVC

Table 8.2: Currently operating stations of the BARD GPS network maintained by other agencies in the Parkfield and Long Valley caldera regions. Other agencies include: CVO = USGS Cascade Volcano Observatory (see also Table 1.1). Receivers: A = Ashtech. Data from other agencies retrieved or pushed by ftp or from the web.

In the remainder of this section, we describe the standard BARD station and some of the BARD-related activities the BSL has performed over the last year, including maintenance to existing stations, installation of a new station and an experimental single-frequency receiver profile, improvement in processing methods, and analysis of the data to estimate deformation signals monitored by the network.

## 2. BARD Stations

A BSL continuous GPS station uses a low-multipath choke-ring antenna mounted to a reinforced concrete pillar approximately 0.5 meter above local ground level. The reinforcing steel bars of the pillar are drilled and cemented into rock outcrop to improve long-term monu-

ment stability. It uses a low-loss antenna cable to minimize signal degradation on the longer cable setups that normally would require signal amplification. Low-voltage cutoff devices are installed to improve receiver performance following power outages. The Ashtech Z-12 receiver is programmed to record data once every 30 seconds, observing up to 12 satellites simultaneously at elevations down to the horizon.

Tests performed by UNAVCO on low antenna mounts revealed that estimates of tropospheric water vapor from the GPS data are strongly correlated with signal multipath errors, which can degrade the precision of the vertical position estimates. Most of the BSL GPS stations use monuments that elevate the antennas 0.5–1.0 m above the ground surface, which helps to minimize the correlations between multipath and tropospheric parameters.

The stations are equipped with SCIGN-designed hemispherical domes. Domes cover the antennas to provide security and protection from the weather and other natural phenomenon. The SCIGN dome is designed for the Dorne-Margolin antennas and minimizes differential radio propagation delays by being hemispherical about the phase center and uniform in thickness at the 0.1 mm level. It is also very resistant to damage and, in its tall form combined with the SCIGN-designed antenna adapter, can completely cover the dome and cable connections for added protection. All new stations use the adapters and tall domes. Some of the older stations in well protected areas use the short domes.

Data from all BSL-maintained stations are collected at 30-second intervals and transmitted continuously over serial connections (Table 8.1). Station TIBB uses a direct radio link to Berkeley, and MODB uses VSAT satellite telemetry. The 18 stations use frame relay technology, either alone or in combination with radio telemetry. Twelve GPS stations are collocated with broadband seismometers and Quanterra data collectors (Table 4.2). With the support of IRIS we developed software that converts continuous GPS data to MiniSEED opaque blockettes, which can be stored and retrieved from the Quanterra data loggers (*Perin et al.*, 1998). The MiniSEED approach provides more robust data recovery from onsite backup on the Quanterra disks following telemetry outages. Our comparisons also show the loss of individual records is fewer when using the Quanterra MiniSEED rather than direct serial method due to the superior short-term data buffer in the Quanterra. Data from the 12 collocated stations plus SUTB are retrieved in this manner.

### 3. 2001-2002 Activities

During July 2001–June 2002, we performed maintenance on existing BARD stations, installed a new station, and prepared for new stations near the Hayward fault, on the San Francisco peninsula, and north Bay area regions.

#### 3.1 Station Maintenance

In March 2002, “copper-miners” took advantage of the poor security at the decommissioned Point Molates naval facility to fell the power poles and remove high tension copper power lines that were used by the MOLA station. The property has been put aside for environmental cleanup before the ownership is transferred from the Navy to the City of Richmond. Due to the status of the property, the high costs to reestablish power, and the unsecured nature of the area, the station was removed from continuous GPS service. The monument and enclosure were left intact and the site is being periodically reoccupied, approximately 2–3 days per month, in a semi-permanent mode.

In May 2002, forced entry in the building housing the GPS equipment at SAOB resulted in theft of GPS receiver and damage to building and telemetry system. We reinforced the plywood building walls with a layer of wire mesh followed by a surface layer of plywood secured with screws and liquid adhesive. Inside the building, the GPS receiver and short-haul modems were replaced and stored within a double locked large metal “Hoffman” box.

Also in May 2002, the receiver and Freewave radio at Sutter Buttes (SUTB) were replaced due to a data outage following an electrical storm and possible lightning strike. The site is located on top of the South Butte, 2000 feet above the Central Valley.

### 3.2 New Installations

#### Mini-PBO sites

In the summer and fall of 2001, we helped to do site reconnaissance, permitting, and installations for the NSF-funded mini-PBO project establishing collocated GPS/seismometer/borehole strainmeter observatories in the Bay Area. Boreholes were drilled to around 200 m at 4 sites, and strainmeter and seismometer instruments were installed in 3 of the boreholes (the fourth proved problematic and could not be completed until August 2002). Due to delays by utility companies in establishing power and telemetry, only the station OHLN at Ohlone Park in Hercules, about 5 km west of the northern Hayward fault, became fully operational. The GPS antenna is mounted on the top of the 6” borehole casing, in an experimental approach to obtain a stable, compact monument. GPS data from OHLN is now publicly available from the NCEDC, and included in the automated BARD processing for hourly and daily site positions. For more details about the OHLN station installation, and the other mini-PBO sites, see Chapter 9).

#### L1-system Profile

The BSL staff is evaluating the performance of the UNAVCO-designed L1 system in an urban setting. This single-frequency receiver is relatively inexpensive but is less accurate than dual-frequency receiver systems that can completely eliminate first-order ionospheric effects. Hence we expect the L1 system to be most useful for short baseline measurements where ionospheric effects tend to cancel due to similar propagation paths. The systems are self-contained, using solar power and integrated radio modems. During 1999, the BSL borrowed 2 receivers and a master radio from UNAVCO to perform the evaluation, but persistent hardware and software problems limited progress on this project. UNAVCO subsequently resolved many of the problems and in summer 2000, we received new, improved equipment and software for 4 systems and a master radio.

During 2000 and 2001, we completed permitting at 4

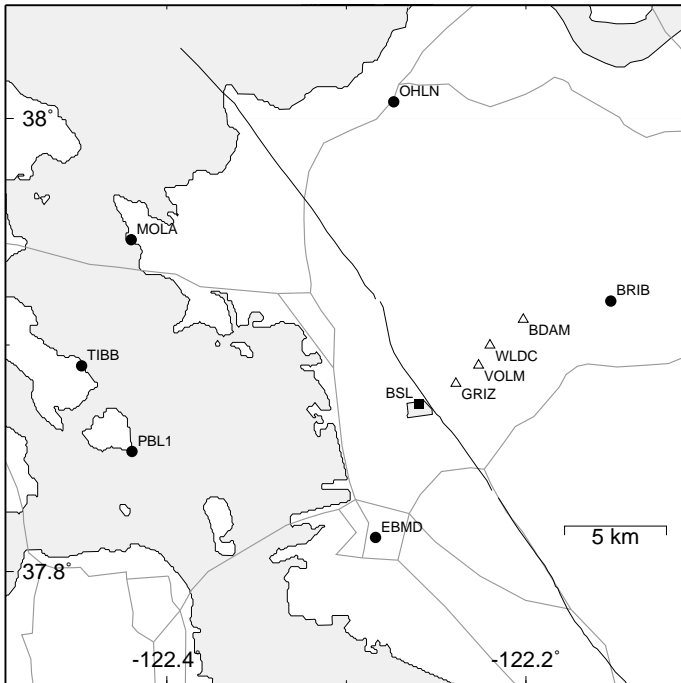


Figure 8.2: Location of L1-system (open triangles) and BARD (closed circles) stations. BSL, just southwest of the Hayward fault, is the location of the Berkeley Seismological Laboratory, where data from the 4 L1-system receivers northeast of the Hayward are telemetered.

sites on a 10-km profile extending normal to the Hayward fault between the UC Berkeley campus and the permanent BRIB site (Fig. 8.2). This profile, complemented by BRIB and EBMD to the west of the fault, will be most sensitive to variations in locking at 2-8 km depth. We expect that these systems will provide useful constraints on relative displacements near the Hayward fault in 3-5 years, and should help to resolve variations in creeping and locked portions of the fault (e.g., Bürgmann *et al.*, 2000).

Three sites are located on East Bay Municipal Utilities District (EBMUD) property. The station BDAM is located just east of the Briones Dam and a few km west of the Briones (BRIB) continuous BARD station. Wildcat (WLDC) is located near the San Pablo Reservoir, and VOLM is located on the ridge of the East Bay Hills close to Volmer Peak. The fourth site, Grizzly Flat (GRIZ), is located on East Bay Regional Park property just west of Grizzly Peak. Finding suitable stations with line-of-sight telemetry across the East Bay Hills proved challenging. Data from WLDC must pass through all the other stations, with its relay path being (in order) BDAM, VOLM, GRIZ, a repeater on the UC Berkeley Space Sciences Building, and then finally the master radio on the roof of McCone Hall where the BSL is located



Figure 8.3: L1 system installation at GRIZ. This autonomous system uses solar panels (mounted in back) and Freewave radios (with Yagi antenna mounded on pole below GPS antenna). GPS receiver, radio, solar power regulators, and backup batteries are in the electronics box mounted in front.

on campus.

In April 2002, we installed the L1 Profile with assistance from two engineers from UNAVCO. We used a large gas powered hand drill to bore a 2" diameter, 18" deep hole into bedrock at the BDAM and VOLM sites, and cemented in a galvanized pipe using expansive grout. GRIZ and WLDC are located in areas where we could not easily access bedrock. GRIZ is located on top of a small plateau covered in volcanic deposits that have weathered to clay. Bedrock was observed nearby uphill of the WLDC site, but could not be used due to telemetry constraints. At both of these sites a subsurface concrete pier was constructed, laced with chicken wire to reduce cement fracturing during drying, and anchored by steel rebar pounded into the ground at several angles.

The electronics, including gps/radio unit, battery and solar power manager, are securely stored within a medium-sized Hoffman box, or locking metal enclosure, attached to pipe. Whenever possible access to the in-

side of box is necessary to remove bolts attaching the box itself. GPS antenna is mounted on a fiberglass rod attached to top of pipe. All loose cables are zip-tied in place and all stainless steel bolts are epoxied to discourage theft. A typical site, with a Yagi antenna for communications, is shown in Figure 8.3.

Since April, we have been assessing the data quality and processing the data to estimate daily site positions. Problems with telemetry outages at WLDC during the early morning, pre-dawn hours, were found to be due to a faulty battery, and were corrected when we installed new batteries at all the sites. GRIZ currently is experiencing intermittent data outages which were not solved by the new battery or by replacing the receiver/radio unit. We are currently investigating possible problems with the solar power regulator. We are also in the process of obtaining 2 additional systems from UNAVCO that will be installed on the roofs of the Space Sciences and McCone Hall buildings, which will make the profile cross the Hayward fault and allow direct measurement of surface creep in this region.

We are developing techniques to process the data using the GAMIT/GLOBK analysis package. We corrected software provided by UNAVCO to synchronize the phase, pseudorange, and clock offset observables, which allows the data to be cleaned in an automatic fashion. Preliminary results suggest that repeatabilities of 1–2 mm in daily horizontal positions on the shortest (several km) baselines can be achieved (Figure 8.4), but these degrade to 3–4 mm on the longer (10 km) baselines. We are investigating ways to simultaneously process the dual-frequency data from nearby BARD stations (e.g., BRIB, OHLN), with the single-frequency L1 data to improve these results. Currently data from second frequency on the BARD stations is not used, which degrades the definition of the local reference frame and repeatability of the baselines.

## 4. Data Analysis and Results

The data from the BARD sites generally are of high quality and measure relative horizontal positions at the 2–4 mm level. The 24-hour RINEX data files are processed daily with an automated system using high-precision IGS orbits. Final IGS orbits, available within 7–10 days of the end of a GPS week, are used for final solutions. Preliminary solutions for network integrity checks and rapid fault monitoring are also estimated from Predicted IGS orbits (available on the same day) and from Rapid IGS orbits (available within 1 day). Data from 5 primary IGS fiducial sites located in North America and Hawaii are included in the solutions to help define a global reference frame. Average station coordinates are estimated from 24 hours of observations using the GAMIT software developed at MIT and SIO, and

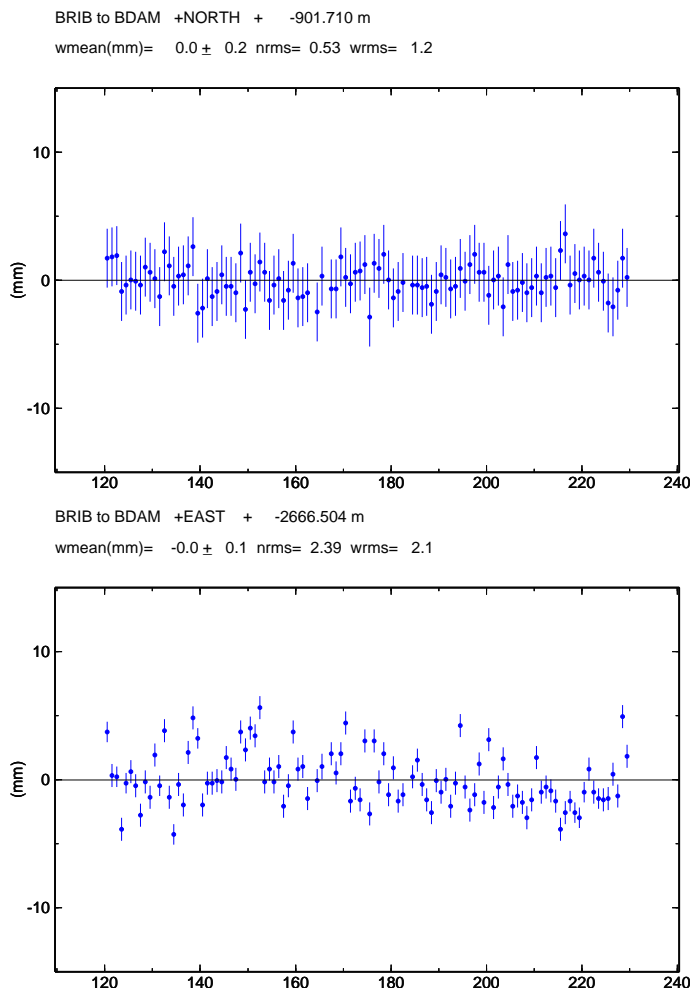


Figure 8.4: Daily estimates of the north and east components of the BRIB to BDAM 3-km baseline. Daily repeatabilities are about 1 mm in north, and 2 mm in east.

the solutions are output with weakly constrained station coordinates and satellite state vectors.

Processing of data from the BARD and other nearby networks is split into 7 geographical subregions: the Bay Area, northern California, Long Valley caldera, Parkfield, southern and northern Pacific Northwest, and the Basin and Range Province. Each subnet includes the 5 IGS stations and 3 stations in common with another subnet to help tie the subnets together. The weakly constrained solutions are combined using the GLOBK software developed at MIT, which uses Kalman filter techniques and allows tight constraints to be imposed a posteriori. This helps to ensure a self-consistent reference frame for the final combined solution. The subnet solutions for each day are combined assuming a common orbit to estimate weakly constrained coordinate-only solutions. These daily coordinate-only solutions are then combined

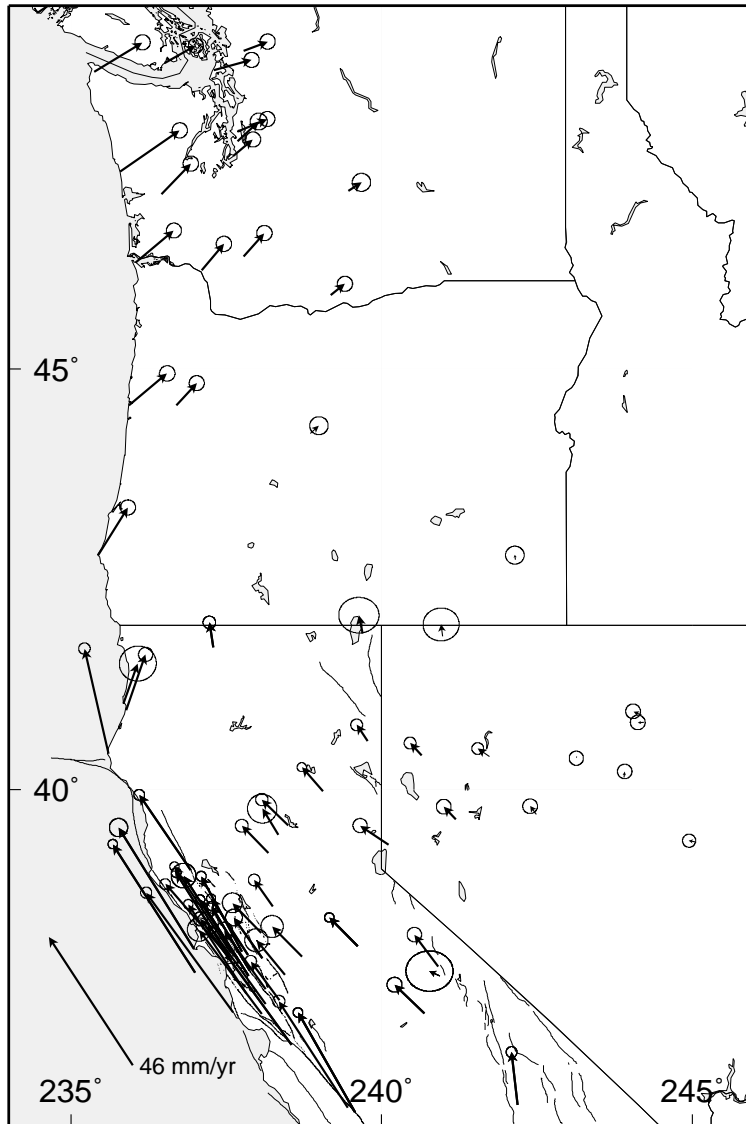


Figure 8.5: Velocities relative to stable North America for the BARD stations and other stations operated in nearby networks. Data from November 1993 to July 2000 was processed by the BSL using GAMIT software. Ellipses show 95% confidence regions, assuming white noise and  $1\text{mm}/\sqrt{\text{yr}}$  random-walk noise, with the predicted Pacific–North America relative plate motion in central California shown for scale.

with tight coordinate constraints to estimate day-to-day coordinate repeatabilities, temporal variations, and site velocities.

The estimated relative baseline determinations typically have 2–4 mm WRMS scatter about a linear fit to changes in north and east components and the 10–20 mm WRMS scatter in the vertical component. Average velocities for the longest running BARD stations during 1993–2000 are shown in Figure 8.5, with 95% confidence regions. We have allowed  $1\text{mm}/\sqrt{\text{yr}}$  random-walk variations in the site positions in order to more accurately characterize the long-term stability of the site monuments and day-to-day correlations in position. The velocities are relative to stable North America, as defined by the IGS fiducial stations, which we assume have relative

motions given by *Kogan et al.*, (2000).

Most of the Sierra Nevada sites (CMBB, QUIN, and ORVB), as well as SUTB in the Central Valley, show little relative motion, indicating that the northern Sierra Nevada–Central Valley is tectonically stable. The motion of these sites relative to North America differs from the inferred motion of the western Basin and Range Province, suggesting 3 mm/yr right-lateral shear across the Walker Lane–Mt. Shasta seismicity trend. Deformation in the Pacific Northwest is generally consistent with interseismic strain accumulation along the Cascadia megathrust, the interface between the Juan de Fuca and North America plates, particularly in Washington where the velocity vectors are nearly parallel to the oblique convergence direction. Greater arc-parallel motion in Oregon and

northern California may be due to the influence of the SAF system to the south and clockwise rotation of the southern Oregon forearc (*Savage et al.*, 2000).

Deformation along the coast in central California is dominated by the active SAF system, which accommodates about 35 mm/yr of right-lateral shear. The Farallon Island site (FARB) off the coast of San Francisco is moving at nearly the rate predicted by the NUVEL-1A Pacific–North America Euler pole. Two-dimensional modeling of the observed fault-parallel strain accumulation predicts deep slip rates for the San Andreas, Hayward, and Calaveras/Concord faults are  $19.3\pm 1.8$ ,  $11.3\pm 1.9$ , and  $7.4\pm 1.6$  mm/yr, respectively, in good agreement with estimated geologic rates ( $17\pm 4$ ,  $9\pm 2$ , and  $5\pm 3$  mm/yr, respectively). Most of the 46 mm/yr of relative motion is accommodated within a 100-wide zone centered on the SAF system and a broader zone in the Basin and Range Province in Nevada.

## 5. Real-Time Processing

We are also developing real-time analysis techniques that will enable rapid determinations ( $\sim$ minutes) of deformation following major earthquakes to complement seismological information and aid determinations of earthquake location, magnitude, geometry, and strong motion (*Murray et al.*, 1998c). We currently process data available within 1 hour of measurement from the 18 continuous telemetry BSL stations, and several other stations that make their data available on an hourly basis. The data are binned into 1 hour files and processed simultaneously. The scatter of these hourly solutions is much higher than the 24-hour solutions: 10 mm in the horizontal and 30–50 mm in the vertical. Our simulations suggest that displacements 3–5 times these levels should be reliably detected, and that the current network should be able to resolve the finite dimensions and slip magnitude of a  $M=7$  earthquake on the Hayward fault. We are currently investigating other analysis techniques that should improve upon these results, such as using a Kalman filter that can combine the most recent data with previous data in near real-time. The August 1998  $M=5.1$  San Juan Bautista earthquake (*Uhrhammer et al.*, 1999) is the only event to have produced a detectable earthquake displacement signal at a BARD GPS receiver.

## 6. Acknowledgements

Mark Murray oversees the BARD program. André Basset, Bill Karavas, John Friday, Dave Rapkin, Doug Neuhauser, and Rich Clymer contribute to the operation of the BARD and L1 networks. Mark Murray and André Basset contributed to the preparation of this chapter.

## 7. References

- Bürgmann, R., D. Schmidt, R. M. Nadeau, M. d’Alessio, E. Fielding, D. Manaker, T. V. McEvilly, and M. H. Murray, Earthquake potential along the northern Hayward fault, California, *Science*, 289, 1178–1182, 2000.
- King, N. E., J. L. Svarc, E. B. Fogleman, W. K. Gross, K. W. Clark, G. D. Hamilton, C. H. Stiffler, and J. M. Sutton, Continuous GPS observations across the Hayward fault, California, 1991–1994, *J. Geophys. Res.*, 100, 20,271–20,283, 1995.
- Kogan, M. G., G. M. Steblov, R. W. King, T. A. Her-ring, D. I. Frolov, S. G. Egorov, V. Y. Levin, A. Lerner-Lam, A. Jones, Geodetic constraints on the rigidity and relative motion of Eurasia and North America, *Geophys. Res. Lett.*, 27, 2041–2044, 2000.
- Murray, M. H., and P. Segall, Continuous GPS measurement of Pacific–North America plate boundary deformation in northern California and Nevada, *Geophys. Res. Lett.*, 28, 4315–4318, 2001.
- Murray, M. H., R. Bürgmann, W. H. Prescott, B. Romanowicz, S. Schwartz, P. Segall, and E. Silver, The Bay Area Regional Deformation (BARD) permanent GPS network in northern California, *EOS Trans. AGU*, 79(45), Fall Meeting Suppl., F206, 1998a.
- Murray, M. H., W. H. Prescott, R. Bürgmann, J. T. Freymueller, P. Segall, J. Svarc, S. D. J. Williams, M. Lisowski, and B. Romanowicz, The deformation field of the Pacific–North America plate boundary zone in northern California from geodetic data, 1973–1989, *EOS Trans. AGU*, 79(45), Fall Meeting Suppl., F192, 1998b.
- Murray, M. H., D. S. Dreger, D. S. Neuhauser, D. R. Baxter, L. S. Gee, and B. Romanowicz, Real-time earthquake geodesy, *Seismol. Res. Lett.*, 69, 145, 1998c.
- Perin, B. J., C. M. Meertens, D. S. Neuhauser, D. R. Baxter, M. H. Murray, and R. Butler, Institutional collaborations for joint seismic and GPS measurements, *Seismol. Res. Lett.*, 69, 159, 1998.
- Romanowicz, B., B. Bogaert, D. Neuhauser, and D. Oppenheimer, Accessing northern California earthquake data via Internet, *EOS Trans. AGU*, 75, 257–260, 1994.
- Savage, J. C., J. L. Svarc, W. H. Prescott, and M. H. Murray, Deformation across the forearc of the Cascadia subduction zone at Cape Blanco, Oregon, *J. Geophys. Res.*, 105, 3095–3102, 2000.
- Uhrhammer, R., L. S. Gee, M. Murray, D. Dreger, and B. Romanowicz, The  $M_w$  5.1 San Juan Bautista, California earthquake of 12 August 1998, *Seismol. Res. Lett.*, 70, 10–18, 1999.

## Chapter 9

# Plate Boundary Deformation Project

### 1. Introduction

The Integrated Instrumentation Program for Broadband Observations of Plate Boundary Deformation, commonly referred to as “Mini-PBO”, is a joint project of the BSL, the Department of Terrestrial Magnetism at Carnegie Institution of Washington (CIW), the IGPP at UC San Diego (UCSD), and the U.S. Geological Survey (USGS) at Menlo Park, Calif. It augments existing infrastructure in central California to form an integrated pilot system of instrumentation for the study of plate boundary deformation, with special emphasis on its relation to earthquakes. This project is partially funded through the EAR NSF/IF program with matching funds from the participating institutions and the Southern California Integrated Geodetic Network (SCIGN).

Because the time scales for plate boundary deformation range over at least 8 orders of magnitude, from seconds to decades, no single technique is adequate. We have initiated an integrated approach that makes use of three complementary and mature geodetic technologies: continuous GPS, borehole tensor strainmeters, and interferometric synthetic aperture radar (InSAR), to characterize broadband surface deformation. Also, ultrasensitive borehole seismometers monitor microearthquake activity related to subsurface deformation.

The project has three components. The first augments existing instrumentation along the Hayward and San Andreas faults in the San Francisco Bay area (Figure 9.1). During July 2001 to August 2002, five boreholes were drilled and equipped with tensor strainmeters and 3-component L22 (velocity) seismometers (Table 9.1). The strainmeters were recently developed by CIW and use 3 sensing volumes placed in an annulus with 120 degree angular separation, which allows the 3-component horizontal strain tensor to be determined. One borehole station has also been equipped with a GPS receiver, Quanterra recording system, and downhole pore pressure sensor, and will eventually also include a tilt sensor. The other stations are in various stages of completion, primarily waiting for power and telemetry to be established. The GPS antennas at these stations are mounted at the

top of the borehole casings in an experimental approach to achieve stable compact monuments. The GPS stations complement existing Bay Area stations of the BARD continuous network.

The 30-second GPS, and 100-Hz strainmeter and seismometer data is acquired on Quanterra data loggers and continuously telemetered by frame relay to the BSL. Low frequency (600 second) data (including strainmeters, for redundancy) is telemetered using the GOES system to the USGS. All data is available to the community through the Northern California Earthquake Data Center (NCEDC) in SEED format, using procedures developed by the BSL and USGS to archive similar data from 139 sites of the USGS ultra-low-frequency (UL) geophysical network, including data from strainmeters, tiltmeters, creep meters, magnetometers, and water well levels.

The second component of this project is to link the BARD network in central and northern California to the SCIGN network in southern California. The distribution of these sites allows measurement of both near-field deformation from fault slip on the San Andreas and regional strain accumulation from far-field stations. During Summer 2001, nine new continuous GPS sites were installed (see Table 8.2) in the Parkfield area spanning about 25 km on either side of the San Andreas fault. One of the receivers was contributed by the USGS and the other eight were contributed by SCIGN, while the braced monuments for all the sites were constructed using Mini-PBO funding. The new array augments the considerable geophysical instrumentation already deployed in the area and contributes to the deep borehole drilling on the San Andreas fault (SAFOD) component of Earthscope. The data are currently downloaded daily by SCIGN and archived by SOPAC. The NCEDC is currently assuming the responsibility for retrieving the data from these sites over their existing frame relay circuit at Parkfield. A subset of these sites will eventually be upgraded to real-time streaming and analyzed in instantaneous positioning mode.

The third component is InSAR, which supports skeletal operations of a 5-m X-band SAR downlink facility in San Diego to collect and archive radar data, and develop

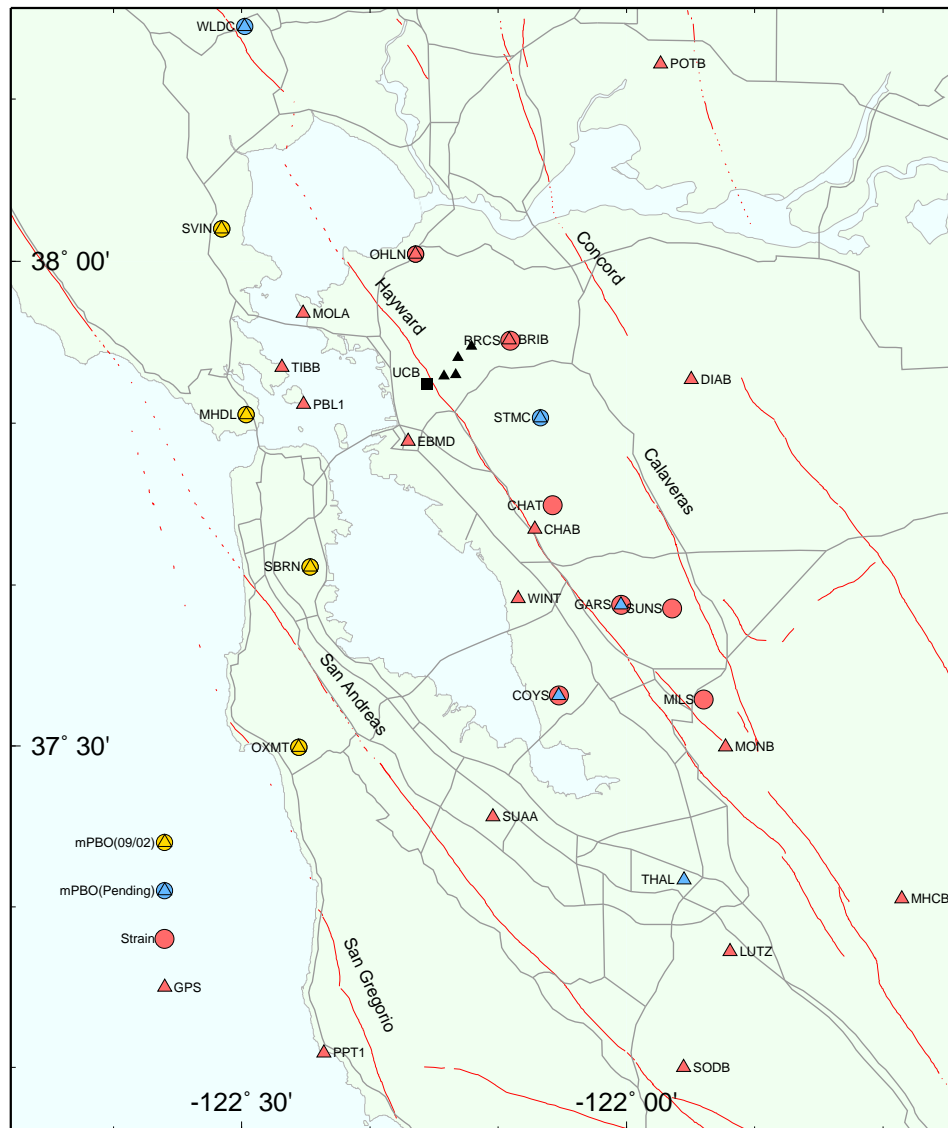


Figure 9.1: Location of existing (red), in preparation (yellow), and pending (blue) Mini-PBO sites in the San Francisco Bay area. Shown also (red) are currently operating strainmeter (circles) and BARD (triangles) stations. Blue triangles are other pending BARD stations. Black triangles are L1-system profile sites near the Hayward fault and the UC Berkeley campus.

an online SAR database for WInSAR users. The ERS-1/2 SAR data, which extend from 1992 until present, offer the only means for monitoring plate boundary deformation at high spatial resolution over all of western North America. This data set is largely unexplored mainly because data distribution is restricted by ESA and the time consuming nature of processing phase information. Our objective is to improve access to these data for plate boundary research within the strict guidelines set by ESA.

## 2. New Site Installations

During this last year, the BSL and USGS installed the first Mini-PBO stations. Boreholes were drilled by the USGS Water Resources Division crew at five sites. The drillers used a newly purchased rig (Figure 9.2) that experienced numerous problems (hydraulics, stuck bits, etc.), which delayed the drilling considerably at several of the sites and significantly increased the costs of the project.

Figure 9.3 shows the configuration of the borehole instrument installation at the first site at Ohlone Park in Hercules (OHLN). A 6.625" steel casing was cemented into a 10.75" hole to 625'4" depth to prevent the upper,

Code	Latitude	Longitude	Installed	Strainmeter depth (ft)	Seismometer depth (ft)	Location
OHLN	38.00742	-122.27371	2001/07/16	670.5	645.5	Ohlone Park, Hercules
SBRN	37.68562	-122.41127	2001/08/06	551.5	530.0	San Bruno Mtn. State Park, Brisbane
OXMT	37.49795	-122.42488	2002/02/06	662.7	637.3	Ox Mtn., Half Moon Bay
MHDL	37.84227	-122.49374	2002/08/06	520.6	489.2	Golden Gate Nat. Rec. Area, Sausalito
SVIN	38.03325	-122.52638	2002/08/29	527.0	500.0	St. Vincent CYO School, San Rafael
SMCB	37.83881	-122.11159				St. Mary's College, Moraga
WDCB	38.24088	-122.49628				Wildcat Mt., Sears Pt.

Table 9.1: Currently operating and planned stations of the Mini-PBO network. Strainmeter installation date is given. Depth to tensor strainmeter and 3-component seismometers in feet.

most unconsolidated materials from collapsing into the hole. Below this depth a 6" uncased hole was drilled to 676'. Coring was attempted with moderate success below 540' through poorly consolidated mudstone to about 570', and increasingly competent sandstone below. Moderately good core was obtained from 655' to 669', so this region was selected for the strainmeter installation. The section of the hole below about 645' was filled with a non-shrink grout into which the strainmeter was lowered, allowing the grout to completely fill the inner cavity of the strainmeter within the annulus formed by the sensing volumes to ensure good coupling to the surrounding rock.

The 3-component seismometer package was then lowered to 645.5', just above the strainmeter, on a 2" PVC pipe, and neat cement was used to fill the hole and PVC pipe to 565'. The pipe above this depth was left open for later installation of the pore pressure sensor in the 520-540' region. To allow water to circulate into the pipe from the surrounding rock for the pore pressure measurements, the the steel casing was perforated, a sand/gravel pack was emplaced, and a PVC screen was used at this depth. The casing was then cemented inside to 192', and outside to 16' depth. A 12" PVC conductor casing was cemented on the outside from the surface to 16' to stabilize the hole for drilling and to provide an environmental health seal for shallow groundwater flow. The annulus between the 12" conductor casing and the 6.625" steel casing was cemented from 16' to 10' depth and above was left decoupled from the upper surface to help minimize monument instability for the GPS antenna mounted on top of the steel casing.

The drilling procedures and hole instrument configuration were similar at the other four sites. At San Bruno Mt (SBRN) near Brisbane, the hole was drilled to 550' with good core through competent graywacke below 520'. Reaming of the bottom hole from the 4" core diameter to 6" was delayed considerably for retrieval of the reaming bit that broke and got lodged in the bottom of the hole. At Scarper's Ridge (OXMT) near Half Moon Bay, the hole was drilled to 712.7' depth with coring attempted

below 653' through granite. Because core was poorly recovered at the lowest depths due to inadequacies with the coring system that broke up the rock, a slightly shallower depth of 660' was chosen for the strainmeter installation.

At the Marin Headlands (MHDL) site, the drilling in October 2001 encountered hard greenstone with some fractures and clay layers between 410-608' and red and green chert below to 659'. Coring at around 545' was slow and poorly recovered. A video log of the hole showed several promising strainmeter installation regions at 500-550' depths. However, containment of high volumes of artesianing fluids from the well became increasing problematic. The hole was cased to 278', sand filled on the bottom, and cemented and plugged at the top in mid-October. In August 2002, the cement and sand were rapidly drilled out, without any artesianing problems, allowing the strainmeter and seismometer packages to be successfully installed.

At the St Vincents (SVIN) site near San Rafael, drilling in August 2002 also entailed no shortage of problems. The first hole had to be abandoned after some tungsten grinding buttons from a defective bit dislodged and could not be retrieved from the bottom of the hole. Hammer drilling through the very hard graywacke encountered throughout the hole also proved difficult due to the lack of proper stabilization on the drill string. Rotary drilling, although relatively slow, enabled penetration to 528' in the limited time available. A video log showed a promising region devoid of open fractures near the bottom of the hole where the strainmeter and seismometer packages were installed without any further difficulties.

Due to the unexpectedly high costs of drilling, only 5 boreholes could be completed under the NSF/IF grant, although additional instrumentation was purchased in anticipation of acquiring more sites. Caltrans intends to drill boreholes at several locations for the HFN project in the coming year that might be suitable for Mini-PBO installations, depending on the quality of the rock encountered at about 600' depth. Two of the already permitted potential sites, St. Mary's College (SMCB) and Wildcat Mt. (WDCB) (Figure 9.1 and Table 9.1), would



Figure 9.2: USGS Water Resources Division rig used to drill the Mini-PBO boreholes at the St. Vincents site.

### HERCULES (Ohlone) Status 8/20/01 BOREHOLE STRAINMETER AND SEISMIC MONITORING INSTALLATION

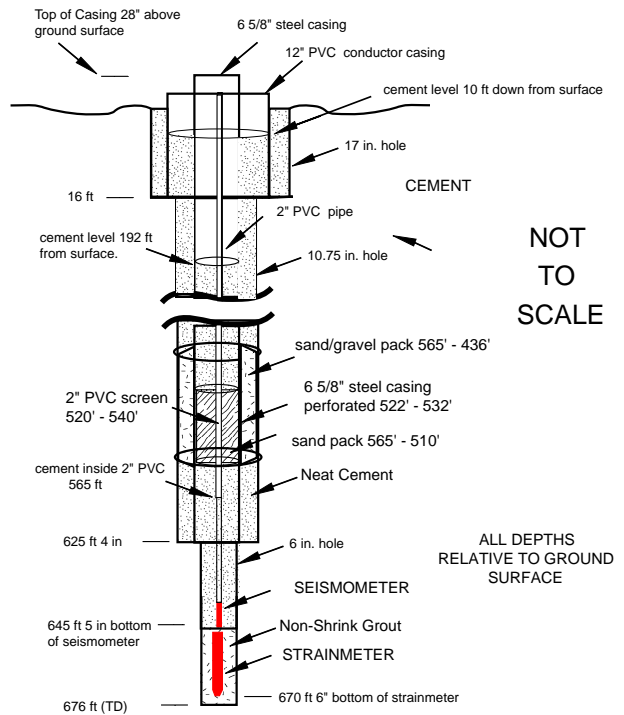


Figure 9.3: The Mini-PBO borehole configuration at Ohlone, showing the emplacement of the strainmeter and seismometer instruments downhole. The GPS receiver is mounted on the top. Figure courtesy B. Mueller (USGS).

nicely complement existing instrumentation, providing additional monitoring of the northern Hayward fault and initiating monitoring of the southern Rodgers Creek fault north of San Pablo bay.

The BSL is supervising GPS, power, frame relay telemetry, and Quanterra 4120 datalogger installation at all the Mini-PBO stations. Power, telemetry, and dataloggers are currently installed at OHLN and SBRN. The frame relay circuit at MHDL is also installed, but the power hookup has been delayed due to permitting complications that should be resolved in Fall 2002. We are currently establishing power and telemetry at the most recently installed MHDL and SVIN stations. The USGS has installed solar panels at OXMT, and soon at MHDL and SVIN, to collect the low-frequency strainmeter data prior to establishing DC power at the sites.

The BSL is developing an experimental GPS mount for the top of the borehole casings to create a stable, compact monument (Figure 9.4). The antennas, using standard SCIGN adapters and domes for protection, are attached to the top of the 6-inch metal casing, which will be mechanically isolated from the upper few meters of

the ground. The casing below this level will be cemented fully to the surrounding rock. We have installed a GPS antenna at OHLN (Figure 9.5). The antenna is attached to a metal pipe symmetrically centered with respect to the casing that is welded to a cross beam and bolted inside the top of the casing, which allows access through the top of the casing to the 2" pipe for heat flow measurements. A similar mount was constructed at OXMT, but it was found to have too much play in the area where the bolts are attached to ensure long-term stability of the monument. We are currently redesigning the mount to minimize such non-tectonic motions. Preliminary analysis of 100 days of the GPS observations at OHLN shows that the short-term daily repeatabilities in the horizontal components are about 0.5-1 mm. These values are similar to those obtained with more typical monuments, such as concrete piers or braced monuments, but it is too early to assess the long-term stability of the borehole casing monument, which might also be affected by annual thermal expansion effects on the casing.

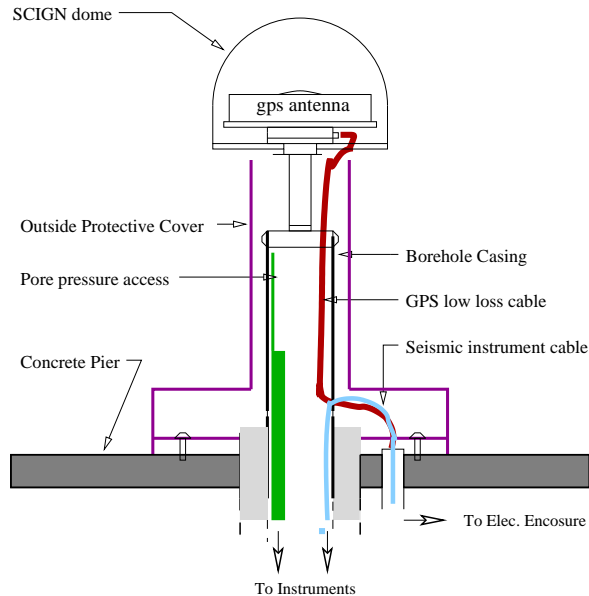


Figure 9.4: Design of the Mini-PBO GPS antenna mount on top of casing.

### 3. Strainmeter Data

We are in the initial stages of assessing the data quality of the Mini-PBO instrumentation. The newly designed tensor strainmeters appear to faithfully record strain signals over a broad frequency range. During the 9 months that the strainmeter at OHLN has been providing high-frequency data, the strain has been exponentially decaying (top, Figure 9.6). This large signal is most likely due to cement hardening effects and re-equilibration of stresses in the surrounding rock in response to the sudden appearance of the borehole. These effects can last for many years and are the principal reason that borehole strainmeters can not reliably measure strain at periods greater than a few months.

At periods around 1 day, tidally induced strains are the dominant strain signal, about 3 orders of magnitude smaller than the long-term decay signal (bottom, Figure 9.6). Since the response of the strainmeter volumes is difficult to estimate independently, theoretically predicted Earth tides are typically used to calibrate the strainmeters. Figure 9.7 shows the calibrated signals in microstrain of the OHLN strainmeter over a several day interval.

At higher frequencies, strains due to seismic events are also evident. Figure 9.8 shows a comparison of the OHLN vertical velocity seismometer and one component of the strainmeter for an  $M=2$  event that occurred within 15 km of the station. Strains from this event are about an order of magnitude smaller than the tidal strains. We are



Figure 9.5: GPS antenna mounted on top of casing at OHLN. The final installation includes a SCIGN antenna dome and a steel protective shroud that envelopes the casing.

beginning to examine the strain data for other types of transient behavior, such as episodic creep or slow earthquake displacements.

### 4. Acknowledgements

This project is sponsored by the National Science Foundation under the Major Research Instrumentation (MRI) program with matching funds from the participating institutions and the Southern California Earthquake Center (SCEC).

Under Mark Murray's supervision, André Basset, Bill Karavas, John Friday, Dave Rapkin, Doug Neuhauser, Tom McEvelly, Wade Johnson, and Rich Clymer have contributed to the development of the BSL component of the Mini-PBO project. Several USGS colleagues, especially Malcolm Johnston, Bob Mueller, and Doug Myren, played critical roles in the drilling and instrument installation phases. Mark Murray and Barbara Romanowicz contributed to the preparation of this chapter.

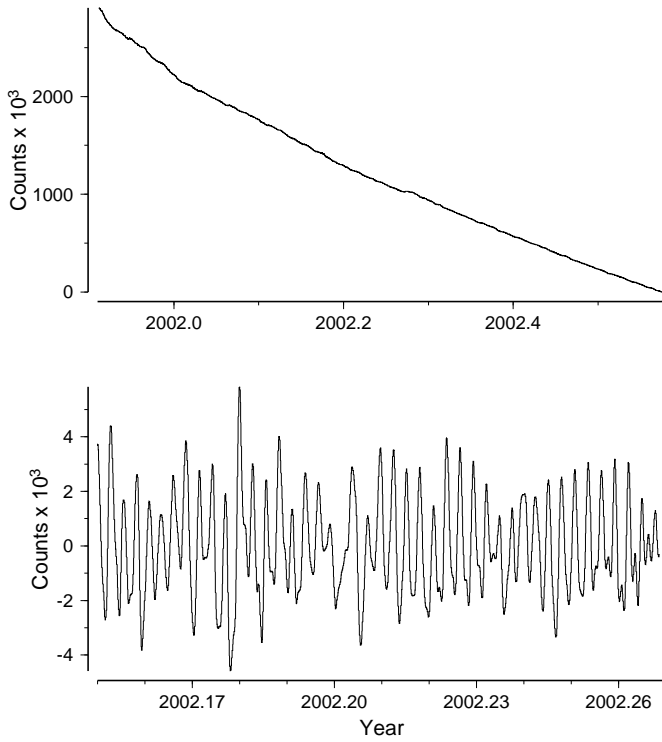


Figure 9.6: 100-second strainmeter data measured by Component 1 at OHLN, in instrumental counts. Top, 9-month timeseries with instrumental offsets due to reservoir resetting removed. Bottom, 1-month timeseries bandpass filtered at 0.5-2 day to show tidal strain signals. Note the different vertical scales.

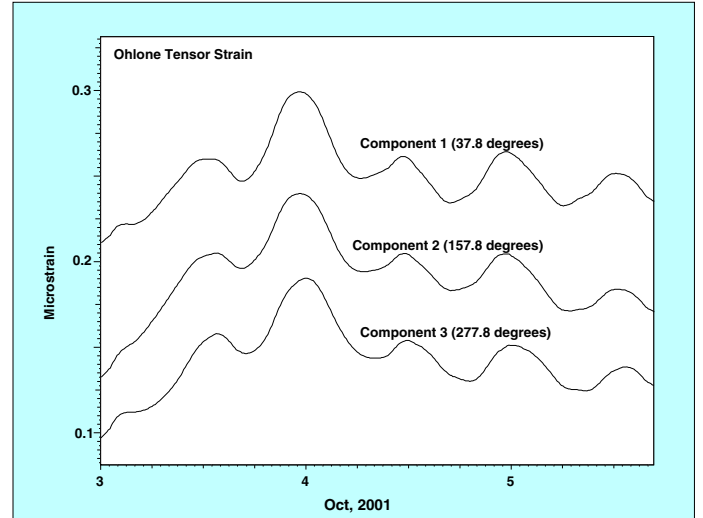


Figure 9.7: Three-component strainmeter data measured at OHLN, in microstrain. Tidal strain is used to calibrate the sensors, allowing instrument counts to be converted to microstrain. Figure courtesy M. Johnston (USGS).

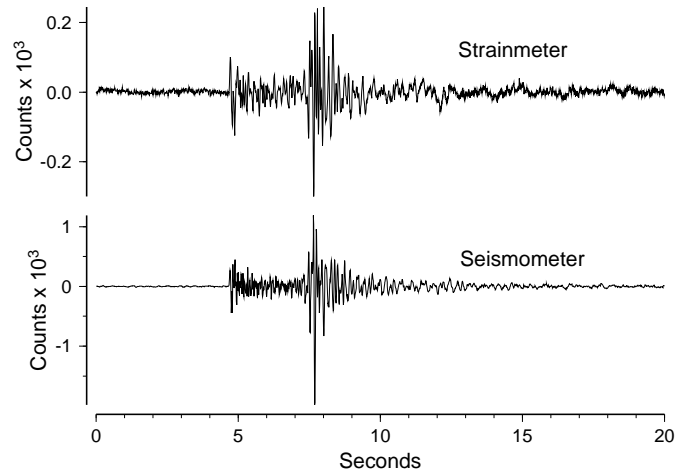


Figure 9.8: 100-Hz strainmeter and seismometer data measured at OHLN, in instrumental counts, showing response to a M=2.3 May 2002 earthquake within 15 km of the station. Seismometer is vertical component. Strainmeter is Component 1.

# Chapter 10

## Ocean Floor Broadband Station in Monterey Bay

### 1. Introduction

This is a collaborative project between the Monterey Bay Aquarium Research Institute (MBARI) and the BSL. Supported by funds from the Packard Foundation to MBARI, NSF/OCE funds and U.C. Berkeley funds to BSL, its goal is to install and operate a permanent seafloor broadband station as a first step towards extending the on-shore broadband seismic network in northern California, to the seaside of the North-America/Pacific plate boundary, providing better azimuthal coverage for regional earthquake and structure studies.

This project follows the 1997 MOISE experiment, in which a three component broadband system was deployed for a period of 3 months, 40 km off shore in Monterey Bay, with the help of MBARI's Point Lobos ship and ROV Ventana (Figure 10.1). MOISE was a cooperative program sponsored by MBARI, UC Berkeley and the INSU, Paris, France (*Stakes et al.*, 1998; *Romanowicz et al.*, 1998; *Stutzmann et al.*, 2001). During the MOISE experiment, valuable experience was gained on the technological aspects of such deployments, which contributed to the success of the present MOBB installation.

The successful MOBB deployment took place April 9-11, 2002 and the station is currently recording data autonomously. Eventually, it will be linked to the planned (and recently funded) MARS (Monterey Accelerated Research System; <http://www.mbari.org/mars/>) cable and provide real-time, continuous seismic data to be merged with the rest of the northern California real-time seismic system. The data are archived at the NCEDC, as part of the Berkeley Digital Seismic Network (BDSN).

### 2. Instrumentation

The ocean-bottom MOBB station currently comprises a three-component seismometer package, a current-meter, and a recording and battery package. A differential pressure gauge (DPG) with autonomous recording (e.g. *Cox et al.*, 1984) will be deployed in the vicinity of

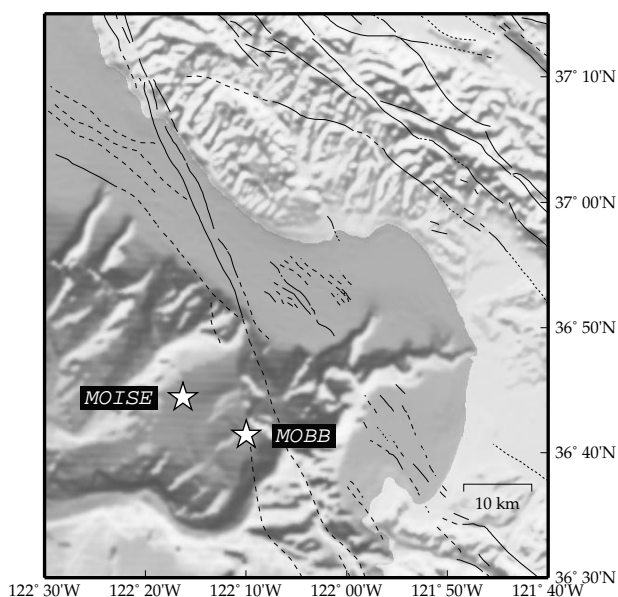


Figure 10.1: Location of the MOBB and MOIS stations in Monterey Bay, California, against safloor and land topography. Fault lines are from the California Geological Survey database. MOBB is located at 1000 m below sea-level.

the seismometer package during the next data recovery dive, in September 2002.

The seismic package contains a low-power (2.2W), three-component CMG-1T broadband seismometer system, built by Guralp, Inc., with a three-component 24-bit digitizer, a leveling system, and a precision clock. The seismometer package is mounted on a cylindrical titanium pressure vessel 54 cm in height and 41 cm in diameter, custom built by the MBARI team and outfitted for underwater connection.

Because of the extreme sensitivity of the seismometer, air movement within the pressure vessel must be minimized. In order to achieve this, after extensive testing at BSL (Chapter 11), the top of the pressure vessel was thermally isolated with two inches of insulating foam and reflective Mylar. The sides were then insulated with multiple layers of reflective Mylar space blanket, and the vessel was filled with argon gas.

The current-meter is a Falmouth Scientific 2D-ACM acoustic current meter. It is held by a small standalone fixture and measures the magnitude and direction of the currents about 1 meter above the seafloor.

The recording system is a GEOSense LP1 data logger with custom software designed to acquire and log digital data from the Guralp system and digital data from the current meter over RS-232 serial interfaces. The seismic data are sampled at 20 Hz and current-meter data at 1 Hz, and stored on a 3 GB, 2.5 in disk drive. All the electronics, including the seismometer and the current meter, are powered by a single 10kWh lithium battery.

### 3. Deployment

All installations were done using the MBARI ship Point Lobos and the ROV Ventana. Prior to the instrumentation deployment, the MBARI team manufactured and deployed a 1181 kg galvanized steel trawl-resistant bottom mount to house the recording and power systems, and installed a 53 cm diameter by 61 cm deep cylindrical PVC caisson to house the seismometer pressure vessel. The bottom mount for the recording system was placed about 11m away from the caisson to allow the future exchange of the recording and battery package without disturbing the seismometer. Prior to deployment, the seismometer package was tested extensively at BSL, then brought to MBARI where its internal clock drift was calibrated in the cold room against GPS time.

The actual deployment (04/09/02-04/11/02) occurred over 3 days. On the first dive, the seismometer package was lowered into the PVC caisson (Figure 10.2), and its connection cable brought to the site of the recording unit. On the second dive, the recording package was emplaced in its trawl-resistant mount, and connected to the seismometer package. Tiny (0.8 mm) glass beads were poured into the caisson until the seismometer was completely covered, to further isolate it from water circulation. The seismometer package is now buried at least 10 cm under the seafloor level. On the third dive, the ROV buried the cable between the seismometer and recording packages, then connected to the seismometer through the recording system, levelled and recentered the seismometer and verified that it was operational. The current-meter was also installed and connected to the recording system.

On April 22nd, the ROV returned to the MOBB site to



Figure 10.2: Installation of the seismometer package inside the PVC caisson. This was later completely covered by glass beads

check the functioning of the seismometer and recording system. Some slight settling of the seismometer pressure vessel had occurred, and so the seismometer was commanded to recenter electronically. Over 3 MB of data were then downloaded from the recording system over a period of about two and a half hours, including the recordings of two regional earthquakes in California and two teleseismic events that occurred in Guerrero, Mexico and in Northern Chile.

The site was revisited two months later, on June 27th, to check the functioning of the system and replace the data recording and battery module, in the first of a series of such dives planned for the next 3 years. The following functions were performed:

1. Disconnected the current meter and seismometer from old data logger frame
2. Removed old data logger from from the trawl-resistant mount.
3. Installed new data logger frame in the trawl-resistant mount.
4. Connected the current meter to the new data logger frame.
5. Connected the ROV to the new data logger frame, and verified that the data logger was alive.
6. Connected the seismometer to the new data logger frame, and watched it reboot.
7. Centered the seismometer.
8. Turned on auto-centering on the seismometer.
9. Verified that the Guralp was seeing the GPS clock signals (NMEA time messages and pulse per second), and recorded the clock offset. During this dive, the Guralp clock was not resynchronized to GPS time.
10. Brought the old data logger frame with data logger and batteries back to the ship.

During two months of recording, many regional and teleseismic events were recorded. These data have just

started being analyzed. The plan is to revisit the site every three months to replace the data recording and battery module. Between each dive, improvements to the data acquisition software can be made. During each visit, the seismometers can be recentered, and the clock resynchronized to GPS time. Eventually, the data recording package will be plugged into the MARS cable, enabling continuous real-time data acquisition on land.

## 4. Examples of data

First, we show in Figure 10.3, the horizontal component tilt signal obtained from the seismometer mass position channels (MME, MMN). These data indicate that the seismometer package has been experiencing an exponentially decaying tilt in a south-southwesterly direction, which is also the down slope direction (e.g. Figure 10.1). The large step on day 112 (04/22/02) was caused by recentering, when the instrument was checked 12 days after installation. The small step on day 134 (05/14/02) is coincident with the occurrence of a  $M_w$  4.96 earthquake which occurred 5 km N59W of MOBB on the San Andreas fault near the town of Gilroy. The instruments were recentered again on day 178 (06/27/02), and, with the gradual settling of the package, we expect that the subsequent tilt decay will take at least two months to reach saturation (which it did between days 161-178 on the MMN component), in time for the next planned dive and recentering operation. On the MMZ component, the semidiurnal gravitational tide is visible, riding on the tilt signal. This signal has been detrended with a 2 day running average and the scale was expanded to emphasize the fortnightly beating of the semidiurnal gravitational tides. As with the horizontal components, the largest signals are associated with rapid changes in the second derivative of the tilt, caused by recentering or by significant ground shaking (day 134).

Figures 10.4 and 10.5 show a component by component comparison of the recording of the 04/26/02  $M_w$  7.1 teleseism in the Mariana Islands at MOBB and 3 nearby stations of the BDSN. In Figure 10.5, only the P-wave portion of the seismograms is displayed. The comparison shows consistency between the recordings of MOBB and nearby stations. On the horizontal components, there appears to be some signal-generated noise following the S waves and the Love wave, which is likely associated with ringing in the shallow mud layers. It is less apparent in the P waves in the pass-band shown, however at higher frequency the P wave shows a 3 min long coda. Such observations should be helpful in understanding the triggering of submarine landslides in strong motion events, and may be relevant for ocean floor structures such as oil platforms and pipelines. On the other hand, this type of noise may be unavoidable in a shallow buried installation. Our plan is to evaluate it further and investigate

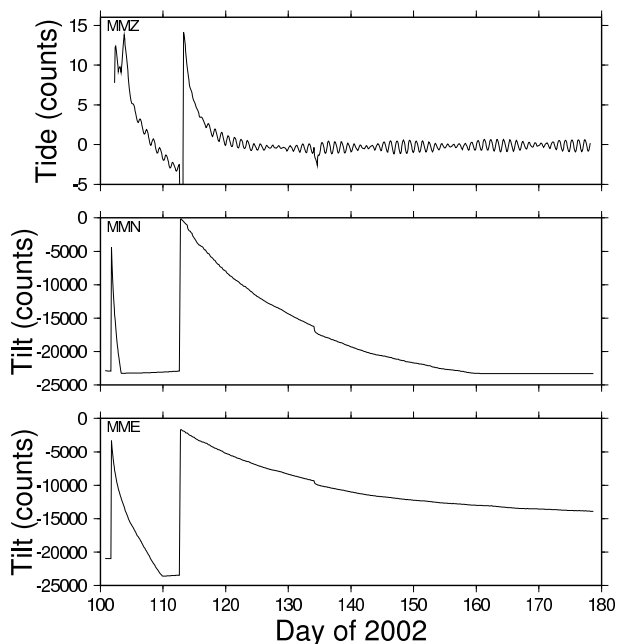


Figure 10.3: Mass position data for the time period 04/11/02-06/27/02. The large steps are associated with: 1) installation (day 100); 2) recentering (day 112), and a smaller step with a local  $M_w$  4.95 earthquake on day 134. The tide signal is clearly visible on the vertical component.

ways to suppress it by modelling and post-processing.

To further demonstrate the consistency of the MOBB data, we also show the results of a single station moment tensor inversion using only MOBB, and the comparison of the corresponding synthetic predictions with the actual data at the four other BDSN stations, for a  $M_w$  3.63 regional event which occurred on 04/23/02 on the San Andreas fault at a distance of 53.4 km from MOBB. The single station solution results in nearly identical focal mechanisms, but a slightly larger CLVD component and scalar moment, which is not unlike other single station inversions (Figure 10.6).

We plan to systematically analyze MOBB data acquired over the next year to assess the data quality and possible improvements, through post-processing and/or installation adjustments. We plan to evaluate the long term time evolution of background noise, as the system continues to settle and stabilize, and the shorter term noise fluctuations in relation to tides and currents as recorder by the current-meter (e.g. Figure 10.7) as well as the DPG (after the installation of the DPG in September 02). Since the auxiliary data are sampled at sufficiently high rates (1 sps) compared to what was available for the MOISE experiment, we will be able to investigate ways to reduce the background noise correlated with the pressure and current data at periods longer than 10 sec.

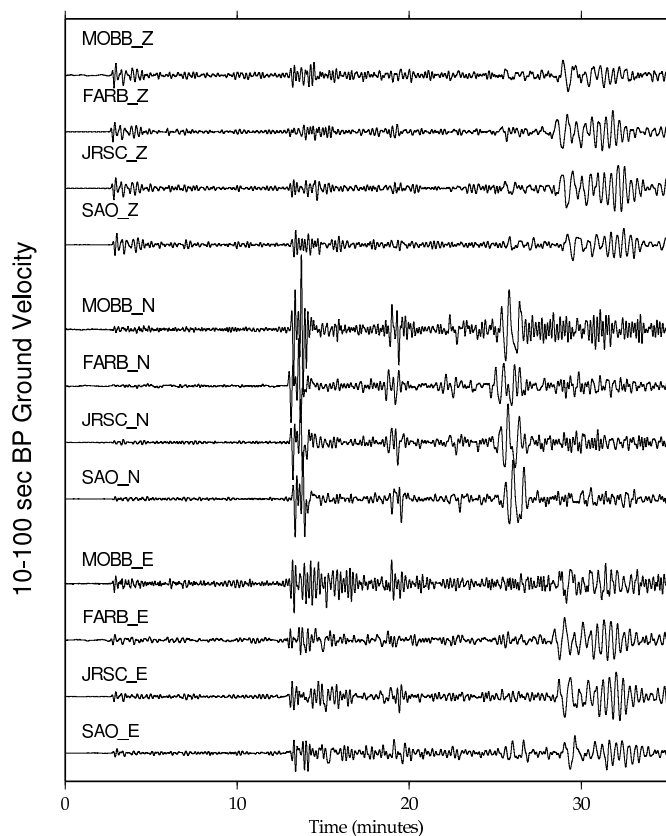


Figure 10.4: Comparison of vertical, N and E component records of the 04/26/02  $M_w$  7.1 Mariana earthquake (depth = 85.7 km, distance =  $85.2^\circ$ , azimuth =  $283^\circ$  from MOBB, at MOBB and 3 stations of the BDSN. The records have been band-pass filtered between 10-100 sec.

## 5. Acknowledgements

MOBB is a collaboration between the BSL and MBARI, involving Barbara Romanowicz, Bob Uhrhammer, and Doug Neuhauser from the BSL and Debra Stakes and Paul McGill from MBARI. The MBARI team also includes Steve Etchemendy (Director of Marine Operations), Jon Erickson, John Ferreira, Tony Ramirez and Craig Dawe.

The MOBB effort at the BSL is supported by funds from NSF/OCE and UC Berkeley.

## 6. References

Cox, C., T. Deaton and S. Webb, A deep-sea differential pressure gauge, *J. Atm. Ocean. Tech.*, 1, 237-245, 1984.

Romanowicz, B., D. Stakes, J. P. Montagner, P. Tarits, R. Uhrhammer. M. Begnaud, E. Stutzmann, M. Pasyanos, J.F. Karczewski, S. Etchemendy, MOISE: A pilot experiment towards long term Sea-floor geophysical

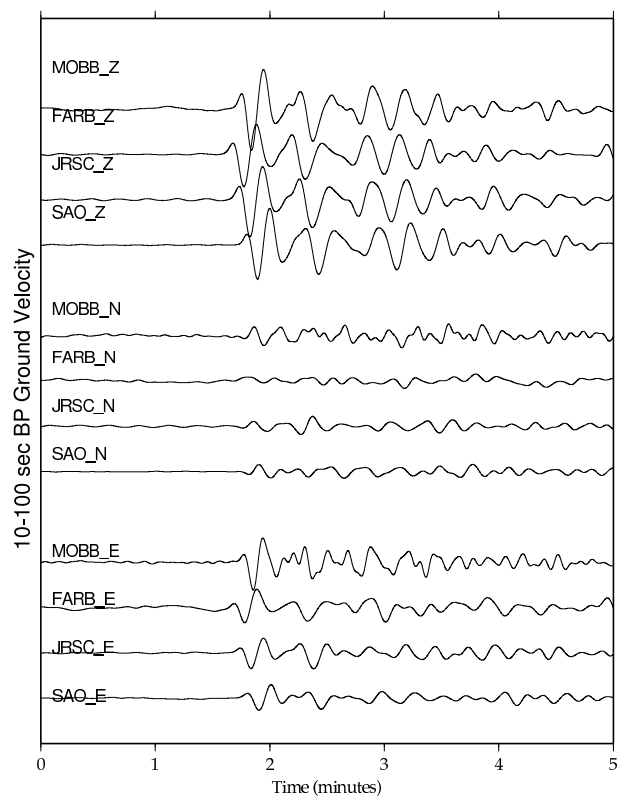


Figure 10.5: Same as Figure 10.4, zoomed in on the P wave portion of the seismograms

observatories, *Earth Planets Space*, 50, 927-937, 1999.

Stakes, D., B. Romanowicz, J.P. Montagner, P. Tarits, J.F. Karczewski, S. Etchemendy, D. Neuhauser, P. McGill, J-C. Koenig, J.Savary, M. Begnaud and M. Pasyanos, MOISE: Monterey Bay Ocean Bottom International Seismic Experiment, *EOS Trans., A.G.U.*, 79, 301-309, 1998.

Stutzmann, E., J.P. Montagner et al., MOISE: a prototype multiparameter ocean-bottom station, *Bull. Seism. Soc. Am.*, 81, 885-902, 2001.

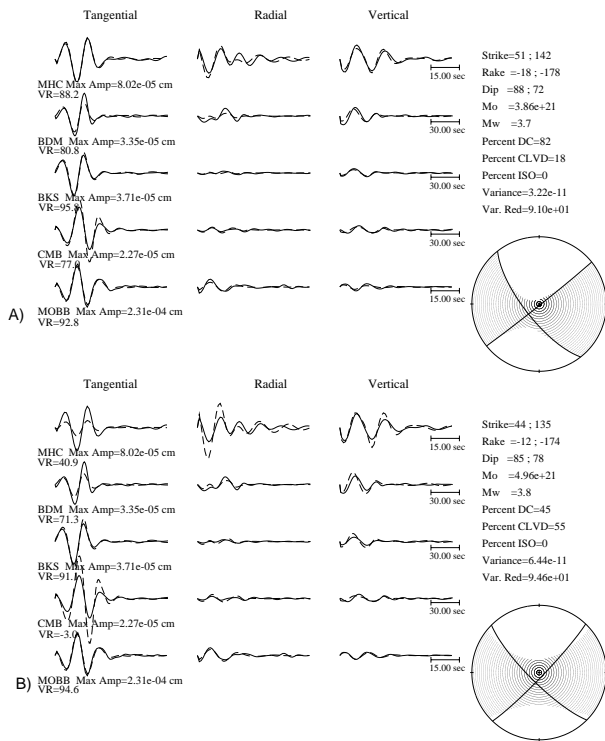


Figure 10.6: Results of moment tensor inversions for the M 3.63 regional event shown in Figure 10. Top: inversion using 4 stations of the BDSN and MOBB (BDM, BKS, and CMB are bandpassed between 0.02 and 0.05Hz; MHC and MOBB, between 0.05 and 0.10Hz). Bottom: results of inversion using only MOBB, showing the good fits of the single station solution to the other BDSN data. Courtesy of D. Dreger.

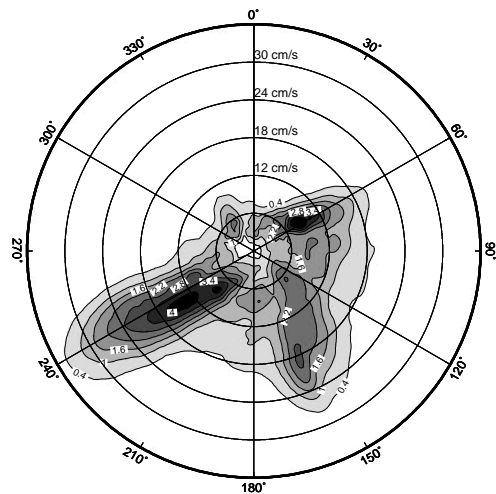


Figure 10.7: Distribution of currently available current velocity data as a function of azimuth. The contour label units are fractions of the average density distribution of the current. The two dominant maxima (centered at  $60^\circ$  and  $240^\circ$ , i.e. orthogonal to the continental shelf) are associated with the semi-diurnal tidal currents. The third directional peak is roughly parallel to the coastline and appears to be related to the dominant ocean circulation.

# Chapter 11

## Data Acquisition and Quality Control

### 1. Introduction

Stations from nearly all networks operated by the BSL transmit data continuously to the BSL facilities on the UC Berkeley campus for analysis and archive. In this chapter, we describe activities and facilities which cross-cut the individual networks described in Chapters 4 - 10, including the facilities in McCone Hall, procedures for data acquisition and quality control, sensor testing capabilities and procedures, and a collaborative experiment in early warning.

While some of these activities are continuous from year to year, we have identified changes or activities which are specific to 2001-2002.

### 2. McCone Hall Facilities

The routine data acquisition, processing, and archiving activities of the BSL are carried out in McCone Hall. The BSL facilities in McCone are designed to provide air conditioning, 100-bit switched network, and reliable power with UPS and generator.

Because of the mission-critical nature of the automated earthquake processing, most computer systems operated by the BSL run on circuits with both UPS and generator power. Air conditioning is provided through both "building air" and a separate room AC unit.

Over the years, the BSL has experienced problems with the McCone generator system, including a failure in 1999 due to a combination of a weakened power system and a leak in the water pump.

#### 2.1 March 7th Power outage

On March 7, 2002, a campus-wide power outage occurred when moisture seeped into a UC Berkeley electric substation. The power failed a few minutes before 5:00 PM local time. BSL staff immediately noticed that the McCone generator failed to start (and the BKS generator as well). Phone calls were made to Physical Plant and Campus Services (PPCS), but the extended nature of the outage prevented PPCS staff from responding for over two hours.

During this time, BSL staff made several attempts to bring the McCone generator online. The initial failure of the generator was traced to a weak battery. When BSL staff replaced the battery, the generator started up and then shut itself off after several minutes, due to a leak in the water pump.

As a result of the failure of the generator, the BSL earthquake monitoring system went off the air around 5:30 PM when the UPS system shut down due to a low battery condition (the UPS is designed to carry the electrical load until the generator comes online). A subset of critical computers were brought back online when a personal generator belonging to Bob Uhrhammer was brought in around 8:00 PM. A temporary fix to the generator was provided by PPCS around 8:30 PM, which allowed the rest of the processing system to be restored. The generator was not fully repaired until March 26th, 19 days after the power outage.

The failure of the McCone generator was due to poor maintenance. Similar to the situation in 1999, it failed due to problems in the power system combined with a leak in the water pump. The BSL is working with PPCS to establish a routine of regular load tests, which should improve screening for problems such as this, as well as working with other groups to relocate the critical activities to more robust campus facilities.

The failure of the generator at Byerly Vault was traced to PPCS error. The generator had been left in a mode where it would not automatically start when power was lost. A BSL staff member went up to Byerly during the power outage and brought the generator online.

#### 2.2 New facilities

The BSL is actively working with the campus to relocate the critical operations of data acquisition, processing, archiving, and distribution to a more robust facility. With assistance from the Office of the Vice Chancellor for Research, the BSL has been granted space in a building currently under construction. The building is designed to current codes and has been given special attention for post-earthquake operations. Anticipated occupancy is in FY 2004-2005.

### 3. Data acquisition

Central-site data acquisition for the BDSN/NHFN/MPBO is performed by two computer systems located at the BSL (Figure 11.1). These acquisition systems are also used for the Parkfield-Hollister electromagnetic array and for the BARD network. A third system is used primarily as data exchange system with the USNSN receives a feed from CMB, MOD, SAO, and WDC from the the NSN VSAT. This system transmits data to the USNSN from HOPS, CMB, SAO, WDC, and YBH. Data acquisition for the HRSN follows a more complicated path, as described in Chapter 6.

Data acquisition and communication with the Quanterra data loggers depends both on the software on the recording systems and at the central site.

#### 3.1 MultiSHEAR

In late 1998, Quanterra provided the first release of MultiSHEAR, an enhanced version of its data acquisition software that was year 2000 compliant, and updated components of the OS/9 operating system to address the year 2000 problem. MultiSHEAR contained a number of enhancements, especially in the area of multi-site data collection, and introduced a totally new configuration procedure. The BSL worked with Quanterra during 1999 to enhance the configuration procedures to address the diverse needs of the BDSN and HFN station configurations. During November and December 1999, all of the BSL Quanterra data loggers were updated to MultiSHEAR with the corresponding OS/9 modifications, which addressed the year 2000 problems.

The two significant features of MultiSHEAR that affected the BSL were the correction of a systematic timing error of the decimated channels from SHEAR and UltraSHEAR software in the Quanterra data logger (previously described in the 1999-2000 and 2000-2001 Annual Reports), and the addition of multi-site data collection.

The BSL will use this multi-site data collection feature to create "hub" systems, which will acquire, store, and transmit data from several remote data loggers as well as the hub's own data. The San Francisco/Oakland Bay Bridge network will consist of two Quanterra 4120 hubs (Figure 11.2), each of which will acquire data from its own digitizers as well data from three remote diskless Quanterra Q730 systems. Each hub will provide local storage for all four sites, and will transmit the real-time the data from all four sites to the BSL over a 512Kb spread spectrum radio. The BSL developed the initial MultiSHEAR hub configuration procedure, and worked with Quanterra to refine and test the hub configurations.

#### 3.2 Comserv

The BSL uses the `comserv` program for central data acquisition, which was developed by Quanterra. The

`comserv` program receives data from a remote Quanterra data logger, and redistributes the data to one or more `comserv` client programs. The `comserv` clients used by REDI include `datalog`, which writes the data to disk files for archival purposes, `cdafill`, which writes the data to the shared memory region for REDI analysis, and other programs such as the seismic alarm process, the DAC480 system, and the feed for the Memento Mori Web page (Figure 11.3).

The two computers that perform data acquisition also serve as REDI processing systems. In order to facilitate REDI processing, each system maintains a shared memory region that contains the most recent 30 minutes of data for each channel used by the REDI analysis system. All REDI analysis routines first attempt to use data in the shared memory region, and will only revert to retrieving data from disk files if the requested data is unavailable in the shared memory region.

Most stations transmit data to only one or the other of the two REDI systems. The `comserv` client program `cs2m` receives data from a `comserv` and multicasts the data over a private ethernet. The program `mcast`, a modified version of Quanterra's `comserv` program, receives the multicast data from `cs2m`, and provides a `comserv`-like interface to local `comserv` clients. This allows each REDI system to have a `comserv` server for every station.

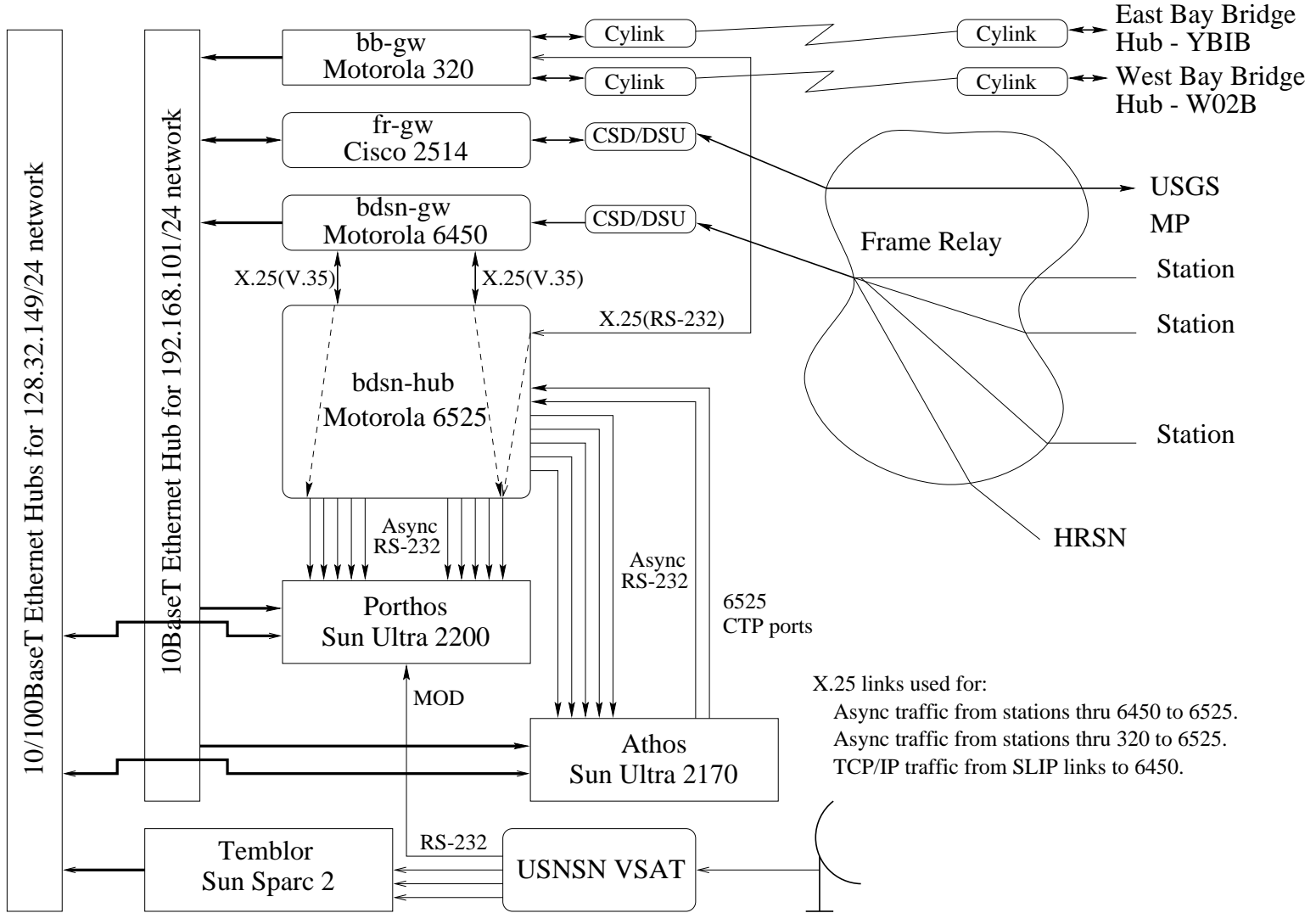
We have extended the multicasting approach to handle data received from other networks such as the NCSN and UNR. These data are received by Earthworm data exchange programs, and are then converted to MiniSEED and multicast in the same manner as the BSL data. We use `mserv` on both REDI computers to receive the multicast data, and handle it in an identical fashion to the BSL MiniSEED data.

### 4. Seismic Noise Analysis

BSL seismic data are routinely monitored for state-of-health. An automated analysis is computed weekly to characterize the seismic noise level recorded by each broadband seismometer. The estimation of the Power Spectral Density (PSD) of the ground motion recorded at a seismic station, provides an objective measure of background seismic noise characteristics over a wide range of frequencies. When used routinely, the PSD algorithm also provides an objective measure of seasonal and secular variation in the noise characteristics and aids in the early diagnoses of instrumental problems. A PSD estimation algorithm was developed in the early 1990's at the BSL for characterizing the background seismic noise and as a tool for quality control. As presently implemented, the algorithm sends the results via email to the engineering and some research staff members and generates a bargraph output which compares all the BDSN broadband stations by components. A summary of the

# BDSN and REDI Telemetry and Data Flow

2001/08/29



X.25 links used for:  
 Async traffic from stations thru 6450 to 6525.  
 Async traffic from stations thru 320 to 6525.  
 TCP/IP traffic from SLIP links to 6450.

Figure 11.1: Data flow from the BDSN, NHFN, MPPBO, HRSN, and BARD network into the BSL central processing facility.

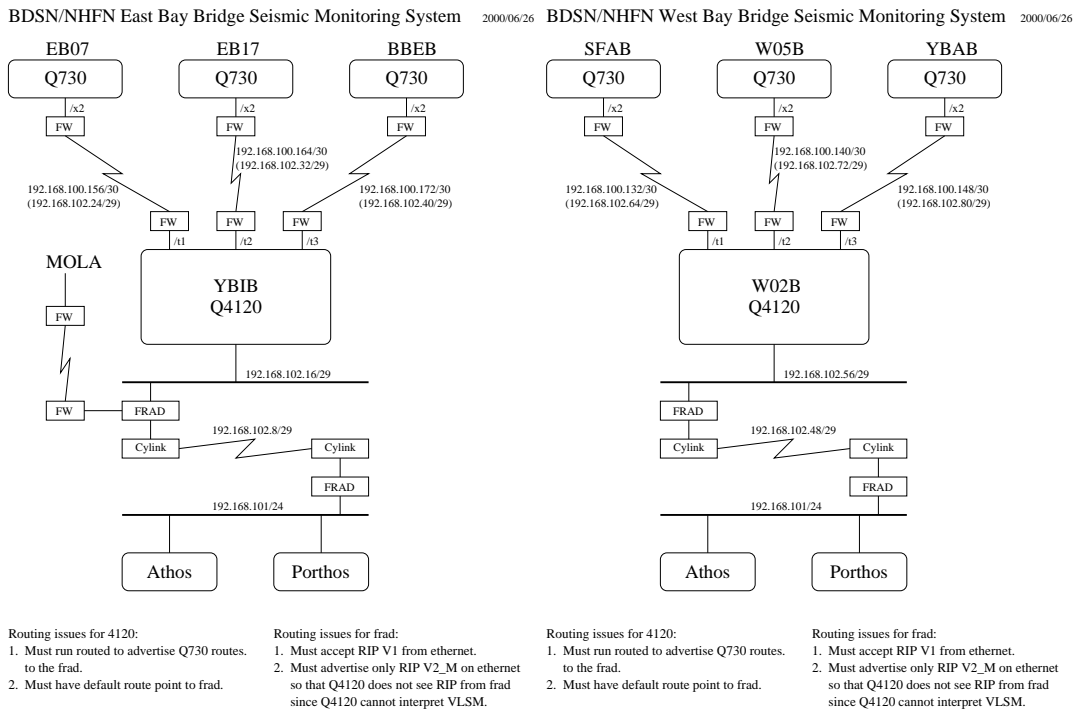


Figure 11.2: Planned data flow from the East and West Bay Bridge seismic monitoring hubs.

results for 2001-2002 is displayed in Figure 4.3.

Last year, we expanded our use of the weekly PSD results to monitor trends in the noise level at each station. In addition to the weekly bar graph, additional figures showing the analysis for the current year are produced. These cumulative PSD plots are generated for each station and show the noise level in 5 frequency bands for the broadband channels. These cumulative plots make it easier to spot certain problems, such as failure of a sensor. In addition to the station-based plots, a summary plot for each channel is produced, comparing all stations. These figures are presented as part of a noise analysis of the BDSN on the WWW at <http://www.seismo.berkeley.edu/seismo/bdsn/psd/>.

The PSD algorithm has been documented in previous annual reports. As reported in the past, this tool was originally written in Fortran and recently converted to C using the f2c utility in response to interest from the community. However, the resulting code was impenetrable. As a result, a BSL undergraduate, Steve Chu, worked with Bob Uhrhammer in the spring of 2002 to write the code in C.

## 5. Sensor Testing Facility

### 5.1 Introduction

The BSL has set up an instrumentation test facility in the Byerly Seismographic Vault in order to systemati-

cally determine and to compare the characteristics of up to eight sensors at a time. The test equipment consists of an eight-channel Quanterra Q4120 high-resolution data logger and a custom interconnect panel that provides isolated power and preamplification when required to facilitate the connection and routing of signals from the sensors to the data logger with shielded signal lines. Upon acquisition of the 100 samples-per-second (sps) data from the instruments under test, PSD analysis and spectral phase coherency analysis are used to characterize and compare the performance of each sensor. Tilt tests and seismic signals with a sufficient signal level above the background seismic noise are also used to verify the absolute calibration of the sensors. A simple vertical shake table is used to access the linearity of a seismic sensor.

### 5.2 Background

BSL personnel have tested numerous sensors during the past several years and each test has been *ad hoc* in its implementation and execution. In order to expedite the setup and testing of the instruments for both BSL in-house use and well as for other groups, such as IRIS, we dedicated an eight-channel Quanterra Q4120 data logger (see Figure 11.4) and constructed cabling and a patch panel (see Figure 11.5) to enable the simultaneous testing of up to eight sensors with high (24-bit integer) resolution sampling at 100 samples per second (for a usable bandwidth of 0-32 Hz). We housed the test equip-

# REDI Data Acquisition and Data Flow

2001/03/19

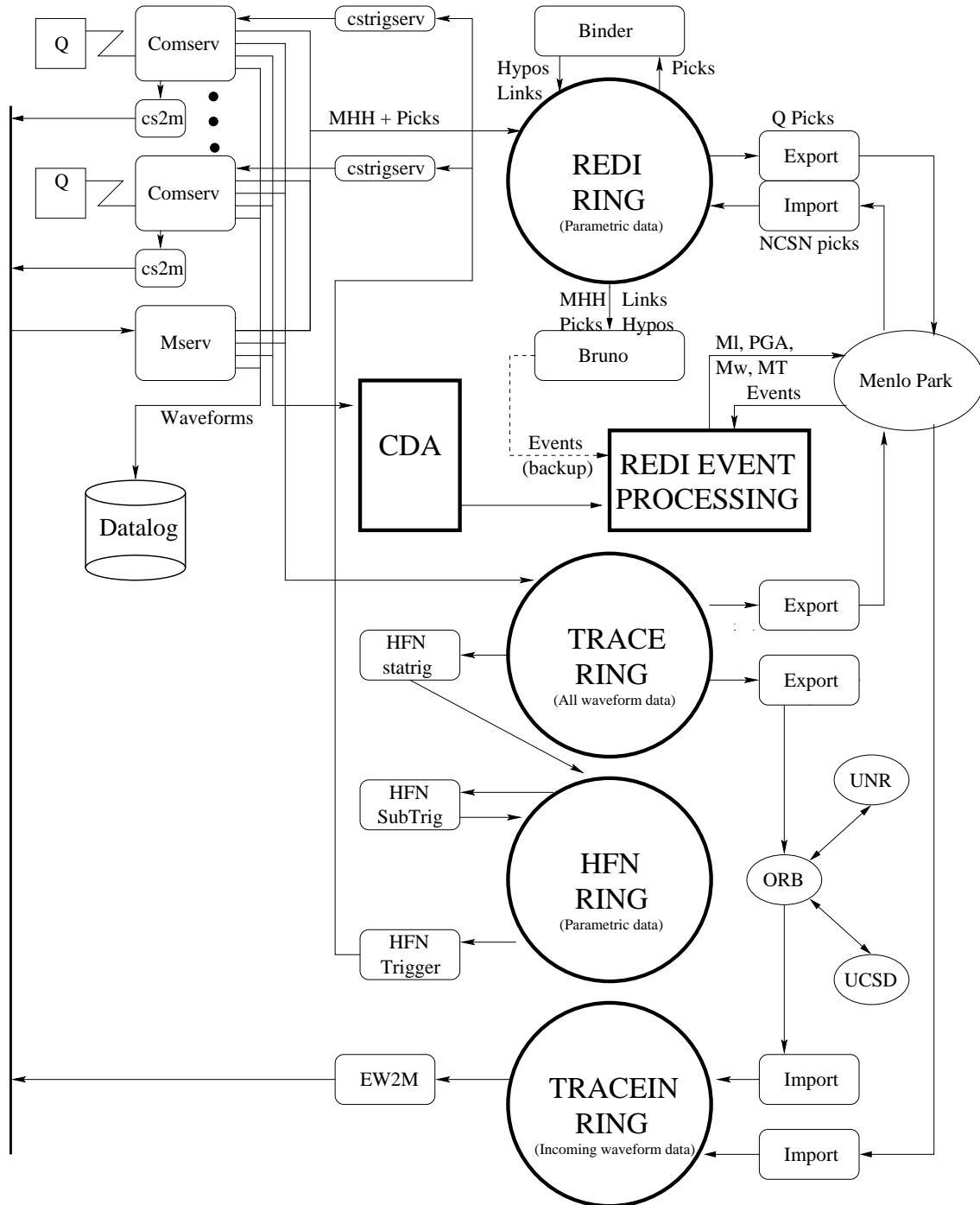


Figure 11.3: Dataflow in the REDI processing environment, showing waveform data coming in from the Quanterra data loggers (Q) into *comserv*. From *comserv*, data are logged to disk (via *datalog*), distributed to other computers (*mserv*), fed into the CDA for REDI processing, and spooled into a tracing for export.



Figure 11.4: Quanterra Q4120 data logger (lower left) that records the data from the instruments undergoing testing in the Byerly Vault.

ment in the Byerly Seismographic Vault, located in an old mining drift in the Claremont shales and cherts formation in Strawberry Canyon behind the Botanical Garden. The Byerly Seismographic Vault is ideal for a test facility because it is seismically quieter than the BSL facilities on the Berkeley campus, it has all the necessary infrastructure, and because the BDSN station BKS, housed in the same vault, includes a set of Streckeisen STS-1 broadband seismometers and a Kinemetrics FBA-23 strong motion accelerometer which provide reference seismic recordings of the ground motion.



Figure 11.5: Interconnecting patch panel (top center) which routes the signals from the sensors under test (lower left and STS-2 reference sensor center right) to the Q4120 data logger.

### 5.3 Sensor Testing Methodology

Sensor testing has three aspects: 1) data acquisition; 2) sensor calibration; and, 3) sensor performance.

The acquisition of high resolution digital data is absolutely essential for the testing of modern sensors. The Quanterra Q4120 data logger, which has 24-bit integer resolution (144 dB dynamic range) with a LSB of  $2.38 \mu\text{V}$  and a 40 V P-P signal handling capability, is ideally suited for this task. Data acquisition has two modes, active and passive. In the active acquisition mode, a signal is induced by appropriate means as described below. In the passive acquisition mode, the sensors signals are recorded for extended periods of time, typically from a day or so to a couple of weeks or more, to acquire samples of both the background noise level as well as various natural seismic, gravitational tide, and atmospheric signals.

The calibration methodology employed is sensor dependent. In the case of broadband seismometers, induced tilting, dynamic shaking, dynamic driving of a calibration coil, the gravitational tide signal, and comparison with ground motions inferred from known sensors are used as appropriate. In the case of strong motion accelerometers, induced tilting, dynamic shaking, and comparison with ground motions inferred from known sensors are used as appropriate. In the case of barometric pressure sensors, static elevation changes and comparison with the atmospheric pressure inferred from known sensors are used as appropriate.

Performance of a sensor is primarily characterized by determining the usable dynamic range, the linearity, and the noise characteristics. The usable dynamic range is the difference, usually expressed in dB, between the sensor saturation signal level and the sensor or background noise level. The usable dynamic range is usually frequency dependent. Characterization of the linearity and dynamic range of a broadband seismic sensor is problematic because seismic signals are a wide bandwidth transient phenomena (see the linearity and dynamic range section below). The linearity is characterized by determining the third-order intercept point. The usable dynamic range is quantified by the difference between the sensor saturation (full scale) signal level and the background signal or sensor noise floor and it is usually expressed in dB. PSD estimates of the background seismic (or sensor self noise), plotted as a function of frequency, are used to concisely quantify the performance of a broadband sensor (and also to quantify differences in the noise levels observed in various seismic vaults housing broadband seismic sensors). Another approach for characterizing the bandwidth and performance of a particular type of sensor is to simultaneously record two identical sensors placed on the same pier and calculate the phase coherency of their outputs as a function of frequency.

All of the above approaches to sensor testing have been

employed in our analysis during the past year.



Figure 11.6: Simple vertical shake table, constructed using a Johnson-Matheson Model 6840 short-period seismometer, with a PMD sensor mounted on top of the shake table for testing.

#### 5.4 Shake Table

The problem of how to shake the seismic sensors in order to test the linearity was solved by constructing a vertical component shake table from a Johnson-Matheson (J-M) Model 6840 short-period vertical seismometer as shown in Figure 11.6. The large and stiff suspension of the J-M was ideally suited for modification to a simple shake table. A platform to hold the sensor and extra springs to support the additional weight were added to the J-M seismometer so that vertical shaking could be induced by actively driving the J-M signal coil at relatively low current levels. The natural frequency of the resulting shake table was  $\sim 1.6$  Hz. We found that the

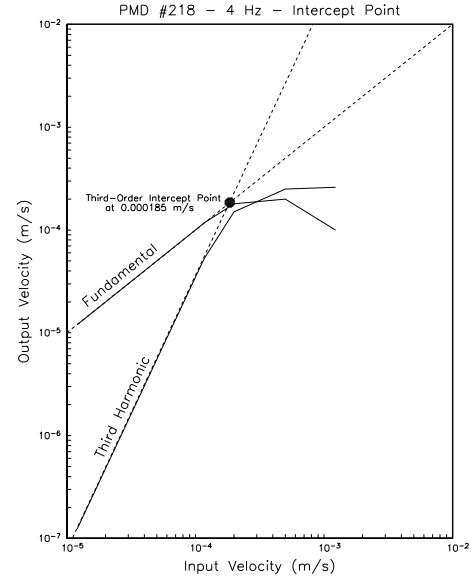


Figure 11.7: Third-order intercept point plot for PMD sensor, measured at 4 Hz.

shake table could be driven over a useful range of  $\sim 50$  dB, from  $\sim 3.4 \times 10^{-6}$  m rms (limited by the background noise PSD level of  $\sim -136$  dB at BKS) to  $\sim 10^{-3}$  m rms (limited by the shake table suspension travel), and over a 0.2-5 Hz frequency range by driving the signal coil sinusoidally with a WaveTek function generator. Vertical and horizontal Wilcoxon 731A accelerometers are attached to the housing of the sensor under test to directly measure the amplitude and spectral characteristics of the induced shaking for reference to output of test sensor. The table and sensor were arranged so that their center of mass was on the center line of the J-M suspension axis in order to minimize cross axis coupling.

#### 5.5 Linearity and Dynamic Range

Characterization of the linearity and dynamic range of a broadband seismic sensor is problematic because seismic signals are a wide bandwidth transient phenomena while typical linearity tests utilize a narrow bandwidth continuous signal. One figure of merit that is indicative of the quality with which a seismic sensor can record the ground motion signal is Total Harmonic Distortion (THD). The THD, in percent, is defined as:

$$THD = 100 \frac{\sqrt{\sum_{k=2}^N a_k^2}}{a_1}$$

where:  $a_1$  is the rms level of the fundamental drive signal and the  $a_k$  are the rms levels of the harmonics that result from non-linear processes in the seismic sensor. Given the difficulties in reliably determining the sum

of the  $a_k$ 's, we opted to measure instead the size of the third-order harmonic ( $a_3$ ) as a function of the sinusoidal drive signal ( $a_1$ ) and to determine the third-order intercept point. The third-order intercept point, i.e. the projected asymptotic point at which the fundamental and third harmonic signal levels are equal in amplitude, provides a useful figure of merit for the quality of a ground motion signal recorded by a seismic sensor. The methodology for determining the third-order intercept point is shown in Figure 11.7 for a PMD sensor where the fundamental and third harmonic output velocities are plotted as a function of the sinusoidal input velocity at a given frequency. Asymptotes are drawn through the fundamental and third harmonic slopes and their intersection is the third-order intercept point.

## 6. Sensor testing in 2001-2002

### 6.1 Guralp CMG-1T Ocean Bottom Seismometer

Prior to deployment of the Guralp CMG-1TD OBS (Serial Number T1045) sensor package (Figure 11.8) on the ocean floor in Monterey Bay (MOBB - Chapter 10), we did extensive testing to verify the operation of the seismometers and the wide range leveling system (Figure 11.9), to verify the calibration of the seismometer, to determine the drift rate of the OBS clock, to characterize the background noise PSD performance of the seismometers and to calibrate the magnetometer used to determine the sensor orientation on the ocean floor.

The testing of the OBS system in the Byerly Seismographic Vault (BKS) started on 2 November with the arrival and installation of the CMG-1TD seismometer and learning the commands for unlocking, centering and checking the status of the seismometers. We determined then that the internal flux gate magnetometer was not operating properly. The test data from the CMG-1TD was telemetered to McCone Hall via a frame relay serial port. A plastic garbage can was placed over the CMG-1TD to keep dust and breezes off of the exposed sensors and electronics.

On 14 December, Cansun Guralp visited BSL to replace the flux gate magnetometer and determine the offset of the CMG-1TD internal clock. The new magnetometer was calibrated using a Guralp-supplied turntable. The Garmin GPS receiver was connected to the CMG-1TD to check the clock offset and, based on the software reports, it appears that the CMG-1TD internal clock was 18-19 msec faster than the GPS clock. We verified the offset by connecting a 1 PPM signal (generated by external diagnostics board from Guralp's Garmin GPS receiver) into the Guralp Z digitizer, in place of the Z component seismometer and observed the same 18-19 msec difference.

During January, the CMG-1TD was operated contin-



Figure 11.8: Photo of the Guralp CMG-1TD Serial Number T1045 seismometer in the Byerly Vault (BKS). Shown are the various circuit boards on the sides and the top of the sensor package. Three of the nine batteries used by the leveling system are on the left front and the system clock is on the circuit board on the right. The seismometers are in the mu metal shielded container mounted on leveling gimbals in the center.



Figure 11.9: Photo taken after the seismometers were leveled with the base tilted in order to verify the operation of the wide range leveling system. Given the extreme tilt sensitivity of the CMG-1TD's 360 second pendulums, the leveling system is crucial for successful operation on the ocean floor. Note that the central gimbal system containing the seismometers is tilted relative to the outside frame.

uously and the ground motions, inferred from the CMG-1TD and from the STS-1's operating at BKS, were compared for some large teleseisms and regional earthquakes and we verified that the transfer function of the CMG-1TD was correct. However background noise PSD analysis showed that the Z component of the CMG-1TD was very noisy at periods longer than 10 seconds, as shown in Figure 11.10. The high noise level observed on the CMG-1TD vertical component is most likely caused by air circulation around the seismometer and the noise is expected to decrease significantly when the CMG-1TD is installed in the pressure vessel. During this time it was also determined that the CMG-1TD internal clock drift rate is  $-236.59 \pm 1.98$  microseconds/day.

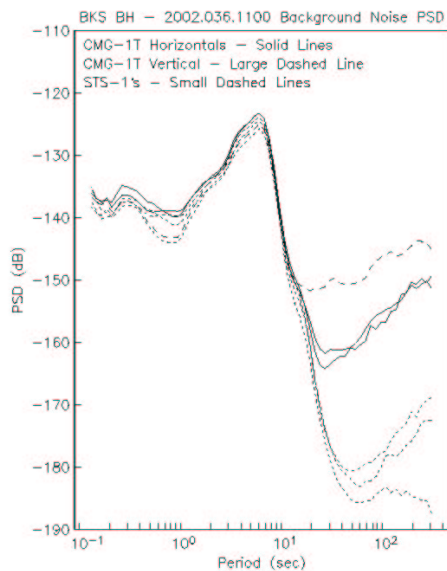


Figure 11.10: Comparison of typical background noise PSD levels observed by the CMG-1TD and the co-sited STS-1 in the BKS vault. The large dashed line and the solid lines are the Z component and horizontal component PSD's, respectively, and the small dashed lines are the STS-1 PSD's.

The CMG-1TD was installed in the titanium pressure vessel on 30 January and the pressure vessel was placed on a bed of sand as shown in Figure 11.11. Subsequent background noise PSD analysis indicated that the CMG-1TD vertical component was still very noisy at periods longer than 10 seconds. Communication with Guralp suggested several possible causes for the observed long-period noise: 1) the sand may be creaking under the weight of the pressure vessel and seismometer; 2) one or more of the calibration relays may have been left in the

cal-enable position at boot-up; 3) the air inside the pressure vessel may be convecting; or 4) something is amiss with the Z component seismometer. Tests subsequently ruled out the sand creaking and the calibration relays as the source of the problem.



Figure 11.11: Photo of the titanium pressure vessel resting on a  $\sim 1$  cm thick bed of kiln dried fine sand on the concrete pier.

In a one week interval, starting on 26 February, a series of tests were done to determine their effect on the CMG-1TD background noise PSD level. The first test was to construct and install a baffle and insulating sleeve around and over the seismometer inside the pressure vessel as shown in Figure 11.12. The result was that background noise PSD at periods longer than  $\sim 10$  seconds decreased by  $\sim 17$  dB on the Z component. This is evidence that the air inside the pressure vessel was in fact convecting and inducing noise on the Z component. The insulation and baffle served to stratify the air and inhibit convection inside the pressure vessel. The second test was to purge the pressure vessel with dry argon gas (argon is 37% denser than air and has thermal conduction properties which tends to inhibit convection). The argon gas indeed lowered the background noise PSD level by another 6+ dB at long periods. To test the idea that the power supply may be inducing some long period noise into the system, we disconnected the power supply and powered the CMG-

1TD solely from a 12 Volt battery. The background noise PSD level subsequently decreased by another 6+dB at long periods. Finally we added insulation to the outside of the pressure vessel by draping a space blanket over the vessel and covering the vessel with a two inch thick foam box with all seams taped. The background noise PSD performance of all three CMG-1TD seismometer components are now within 5 dB of the performance of the BKS STS-1 sensors (which are more heavily insulated and installed in a nearly ideal observatory environment), as shown in Figure 11.13. The result of this testing is that CMG-1T must be appropriately insulated and the pressure vessel purged with argon gas in order to obtain the performance of which the CMG-1T is capable.



Figure 11.12: Photo of the space blanket insulation and the space filling urethane foam space filling plug in the titanium pressure vessel with the titanium end cap removed.

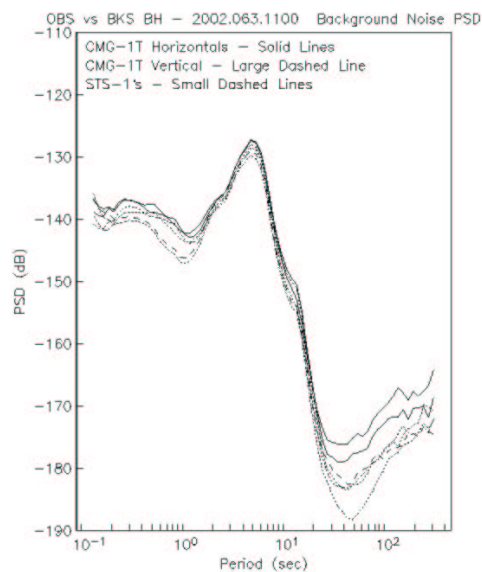


Figure 11.13: Observed background noise PSD levels for the CMG-1TD after it had been installed in the titanium pressure vessel, appropriately insulated and purged with argon gas. Note that the CMG-1TD PSD levels are within ~5 dB of the STS-1 PSD levels at long periods.

For the final phase of the testing, the CMG-1TD and the pressure vessel were transported to MBARI on 26 March for testing in their cold room at the ~4 degrees C temperature of the ocean floor. The cultural environment at MBARI, owing to its being situated on sand and in close proximity to the surf, makes for noisy seismic recordings with a large seven-second microseismic peak. The clock drift while operating in the cold room increased by an order of magnitude to  $-3191.39 \pm 2.656$  microseconds/day. This was a surprise because the expectation was that the drift rate would be smaller at 4 degrees C

than at room temperature. There was insufficient time, however, to retrain the clock prior to the scheduled deployment on the ocean floor. We also did a rough check of the calibration of the flux gate magnetometer because there was some concern that the metal in the BKS Vault may have biased the original calibration results.

For details on the deployment of the MOBB system, please see Chapter 10.

## 6.2 Quanterra 680 Data Logger Noise

The question arose as to what is the typical self-noise of a Quanterra 680-family Very-Broad-Band data acquisition system (aka "Pumpkin"). The digitizer package contains identical sets of independently optically-isolated three-channel 24-bit digitizers operating at 80 Hz sampling with a least significant bit (LSB) of 2.38 microvolts and a  $\pm 20$  Volt full scale range. The self-noise was tested by operating a Q680 (s/n 921209) in the BSL lab for a couple of weeks with open inputs to the six high-resolution channels. The result, shown in Figure 11.14, is a composite based on the noise PSD observed on all six channels. The lowest self-noise occurs at 2-4 Hz frequencies and the lowest median self-noise PSD of -136.6 dB relative to  $1 \text{ V}^2/\text{Hz}$  occurs at 2.5 Hz. Most of the self-noise of the Q680 occurs at high frequencies (above  $\sim 10$  Hz). A -136.6 dB PSD level integrated over 1 Hz (the 2 to 3 Hz interval) is equivalent to a rms noise level of 0.067 LSB (or 0.159 microvolts) and the median value integrated over the 0-32 Hz bandwidth limited by the FIR anti-aliasing filters of the 80 Hz sampled channel is 0.601 LSB (or 1.43 microvolts). The 1.43 microvolt rms 0-32 Hz self-noise of the Q680 is approximately an order of magnitude lower than the quietest broadband sensors used by BDSN. The asymmetric variation in the inter-quartile range, given by the spacing between the medium dashed lines, is due to individual differences in the self-noise of the six high-resolution digitizer channels. There is a  $\sim 6$  dB variation in the observed self-noise PSD which is mostly due to differences in the self-noise of the individual digitizers and partly due to variations in the environmental conditions (primarily temperature variation) in the lab.

## 6.3 BDSN Instrumentation

In addition to the above testing, we tested several new broadband seismometers and strong motion accelerometers. New, and recently repaired, sensors are routinely tested before deployment in the field. We also had a few BDSN sensors, both accelerometers and broadband sensors, which either become noisy or malfunctioned during the past year and they were tested at the test facility in the Byerly Seismographic Vault to identify and characterize the problem. Most notably we have two horizontal Streckeisen STS-1 broadband seismometers which

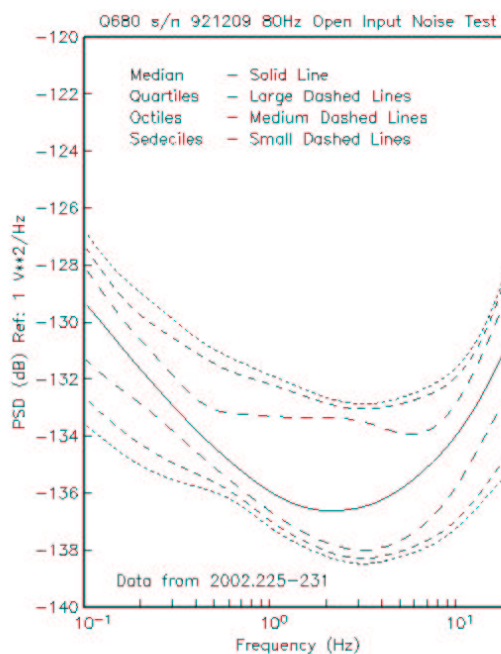


Figure 11.14: Composite open input self-noise PSD of Quanterra Q680 data logger s/n 921209. The median of the ranked PSD values is presented by the solid line, the quartiles by the large dashed lines, the octiles by the medium dashed lines, and the sedeciles (6.25 percent and 93.75 percent thresholds) are given by the small dashed lines.

became noisy over the past year and the problem was traced to rusty hinges, probably caused by operating at atmospheric pressure in a humid environment for several years. We are currently experimenting with different hinge materials for replacing the hinges.

## 7. UrEDAS Project

### 7.1 Introduction

The established joint notification system in Northern California (Chapter 12) provides accurate and reliable determination of earthquake parameters, but there is a time delay between the occurrence of an event and the determination of its size. In an emergency, this time delay prevents actions which could mitigate damage from strong ground shaking. The present configuration of the system could be improved with the capability of rapid size determination. In addition, it will be advantageous to have detection capabilities independent of the dense short-period network, especially in an emergency when

communications may be disrupted.

In an effort to develop such capability with the BDSN, we have started an experiment collocating a set of UrEDAS (Urgent Earthquake Detection and Alarm System; see *Nakamura, 1996*), an integrated real-time earthquake warning system, at BKS. The UrEDAS detects an earthquake using only 3 sec of the P-wave recorded at a single station and has been used in Japan for over a decade to alert bullet trains to strong shaking in progress. While the weakness of UrEDAS is that it is less accurate in event parameter determination, its advantage is speed. Through this experiment we explore the development of a single-station capability of rapid earthquake detection and location/magnitude estimate using data from the BDSN stations.

## 7.2 UrEDAS Overview

UrEDAS was developed to mitigate earthquake hazards for Japanese railways, especially bullet trains that travel at a peak speed close to 200 kph. Because of the speed of the bullet trains, it is extremely important to rapidly detect hazardous earthquakes and send alarm signals to the automatic train stop system. Empirically, damage to railways occurs for events with  $M \geq \sim 5.5$ , with the damaged area generally confined within a certain distance range of the epicenters. For example, earthquakes with M6, M7 and M8 can cause damages within epicentral distances of 12, 60, and 300 km, respectively. The target area of event detection of UrEDAS is designed to be  $\sim 200$  km from its location along the railways. Dr. Yukata Nakamura, who was formerly at the Railway Technical Research Institute and is now the president of System and Data Research (SDR) Co., Ltd. in Tokyo, Japan, is the leader of the UrEDAS system development.

The philosophy of the UrEDAS "front alarm" system is to detect earthquake motions as early as possible before strong ground shaking reaches the site (*Nakamura, 1996*). The concept of such a system was originally published by Dr. J. D. Cooper in the San Francisco Daily Evening Bulletin, 3<sup>rd</sup> November 1868. At the time Cooper addressed the importance of an automated early warning system alarm as well as the likely problems of false alarms and the necessity of public education for the warning. However, the technical expertise at the time was inadequate for construction such an alarm system. In 1972 the Earthquake Research Institute of the University of Tokyo proposed the development of an automated system similar to that suggested by Cooper. The Japanese National Railways (JNR) was interested in this concept and they promoted the system development. The JNR completed the development of a Coast-line Detection System for the Tohoku Bullet Train Line in 1982 (*Nakamura and Saito, 1982*), and it was the prototype that has the same basic function of the present UrEDAS system.

UrEDAS utilizes a single system that consists of two

sets of three-component seismometers, a set of velocity sensors with  $T_o=1$  sec (short-period sensors with moving coil designed for events up to  $M \sim 6$ ) and a set of force feedback velocity sensors with a 0.1-10 Hz frequency pass-band (long-period sensors designed for larger events), for stable determination of small to large events. The system uses a velocity threshold to detect events and the epicentral azimuth is estimated from the direction of the initial motion projected on the horizontal plane. An estimate of the distance and magnitude is based on frequency content and amplitudes of the first three seconds of the P-wave motion. If the S-wave is detected, the estimates of distance and magnitude are revised. The epicentral distance ( $R$ ) is estimated using the relation  $\log R = a \cdot \log A + b \cdot \log T + c$  where  $A$  is the amplitude of the initial P-wave motion (in m/kin),  $T$  its prominent period, and  $a, b$ , and  $c$  are constant. The magnitude is estimated from the prominent period ( $T$ ) of the initial P-wave motion using the relation  $M = 3.2 \cdot \log T + 5.26$ .

An alarm can be issued if hazardous earthquake is detected from the P-wave motions. However, it is not always easy to detect an event from the P-wave alone and there is a trade-off between the detection threshold and the rate of false alarms. The primary advantage of UrEDAS is that the system can provide event information in  $\sim 3$  seconds following the detection of a P-wave at a single site. The quality of the parameter determination depends on the conditioning and tuning of the system for site specific effects and thus the pre-conditioning is important in the determination procedure. Also, the magnitude estimation using just the first three seconds of the P-wave motions may not always be reliable. It is also possible that the station location happens to be near a P-wave node of the focal mechanism. To overcome the weakness of the single system algorithm, each of the UrEDAS stations distributed along the railways is linked to a centralized system to provide better estimates of the event parameters.

## 7.3 UrEDAS Installation at BKS

Since 1984, JNR has tested the UrEDAS system in various areas where high-quality location and magnitude determinations are available from dense regional short-period networks. In November 1999 the crew of SDR visited BSL to discuss a possible joint experiment with UrEDAS. The seismologists at BSL agreed to test the UrEDAS performance by collocating it at one of the BDSN stations. We chose the Byerly Vault (station BKS) for its low noise level and accessibility and because it includes a set of Streckeisen STS-1 seismometers and a Kinematics FBA-23 strong motion accelerometer and because the station has been operational since June 1962 and the site specific characteristics of the seismic wave propagation are fairly well known.

The initial system installation was completed with the

event detection and notification in February 2001 and was upgraded to transmit waveform data to the BSL in July 2001. The SDR crew visited the site in July 2002 to check on the equipment and to revise the values of the parameters used by the UrEDAS algorithms. Figure 11.15 shows the UrEDAS sensors and Figure 11.16 shows an illustration of the UrEDAS network configuration.

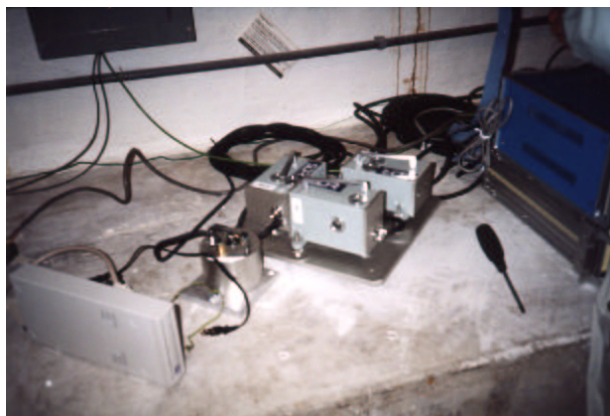


Figure 11.15: UrEDAS sensors installed at BKS site. The dedicated PC-based processing system (not shown here) is located in an adjacent room.

## 7.4 Discussion

Since February 2001, there have been 283 UrEDAS detected events, and 151 of these correspond to events in the NCSN earthquake catalog (within a 500 km radius and with a theoretical P-wave onset time at BKS within 20 seconds of the UrEDAS detection time). The 132 uncorrelated UrEDAS events are presumably a mix of teleseisms (which UrEDAS has a tendency to mislocate as local events), some small local events near Berkeley (which are below the NCSN magnitude threshold), and a few random noise triggers.

To date UrEDAS readily detects the occurrence of local/regional events from the P-wave signal as shown in Figure 11.17. It also does a fair job of determining the source distance out to 160 km or so (see Figure 11.18) but the azimuth determination is basically unusable as shown in Figure 11.19. UrEDAS also has biased magnitude estimates as shown in Figure 11.20. The UrEDAS algorithm assumes a one-dimensional velocity model with straight line propagation paths and a three-dimensional model of the crustal structure will likely be required to significantly improve the azimuthal estimates. Also, the magnitude estimation algorithm needs further tuning.

Assuming that the primary goal is to determine the event location and size as rapidly as possible, the fastest approach will prove to be a hybrid approach where the remote stations determine the azimuth and ramp growth

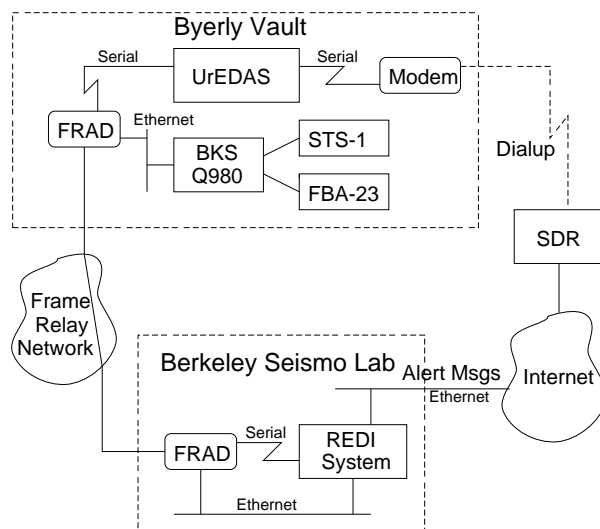


Figure 11.16: Schematical illustration of the UrEDAS collocation experiment with a Streckeisen STS-1 broadband instrument and a Kinemetrics FBA-23 strong motion accelerometer with a Quantera Q980 data logger at BKS.

rate and associated uncertainties and the central site uses a fuzzy logic algorithm to determine the location and size of the event. The primary advantage of this hybrid method is that the ramp growth rate can be reliably determined before the S-wave arrives. In the limiting case, and with a sufficiently high station density, one could even go so far as to determine and report from the remote sites using only the broadband P-wave impulse, and associated azimuth and apparent angle of incidence and estimates of their resolution and have the central site coalesce the data into a viable and rapid event report.

The critical issue for a successful installation of a UrEDAS type system in the BDSN is the calibration of specific site effects at individual stations. A joint use of the single station detection system with the current northern California earthquake notification system would significantly increase the capability of real-time earthquake warning system.

The current UrEDAS system uses a dedicated PC and the SDR personnel have indicated that a UrEDAS/UNIX version of the algorithm is available. The UNIX version generates the same message format as does the PC-based system. The advantage of the UNIX based system is that, besides running on the BSL computers, it can process data from any seismometer or seismometer/filter system that can output ground acceleration in the 0.1-10 Hz passband at 100 sps. The UNIX version of the UrEDAS algorithm is hard wired for 100 sps acceleration data provided in Gals (to four decimal places) so we would need to generate a structure which supplies the algorithm with

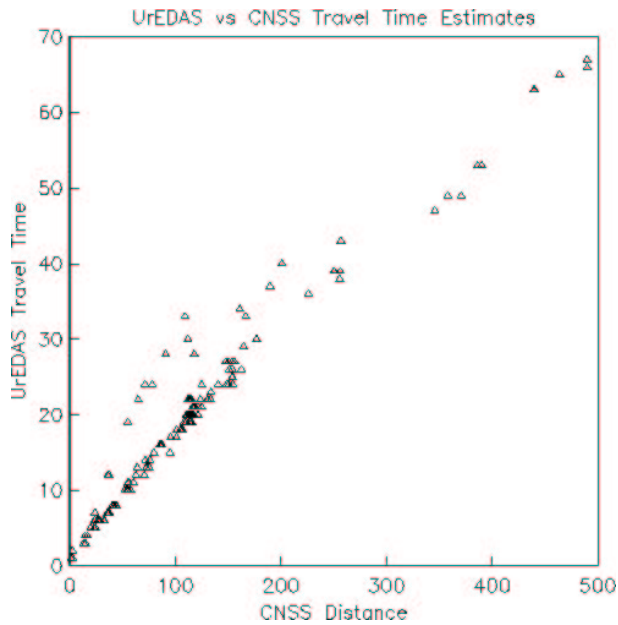


Figure 11.17: UrEDAS inferred travel time (detection time minus origin time) versus CNSS epicentral distance to BKS. The UrEDAS detection time mostly correspond to the P-wave arrival time for a majority of the detected events at distance less than  $\sim 160$  km. At larger distances there is increased scatter and fewer events detected.

a date/time stamp and the three acceleration components (Z,N,E) in Gals and a rate of 100 per second with a specific comma delimited format: "20020607114810.00,+24.4356,-21.5642,+14.9547" (for example). The primary disadvantage of the UrEDAS/UNIX processing is that it will lag several seconds behind real-time ( $\sim 5$ -10, say), due to the packet transmission protocol that we use to transmit the data to BSL. The UrEDAS/UNIX source code is proprietary property of SDR and will not be made available to BSL.

## 8. Acknowledgements

Doug Neuhauser, Bob Uhrhammer, Lind Gee, Pete Lombard, and Rick McKenzie are involved in the data acquisition and quality control of BDSN/NHFN/MBPO data.

Development of the sensor test facility and analysis system was a collaborative effort of Bob Uhrhammer, Tom McEvelly, John Friday, and Bill Karavas. IRIS and DTRA provided, in part, funding and/or incentive to set up and operate the facility and we thank them for their support.

Bob Uhrhammer led the testing and problem solving effort of the MOBB sensor, with help from John Friday, Doug Neuhauser, and Bill Karavas.

Fumiko Tajima initiated the collaboration with SDR

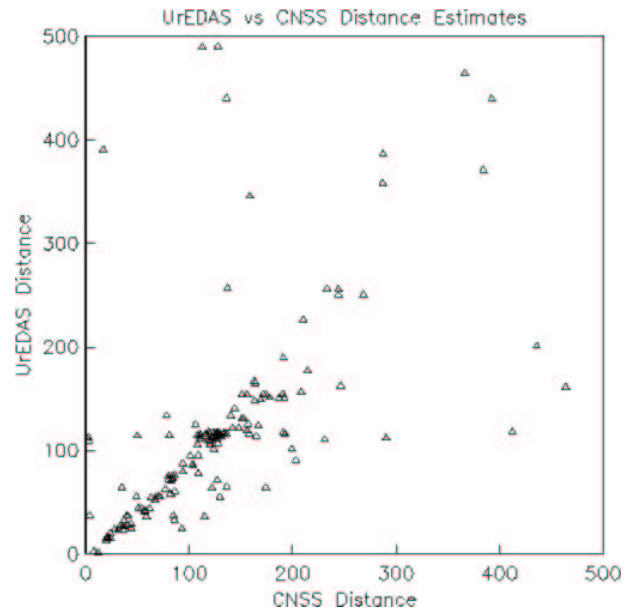


Figure 11.18: UrEDAS reported distance versus CNSS epicentral distance to BKS. The correlation is best at distances of less than  $\sim 160$  km and poor at larger distances.

on testing the UrEDAS system, which is now coordinated by Bob Uhrhammer. Doug Neuhauser, Bill Karavas, John Friday, and Dave Rapkin helped with installation and maintenance. We thank Yutaka Nakamura and his colleagues at SDR for providing us with the installation of UrEDAS system and information on the accumulated data by this system.

Bob Uhrhammer, Lind Gee, and Doug Neuhauser contributed to the preparation of this chapter.

## 9. References

Abramovich, I. A., V. M. Agafonov, M. E. Cobern, and V. A. Kozlov, Improved Wide-Band Molecular Electronic Seismometer and Data Acquisition system, Poster Session S31B-18, AGU Fall Meeting, San Francisco, 1997.

Halbert, S. E., R. Buland, and C. R. Hutt, Standard for the Exchange of Earthquake Data (SEED), Version V2.0, February 25, 1988. United States Geological Survey, Albuquerque Seismological Laboratory, Building 10002, Kirtland Air Force Base East, Albuquerque, New Mexico 87115, 82 pp., 1996.

Nakamura, Y. and A. Saito, Train stopping system for the Tohoku Shinkansen (in Japanese), *Proc. of Semianual meeting of the Seismological Society of Japan*, 82, 244, 1982.

Nakamura, Y., Real-time information systems for seismic hazards mitigation UrEDAS, HERAS, and PIC, *Quarterly Report of Railway Technical Research Insti-*

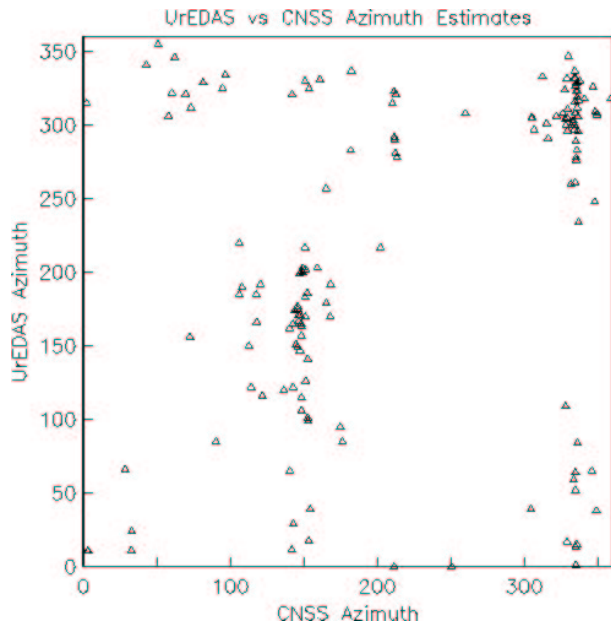


Figure 11.19: UrEDAS reported azimuth versus CNSS epicentral azimuth from BKS. The UrEDAS azimuth estimate is highly biased by the local lateral structure across the Hayward Fault zone. The azimuth estimates tend to cluster around  $\sim 150$  and  $\sim 340$  degrees owing to refraction of the P-wave along the SW (fast) side of the fault zone.

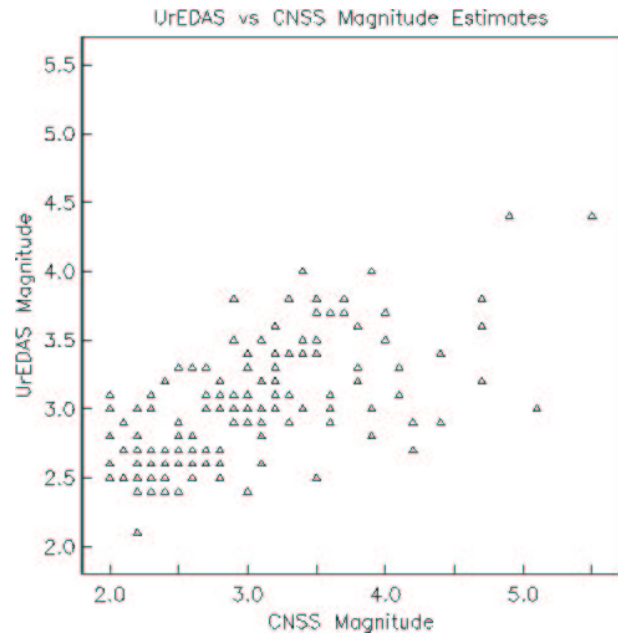


Figure 11.20: UrEDAS reported magnitude versus CNSS reported magnitude. The UrEDAS magnitude estimate is biased high for small events  $M < \sim 3$  and low for larger events.

*tute*, 37, 112-127, 1996.

Peterson, J. Observations and Modeling of Seismic Background Noise, *U.S. Geological Survey Open File Report 93-322*, 94 pp., 1993.

Tapley, W. C. and J. E. Tull, SAC - Seismic Analysis Code: Users Manual, *Lawrence Livermore National Laboratory*, Revision 4, 388 pp., March 20, 1992.

Uhrhammer, R. A. and T. V. McEvelly, IRIS Sensor Tests: an interim report, Poster Presentation, 2001 IRIS Workshop, Jackson Lake Lodge, Moran, WY, June 6-9, 2001.

## Chapter 12

# Northern California Earthquake Monitoring

### 1. Introduction

Analysis of the data produced by BSL networks begins as the waveforms are acquired by computers at UC Berkeley, and ranges from automatic processing for earthquake response to analyst review for earthquake catalogs and quality control.

Over the last 9 years, the BSL has invested in the development of the hardware and software necessary for an automated earthquake notification system (*Gee et al., 2002; Gee et al., 1996*). The Rapid Earthquake Data Integration (REDI) project is a research program at the BSL for the rapid determination of earthquake parameters with three major objectives: to provide near real-time locations and magnitudes of northern and central California earthquakes; to provide estimates of the rupture characteristics and the distribution of ground shaking following significant earthquakes, and to develop better tools for the rapid assessment of damage and estimation of loss. A long-term goal of the project is the development of a system to warn of imminent ground shaking in the seconds after an earthquake has initiated but before strong motions begin at sites that may be damaged.

In 1996, the BSL and USGS began collaboration on a joint notification system for northern and central California earthquakes. The current system merges the programs in Menlo Park and Berkeley into a single earthquake notification system, combining data from the NCSN and the BDSN.

This year, significant progress was made in the development of the California Integrated Seismic Network.

### 2. Joint Notification System Overview

Figure 12.1 illustrates the distributed nature of the current joint notification system in northern California.

On the USGS side, incoming analog data from the NCSN are digitized, picked, and associated as part of

the Earthworm system (*Johnson et al., 1995*). Preliminary locations, based primarily on phase picks from the NCSN, are available within seconds, while final locations and preliminary coda magnitudes are available within 2-4 minutes. Earthworm reports events - both the "quick-look" 25 station hypocenters (without magnitudes) and the final (unreviewed) solutions (with coda magnitudes) to the Earlybird alarm module in Menlo Park. This system sends the Hypoinverse archive file to the BSL for additional processing, generates pages to USGS and UC Berkeley personnel, and distributes information via the Quake Data Distribution System (QDDS).

Once an event is declared, additional Earthworm processing at the USGS generates ground motion amplitudes from NCSN and NSMP stations and loads them into a database. A process known as ShakeMapFeeder extracts amplitudes from the database and pushes them to the ShakeMap system (*Wald et al., 1999*) implemented in Menlo Park.

On the UC Berkeley side, the Hypoinverse archive file is normally used to drive the REDI processing system. The REDI processing is divided into two systems - routine or "standard" processing (local magnitude, ground motion amplitudes, and moment tensors) - and the finite-fault processing added last year (Figure 12.2). Each REDI system provides several "stages" of processing, and the attributes of events such as magnitude, the "age" (time since origin), and number of associated phases are used to determine the appropriate processing. The REDI stage structure allows processing to be scheduled (for example, wait 5 minutes after the origin time before scheduling a moment tensor computation) as well as prioritized (for example, process the magnitude 6 before the magnitude 2).

In "abnormal" situations, such as when communication links between the BSL and the USGS are disrupted, the BSL can drive the REDI system using events detected based on BDSN data alone. The BSL has implemented the same association algorithm used in the Earthworm system in Menlo Park, using Murdock-Hutt phase detec-

## Northern California Earthquake Notification System Current Implementation

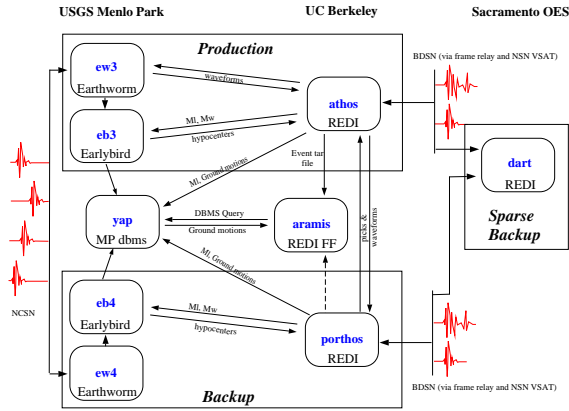


Figure 12.1: Schematic diagram illustrating the connectivity between the real-time processing systems at the USGS Menlo Park and UC Berkeley. This figure also illustrates the newly added finite-fault and ShakeMap capability, which is handled on a separate system, as well as the independent processing system in Sacramento.

tions and/or picks from an Earthworm picker.

### 2.1 Standard Processing

Stage 0 of the "standard" processing provides initial event handling. It can accept either Hypoinverse files from the USGS (the normal source of event information) or events generated from the local associator. If the preliminary magnitude estimate is less than 3.0, no additional processing is performed and event information is distributed if appropriate.

Stage 1 is initiated for all events with preliminary magnitudes greater than 3.0 and for events with no preliminary magnitude. In this stage, broadband waveforms are processed to produce Wood-Anderson synthetics and estimates of local magnitude are generated. This stage uses the preliminary magnitude and a distance criterion to decide which channels to analyze.

Stage 2 generates ground-motion amplitudes for use in ShakeMap and other applications. Stage 2 currently generates estimates of peak ground acceleration, peak ground velocity, and peak ground displacement from BDSN acceleration records, but does not produce estimates of spectral acceleration.

Stage 3 performs the automated moment tensor analysis. In this stage of REDI processing, both the waveform modeling method of Dreger and Romanowicz (1994) and the surface wave inversion technique of Romanowicz et al. (1993) are run for every qualifying event (earthquakes with  $M_L$  greater than 3.5). Each algorithm produces an estimate of the seismic moment, the moment tensor solu-

tion, the centroid depth, and solution quality. The REDI system uses the individual solution qualities to compute a weighted average of moment magnitude, to compare the mechanisms using normalized root-mean-square of the moment tensor elements (Pasyanos et al., 1996), and to determine a "total" mechanism quality.

In 2000-2001, two new stages were added to standard REDI processing. Stage 4 extracts the waveform data required for the finite-fault processing and Stage 5 "packs" the event up and ships it to the REDI finite-fault system running on aramis.

### 2.2 Finite-Fault Processing

During 2000-2001, the estimation of finite-fault parameters was migrated from the development platform to the REDI operational environment, new modules were developed to use the finite-fault parameters to simulate near-fault strong ground motions, and the results integrated into the generation of ShakeMap (Dreger and Kaverina, 2000; Dreger and Kaverina, 1999).

In Stage 0, waveform data are prepared for inversion and rough estimates of the fault dimensions are derived using the empirical scaling relationships of Wells and Coppersmith (1994). Using these parameters to constrain the overall dimensions of the extended source, the stage tests the two possible fault planes obtained from the moment tensor inversion over a range of rupture velocities by performing a series of inversions using a line-source representation. In addition to the identification of the fault plane and apparent rupture velocity, this stage yields preliminary estimates of the rupture length, dislocation rise time, and the distribution of slip in one dimension.

Stage 1 combines the results of the line-source inversion with the directivity-corrected attenuation relationships of Somerville et al. (1997) to simulate ground motions in the near-source region. "FFShake" computes peak ground acceleration, peak ground velocity, and spectral response at 0.3, 1.0, and 3.0 sec period, which are the values used in ShakeMap, for a grid of pseudo-stations in the vicinity of the epicenter. The predicted ground motions are automatically incorporated in ShakeMap updates as described below.

In Stage 2, the second component of the finite-fault parameterization uses the best-fitting fault plane and rupture velocity from Stage 0 to obtain a more refined image of the fault slip through a full two-dimensional inversion. If line-source inversion fails to identify the probable fault (due to insufficient separation in variance reduction), the full inversion is computed for both fault planes. In the present implementation, the full inversion requires 20-30 minutes per plane, depending on the resolution, on a Sun UltraSPARC1/200e.

Stage 3 completes the cycle by simulating the near-fault strong ground motion parameters by convolving the velocity structure response with the finite-fault slip dis-

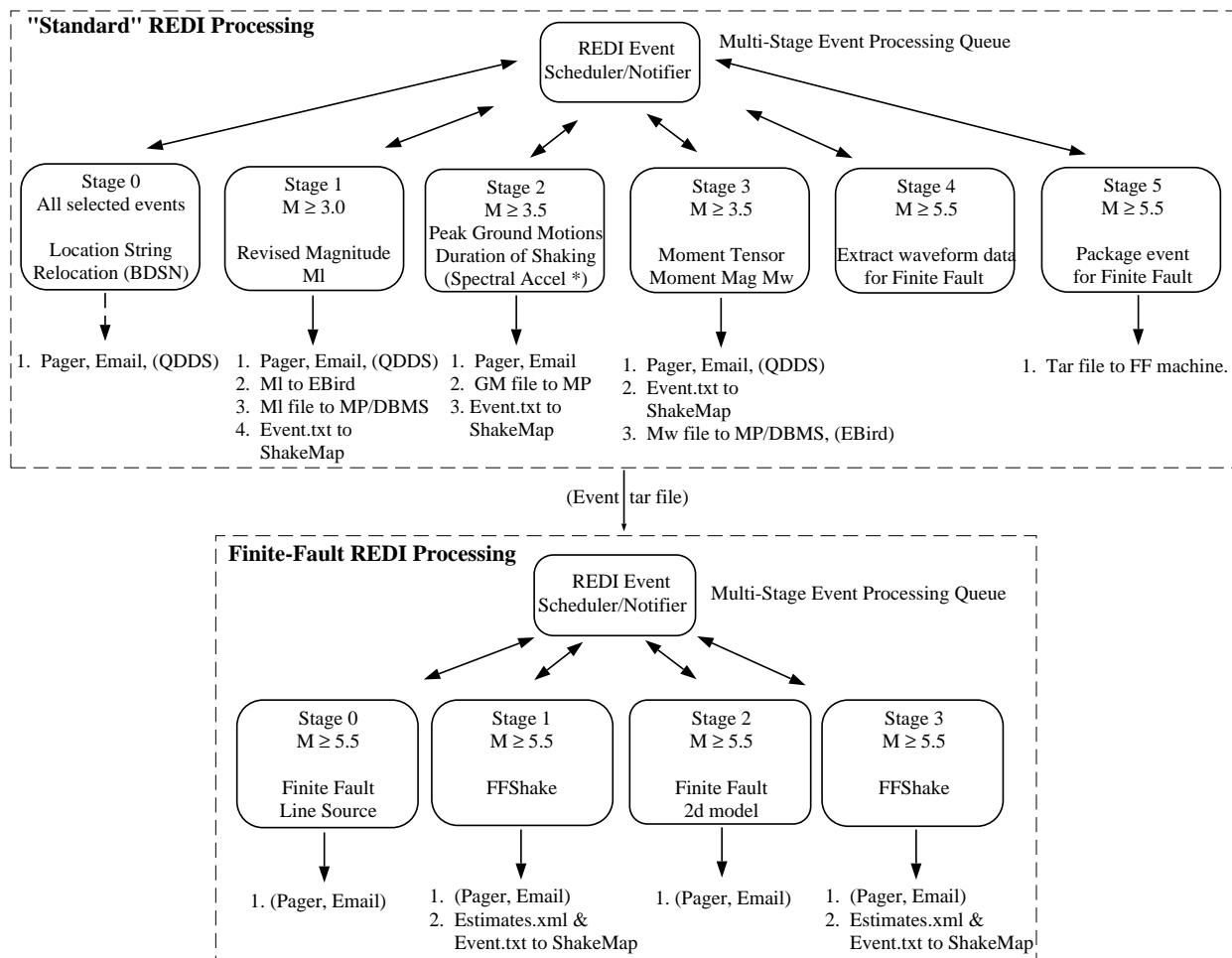


Figure 12.2: Diagram showing the two levels of REDI processing. The "Standard" processing is conducted on the two main data acquisition systems and includes the computation of  $M_L$ , ground-motion processing, and the determination of the seismic moment tensor. The "Finite-fault" system is an expansion of REDI processing. Items in parentheses are planned expansions.

tribution. As in Stage 1, "FFShake" computes peak ground acceleration, peak ground velocity, and spectral response at 0.3, 1.0, and 3.0 sec period for a grid of pseudo-stations in the vicinity of the epicenter and pushes these ground motions to the ShakeMap system.

## 2.3 ShakeMap

As part of the development of the finite-fault project, the BSL worked with the USGS Menlo Park to install ShakeMap V2.0 at UC Berkeley. Although USGS personnel had done most of the work to adapt the program to northern California, development was required to integrate the ShakeMap package into the REDI environment. In the process, BSL staff identified and fixed some minor bugs in the software.

The motivation for this effort is the desire to integrate the ground motions predicted from the finite-fault inversions into the ShakeMap generation. The goal is to provide updated ShakeMaps as more information about the earthquake source is available. Versions 2.0 and higher of ShakeMap are structured to allow the use of different "estimates" files, that is, to incorporate ground motions predicted by alternate means.

As shown in Figure 12.2, the REDI processing system is integrated with the ShakeMap software at several levels. "Event.txt" files are generated at several stages - these files tell the ShakeMap software to wake-up and process an event. A ShakeMap is generated following Stage 2 in the Standard processing and updated if a revised estimate of magnitude is obtained following Stage 3.

For events which trigger the finite-fault processing, estimates of ground motions based on the results of the line-source computation and the full 2D inversion are produced in the "FFShake" stages. "Estimates.xml" files are generated and pushed to the ShakeMap package. The output of the line source computation produces what we call an "Empirical ShakeMap", while output from the 2D inversion produces a "Conservative ShakeMap".

Figure 12.3 illustrates the three different methodologies with examples from an M6 earthquake which occurred in the Mammoth Lakes region in May 1999. Very few data were available to constrain these maps. This event is somewhat small for this methodology, but the impact of the successive improvements in the ground motion estimates is clearly illustrated.

Future plans include the continued testing and refinement of the procedure, working with the USGS group toward integration into the authoritative ShakeMap method for northern California and other regions, and development of additional capabilities based on the incorporation of BARD GPS data. Figure 12.4 shows the typical processing times associated with the current implementation.

## 2.4 Implementation

At present, two Earthworm-Earlybird systems in Menlo Park feed two "standard" REDI processing systems at UC Berkeley (Figure 12.1). One of these systems is the production or paging system; the other is set up as a hot backup. The second system is frequently used to test new software developments before migrating them to the production environment. The REDI finite-fault processing is installed on a third system, which is always "fed" from the production system. A fourth system is installed in Sacramento as a stand-alone operation in order to provide a redundant notification facility outside of the Bay Area.

This structure has greatly expedited automatic earthquake processing in northern California. The dense network and Earthworm-Earlybird processing environment of the NCSN provides rapid and accurate earthquake locations, low magnitude detection thresholds, and first-motion mechanisms for smaller quakes. The high dynamic range data loggers, digital telemetry, and broadband and strong-motion sensors of the BDSN and REDI analysis software provide reliable magnitude determination, moment tensor estimation, peak ground motions, and source rupture characteristics. Robust preliminary hypocenters are available about 25 seconds after the origin time, while preliminary coda magnitudes follow within 2-4 minutes. Estimates of local magnitude are generally available 30-120 seconds later, and other parameters, such as the peak ground acceleration and moment magnitude, follow within 1-4 minutes (Figure 12.4).

Earthquake information from the joint notification system is distributed by pager, e-mail, and the WWW. The first two mechanisms "push" the information to recipients, while the current Web interface requires interested parties to actively seek the information. Consequently, paging and, to a lesser extent, e-mail are the preferred methods for emergency response notification. The *recenteqs* site has enjoyed enormous popularity since its introduction and provides a valuable resource for information whose bandwidth exceeds the limits of wireless systems and for access to information which is useful not only in the seconds immediately after an earthquake, but in the following hours and days as well.

## 2.5 System Monitoring

In order to ensure that automatic systems are operating correctly, BSL staff and students participate in *alarm response*. Each week, two people are on duty in order to respond to earthquakes - or computer problems. One person is designated as primary and is responsible for earthquake-related issues. The second individual serves as a backup to the second and addresses more operational problems. For earthquake notification, the alarm response team receives pages from several sources including an automatic monitoring of the ground velocity at

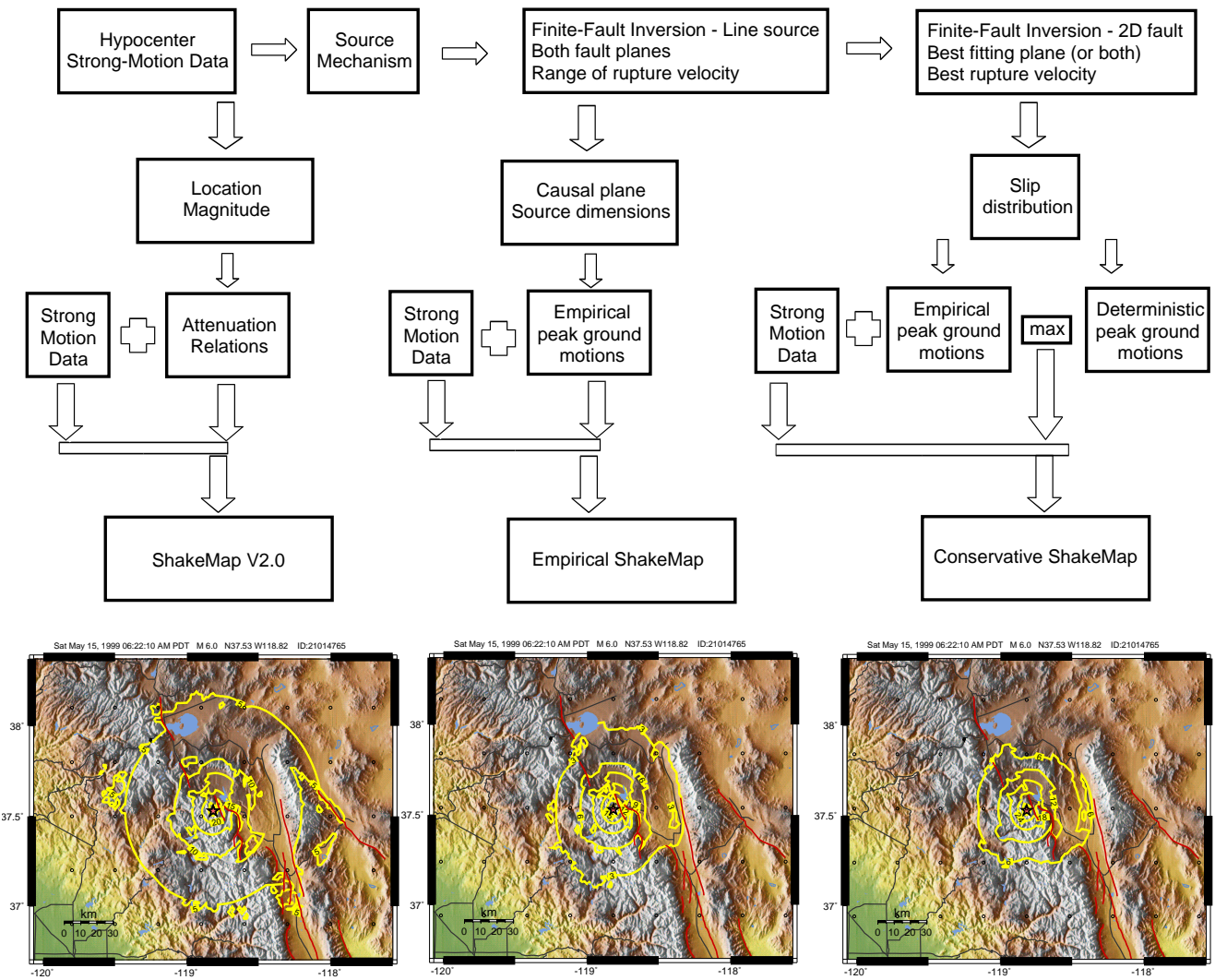


Figure 12.3: Summary of the three levels of ShakeMaps produced by the REDI system, with an example for an M6 earthquake in the Mammoth Lakes region. Note that the contour intervals vary from plot to plot.

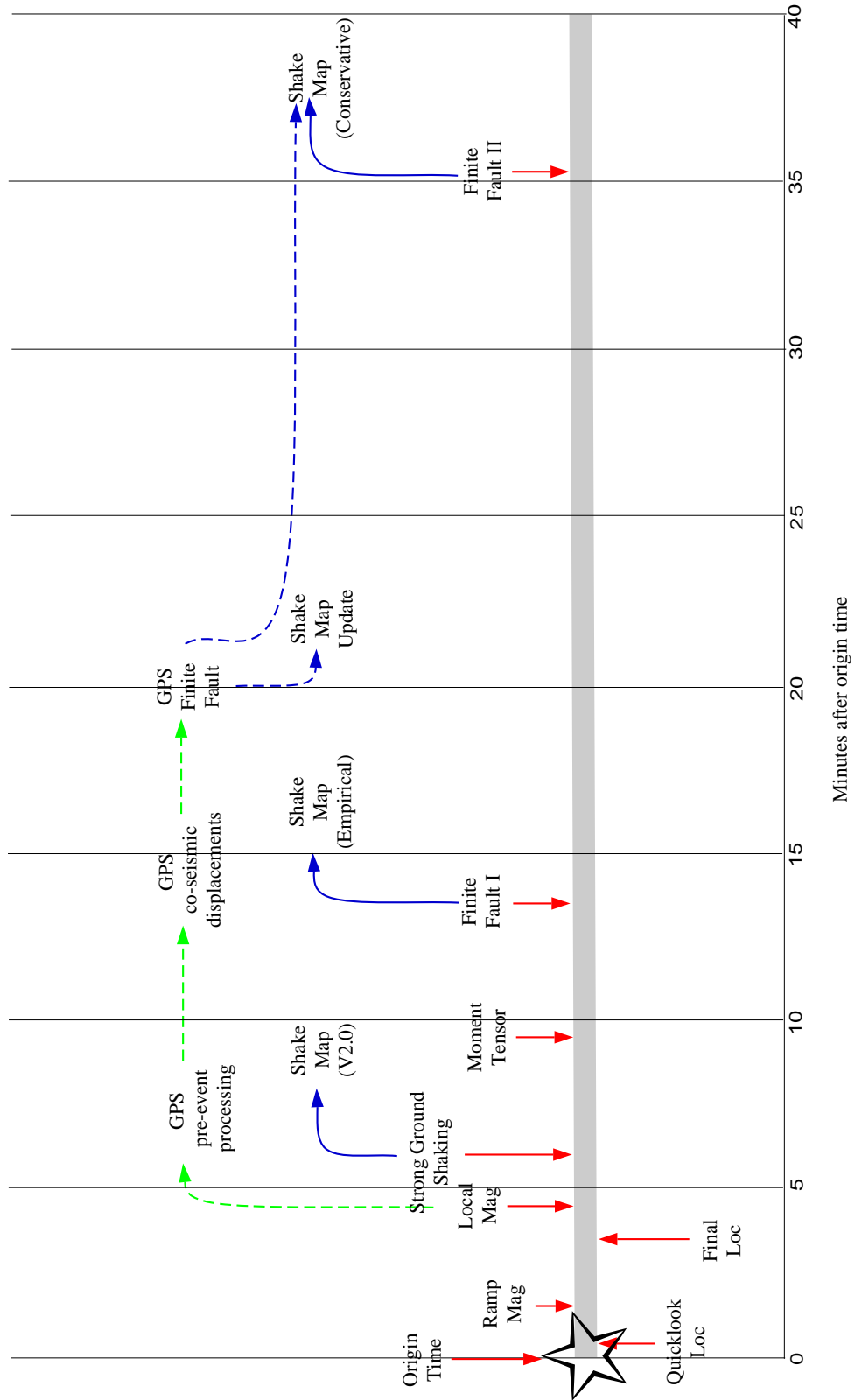


Figure 12.4: Illustration of the current (solid lines) and planned/proposed (dotted lines) development of real-time processing in northern California. The Finite Fault I and II are fully implemented within the REDI system at UC Berkeley and are integrated with ShakeMap. The resulting maps are still being evaluated and are not currently available to the public.

BKS (known as the SEismic ALarm or SEAL), a human-initiated alarm from the UCB Police Department, and separate notifications from REDI and the USGS. For operational monitoring, we have developed a component of the REDI system for tracking the heartbeats and data flow from critical systems and processes. Because this is inherently a distributed system, it is critical to monitor the "health" of every component. In the REDI system, the monitor program is a master scheduler that can perform several types of monitoring. As presently implemented, the monitor program watches critical computers and network components, disk resources, specified processes, and particular subsystems, such as data acquisition.

### 3. 2001-2002 Activities

#### 3.1 Queueing of event messages

Working with the USGS, we have implemented a mechanism to queue event messages transmitted from the USGS to the REDI system. Previously, Earlybird opened a socket connection to the REDI computers. This approach was vulnerable to loss of data during times of connectivity problems. This socket-based approach has been replaced with a "file flinger", which provides the capability to queue or store event messages if connectivity between Berkeley and Menlo Park is lost.

#### 3.2 Support for SNCL

Over the last year, we completed the implementation of full SEED channel names. In the past, the REDI system had used Station/Network/Channel (SNC) to describe a unique waveform channel. However, the evolution of the BDSN and experience with other networks led to the implementation of Location code or the full SNCL convention. This involved revisiting a number of REDI modules which handle waveform data.

This modification provided the opportunity to enhance the way REDI selects waveforms for processing. The "redi.avail" file allows for control of which channels are used for REDI modules and makes it easy to turn channels off and on if sensors or data loggers fail or telemetry problems are experienced.

#### 3.3 Moment Tensor codes

As part of the changes for supporting SNCL, BSL staff put considerable time into recasting some of the moment tensor codes. Pete Lombard worked with Doug Dreger to modify the complete waveform codes. Changes included the ability to handle acceleration as well as velocity data, generalizing assumptions about data rates and channel orientation, and enhancements to how channels are selected, based on the distribution of stations.

#### 3.4 $M_w$

The REDI system has routinely produced automatic estimates of moment magnitude ( $M_w$ ) for many years. However, these estimates have not routinely used as the "official" magnitude, due in part to questions about the reliability of the automatic solutions. However, in response to the 05/14/2002 Gilroy earthquake ( $M_w$  4.9,  $M_L$  5.1) and the complications created by the publication of multiple magnitudes, the BSL and USGS Menlo Park have agreed to use automatically determined moment magnitudes, when available, to supplement estimates of local magnitude ( $M_L$ ).

We have taken steps to use  $M_w$  automatically and hope to complete this work in the early fall of 2002. In parallel, this work will allow both the USGS and the BSL components of the joint notification system to report earthquake information to Web independently (currently, only the USGS component distributes information to the Web using QDDS). As a result of this development, both the USGS and BSL components will distribute information to the Web, enhancing the robustness of the Northern California operations.

#### 3.5 Collaboration with UNR

As part of our collaboration with UNR Seismological Laboratory, we implemented the capability to "forward" event messages from UNR over the REDI paging system in January. UNR sends Qpager format messages to the BSL via email, where a program extracts the message, evaluates the location, and then sends a page if the event is inside the UNR paging polygon. As part of this collaboration, the USGS Menlo Park and the BSL modified their paging polygon to align with the California/Nevada border.

#### 3.6 ShakeMap

During 2001-2002, the ShakeMap software at the BSL was upgraded to version 2.4, in order to stay synchronized with the implementation in Menlo Park. V2.5 is currently being tested in Menlo Park and we anticipate upgrading in the next quarter.

#### 3.7 Northern California Management Center

As part of ongoing efforts to improve the monitoring systems in northern California, the BSL and the USGS Menlo Park have begun to plan for the next generation of the northern California joint notification system.

Figure 12.1 illustrates the current organization of the two systems. As described above, an Earthworm/Earlybird component is tied to a REDI component and the pair form a single "joint notification system". Although this approach has functioned reasonably well over the last 5 years, there are a number of potential problems

## Northern California Earthquake Notification System

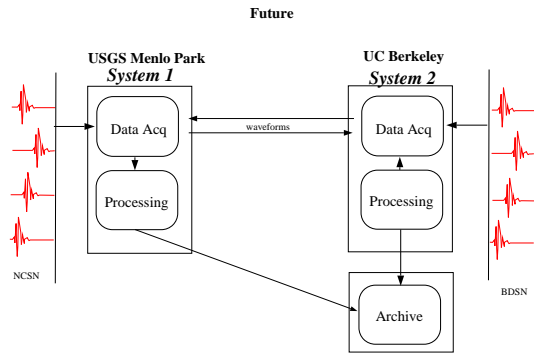


Figure 12.5: Future design of the Northern California Earthquake Notification System. In contrast with the current situation (Figure 12.1), the system is being redesigned to integrate the Earthworm/Earlybird/REDI software into a single package. Parallel systems will be run at the Berkeley and Menlo Park facilities of the Northern California Operations Center.

associated with the separation of critical system elements by 30 miles of San Francisco Bay.

Recognizing this, we intend to redesign the northern California operations so that a single independent system operates at the USGS and at UC Berkeley. Figures 12.5 and 12.6 illustrate the planned configuration. Our discussions have proceeded to the stage of establishing specifications and determining the details required for design. In the last year, the BSL and the USGS Menlo Park have met several times to discuss designs for the proposed system. In October, the BSL and the USGS Menlo Park asked representatives from the USGS Golden, USGS Pasadena, and Caltech to participate in a 2-day meeting.

## 4. Routine Earthquake Analysis

On a daily basis, the BSL continues to locate and determine the magnitude of earthquakes in northern California and adjacent regions. As a general rule, events are analyzed if their magnitude is greater than 2.8 in the Central Coast ranges, greater than 3.0 in all of northern California, or greater than 3.8 in the bordering regions. Traditionally, these events were located using hand-picked arrival times from the BDSN stations in conjunction with P-arrival times from the NCSN using the program st-relp. Over the past several years, the BSL has made a transition in the daily analysis to take advantage of the automatic processing system. As part of this transition, events which have been processed by the automatic system are not generally relocated, although phase arrivals are still hand-picked and the synthetic Wood-Anderson

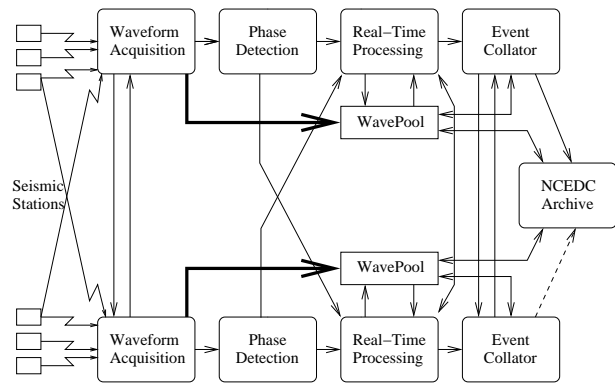


Figure 12.6: Illustration of the design currently being considered for the development of the Northern California Management Center.

readings are checked. Instead, analysts are focusing on the determination of additional parameters, such as the seismic moment tensor, phase azimuth, and measures of strong ground shaking.

From July 2001 through June 2002, BSL analysts reviewed nearly 200 earthquakes in northern California and adjoining areas, ranging from M2.8 to 5.9. Reviewed moment tensor solutions were obtained for 28 events (through 6/30/2002). Figure 12.7 and Table 12.1 displays the earthquakes located in the BSL catalog and the moment tensor solutions.

In addition to the routine analysis of local and regional earthquakes, the BSL also processes teleseismic earthquakes. Taking advantage of the CNSS catalog, analysts review teleseisms of magnitude 5.8 and higher. All events of magnitude 6 and higher are read on the quietest BDSN station, while events of magnitude 6.5 and higher are read on the quietest station and BKS. Earthquakes of magnitude 7 and higher are read on all BDSN stations.

The locations and magnitude determined by the BSL are cataloged on the NCEDC. The phase and amplitude data are provided to the NEIC, along with the locations and magnitudes, as contributions to the global catalogs, such as that of the ISC.

## 5. Acknowledgements

Lind Gee leads the development of the REDI system and directs the routine analysis. Peter Lombard, Doug Neuhauser, and Jim Yan contribute to the development of software. Rick McKenzie, Doug Dreger, Hrvoje Tkalčić, and Dennise Templeton contribute to the routine analysis. Lind Gee, Doug Neuhauser, and Dennise Templeton contributed to the writing of this chapter.

Partial support for the develop of the REDI system is provided by the USGS.

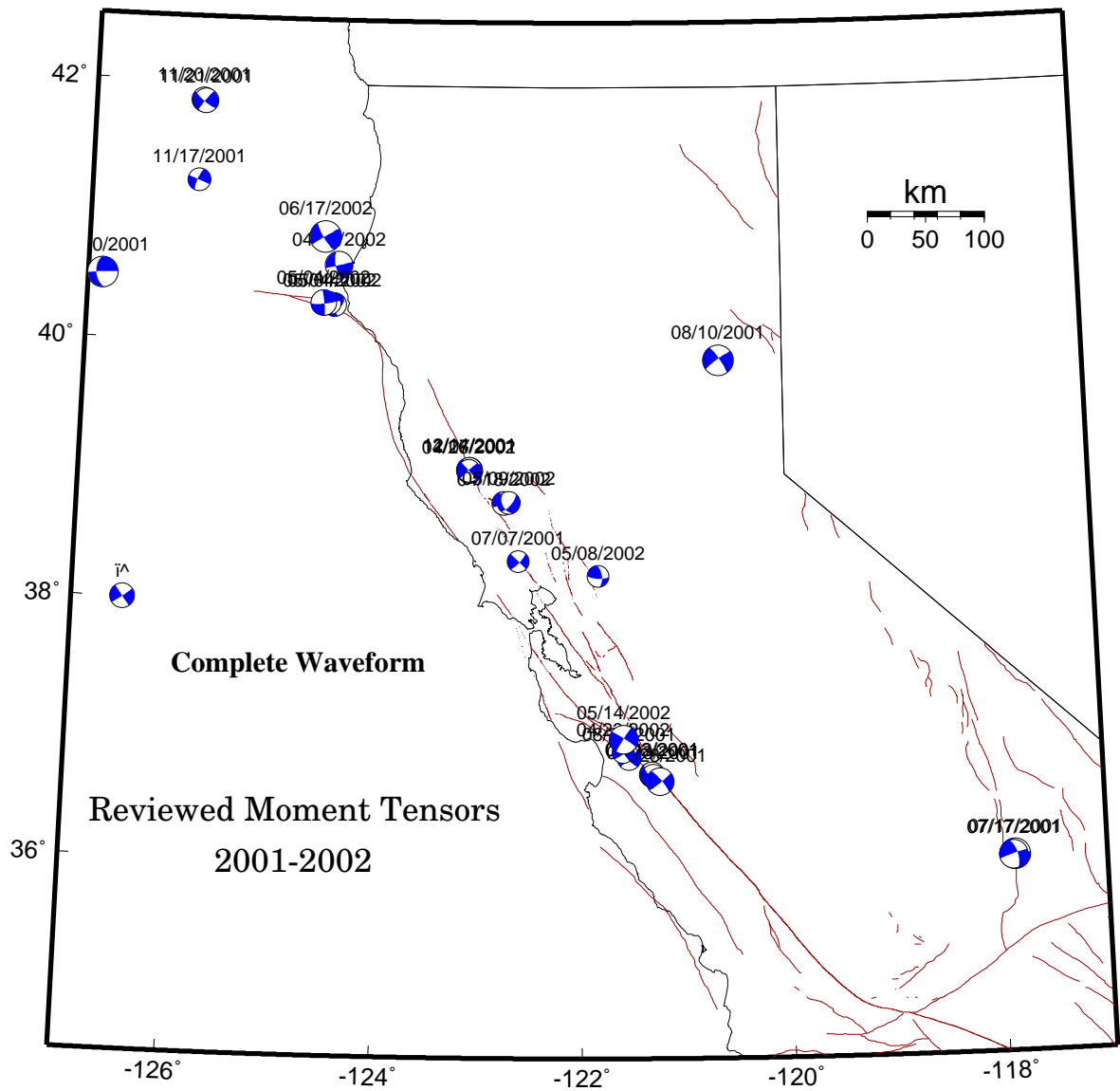


Figure 12.7: Map comparing the reviewed moment tensor solutions from the joint notification system. Solutions from the complete waveform inversion are plotted in black.

Location	Date	Time	Lat.	Lon.	MT Dep.	$M_L$	$M_w$	$M_o$	Str.	Dip	Rake	Meth.
Tres Pinos	07/02/2001	17:33:53.0	36.694	-121.333	8.0	4.1	4.1	1.80e22	60	89	-6	1
					11.0	4.1	4.1	1.69e22	133	87	-158	2
Tres Pinos	07/03/2001	19:02:50.0	36.696	-121.329	6.0	4	4.2	2.30e22	221	85	28	1
					11.0	4	4.1	2.05e22	138	77	-176	2
Tres Pinos	07/03/2001	19:07:16.0	36.683	-121.319	6.0	3.9	4.0	1.10e22	36	70	-35	1
					11.0	3.9	4.0	1.23e22	133	76	-154	2
Rohnert Park	07/07/2001	15:07:31.0	38.344	-122.630	11.0	3.7	3.7	3.34e21	133	90	-166	2
Coso Junction	07/17/2001	12:07:25.0	36.017	-117.878	8.0	4.9	5.2	6.89e23	352	83	171	2
Coso Junction	07/17/2001	12:59:58.0	36.013	-117.893	5.0	4.7	4.9	2.76e23	344	66	-176	2
Portola	08/10/2001	20:19:26.0	39.893	-120.638	24.0	5.1	5.1	4.60e23	139	89	161	1
					24.0	5.1	5.2	6.80e23	326	81	-173	2
San Benito	08/26/2001	05:03:02.0	36.820	-121.550	5.0	3.9	4.0	1.12e22	135	80	-179	2
Trinidad	11/17/2001	02:17:00.0	41.234	-125.915	21.0	3.8	3.9	8.18e21	292	90	-167	2
Oregon	11/20/2001	16:58:11.0	41.854	-125.900	24.0	3.8	4.1	1.40e22	225	74	13	2
Oregon	11/21/2001	02:01:28.0	41.844	-125.878	24.0	3.9	4.1	1.48e22	218	84	10	2
Punta Gorda	11/30/2001	07:46:56.0	40.490	-126.850	18.0	4.7	4.9	2.20e23	269	79	145	1
					11.0	4.7	5.1	4.69e23	265	88	-144	2
Ukiah	12/07/2001	14:29:08.0	39.043	-123.117	8.0	4.1	4.3	3.09e22	326	81	162	2
Ukiah	12/14/2001	09:41:05.0	39.045	-123.120	11.0	4	4.4	3.92e22	328	76	179	2
Tres Pinos	12/28/2001	21:14:01.0	36.641	-121.252	5.0	4.7	4.6	9.99e22	320	80	174	2
Punta Gorda	01/07/2002	20:23:15.0	40.309	-127.108	11.0	4.7	5.0	3.38e23	345	72	-79	2
Geysers	04/18/2002	11:35:40.0	38.791	-122.774	5.0	3.5	4.0	9.97e21	162	74	-175	2
San Jose	04/23/2002	11:59:20.0	36.866	-121.607	8.0	3.6	3.7	3.45e21	324	89	171	2
Ukiah	04/26/2002	11:01:26.0	39.040	-123.125	8.0	3.5	3.8	5.48e21	228	85	-2	2
Ferndale	04/29/2002	00:43:29.0	40.609	-124.462	27.0	4.4	4.6	1.00e23	166	68	179	2
Punta Gorda	05/04/2002	12:17:00.0	40.305	-124.501	5.0	3.9	4.0	9.85e21	160	73	44	2
Punta Gorda	05/04/2002	12:54:23.0	40.313	-124.549	8.0	3.7	3.8	5.69e21	347	74	2	2
Punta Gorda	05/04/2002	13:56:31.0	40.319	-124.611	5.0	4.3	4.4	4.54e22	353	85	-8	2
Fairfield	05/08/2002	14:59:36.0	38.229	-121.845	14.0	3.7	3.7	3.90e21	353	62	160	2
Geysers	05/09/2002	11:07:55.0	38.797	-122.728	5.0	3.6	3.9	8.11e21	155	43	-147	2
Gilroy	05/14/2002	05:00:29.0	36.967	-121.600	8.0	5.2	4.9	2.86e23	212	87	-6	2
Nevada	06/14/2002	12:40:49.0	36.715	-116.300	8.0	4.4	4.6	7.86e22	2	75	-121	2
Eureka	06/17/2002	16:55:07.0	40.829	-124.606	21.0	5.1	5.3	8.98e23	238	88	12	2

Table 12.1: Moment tensor solutions for significant events from July 1, 2001 to June 30, 2002 using both regional methodologies. Epicentral information from the UC Berkeley/USGS Northern California Earthquake Data Center. Moment is in dyne-cm and depth is in km. Key to methods: (1) Complete waveform fitting inversion; (2) Regional surface wave inversion.

## 6. References

Dreger, D. and A. Kaverina, Seismic remote sensing for the earthquake source process and near-source strong shaking: A case study of the October 16, 1999 Hector Mine earthquake, *Geophys. Res. Lett.*, *27*, 1941-1944, 2000.

Dreger, D., and A. Kaverina, Development of procedures for the rapid estimation of ground shaking, *PGE-PEER Final Report*, 1999.

Dreger, D., and B. Romanowicz, Source characteristics of events in the San Francisco Bay region, *USGS Open-File-Report 94-176*, 301-309, 1994.

Gee, L., D. Neuhauser, D. Dreger, M. Pasyanos, R. Uhrhammer, and B. Romanowicz, The Rapid Earthquake Data Integration Project, *Handbook of Earthquake and Engineering Seismology*, IASPEI, in press, 2002.

Gee, L., D. Neuhauser, D. Dreger, M. Pasyanos, B. Romanowicz, and R. Uhrhammer, The Rapid Earthquake Data Integration System, *Bull. Seis. Soc. Am.*, *86*, 936-945, 1996.

Johnson, C., A. Bittenbinder, B. Bogaert, L. Dietz, and W. Kohler, Earthworm: A flexible approach to seismic network processing, *IRIS Newsletter*, *XIV (2)*, 1-4, 1995.

Kanamori, H., P. Maechling, and E. Hauksson, Continuous monitoring of ground-motion parameters, *Bull. Seis. Soc. Am.*, *89*, 311-316, 1999.

Murdock, J., and C. Hutt, A new event detector designed for the Seismic Research Observatories, *USGS Open-File-Report 83-0785*, 39 pp., 1983.

Romanowicz, B., D. Dreger, M. Pasyanos, and R. Uhrhammer, Monitoring of strain release in central and northern California using broadband data, *Geophys. Res. Lett.*, *20*, 1643-1646, 1993.

Pasyanos, M., D. Dreger, and B. Romanowicz, Toward real-time estimation of regional moment tensors, *Bull. Seis. Soc. Am.*, *86*, 1255-1269, 1996.

Somerville, P., N. Smith, R. Graves, N. Abrahamson, Modification of empirical strong ground motion attenuation results to include the amplitude and duration effects of rupture directivity, *Seismol. Res. Lett.*, *68*, 199-222, 1997.

Wald, D., V. Quitoriano, T. Heaton, H. Kanamori, C. Scrivner, and C. Worden, TriNet "ShakeMaps": Rapid generation of peak ground motion and intensity maps for earthquakes in southern California, *Earthquake Spectra*, *15*, 537-556, 1999.

## Chapter 13

# Northern California Earthquake Data Center

### 1. Introduction

The Northern California Earthquake Data Center, a joint project of the Berkeley Seismological Laboratory and the U.S. Geological Survey at Menlo Park, serves as an "on-line" archive for various types of digital data relating to earthquakes in central and northern California. The NCEDC is located at the Berkeley Seismological Laboratory, and has been accessible to users via the Internet since mid-1992.

The primary goal of the NCEDC is to provide a stable and permanent archival and distribution center of digital geophysical data for northern and central California such as seismic waveforms, electromagnetic data, GPS data, and earthquake parametric data. The principal networks contributing seismic data to the data center are the Berkeley Digital Seismic Network (BDSN) operated by the Seismological Laboratory, the Northern California Seismic Network (NCSN) operated by the USGS, and the Bay Area Regional Deformation (BARD) GPS network. The collection of NCSN digital waveforms date from 1984 to the present, the BDSN digital waveforms date from 1987 to the present, and the BARD GPS data date from 1993 to the present.

The NCEDC continues to use the World Wide Web as a principal interface for users to request, search, and receive data from the NCEDC. The NCEDC has implemented a number of useful and original mechanisms of data search and retrieval using the World Wide Web, which are available to anyone on the Internet. All of the documentation about the NCEDC, including the research users' guide, is available via the Web. Users can perform catalog searches and retrieve hypocentral information and phase readings from the various earthquake catalogs at the NCEDC via easy-to-use forms on the Web. In addition, users can peruse the index of available broadband data at the NCEDC, and can request and retrieve broadband data in standard SEED format via the Web. Access to all datasets is available via research accounts at the NCEDC. The NCEDC's Web address is

<http://quake.geo.berkeley.edu/>

### 2. NCEDC Overview

The NCEDC is located within the computing facilities at the Berkeley Seismological Laboratory in McCone Hall. The BSL facility provides the NCEDC with air conditioning, 100 bit switched network, and reliable power from a UPS with generator backup.

The current NCEDC facilities consist of a Sun Ultra 450 computer, a 2.5 TByte capacity DISC 517 slot jukebox with four 5.2 GByte MO drives and 5.2 GB MO media, an 15-slot AIT tape jukebox which holds 25 GBytes per tape, and the SAM-FS hierarchical storage management (HSM) software. A dual processor Sun Ultra 60 provides Web services and research account access to the NCEDC.

The hardware and software system can be configured to automatically create multiple copies of each data file. The NCEDC uses this feature to create an online copy of each data file on MO media, and another copy on AIT tape which is stored offline.

### 3. 2001-2002 Activities

By its nature, data archiving is an ongoing activity. In 2001-2002, the NCEDC continued to expand its data holdings and enhance access to the data. Projects and activities of particular note include:

- Establishment of a continuous archive for NCSN broadband data
- Development of procedures to populate NCSN hardware information, instrument response, and waveform inventory in the NCEDC database
- Development of *CalQC* program to facilitate quality control procedures for continuous data channels

- Design of waveform protocol to exchange data with the SCEDC
- Adaption of *STP* to the NCEDC
- Initiation of project to archive the remaining 16-bit BDSN data to MiniSEED
- Development of new Web pages

These activities and projects are described in detail below.

## 4. Data Collections

The bulk of the data at the NCEDC consist of waveform and GPS data from northern California. The total size of the datasets archived at the NCEDC is shown in Table 13.1. Figure 13.1 shows the geographic distribution of data archived by the NCEDC.

### 4.1 BDSN/NHFN/MPBO Seismic Data

The archival of current BDSN (Chapter 4), NHFN (Chapter 5), and Mini-PBO (Chapter 9) (all stations using the network code BK) seismic data is an ongoing task. These data are telemetered from more than 30 seismic data loggers in real-time to the BSL, where they are written to disk files. Each day, an extraction process creates a daily archive by retrieving all continuous and event-triggered data for the previous day. The daily archive is run through quality control procedures to correct any timing errors, triggered data is reselected based on the REDI, NCSN, and BSL earthquake catalogs, and the resulting daily collection of data is archived at the NCEDC.

All of the data acquired from the BDSN/NHFN/MPBO Quanterra data loggers are archived at the NCEDC. The NCEDC has made an effort to archive older digital data, and the 16-bit BDSN digital broadband data from 1987-1991 have been converted to MiniSEED and are now online. In late June 2002, the NCEDC initiated a project to convert the remaining 16-bit BDSN data (MHC, SAO, and PKD1) from late 1991 through mid-1992 to MiniSEED. An undergraduate student has been hired to read the old tapes and to work on the conversion. Data acquired by portable 24-bit RefTek recorders before the installation of Quanterra data loggers at NHFN sites has not yet been converted to MiniSEED and archived.

### 4.2 NCSN/SHFN Seismic Data

NCSN and SHFN waveform data are sent to the NCEDC via the Internet. The NCSN event waveform files are automatically transferred from the Menlo Park to the NCEDC as part of the routine analysis procedure

by the USGS, and are automatically verified and archived by the NCEDC.

A few corrupt NCSN event files were discovered at the NCEDC several years ago, and were eventually traced down to suspected flaws in the 12-inch WORM media and/or firmware problems on the Sony WDA-600 series jukeboxes used by the NCEDC. When we transcribed the data from the 12-inch WORM media to the current 5.25 inch magneto-optical media, we verified that all files were transcribed accurately. In 2000-2001, using software developed at the NCEDC to detect possibly corrupt NCSN files, we identified 4704 possibly corrupted NCSN waveform event files. We re-read the original NCSN tapes for all of these events, discovered that only 71 of the files were actually corrupt, and replaced the corrupted event waveform files.

The NCEDC maintains a list of teleseismic events recorded by the NCSN, which is updated automatically whenever a new NCSN event file is received at the NCEDC, since these events do not appear in the NCSN catalog.

The NCSN has installed 9 continuously telemetered digital broadband stations in northwest California and southwest Oregon in support of the USGS/NOAA Consolidated Reporting of EarthquakeS and Tsunamis (CREST) system. This year, the NCEDC established procedures to create an archive of continuous data from these stations, in addition to the event waveform files. These data initially included channels at 50 and 100 Hz, but now are all 100 Hz sampling. The NCEDC hoped to generate an archive of 20 Hz data (for consistency with the BDSN data) from these 100 Hz waveforms, but problems with missing data has made this difficult. At this point, the NCEDC is archiving the 100 Hz data without decimation.

### 4.3 Parkfield HRSN Data

Event seismograms from the Parkfield High Resolution Seismic Network (HRSN) from 1987 through June 1998 are available in their raw SEG-Y format via NCEDC research accounts. A number of events have faulty timing due to the lack or failure of a precision timesource for the network. Due to funding limitations, there is currently no ongoing work to correct the timing problems in the older events or to create MiniSEED volumes for these events. However, a preliminary catalog for a significant number of these events has been constructed, and the catalog is available via the web at the NCEDC.

As described in Chapter 6, the original HRSN acquisition system died in late 1998, and an interim system of portable RefTek recorders were installed at some of the sites. Data from this interim system are not currently available online.

In 2000 and 2001, 3 new borehole sites were installed, and the network was upgraded to operate with Quan-

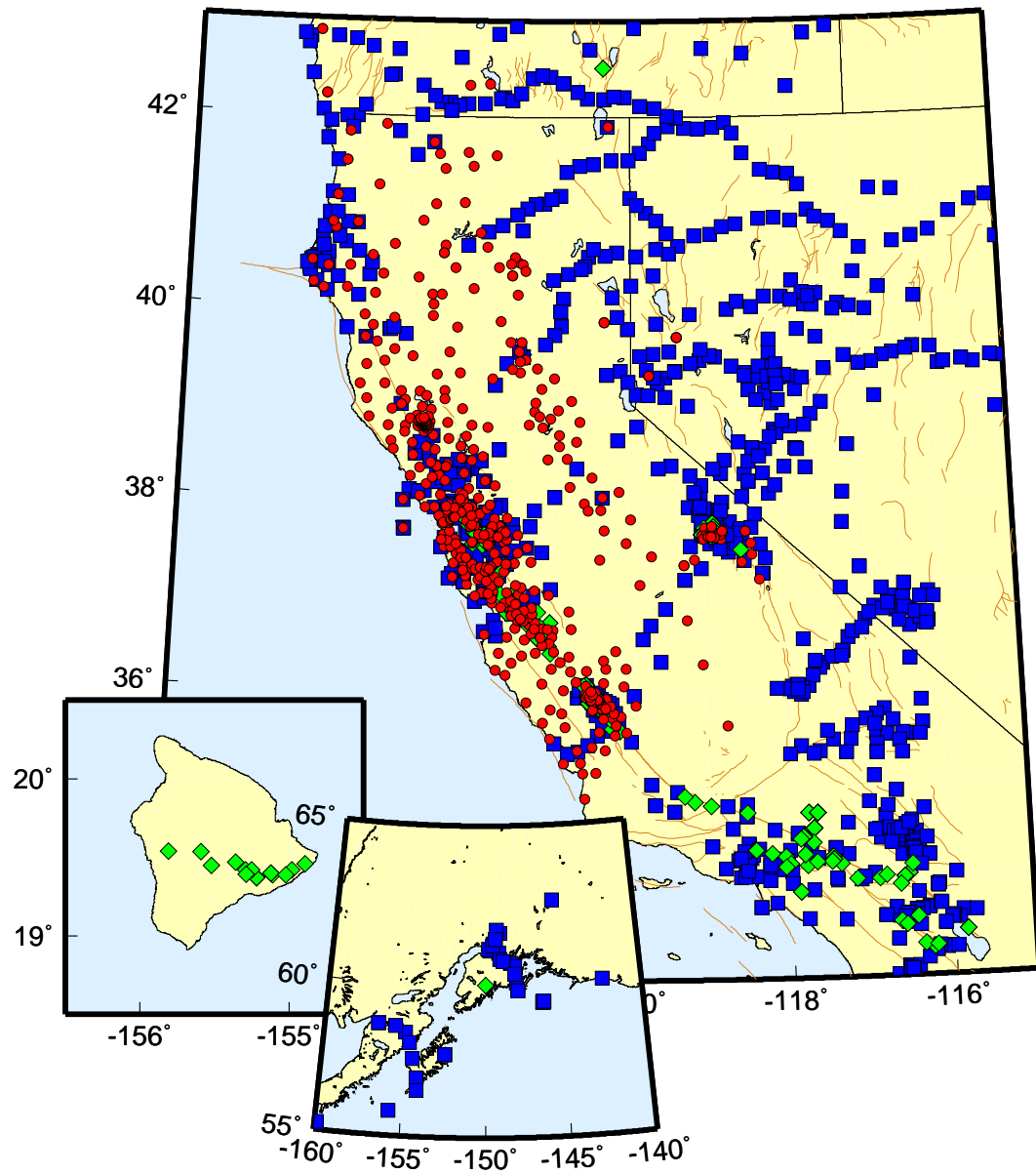


Figure 13.1: Map showing the location of stations whose data are archived at the NCEDC. Circles are seismic sites; squares are GPS sites, and diamonds are the locations of USGS Low-frequency experiments.

# BDSN/NHFN Data Availability

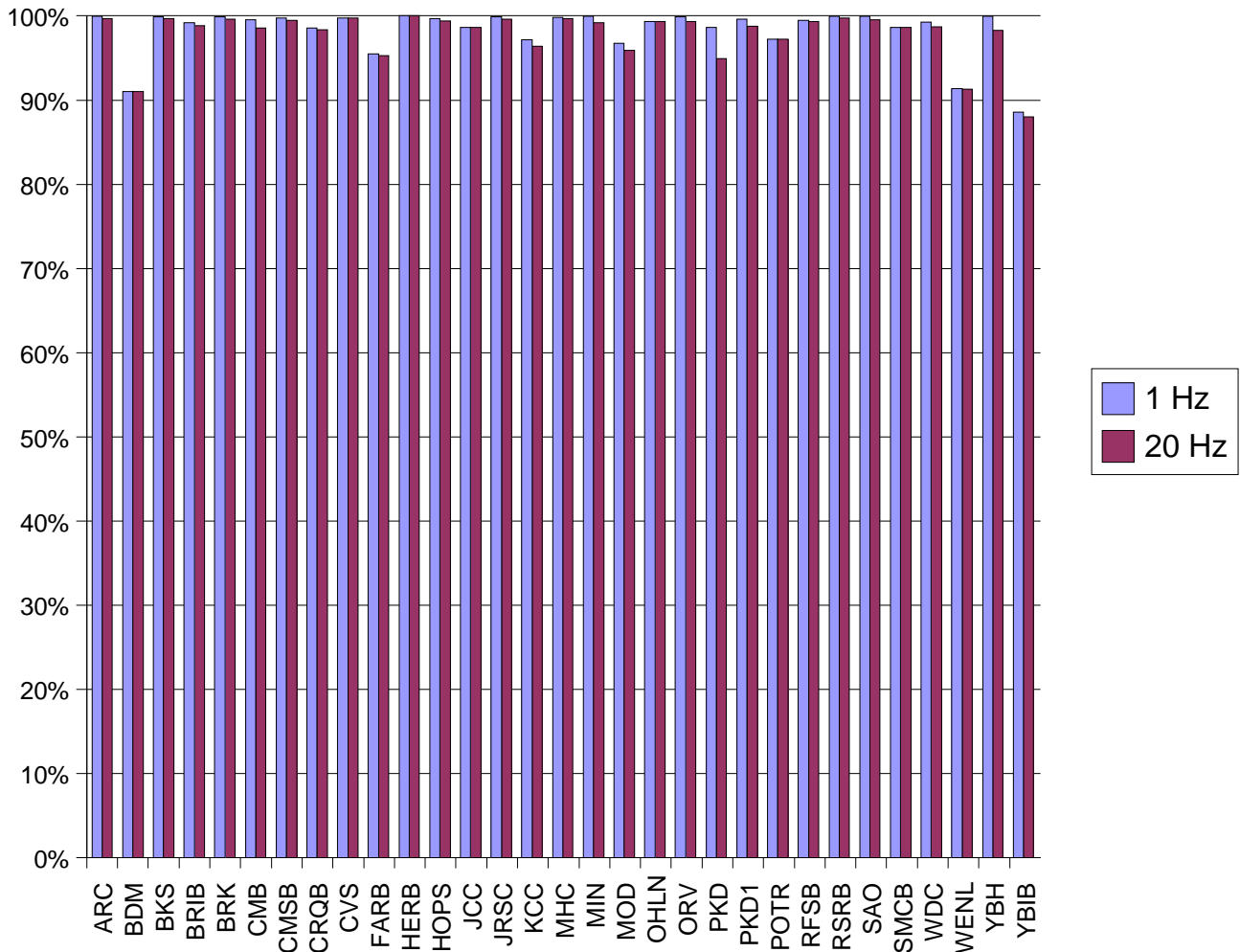


Figure 13.2: Chart showing the availability of BDSN/NHFN/MPBO data at the NCEDC for the 1 Hz and 20 Hz channels from 01/01/1996 - 06/30/2002. The "uptime" of these networks is better than 95% at nearly all stations. Exceptions are BDM (damaged by a lightning strike in May 2000), FARB (power problems when the USFWS generator failed in 1998), MOD (the newest BDSN station which suffered some delays during installation), WENL (flooded during the winter of 1997), and YBIB (damaged during a lightning strike in 1997, and without AC power for the past 2 years). In general, a difference between the 1 and 20 Hz data is indicative of one or more significant telemetry problems. Following a major telemetry outage, BSL staff will recover 1 Hz continuous data but only event data for the 20 Hz channels.

Data Type	MBytes
BDSN/NHFN/MPBO (broadband, electric field, magnetic field, strain) waveforms	848,181
NCSN seismograms	328,467
Parkfield HRSN seismograms	352,860
BARD GPS (RINEX and raw data)	296,172
UNR Nevada seismograms	85,778
Calpine/Unocal Geysers region seismograms	38,658
USGS Low frequency geophysical waveforms	917
Misc data	56,802
Total size of archived data	2,007,835

Table 13.1: Volume of Data Archived at the NCEDC by network

terra Q730 data loggers and digital telemetry. The upgraded acquisition system detects events using the HRSN stations, and through collaboration with the temporarily deployed PASSCAL network (PASO), extracts waveforms from both the HRSN and the PASO stations. The event waveform files are automatically transferred to the NCEDC, where they are made available to the research community via anonymous ftp until they are reviewed and permanently archived.

The HRSN 20 Hz (BP) and state-of-health channels are being archived continuously at the NCEDC. As an interim measure, the NCEDC is also archiving continuous data from the 250 Hz (DP) channels in order to help researchers retrieve events that were not detected during the network upgrade.

#### 4.4 UNR Broadband data

The University of Reno in Nevada (UNR) operates several broadband stations in western Nevada and eastern California that are important for northern California earthquake processing and analysis. Starting in August 2000, the NCEDC has been receiving and archiving continuous broadband data from four UNR stations. The data are transmitted in real-time from UNR to UC Berkeley, where it is made available for real-time earthquake processing and for archiving.

In a situation similar to that of the broadband waveforms from the NCSN, the NCEDC originally planned to create an archive of 20 Hz data from the 100 Hz data. However, frequent gaps in the data complicate the development of a robust decimation process. At this time, the UNR broadband waveforms are being archived at 100 Hz.

#### 4.5 Electro-Magnetic Data

The NCEDC continues to archive and process electric and magnetic field data acquired from data loggers at two sites (SAO and PKD). At PKD and SAO, 3 components of magnetic field and 2 or 4 components of electric field are digitized and telemetered in real-time along with

seismic data to the Seismological Laboratory, where they are processed and archived at the NCEDC in a similar fashion to the seismic data (Chapter 7). The system generates continuous data channels at 40 Hz, 1 Hz, and .1 Hz for each component of data. All of these data are archived and remain available online at the NCEDC. Using programs developed by Dr. Martin Fullerkrug at the Stanford University STAR Laboratory (now at the Institute for Meteorology and Geophysics at the University of Frankfurt), the NCEDC is computing and archiving magnetic activity and Schumann resonance analysis using the 40 Hz data from this dataset. The magnetic activity and Schumann resonance data can be accessed from the Web.

In addition to the electro-magnetic data from PKD and SAO, the NCEDC archives data from a low-frequency, long-baseline electric field project operated by Dr. Steve Park of UC Riverside at site PKD2. This experiment (which is separate from the equipment at PKD1 described in Chapter 7), uses an 8-channel Quanterra data logger to record the data, which are transmitted to the BSL using the same circuit as the BDSN seismic data. These data is acquired and archived in an identical manner to the other electric field data at the NCEDC.

#### 4.6 GPS Data

The NCEDC continues to expand its archive of GPS data through the BARD (Bay Area Regional Deformation) network of continuously monitored GPS receivers in northern California (Chapter 8). The NCEDC GPS archive now includes 67 continuous sites in northern California. There are approximately 50 core BARD sites owned and operated by UC Berkeley, USGS (Menlo Park and Cascade Volcano Observatory), LLNL, UC Davis, UC Santa Cruz, Trimble Navigation, and Stanford. Data are also archived from sites operated by other agencies including East Bay Municipal Utilities District, the City of Modesto, the National Geodetic Survey, and the Jet Propulsion Laboratory.

This year the NCEDC continued to archive non-continuous survey GPS data. The initial dataset to be

archived is the survey GPS data collected by the USGS Menlo Park for northern California and other locations. The NCEDC is the principal archive for this dataset. Significant quality control efforts were implemented by the NCEDC to ensure that the raw data, scanned site log sheets, and RINEX data are archived for each survey. All of the USGS MP GPS data has been transferred to the NCEDC and virtually all of the data from 1992 to the present has been archived and is available for distribution.

#### 4.7 Calpine/Unocal Geysers Seismic Data

The Calpine Corporation currently operates a micro-seismic monitoring network in the Geysers regions of northern California. Prior to 1999 this network was operated by Unocal. Through various agreements with both Unocal and Calpine, the companies have release triggered event waveform data from 1989 to through 2000 along with and preliminary event catalogs for the same time period for archiving and distribution through the NCEDC. This dataset represents over 296,000 events that were recorded by Calpine/Unocal Geysers network, and are available via research accounts at the NCEDC.

#### 4.8 USGS Low Frequency Data

Over the last 26 years, the USGS at Menlo Park, in collaboration with other principal investigators, has collected an extensive low-frequency geophysical data set that contains over 1300 channels of tilt, tensor strain, dilatational strain, creep, magnetic field, water level, and auxilliary channels such as temperature, pore pressure, rain and snow accumulation, and wind speed. In collaboration with the USGS, we assembled the requisite information for the hardware representation of the stations and the instrument responses for many channels of this diverse dataset, and developed the required programs to populate and update the hardware database and generate the instrument responses. We developed the programs and procedures to automate the process of importing the raw waveform data and convert it to MiniSEED format.

We have currently archived timeseries data from 887 data channels from 167 sites, and have instrument response information for 542 channels at 139 sites. The waveform archive is updated on a daily basis with data from 350 currently operating data channels. We will augment the raw data archive as additional instrument response information is assembled for the channels, and will work with the USGS to clearly define the attributes of the "processed" data channels.

### 4.9 Earthquake Catalogs

#### Northern California

Currently both the USGS and BSL construct and maintain earthquake catalogs for northern and central California. The "official" UC Berkeley earthquake catalog begins in 1910, and the USGS "official" catalog begins in 1966. Both of these catalogs are archived and available through the NCEDC, but the existence of 2 catalogs has caused confusion among both researchers and the public. The BSL and the USGS have spent considerable effort over the past year to define procedures for merging the data from the two catalogs into a single northern and central California earthquake catalog in order to present a unified view of northern California seismicity. The differences in time period, variations in data availability, and mismatches in regions of coverage all complicate the task.

#### Worldwide

The NCEDC, in conjunction with the Council of the National Seismic System (CNSS), has producing and distributed a world-wide composite catalog of earthquakes based on the catalogs of the national and various U.S. regional networks for several years. Each network updates their earthquake catalog on a daily basis at the NCEDC, and the NCEDC constructs a composite world-wide earthquake catalog by combining the data, removing duplicate entries that may occur from multiple networks recording an event, and giving priority to the data from each network's *authoritative region*. The catalog, which includes data from 14 regional and national networks, is searchable using a Web interface at the NCEDC. The catalog is also freely available to anyone via ftp over the Internet.

With the demise of the CNSS and the development of the ANSS, the NCEDC has been asked to update the Web pages to present the composite catalog as a product of the ANSS. This conversion will be completed in the fall of 2002.

### 5. Data Quality Control

The NCEDC developed a GUI-based state-driven system *CalQC* to facilitate the quality control processing that is applied to the BK, NC broadband, NN, and BP data sets.

The quality control procedures for these datasets include the following tasks:

- data extraction of a full day of data,
- quickcheck program to summarize the quality and stability of the stations' clock,

- checks for missing data along with procedures to retrieve data from the stations and incorporate it into the day of data,
- optional creation of multi-day timeseries plots for state-of-health data channels,
- optional timing corrections for data,
- optional extraction of event-based waveforms from continuous data channels,
- optional repacking of MiniSEED data,
- creating waveform inventory entries in the NCEDC database,
- publishing the data for remote access on the NCEDC.

*CalQC* uses previously developed the programs to perform each function, but it provides a graphical point-and-click interface to automate these procedures, and to provide the analyst with a record of when each process was started, whether it executed correctly, and whether the analyst has indicated that a step has been completed.

## 6. Database Development

Most of the parametric data archived at the NCEDC, such as earthquake catalogs, phase and amplitude readings, waveform inventory, and instrument responses have been stored in flat text files. Flat file are easily stored and viewed, but are not efficiently searched. Over the last year, the NCEDC, in collaboration with the USGS/SCEC Data Center, and TriNet, has continued development of database schemas to store the parametric data from the joint earthquake catalog, station history, complete instrument response for all data channels, and waveform inventory.

The parametric schema supports tables and associations for the joint earthquake catalog. It allows for multiple hypocenters per event, multiple magnitudes per hypocenter, and association of phases and amplitudes with multiple versions of hypocenters and magnitudes respectively. The instrument response schema represents full multi-stage instrument responses (including filter coefficients) for the broadband data loggers. The hardware tracking schema will represent the interconnection of instruments, amplifiers, filters, and data loggers over time. This schema will be used to store the joint northern California earthquake catalog and the CNSS composite catalog.

The entire description for the BDSN/NHFN/MPBO, HRSN, and USGS Low Frequency Geophysical networks and data archive has been entered into the hardware

tracking, SEED instrument response, and waveform tables. Programs have been developed to perform queries of waveform inventory and instrument responses, and the NCEDC can now generate full SEED volumes from the BDSN network based on information from the database and the waveforms on the mass storage system. The second stage of development will include the NCSN waveform inventory and later the NCSN instrument response data as they are made available. We distributed all of our programs and procedures to populate the hardware tracking and instrument response tables to the SCEDC in order to help them populate their database.

Additional details on the joint catalog effort and database schema development may be found at <http://quake.geo.berkeley.edu/db>

## 7. Data Access & Distribution

The various earthquake catalogs, phase, and earthquake mechanism can be searched using NCEDC web interfaces that allow users to select the catalog, attributes such as geographical region, time and magnitude. The GPS data is available to all users via anonymous ftp. Research accounts are available to any qualified researcher who needs access to the other datasets that currently are not available via the Web.

### 7.1 SeismiQuery

During 2000 and 2001, the NCEDC has developed a generalized database query system to support the development of portable database query applications among data centers with different internal database schemas. The initial goal was to modify the IRIS SeismiQuery web interface program to make installation easier at the NCEDC and other data centers, as well as to introduce a new query language that would be schema independent.

In order to support SeismiQuery and other future database query applications, we defined a set of Generic Data Views (GDV) for the database that encompassed the basic objects that we expect most data centers to support. We introduced a new language we call MSQL (Meta SeismiQuery Language), which is based on generic SQL, and uses the GDV's for its core schema. MSQL queries are converted to Data Center specific SQL queries by the parsing program MSQL2SQL. This parser stores the MSQL parsing tree in a data structure and API's were implemented to browse and modify elements in the parsing tree. These API's are the only datacenter or database specific source codes. We finally modified the SeismiQuery web interface to uniformly generate MSQL requests and to process these requests in a consistent fashion.

We have installed SeismiQuery at the NCEDC, where it provides a common interface for querying attributes

and available data for SEED format data, and have provided both IRIS and the SCEC Data Center with our modified version of SeismiQuery. We envision using this approach to support other database query programs in the future.

## 7.2 NetDC

In a collaborative project with the IRIS DMC and other worldwide datacenters, the NCEDC helped develop and implement NetDC, a protocol which will provide a seamless user interface to multiple datacenters for geophysical network and station inventory, instrument responses, and data retrieval requests. The NetDC builds upon the foundation and concepts of the IRIS BREQ\_FAST data request system. The NetDC system was put into production in January 2000, and is currently operational at three datacenters worldwide – the NCEDC, IRIS DMC, and Geoscope. The NetDC system receives user requests via email, automatically routes the appropriate portion of the requests to the appropriate datacenter, optionally aggregates the responses from the various datacenters, and delivers the data (or ftp pointers to the data) to the users via email.

The NCEDC hosts a web page that allows users to easily query the NCEDC waveform inventory, generate and submit NetDC requests to the NCEDC. The NCEDC currently supports both the BREQ\_FAST and NetDC request formats. As part of our collaboration with SCEDC, the NCEDC provided its BREQ\_FAST interface code to SCEDC, have worked closely with them to implement BREQ\_FAST requests at the SCEDC.

## 7.3 STP

This year, the NCEDC wrote a collaborative proposal with the SCEDC to the Southern California Earthquake Center, with the goal of unifying data access between the two data centers. As part of this project, the NCEDC and SCEDC are working to support a common set of 3 tools for accessing waveform and parametric data: SeismiQuery, NetDC, and STP.

The Seismogram Transfer Program or STP is a GUI-based client-server program, developed at the SCEDC. Access to STP is either through a simple direct interface that is available for Sun or Linux platforms or through a Web interface. With the direct interface, the data are placed directly on a users' computer in several possible formats, with the byte-swap conversion performed automatically. With the Web interface, the selected and converted data are retrieved with a single ftp command. The STP interface also allows rapid access to parametric data such as hypocenters and phases.

The NCEDC has started implementing STP, working with the SCEDC on extensions and needed additions.

## 7.4 GSAC

Since 1997, the NCEDC has collaborated with UNAVCO and other members of the GPS community on the development of the GPS Seamless Archive Centers (GSAC) project. When completed, this project will allow a user to access the most current version of GPS data and metadata from distributed archive locations. The NCEDC is participating at several levels in the GSAC project: as a primary provider of data collected from core BARD stations and USGS MP surveys, as a wholesale collection point for other data collected in northern California, and as a retail provider for the global distribution of all data archived within the GSAC system. We have helped to define database schema and file formats for the GSAC project, and for several years have produced complete and incremental monumentation and data holdings files describing the data sets that are produced by the BARD project or archived at the NCEDC so that other members of the GSAC community can provide up-to-date information about our holdings. Currently, the NCEDC is the primary provider for over 74,000 data files from over 1400 continuous and survey-mode monuments. The data holdings records for these data have been incorporated into a preliminary version of the retailer system currently undergoing testing, which should become publicly available in late 2002.

## 7.5 Web Pages

The NCEDC developed its Web pages in the early days of the Web. Unfortunately, time constraints have kept the pages somewhat static and limited in their use. In June of 2002, the NCEDC began an project to update and expand their Web offerings. This project is still underway and should be completed in the fall of 2002.

## 8. Acknowledgements

The NCEDC is a joint project of the BSL and the USGS Menlo Park and is partially funded by the USGS.

Doug Neuhauser is the manager of the NCEDC. Stephane Zuzlewski, Rick McKenzie, Mark Murray, André Basset, and Lind Gee of the BSL and David Oppenheimer, Hal Macbeth, and Fred Klein of the USGS Menlo Park contribute to the operation of the NCEDC. Steve Chu developed the *CalQC* program. Doug Neuhauser, Lind Gee, and Stephane Zuzlewski contributed to the preparation of this chapter.

# Chapter 14

## Outreach and Educational Activities

### 1. Introduction

The BSL is involved in a variety of outreach activities, ranging from lectures and lab tours to educational displays and the development of classroom materials for K-12 teachers. We maintain an earthquake information tape (510-642-2160) and an extensive set of Web pages, providing basic earthquake and seismic hazard information for northern and central California.

### 2. Outreach Overview

The BSL has several on-going outreach programs, such as the educational displays, WWW development, and the Earthquake Research Affiliates Program.

#### 2.1 Educational Displays

As part of the BSL's outreach activities, we have made REDI earthquake data available to a number of universities, colleges, and museums as educational displays. As noted above, this year marked the expansion of this program to the K-12 environment. Participating organizations receive a REDI pager and the Qpager software to display the earthquake information. The Qpager program maps the previous seven days of seismicity, with earthquake shown as a dot. The size of the dot indicates the magnitude of the event, while the color of the dot indicates its age. These educational displays have been installed at UC Berkeley (McCone Hall, Earthquake Engineering Research Center, LHS), California Academy of Sciences, CSU Fresno, CSU Northridge, CSU Sacramento, Caltech, College of the Redwoods, Fresno City College, Humboldt State University, San Diego State University, Sonoma State University, Stanford University (Blume Engineering Center, Department of Geophysics), UC Davis, UC Santa Cruz, UC San Diego, and USC. In a pilot project initiated two years ago, the San Francisco Unified School District has been given two pager systems for use in middle school classrooms.

In addition to the seismicity displays, the BSL provides local waveform feeds for helicorders at several visitor centers associated with BDSN stations (CMB and

MHC). Organizations such as LHS, KRON, and KPIX receive feeds from BKS via dedicated phone lines for display, while the USGS Menlo Park uses data from CMB for display in the lobby of the seismology building. The BSL has also loaned a seismometer and helicorder display to the San Leandro Unified School District for their use in science classes.

#### 2.2 WWW

Over the last year, we have continued to expand our presence on the WWW. Our primary goal has been to provide a source of earthquake information for the public, although we also provide information about the networks, such as station profiles, which benefits the research community as well. We provide such information as seminar schedules, course advertisements, descriptions of operations and research, updates on recent earthquake activity, details on Bay Area seismicity and hazards, and links to other earthquake and earth science servers. We also use the WWW server for our own information distribution, with such details as the computing and operational resources, rosters, and schedules for various purposes.

#### 2.3 Earthquake Research Affiliates Program

The UC Berkeley Earthquake Research Affiliates (ERA) Program is an outreach project of the BSL, the Department of Geology and Geophysics, and the Earthquake Engineering Research Center. The purpose is to promote the support of earthquake research while involving corporations and governmental agencies in academic investigation and education activities such as conferences and field trips. The ERA program provides an interface between the academic investigation and practical application of earthquake studies.

### 3. 2000-2001 Activities

#### 3.1 Interactive University Project

During 2001-2002, the ISTAT (Integrating Science, Teaching, and Technology) Project drew to a close.

This collaboration, part of the the Interactive University Project (IUP), brought the BSL, the Museum of Paleontology, the Space Sciences Laboratory, and the Center for Particle Astrophysics together in an earth and space science cluster, with a focus on education in "Integrating Science, Teaching, and Technology" (ISTAT) with a focus grades 6-12. We received a small 18 month grant in 1996 to initiate this project. Based on our success, we submitted a second proposal in 1998 and received funding for a 3 year project with Gloria Davis Middle School, Horace Mann Academic Middle School, Galileo High School, Mission High School, and Thurgood Marshall Academic High School in the San Francisco Unified School District (<http://www.UCMP.Berkeley.EDU/IU/>).

During this project, we worked with lead teachers to review the new San Francisco science and math standards and to identify "gaps" between existing resources and materials and the required content. San Francisco has recently adopted new textbooks with the goal of teaching Earth and Space Sciences in the 9th grade. We worked with the teachers to develop a working outline for the curriculum and to supplement the text with activities and resources.

The draft Earth science curriculum now includes a scope and sequence, course outlines for 6, 9, and 12 week modules, and preliminary assessment materials and is available on the Web at <http://seismo.berkeley.edu/seismo/istat/9th/>.

### 3.2 Teachers' Workshop

In the fall of 2001, Dr. Gee joined scientists from UCMP, San Francisco State University, San Jose State University, and the Cal Academy of Sciences to design an earth science course for middle school teachers. The course was composed of 5 workshops and Dr. Gee presented material on earthquakes.

### 3.3 Tours and Presentations

BSL staff have also spent considerable time with public relations activities during the past year. Several tours are given each month, with audiences ranging from middle-school students to scientists and engineers from China and Japan. This year, we saw a sizeable increase in visits from "home-school" students.

The BSL hosted several special groups during 2001-2002. A number of educational groups visited, including a class from Mills College a group of California city managers attending a conference sponsored by the Goldman School of Public Policy.

In addition to the tours, Drs. Romanowicz, Dreger, Uhrhammer, and Gee presented talks on earthquakes and related phenomena to public groups. Dr. Gee gave a presentation for the City of Berkeley, directed at the volunteers participating in the Disaster Resistent Berkeley program.

### 3.4 Take Your Child to Work Day

The BSL was unable to participate in Cal Day this year, due to a scheduling conflict with the annual meeting of the Seismological Society of America. The BSL did participate in "Take Your Child to Work Day" and hosted many UC Berkeley parents and their children. The visitors learned about UC Berkeley's role in earthquake monitoring, found out how many earthquakes occurred on their birthday, played with an "earthquake machine", made P and S-waves, learned about earthquake preparedness, and were given sample seismograms.

### 3.5 Workshops

The BSL co-hosted a workshop with Jack Boatwright of the USGS to discuss coordination of seismic instrumentation in Northern California, the generation and distribution of ShakeMaps, and the evolution of ANSS in March 2002. The workshop included representatives from the BSL, the USGS Menlo Park, the California Geological Survey, the California Office of Emergency Services, and PG&E.

### 3.6 1906 Centennial

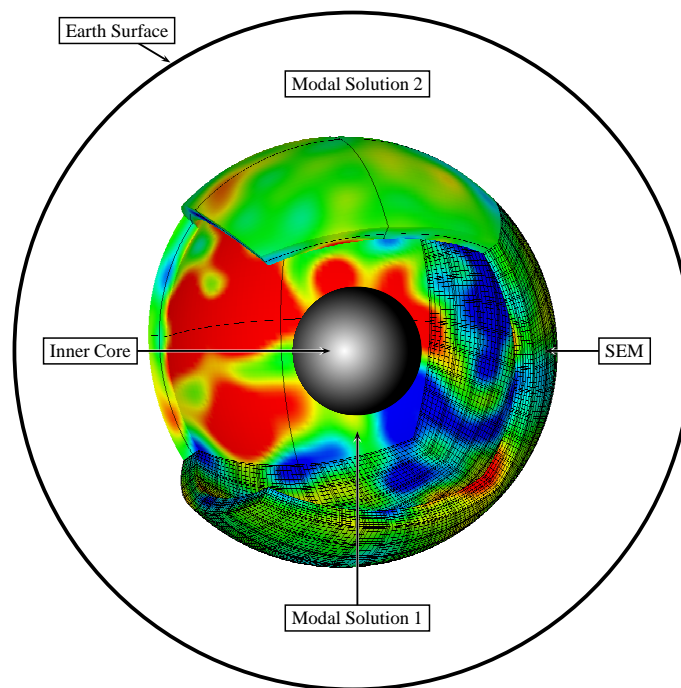
In less than 4 years, the Bay Area will celebrate the centennial of the 1906 earthquake. In June, 2002, the BSL hosted a meeting of representatives from the USGS and the Seismological Society of America (SSA) to begin planning for this historic anniversary. The BSL and the USGS have agreed to co-host the 2006 Annual Meeting of the SSA and discussed several ideas for organizing the meeting with Executive Director Susan Newman. In addition to plans for the scientific meeting, the BSL is collaborating with other campus units on commemorative activities.

## 4. Acknowledgements

Lind Gee oversees the outreach activities at the BSL. Barbara Romanowicz, Bob Uhrhammer, Rick McKenzie, and many other faculty, staff, and students at the BSL contribute to the outreach activities. Lisa Krain helps with the upkeep and development of new web pages. Lind Gee contributed to the preparation of this chapter.

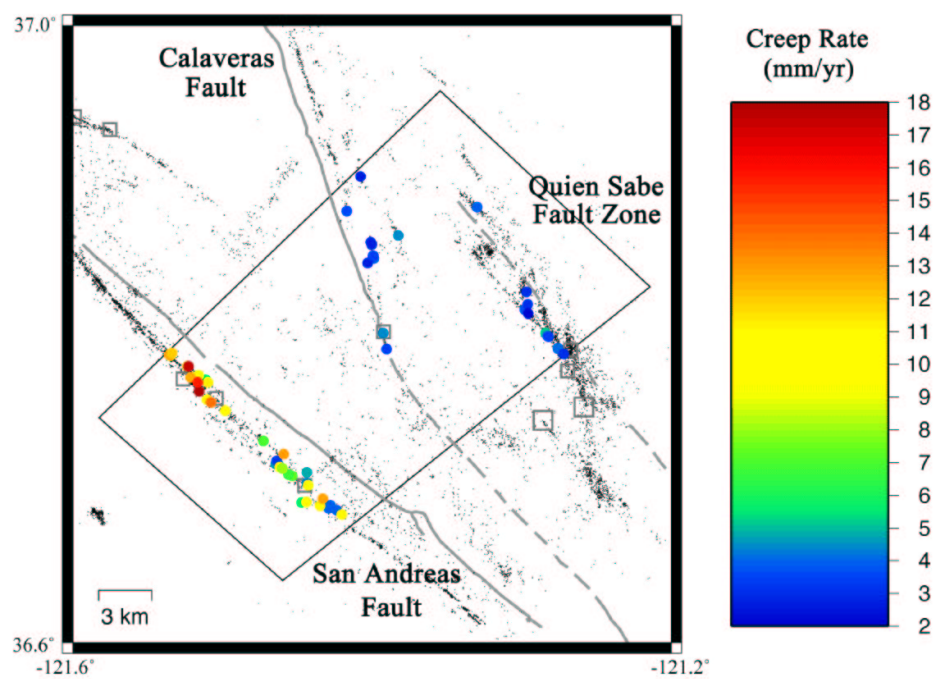
# Part III

## Ongoing Research Projects



# Chapter 15

## Source and Geodetic Studies



# 1. Parkfield Research

R.M. Nadeau, L.R. Johnson, A. Michelini (CRS, Italy), T.V. McEvelly, H.-R. Wenk

## 1.1 Introduction

The HRSN at Parkfield (Chapter 6) was installed in 1987 to provide a direct test of two hypotheses critical to our understanding of the physics of the earthquake process, with implications for earthquake hazard reduction and the possibilities for short-term earthquake prediction - major goals of the NEHRP:

1) That the earthquake nucleation process produces stress-driven perturbations in physical properties of the rocks in the incipient focal region that are measurable, and

2) That the nucleation process involves progressive and systematic failure that should be observable in the ultralow-magnitude microseismicity ( $-1 < M < 2$ ) with high-resolution locations and source mechanisms.

Analyses of the 14+ years of Parkfield monitoring data have revealed significant and unambiguous departures from stationarity both in the seismicity characteristics and in wave propagation details. Within the presumed M6 nucleation zone we also have found a high  $V_p/V_s$  anomaly at depth, where the three M 4.7-5.0 sequences occurred in 1992-94. Synchronous changes well above noise levels have also been seen among several independent parameters, including seismicity rates, average focal depth, S-wave coda velocities, characteristic sequence recurrence intervals, fault creep and water levels in monitoring wells. We have been able to localize the S-coda travel-time changes to the shallow part of the fault zone and demonstrate with numerical modeling the likely role of fluids in the phenomenon. We can connect the changes in seismicity to slip-rate variations evident in other (strain, water level) monitored phenomena. Based on the ubiquitous clusters of repeating microearthquakes, scaling laws have been developed that can be projected to fit earthquakes up to M6, and they predict unprecedented high stress drops and melting on the fault surface for the smallest events. Exhumed fault-zone rocks provide independent evidence for such source conditions. This hypothesis is being debated vigorously in the current literature. Recurrence interval variations in the characteristic event sequences (about one-third of the microearthquake population) have been used to map fault slip rate at depth on the fault surface, and this technique appears to be applicable to other types of faults. Along the way in this exciting discovery process we have challenged the conventional 'constant stress drop' source model, affirmed characteristic earthquake occurrence and developed four-dimensional maps of fault-zone microearthquake processes at the un-

precedented scale of a few meters. The significance of these findings lies in their apparent coupling and interrelationships, from which models for fault-zone process can be fabricated and tested with time. A more fundamental contribution of the project is its production of a continuous baseline, at very high resolution, of both the microearthquake pathology and the subtle changes in wave propagation, providing to the seismological community a dynamic earthquake laboratory available nowhere else. This unique body of observations and analyses has also provided much of the impetus for Parkfield as the preferred site for deep drilling into an active seismogenic fault zone (the SAFOD project), and we have upgraded and expanded the network to improve its view of the drilling target zone on the fault surface.

## 1.2 Recent BSL/Collaborative Research

Over the past year, data and previously derived theoretical and empirical relationships from Parkfield have served as a basis for investigations on a variety of topics by BSL researchers and collaborators at the Department of Terrestrial Magnetism (Carnegie) and Lawrence Berkeley National Laboratory (LBNL).

*Johnson and Nadeau* (2002) developed an empirically based earthquake asperity model that explains previously determined earthquake scaling relationships from characteristically repeating earthquake sequences (CS) at Parkfield. Their model suggests fault strength to be highly heterogeneous.

*Korneev et al.* (2002) have used Fault Zone Guided Waves (FZGW) from HRSN recorded microearthquakes to image the structure of the innermost fault zone using FZGW attenuation.

*Niu et al.* (2002) have used Parkfield CS events as highly repeating illumination sources to reveal the stress-induced migration of scatterers of seismic energy. By examining the systematics of temporal changes in the coda arrivals of CS events and stress changes inferred from the evolution of deformation at Parkfield, they infer that stress-induced redistribution of fluids along fractures in or adjacent to the fault are taking place.

Using the scaling (Tr-Mo) of CS recurrence intervals (Tr) with seismic moments (Mo) (*Nadeau and Johnson*, 1998) and the its calibration with intermediate scale geodetic measurements at Parkfield, *Schmidt et al.* (2002) and *Nadeau and McEvelly* (2002) are mapping areas of deep fault slip and slip rates along the East Bay Area Hayward Fault and along the central creeping section of the San Andreas Fault (SAF) in California.

In ongoing investigations of the Tr-Mo scaling, BSL researchers have extended the range in Mo over which scaling occurs to over 15 orders of magnitude in Mo (Figure 15.1). This relationship serves as a basis for empirical determinations of earthquake source parameters of area (A), seismic slip (d), and stress drop (Nadeau and Johnson, 1998). These determinations involve relatively few model assumptions and are independent of existing models relating the shape and spectra of seismic waveforms to the mechanics of earthquake sources. Results of the CS based approach have implications that are significantly different from the standard models derived from the waveform base methods.

### 1.3 Impetus for External Research

Recently, several independent research groups external to Berkeley have attempted to explain the discrepancy between CS based and standard model scaling of source parameters by providing alternative interpretations to that of Nadeau and Johnson for the observed Tr-Mo (e.g. *Anooshehpour and Brune, 2001; Sammis and Rice, 2001; Beeler et al., 2001; Chen and Sammis, 2002*).

These interpretations involve mechanisms in which loading of the CS patches is magnitude dependent. For example, Beeler et al. have proposed a creep-slip mechanism to explain the Tr-Mo discrepancy at small Mo ( $10^{15}$  to  $10^{18}$  dyne-cm); however, their model does not appear to provide a satisfactory explanation for Tr-Mo at intermediate Mo earthquakes (approx. magnitudes 1.5 to 5) nor for very small events (magnitudes  $< 0$ ) (Figure 15.1).

Interpretations based on slip shielding arguments such as those of Sammis and Rice and Anooshehpour and Brune require CS to be located adjacent to or embedded within large locked patches. However, locations of CS appear to be widely distributed and usually well away from large locked zones (e.g. in the central creeping section of the SAF). Furthermore their relationships in the Tr-Mo scaling generally remain consistent with that expected from local geodetic loading rates regardless of proximity to large locked zones.

### 1.4 Related Research

A number of other recent studies have recognized the significance of the CS systematics and scaling found at Parkfield and have explored their implications from a variety of perspectives. For example with respect to high-precision relative relocations (*Waldhauser and Ellsworth, 2002; Rubin, 2002; Schaff et al., 2002*), and with respect to earthquake physics, seismicity variations and deformation rates along strike-slip and subducting faults in California and Japan (*Matsuzawa et al., 2002; Seno, 2002*).

## 1.5 SAFOD

Another principal focus of BSL's recent research at Parkfield has been the detailed analysis and monitoring of the characteristics of microseismicity within the drilling and penetration zone of the SAFOD component of the NSF initiative EarthScope. Of particular interest is the evolution of fault zone deformation and detailed seismic structure immediately surrounding the repeating SAFOD M2 target zone, and the recurrence behavior and size of the two potential M2 targets (separated by 70 m).

Using a 3-dimensional double-difference code developed by Alberto Michelini in Italy and a preexisting 3-D cubic splines interpolated velocity model developed from HRSN data (*Michelini and McEvilly, 1991*), we have been able to resolve the relative seismic structure in the target zone in great detail (Nadeau et al., 2001) (Figure 15.2). The relocations indicate that the subhorizontally drilled portion of the SAFOD hole may need to penetrate a seismically active (and the existence of CS imply actively slipping) strand some 300m to the SW before entering the M2 target region.

CS exist on both strands and slip rates on the strands inferred from the Tr of the CS in the strands indicate that both are slipping at about 10 to 15 mm/yr. This suggests a distinct possibility of shearing of the deep borehole casing on the SW strand which needs to be taken into account if long term monitoring of the local target is to take place.

The Tr-Mo relationship and ongoing monitoring of the Tr's of the CS local to the M2 target(s) can also be used to help estimate the expected occurrence time of the next M2 repeat (Figure 15.3). This information will be helpful in the planning of SAF penetration and monitoring efforts, as well as for testing of earthquake recurrence forecast models, and for evaluating the conditions surrounding the M2 target(s) leading up to failure.

The SAFOD experiment will also measure deformation along the deep hole which will provide a direct calibration of slip rates at depth with CS Tr's near the target zone. This will provide ground truth for interpretation of the Tr-Mo relationship, and is crucial for establishing an accurate model of CS recurrence behavior, for interpreting Tr-Mo based source parameter scaling relationships, for the extrapolation of fault and earthquake physics based on the Tr-Mo scaling, and for application of the CS deep fault slip rate method to slipping faults generally.

In regards to the drilling operation, the calibration will also provide a better picture of the M2 target size by providing a more accurate estimate of the partitioning of Mo from the expected M2 event ( $Mo = \mu dA$ ) into its seismic slip (d) and rupture area (A) dimensions. Currently, estimates of the dimensions of the M2 target(s) vary significantly depending on the expected stress drop of the M2 events on the patch. Figure 15.4 shows the 2 potential M2 targets and estimated target sizes based on

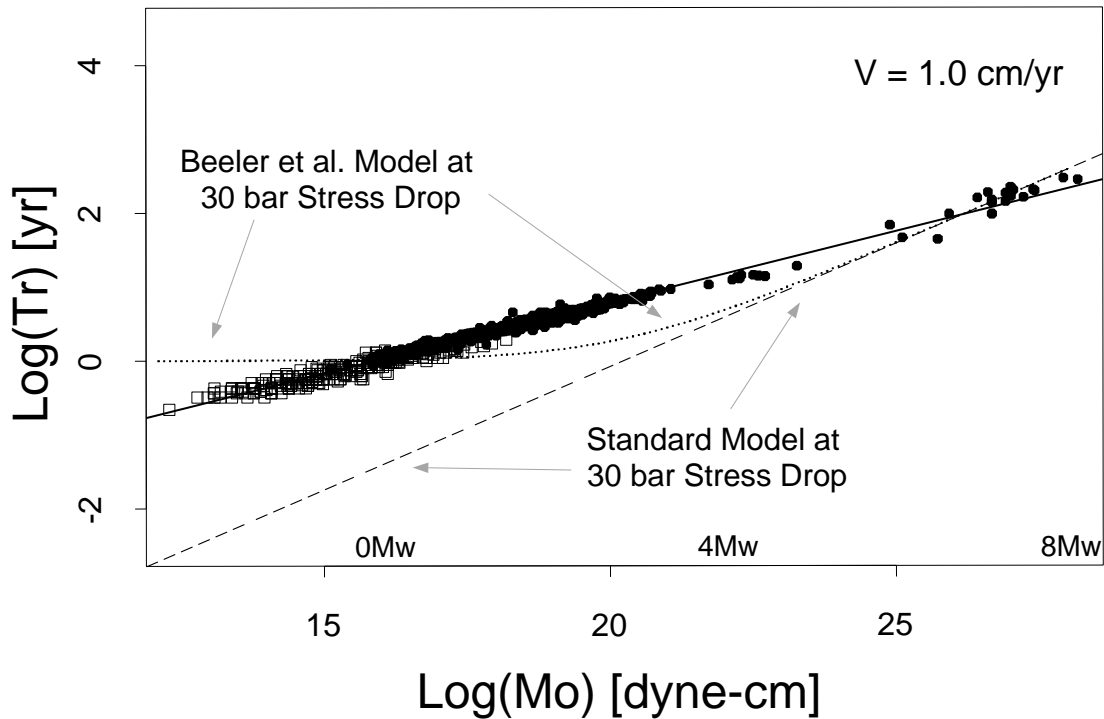


Figure 15.1: Log characteristic sequence recurrence time versus seismic moment normalized to a fault loading rate of 1 cm/yr. Filled circles show data for modern and historical characteristic events in California. Open squares are inferred  $T_r$  and  $M_o$  of fossil earthquakes (pseudotachylites) near Palm Desert California. Black line is a least squares fit to the characteristic earthquake data.

30 bar stress drop (from a standard constant stress drop model) and 2700 bar stress drop suggested by the  $T_r$ - $M_o$  scaling (Nadeau and Johnson, 1998).

More information about the SAFOD project is available on the Web at: <http://www.icdp-online.de/html/sites/sanandreas/objectives/objectives.html> and <http://www.icdp-online.de/html/sites/sanandreas/objectives/proposal.html>

## 1.6 Acknowledgements

We appreciate support for this project by the USGS NEHRP through grant numbers 01HQGR0057 and 02HQGR0067 and by the NSF through award number 9814605.

## 1.7 References

Anooshehpour, A. and J.N. Brune, Quasi-Static Slip-Rate Shielding by Locked and Creeping Zones as an Explanation for Small Repeating Earthquakes at Parkfield, *Bull. Seism. Soc. Am.*, *91*, 401-403, 2001.

Beeler, N.M., A simple stick-slip and creep-slip model for repeating earthquakes and its implication for micro-earthquakes at Parkfield, *Bull. Seism. Soc. Am.*, *91*, 1797-1804, 2001.

Burgmann, R., D. Schmidt, R.M. Nadeau, M. d'Alessio, E. Fielding, D. Manaker, T.V. McEvelly, and

M.H. Murray, Earthquake Potential along the Northern Hayward Fault, California, *Science*, *289*, 1178-1182, 2000.

Chen, Y. and C.G. Sammis, A Numerical Asperity Model for Repeating Earthquakes, *Bull. Seism. Soc. Am.*, submitted, 2002.

Johnson, L.R. and R.M. Nadeau, Asperity Model of an Earthquake-Static Problem, accepted, *Bull. Seism. Soc. Am.*, *92*, 672-686, 2002.

Karageorgi, E., R. Clymer and T.V. McEvelly, Seismological studies at Parkfield. II. Search for temporal variations in wave propagation using Vibroseis, *Bull. Seism. Soc. Am.*, *82*, 1388-1415, 1992.

Karageorgi, E.D., T.V. McEvelly and R.W. Clymer, Seismological Studies at Parkfield IV: Variations in controlled-source waveform parameters and their correlation with seismic activity, 1987-1994, *Bull. Seism. Soc. Am.*, *87*, 39-49, 1997.

Korneev, V.A., T.V. McEvelly and E.D. Karageorgi, Seismological Studies at Parkfield VIII: Modeling the Observed Controlled-Source Waveform Changes, *Bull. Seism. Soc. Am.*, *90*, 702-708, 2000.

Korneev, V.A., R.M. Nadeau and T.V. McEvelly, Seismological Studies at Parkfield IX: Fault Zone Imaging using Guided Wave Attenuation, *Bull. Seism. Soc. Am.*, submitted in revision, 2002.

Matsuzawa, T., T. Igarashi and A. Hasegawa, Char-

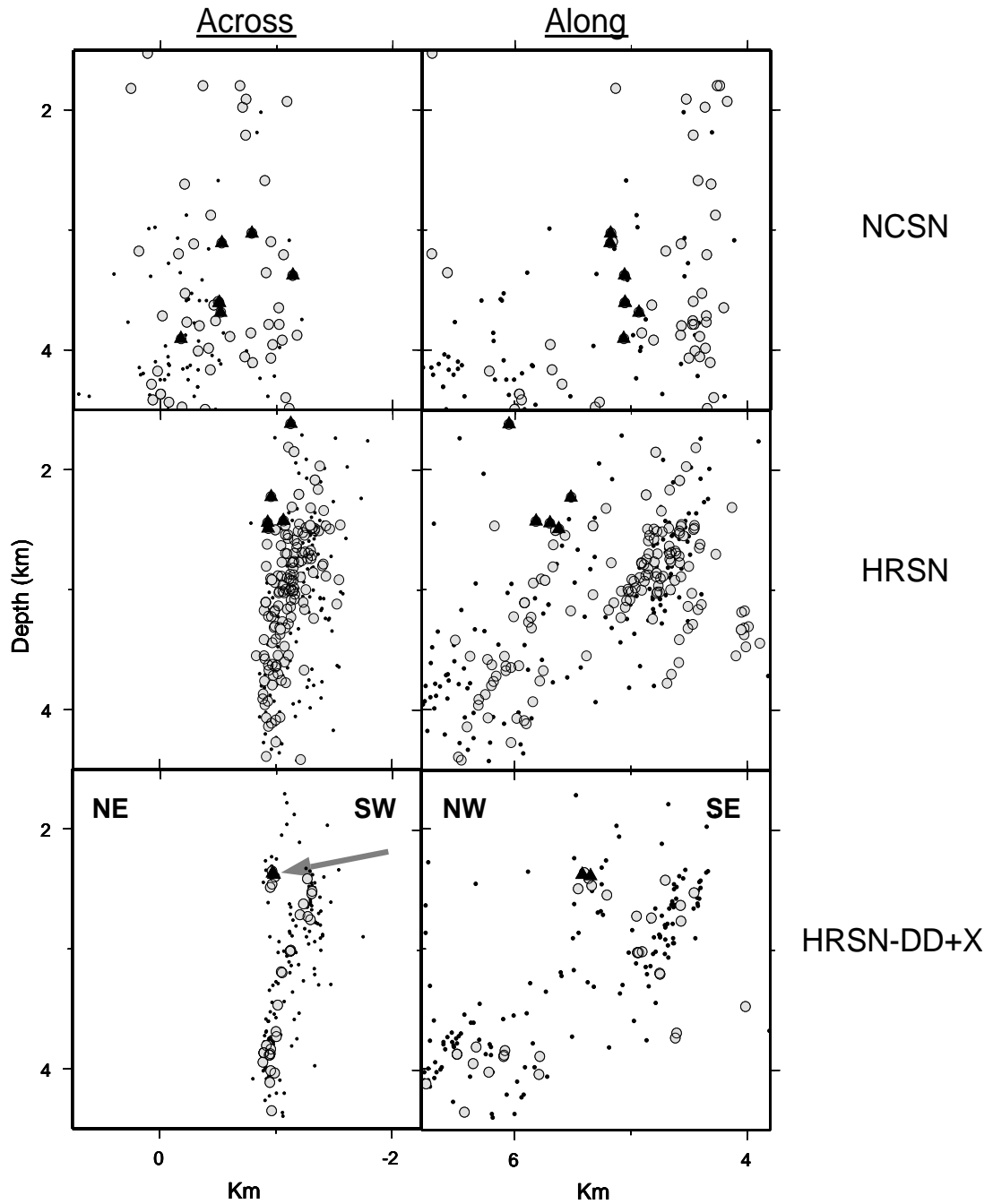


Figure 15.2: A 3x3 km region about the proposed SAFOD drilling target shown in along and across fault sections. Light grey circles show locations of 144 individual characteristically repeating micro-earthquakes from 31 sequences. Black triangles show locations of events from the 2 additional repeating M2 sequences proposed as SAF penetration targets by SAFOD. At lower resolution the repeating quake locations scatter widely. As resolution increases, their locations collapse onto the 33 sites of repeating activity shown in the bottom panels. Black dots are locations of non-repeating seismicity. Note the 2 strands of seismicity shown in the across fault section defining the NE and SW parallel strands. Both are populated with repeating earthquakes (indicating ongoing fault slip). The proposed drilling path direction at penetration (grey arrow) is subhorizontal from the SW to the NE into the M2 targets. Note that both M2 targets occur on the NE strand.

## NEXT?!

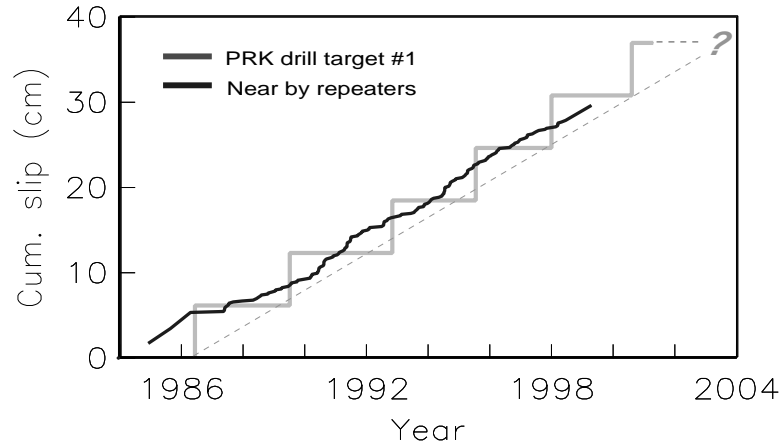


Figure 15.3: Cumulative slip release on characteristically repeating microearthquake sequence (CS) patches in the SAFOD M2 target zone. Gray steps show cumulative release of one of the 2 M2 target sites. Black curve shows cumulative slip of 33 near by CS occurring from 1987-1998.5 normalized to the number of near by CS used. Dashed line shows the average slip release rate of the M2 patch and "?" the approximate repeat date of the M2 target sometime in late 2003 or early 2004, assuming loading rates remain constant. Changes in loading rate on the M2 patch can be inferred from changes in slip release on the nearby patches and used to refine the expected repeat time of the M2.

acteristic Small-earthquake sequence off Sanriku, north-eastern Honshu, Japan, *Geophys. Res. Lett.*, in press, 2002.

Michelini, A. and T.V. McEvelly, Seismological studies at Parkfield I: Simultaneous inversion for velocity structure and hypocenters using B-splines parameterization, *Bull. Seism. Soc. Am.*, 81, 524-552, 1991.

Nadeau, R.M. and L. R. Johnson, Seismological Studies at Parkfield VI: Moment Release Rates and Estimates of Source Parameters for Small Repeating Earthquakes, *Bull. Seism. Soc. Am.*, 88, 790-814, 1998.

Nadeau, R.M., L.R. Johnson and H.-R. Wenk, Are Pseudotachylites Fossil Earthquakes?, *Seism. Res. Lett.*, submitted in revision, 2002.

Nadeau, R.M. and T. V. McEvelly, Seismological Studies at Parkfield V: Characteristic microearthquake sequences as fault-zone drilling targets, *Bull. Seism. Soc. Am.*, 87, 1463-1472, 1997.

Nadeau, R.M. and T.V. McEvelly, Fault slip rates at depth from recurrence intervals of repeating microearthquakes, *Science*, 285, 718-721, 1999.

Nadeau, R.M. and T.V. McEvelly, Spatial and Temporal Heterogeneity of Fault Slip from Repeating Micro-Earthquakes along the San Andreas Fault in Central California, *EOS Trans., Am. Geophys. Union.*, 81, F919, 2000.

Nadeau, R.M., T.V. McEvelly, and A. Michelini, hypocenter Locations at Parkfield and SAFOD Drilling Targets, *Seism. Res. Lett.*, 72, 277, 2001.

Nadeau, R.M. and T.V. McEvelly, Periodic Pulsing of the Tectonic Plate Boundary in Central California, in

prep., 2002.

Niu, F., P.G. Silver, R.M. Nadeau and T.V. McEvelly, Stress-Induced Migration of Seismic Scatterers Associated with the 1993 Parkfield Aseismic Transient, *Science*, submitted, 2002.

Rubin, A., Aftershocks of microearthquakes as probes of the mechanics of rupture, *J. Geophys. Res.*, 107, ESE3 1-16, 2002.

Sammis, C.G. and J.R. Rice, Repeating Earthquakes as Low-Stress-Drop Events at a Border Between Locked and Creeping Fault Patches, *Bull. Seism. Soc. AM.*, 91, 532-537, 2001.

Schaff, D.P., G.H.R. Bokelmann, G.C. Beroza, F. Waldhauser and W.L. Ellsworth, High Resolution Image of Calaveras Fault Seismicity, *J. Geophys. Res.*, in press, 2002.

Schmidt, D.A., R. Burgmann, R.M. Nadeau, and M. d'Alessio, Distribution of aseismic slip-rate on the Hayward fault inferred from seismic and geodetic data, *J. Geophys. Res.*, in prep., 2002.

Seno, T., Fractal asperities, invasion of barriers, and interplate earthquakes, *J. Geophys. Res.*, submitted, 2002.

Waldhauser, F. and W.L. Ellsworth, Fault structure and mechanics of the Hayward Fault, California, from double-difference earthquake locations, *J. Geophys. Res.*, 107, ESE3 1-15, 2002.

Wenk, H.-R., L.R. Johnson, and L. Ratschbacher, Pseudotachylites in the Eastern Peninsular Ranges of California, *Tectonophysics*, 321, 253-277, 2000.

## Target Size

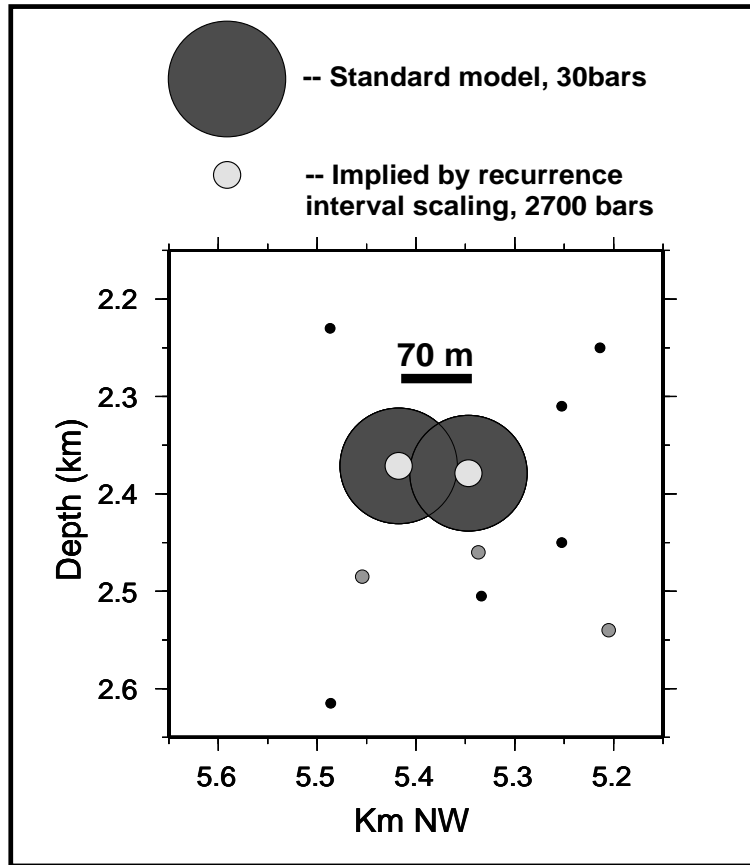


Figure 15.4: Potential M2 targets and estimated dimensions based on 30 bar and 2700 bar stress drops (large dark gray annuli and concentric light gray circles, respectively). Small black circles show near by non-repeating earthquake locations and small gray circles the locations of 3 close in CS, two of which occur on the fault strand some 300 m SW of the strand containing the M2 targets (see discussion in text). The potential targets locate only 70 m apart and yet rupture independently as separate repeated earthquake sequences. At 30 bars their inferred dimensions indicate significant overlap, making their independent rupture difficult to explain. Assuming 2700 bar stress drops, the M2 rupture patches are distinct and separated by some 50 m, making independent rupture more plausible. If patches are indeed this small, they present significantly smaller targets and will require very precise relative locations of the drill-bit relative to the patches in order to achieve monitoring, penetration and sampling of the M2 site as proposed by SAFOD.

## 2. Deep Fault Slip Kinematics from Characteristic Microearthquakes

R.M. Nadeau, D.C. Templeton, R. Burgmann, and T.V. McEvilly

### 2.1 Introduction

Analyses of the 14+ years of Parkfield monitoring data have revealed significant and unambiguous departures from stationarity both in the seismicity characteristics and in wave propagation details. Synchronous with these changes have been changes in the repeat times of characteristic microearthquake sequences,  $T_r$ , which have been related to slip loading rate variations at depth and which have been used to provide a 4-D image of the evolution of slip rates along the 25 km segment of the San Andreas Fault (SAF) spanning the presumed nucleation region of the next Parkfield M6 earthquake (Nadeau and McEvilly, 1999).

Our ongoing research is showing that this technique is applicable to other faults in Central California, and its more widespread application is revealing unexpected attributes of the kinematics of deformation along these faults and on scales ranging from a few meters to 100's of km.

$T_r$ , is also a particularly well constrained observable that can be theoretically related to a variety of physical processes linked to earthquakes, fault structure, and fault deformation (e.g. overall fault strength, stress drops, fault heterogeneity, fault deformation at depth, slip loading of locked segments, fault healing rates, 'in-situ' friction, and event-event triggering). However to provide accurate measurements of these processes in an absolute sense, accurate calibrations between  $T_r$  and various constitutive properties within the fault core (e.g. composition, texture, temperature, stress, slip rate and fluid conditions) are needed. Currently such calibrations must be inferred from surface observations, laboratory experiments and seismic behavior. Ideally, however, they would come from 'in situ' measurement of the fault zone—an expensive proposition.

The National Science Foundation, through its EarthScope initiative (SAFOD component), has recently proposed careful scientific drilling into the seismogenic zone of the active San Andreas (SA) fault at Parkfield. Scientific drilling would sample fault zone properties directly and, as proposed, at the site of a repeating earthquake sequence. This effort promises to significantly enhance our understanding of the physics of of this portion of the SAF and to provide the calibration necessary for relating  $T_r$  to the constitutive properties and processes responsible for earthquakes and fault deformation at Parkfield.

At the same time EarthScope, through its PBO and InSAR components, has proposed to increase the detail and extent of deformation measurements along a ma-

ior plate boundary and throughout the country which should greatly improve estimates of fault slip from surface and space based observations. This information, together with the ongoing discovery of widely distributed repeating earthquake sequences in central CA make it feasible to extrapolate (infer) the physical conditions—relative to those found at Parkfield—on 100's of km of fault in central California and elsewhere.

Small repeating earthquakes continue to be discovered in other regions of the world and on other fault types (e.g. convergent boundaries off the coast of Japan (Matsuzawa *et al.*, 2002) and on normal faults in Greece (Dimitrief and McCloskey, 2000). This suggests the possibility of inferring fault conditions elsewhere.

In the U.S., it is conceivable that a collateral benefit of the USARRAY component of EarthScope will be the discovery of a significant number of new repeating earthquake sequences in regions where low magnitude seismicity has not been studied in detail. This has the potential to greatly expand the geographic coverage where inferential methods based on  $T_r$  can be applied.

The following subsections summarize the current state of repeating earthquake studies at Berkeley, and give examples of how such studies are already changing our understanding of the kinematics of fault deformation.

### 2.2 East Bay Faults

#### Method

The method of determining slip rates from earthquake recurrence has been developed in our research program using data from a borehole network along the active San Andreas fault zone at Parkfield, CA.

Studies at very high resolution of microearthquakes at Parkfield, CA since 1987 revealed a systematic organization in space and time, dominated by spatial clustering of nearly identical, regularly recurring microearthquakes ('characteristic events') on small (meters to 10s of meters) wide patches within the fault zone (Nadeau *et al.*, 1994, 1995; Nadeau and McEvilly, 1997). At Parkfield, nearly half of the 5000+ events in the 1987-1998 catalog exhibit this trait. In general, recurrence intervals (0.5 to 3 yr.) scale with the magnitude of the repeating events for the magnitude range available ( $M_w$  -0.7 to 3). Clusters of these characteristic events occur throughout the slipping fault surface. Scalar seismic moments were estimated for 268 micro-quakes contained in 53 repeating sequences and combined with equivalent estimates from 8 similar but larger event sequences from the Stone Canyon section of the fault and the main Parkfield M6 sequence.

These estimates show that seismic moment is being released as a function of time in a very regular manner where repeating earthquakes occur and for a wide range of earthquake magnitude. Measurements of the moment release rate, combined with an assumed tectonic loading rate, lead to estimates of the seismic parameters source area, slip, and recurrence interval. Such parameters exhibit a systematic dependence upon source size over a range of  $10^{10}$  in seismic moment, which can be described by simple scaling relationships (*Nadeau and Johnson, 1998*). What emerges from this analysis of moment release rates is a quantitative description of an earthquake process that is controlled by small strong asperities that occupy less than 1% of the fault area.

A 26-months period of greatly increased activity during the study interval (M4.2, 4.6, 4.7 and 5.0 events and their aftershocks) accompanied changes exceeding 50% in previously stable recurrence intervals. *Langbein et al. (1999)* report on evidence in deformation measurements for a slip rate increase in 1993 at Parkfield. *Nadeau and McEvilly (1999)* show that it is possible under reasonable assumptions to infer the spatial distribution of variations in slip-rate on the fault surface from the changes in recurrence intervals for the characteristic event sequences. The analysis requires an assumption of constant area for the characteristic repeating sources - one easily supported by the lack of any appreciable change in the seismic moments and waveforms (over the 100 Hz bandwidth) associated with the change in recurrence interval.

### Northern Hayward Fault

Along the northern Hayward Fault (HF) using surface short period NCSN catalog data, a prototype study using the micro-quake based deep fault slip technique was compared to an inversion of surface and space based geodetic data for fault slip. The comparison showed a good match between the two data types and formalization of joint inversion of the two data sets is currently underway. Results of our prototype study on the northern HF were encouraging and have been published in *Science (Burgmann et al., 2000)*. We have subsequently found sufficient repeating earthquake activity along the southern HF, Calaveras (CF) and Mission (MF) faults to determine deep fault slip rates on those faults as well.

A long enough time base of waveform data recorded on the deep borehole Hayward Fault Network (HFN) has also now become available which promises to allow practical application of the repeating quake method to repeating sequences of much lower magnitude and consequent greater temporal and spatial resolution.

### Southern Hayward, Mission and Calaveras Faults

We have completed our initial and computationally intensive search for characteristic sequences on the southern HF, CF and MF faults, using surface NCSN data and

find that seismicity there resembles the clustering found at Parkfield, but at a lower seismicity rate and density. Figure 15.5 shows locations of the NCSN earthquakes that we focused on during the reconnaissance stage of our search for repeaters. This stage of processing characterizes the waveform similarity of all the event pairs separated by 7.5 km or less. Even at reduced catalog completeness (M 1.3) of the NCSN in this area, we see large numbers of highly similar and repeating events (coherency  $> 0.95$ ) distributed widely on all three faults, indicating the presence of substantial repeating earthquake activity (Figure 15.5). Using NCSN surface data we estimate the fractions of identifiable repeaters to be about 10% 15% and 25%, for the northern HF, southern HF, MF and CF segments respectively.

The lowest fractions are explainable in part by lower slip rates and higher magnitude thresholds, since under these conditions recurrence intervals may be longer than observation times. At Parkfield, where the slip rate is much higher and using NCSN data, the fraction of repeaters is about 48%. In our prototype analysis on the northern HF, we showed that sufficient information was available to resolve spatially varying features of slip using surface NCSN data but that monitoring of short-term temporal variations was not practical with the limited resolution of the surface data on such a slowly moving fault. To the southeast, on the faster moving MF and CF, we are finding sufficient rates of quake repetition to allow us to use NCSN data for monitoring transients (Figure 15.5) as is currently being achieved on the faster slipping SAF to the West (*Nadeau and McEvilly, 2002*).

### East-Bay Fault System

Using NCSN arrival times, we have relocated the seismicity along the HF-MF-CF system using the USGS relocation code HypoDD (Figure 15.5) and are evaluating the more highly resolved spatial and temporal seismicity patterns in relation to surface and spaced based deformation estimates, to the spatial and temporal distribution of repeating earthquake sequences and to the post-seismic period following the 1984 Morgan Hill earthquake. Our preliminary findings indicate that, as at Parkfield and on the creeping section of the SAF, the locations of repeating earthquake sequences are confined to the central portion of seismicity on large faults. However, repeating quakes are not ubiquitous on all faults.

For example our search for characteristic quakes in our study region failed to identify any repeating sequences on the CF fault north of its juncture with the MF trend between Fremont and San Jose (Figure 15.5). Furthermore, along the MF and southern HF, repeating sequences only appear in the shallow portion of the seismogenic zone and appear to delineate the proposed locked region of the Hayward fault which is presumably the generation zone of 1868 M7 type events (Figure 15.5). In addition,

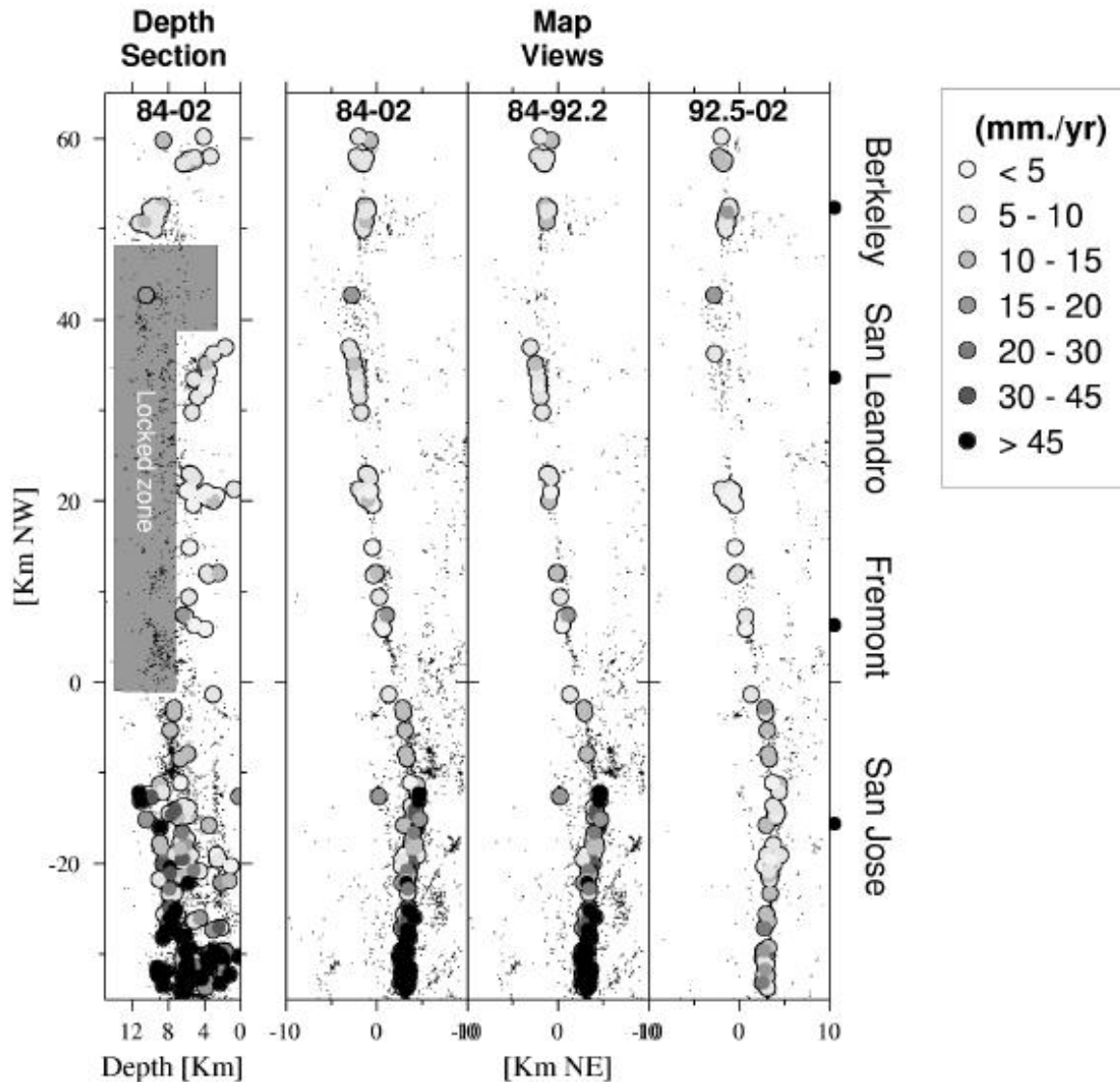


Figure 15.5: Point fault slip rate estimates at depth inferred from recurrence intervals of characteristic micro-earthquakes, superposed on the HypoDD-relocated seismicity along a 120-km-long stretch of the Hayward (HF), Mission (MF) and Calaveras (CF) faults. Locations of characteristically repeating sequences (CS) are shown as large filled (gray) circles. CS and are numerous, widespread and distributed in time and space along these mature actively creeping faults. Rates of slip inferred from the CS recurrence intervals in mm/yr are coded in gray scale as indicated. Black points show locations of non-CS seismicity. Each filled circle represents the average slip rate between time sequential pairs of characteristic events in a sequence. Variations in the rates of repetition are consistent with known variations in slip rate both along strike and through time as determined from surface and space based geodetic methods. For example, sequences NW of Morgan Hill (MH) typically show a steadily decreasing repeat rate with time since the 1984 MH magnitude 6. Left panel shows, in depth section, all slip rate pair estimates and background seismicity for the time period 1984-2002. Second panel shows the same data in map view. Panel three (second from right) shows data in map view for pairs occurring between 1984 to 1992.5, and far left map shows similar data for the period 1992.5 to 2002.2. A time variable slip rate is clear, particularly along the CF where slip rates are high following the 1984 Morgan Hill main shock and slow down significantly afterwards. Slip rate is lowest on the southern HF and MF trends. On these segments, below about 5-6 km, characteristically repeating sequences are absent while background seismicity can clearly be seen. This suggests that the boundary separating the repeating and non-repeating regions delineates the boundary between creeping and non-creeping (locked) fault behavior at depth on this fault system. The locked region of the system, as modeled by *Burgmann et al.*, (2000) shows a reasonable good match to this CS delineated region.

their rate of repetition (indicated by their low, very light gray, slip rates) are low relative to the slip rates on the northern HF and CF segments. Since repeating earthquake activity requires repeated loading from the adjacent slipping fault, we interpret the regions of seismically active but non-repeating seismicity to be non-creeping and locked and the low repeat rates of the shallow repeating sequences to be in response to the shielding effect of the deeper locked section of the southern HF and MF.

If this is the case, high resolution relocations of repeating earthquake activity may prove a valuable tool, generally, for delineating locked fault segment boundaries in more detail at depth. Also of note in this regard is the lack of repeating earthquake activity on two splays of transient earthquake activity emanating from the CF south of San Jose. High precision relocations show that these splays were active during the post-seismic period following the Morgan Hill (MH) earthquake of 1984, but in subsequent years these splays have become aseismic (Figure 15.5, map view, 84-92.5 and 92.5 to 2002). It is not yet clear if the lack of repeating sequences on these splays is due to a relatively minor amount of slip release on the faults after MH or to a fundamental instability in the strength properties of earthquake patches on these subsidiary faults.

In addition to the structural features manifest by the relocations and repeating earthquake analyses, temporal variations are also clearly evident. Shown in the right most panels of Figure 15.5 are map views of the repeating sequences, gray scale coded to their slip rate estimates. On the CF during the period 1984-1992.5 repeat rates (and inferred slip rates at depth) are very high in comparison to repeat rates for sequences from 1992.5 to 2002. In addition, repeating events on the southern HF during the 6 years following the Loma Prieta earthquake nearly ceased, which agrees well with diminished surface deformation rates observed on this fault segment (*Lienkaemper et al.*, 1997; *Burgmann et al.*, 1998).

Our ongoing efforts involve the determination of the the kinematics of slip through joint modeling of surface GPS, creep and space based data so that geologic questions regarding the details of slip in the complex of East Bay faults (particularly the Mission cross over region) can be investigated at much higher resolution (*Schmidt et al.*, (2002).

### 2.3 San Andreas, Calaveras Juncture

We have also applied similar relocation and repeating earthquake techniques further south in the CF and Quien Sabe fault near the bifurcation of the SAF where little surface or space based deformation data is available.

This juncture of the SAF and the southern CF is a highly complex area where subsurface seismicity does not always follow surface fault traces and where secondary sub-parallel faults, such as the Quien Sabe fault zone,

may play an active role in accommodating local shear deformation. The goal of this investigation is to determine the slip rate distribution of these faults at the juncture using repeating earthquake defined subsurface slip rates and surface geodetic measurements.

Currently we are investigating how slip at depth is being partitioned in this complex juncture zone, by determining a lower bound on creep rates at depth using characteristically repeating earthquakes (CREs) and the empirical formula of *Nadeau and McEvilly* (1999). Essentially, the method treats each CRE sequence as a "creep-meter" at depth, and derives slip from the direct relationship between an event's size and repeat interval relative to those found at Parkfield, CA.

In this region, the seismic structure and repeat rates of the characteristic sequences indicate a very complicated and heterogeneous slip regime apparently reflecting the complex fault geometry at depth, rapid slip transients initiated by moderate earthquakes, and the presence of a significantly greater fraction of locked (i.e. non-creeping) fault behavior (*Templeton et al.*, 2001).

We identified 58 CRE sequences (Figure 15.6). Using the double-difference relocation program HypoDD, we relocated the seismicity to see where in the fault zone the CREs were occurring. On the San Andreas and Calaveras faults, CRE sequences occur along the fault plane on horizontal linear streaks of seismicity. These streaks are more pronounced on the San Andreas than on the Calaveras fault. The smaller Quien Sabe fault zone is much more complex than the more mature San Andreas and Calaveras faults. On the northern end of the fault zone, there is only one CRE sequence which is found on one of three side stepping linear fault strands. On the southern part of the fault zone, fault structures become more complex with several fault strands branching off of the one linear fault strand which hosts most of the CRE sequences found on the Quien Sabe fault zone.

Some CRE sequences seemed to be influenced by larger nearby earthquakes, especially those found on fault traces that are discontinuous at depth. For example, on the Quien Sabe fault zone, sequences tended to cluster within approximately 3 km of larger earthquakes. Their recurrence intervals tended to be aperiodic and appeared to be influenced by the timing of larger nearby events. On the San Andreas and Calaveras faults, however, both periodically and aperiodically CRE sequences were found within approximately 3 km of larger earthquakes. We believe that aperiodically CRE sequences are indicating changes in the local stress regime due to the redistribution of stress caused by larger nearby earthquakes. We also showed that CRE recurrence intervals on the Calaveras and Quien Sabe fault zone tended to be larger than those on the San Andreas fault. This is due to the fact that the San Andreas fault is slipping at a much greater rate than the Quien Sabe fault zone and hence would

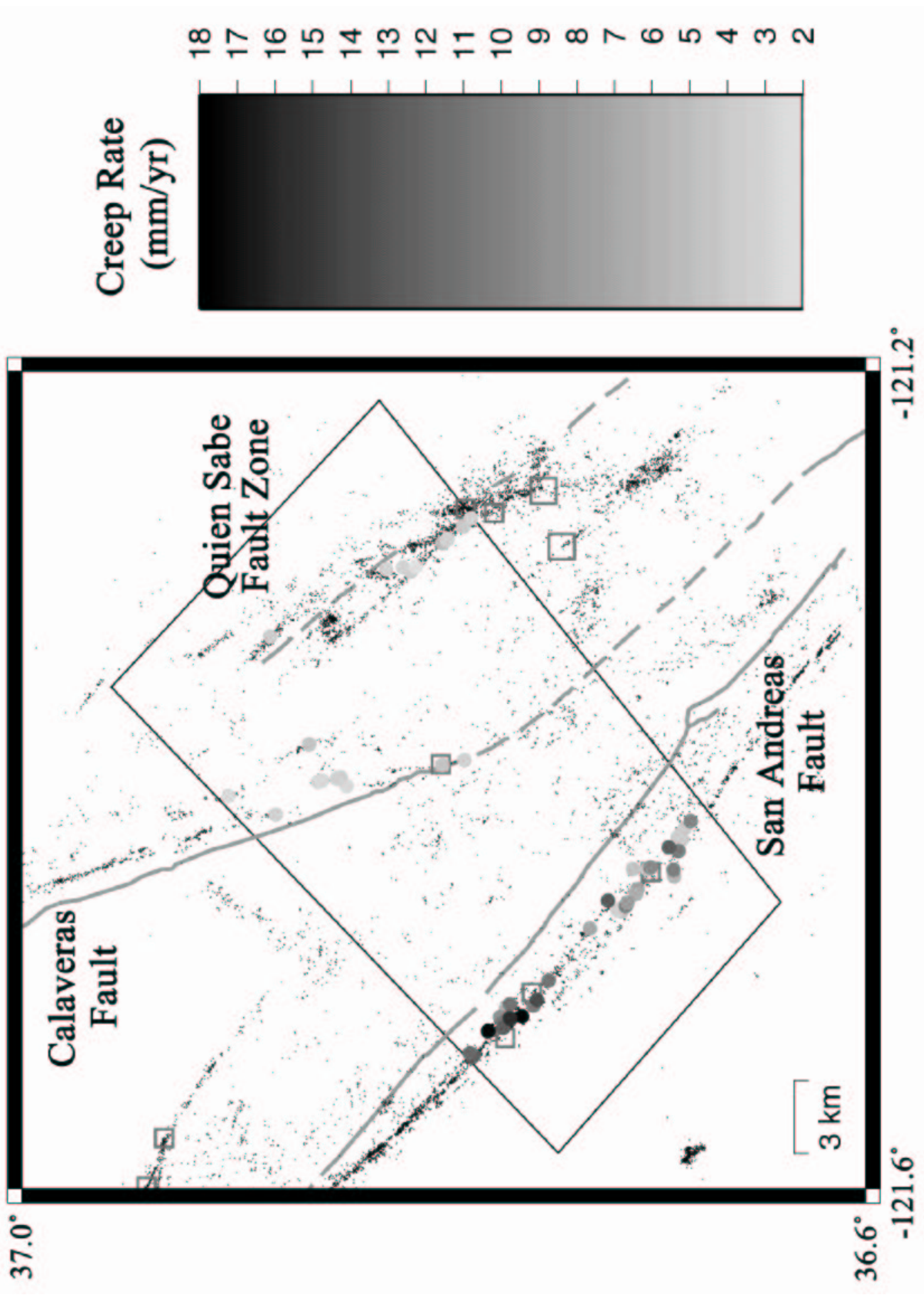


Figure 15.6: San Andreas, Calaveras Fault juncture zone. Location of CREs plotted as filled circles with gray shading scaled to estimated deep slip rates. Grey lines are surface expression of faults and squares indicate location of earthquakes greater than M4.0.

have a greater number of earthquakes over the same time interval.

Since only two or three events per CRE sequence were found on the Calaveras and Quien Sabe fault zone, we chose not to average the creep rates at individual sequence locations. Instead we calculated minimum creep rates. As we expected, creep on the Calaveras and Quien Sabe fault zone was lower, between 2.5-6.9 mm/yr, than that found on the San Andreas fault, between 3.2-18.0 mm/yr. We use these creep rates only as lower end members of creep along the fault trace. Interestingly, the smaller Quien Sabe fault zone seems to be creeping about the same amount as the more mature Calaveras fault in this location.

We plan to combine these subsurface creep rates with surface geodetic data to determine the subsurface creep rate distribution along the fault plane using a homogeneous, linear, elastic half-space model.

## 2.4 The SAF: Parkfield to Loma Prieta

As part of a more ambitious exploration of the extent to which characteristically repeating microearthquakes characterize active fault zones, we have applied the methodology developed at Parkfield (*Nadeau and McEvilly*, 1999) to examine deep slip rate along the San Andreas Fault from South of Parkfield to the Southern extent of rupture of the 1989 Loma Prieta (LP) earthquake from 1984 through 1999 using the NCSN event catalog.

Initial results are fascinating, revealing portions of the fault extending over many tens of kilometers that exhibit coherent pulsing in slip rate. In addition, the pulses appear closely related to the occurrence of the Loma Prieta earthquake in 1989 (*Nadeau and McEvilly*, 2002).

Relative quiescence on the northern end of the segment is observed prior to LP, after which slip rates increase markedly—the LP locked segment appears to have exerted control on the SAF slip rates at distances greater than 30 km from the termination of its rupture. Also of interest is the fact that LP occurred coincidentally with the initiation of an ongoing pulsing cycle some 40 to 80 km further to the South.

Following LP, the periodic pulsing observed to the South appears to extend northward and shows some correspondence to the occurrence of 3 slow silent quakes in the SJB area. The pulsing observed after LP also appears to be superposed on an exponential decay of slip rate corresponding to aftershock decay in the zone adjacent to and following the LP main event (upper right hand time history panel).

In the middle of the examined fault stretch, quasi-periodic pulsing of slip rates with amplitude variations exceeding 50-100 % are pronounced with the north central portion repeating with about 3 year periodicity and 1.7 year periodicity in the south central portion.

From 60 to about 20 km northwest of Parkfield, an apparent migration pulse is also observed. On this segment the SAF appears to act as a strain guide for the transference of the tectonic slip-load at a rate of about 25 km/yr. The migration pattern also appears to repeat itself as part of the more frequent (1.7 yr.) pulsing pattern.

To the South at Parkfield, pulsing is more difficult to define, although considerable slip rate change is observed, in accordance with observations of surface slip-rate change in that area (*Langbein et al.*, 1999). Also noteworthy at Parkfield is a distinct reduction in slip rate beginning after 1995 and continuing through 1999 that perhaps indicates a transition to a phase of relative slip quiescence preparatory to occurrence of the anticipated M6–similar to the quiescence observed prior to LP in the North.

## 2.5 Acknowledgements

We appreciate support for this project by the USGS NEHRP through grant numbers 01HQGR0066 and 02HQGR00226.

## 2.6 References

- Bryant, W.A., Faults in the southern Hollister area, San Benito counties, California, *California Division of Mines and Geology Fault Evaluation Report 164*, 1985.
- Burgmann, R., E. Fielding and J. Sukhatme, Slip along the Hayward fault, California, estimated from space-based synthetic aperture radar interferometry, *Geology*, *26*, 559-562, 1998.
- Burgmann, R., D. Schmidt, R.M. Nadeau, M. d'Alessio, E. Fielding, D. Manaker, T.V. McEvilly, and M.H. Murray, Earthquake Potential along the Northern Hayward Fault, California, *Science*, *289*, 1178-1182, 2000.
- Dimitrief, A. and J. McCloskey, A search for Repeating Microearthquakes in Western Greece (abstract), *EOS Trans. Am. Geophys. U.* *81*, F924, 2000.
- Langbein, J., R. Gwyther, R. Hart, and M.T. Gladwin, Slip rate increase at Parkfield in 1993 detected by high-precision EDM and borehole tensor strainmeters, *Geophys. Res. Lett.*, *26*, 2529-2532, 1999.
- Lienkaemper, J.J., J.S. Galehouse, and R.W. Simpson, Creep response of the Hayward fault to stress changes caused by the Loma Prieta earthquake, *Science*, *276*, 2014-2016, 1997.
- Matsuzawa, T., T. Igarashi and A. Hasegawa, Characteristic Small-earthquake sequence off Sanriku, northeastern Honshu, Japan, *Geophys. Res. Lett.*, in press, 2002.
- Nadeau, R.M., M. Antolik, P. Johnson, W. Foxall, and T.V. McEvilly, Seismological studies at Parkfield III: microearthquake clusters in the study of fault-zone dynamics, *Bull. Seism. Soc. Am.* *84*, 247-263, 1994.

Nadeau, R.M., W. Foxall, and T.V. McEvilly, Clustering and Periodic Recurrence of Microearthquakes on the San Andreas Fault at Parkfield, California, *Science*, 267, 503-507, 1995.

Nadeau, R.M. and T. V. McEvilly, Seismological Studies at Parkfield V: Characteristic microearthquake sequences as fault-zone drilling targets, *Bull. Seism. Soc. Am.*, 87, 1463-1472, 1997.

Nadeau, R.M. and L.R. Johnson, Seismological Studies at Parkfield VI: Moment Release Rates and Estimates of Source Parameters for Small Repeating Earthquakes, *Bull. Seism. Soc. Am.*, 88, 790-814, 1998.

Nadeau, R.M. and T.V. McEvilly, Fault slip rates at depth from recurrence intervals of repeating microearthquakes, *Science*, 285, 718-721, 1999.

Nadeau, R.M. and T.V. McEvilly, Periodic Pulsing of the Tectonic Plate Boundary in Central California, in prep., 2002.

Schmidt, D.A., R. Burgmann, R.M. Nadeau, and M. d'Alessio, Distribution of aseismic slip-rate on the Hayward fault inferred from seismic and geodetic data, *J. Geophys. Res.*, in prep., 2002.

Templeton, D.C., R.M. Nadeau and R. Burgmann, Structure and Kinematics at the Juncture between the San Andreas and Southern Calaveras faults, *Eos Trans. AGU*, 82, F811, 2001.

### 3. Time-dependent depth distribution of aftershocks: Implications for fault mechanics and crustal rheology

Frederique Rolandone, Roland Bürgmann, and Robert Nadeau

#### 3.1 Introduction

A fundamental property of the continental upper crust is the depth distribution of earthquakes. The maximum depth of seismogenic faulting is interpreted either as the brittle-ductile transition, the transition from brittle faulting to plastic flow in the continental crust, or as the transition in the frictional sliding process from unstable to stable sliding. This transition depth depends on four main factors: rock composition, temperature, strain rate, and fluid pressure (e.g., *Sibson* 1982, 1984; *Meissner and Strehlau*, 1982; *Tse and Rice*, 1986; *Scholz*, 1990). Spatial variations in the maximum depth of seismicity in southern California have been correlated with crustal temperature or lithology (e.g., *Magistrale and Zhou*, 1996; *Williams et al.*, 2001). However, little has been done to examine how the maximum depth of seismogenic faulting varies locally (at the scale of a fault segment) with time during an earthquake cycle.

Many models assume a first-order transition from brittle to ductile deformation at a depth that is determined from regional estimates of the geotherm and strain rate. In the vicinity of a large fault this may be misleading because of the effects of strain localization. Strain rate values at depth around active faults are not known but recent mechanical models of strike-slip fault deformation (e.g., *Chery et al.*, 2001; *Rolandone and Jaupart*, 2002) show high strain rate localization around the base of the fault. Thus the brittle-ductile transition is not a sharp and fixed discontinuity in the crust but is expected to vary near the fault with strain rate and therefore to change with time through the earthquake cycle.

The objectives of this study are to apply high-resolution earthquake relocation techniques to resolve the time-dependent depth distribution of aftershocks and thus constrain models of the brittle-ductile transition and the rheology near the base of seismogenic faults.

#### 3.2 Methodology

We investigate the time-dependent depth distribution of aftershocks following moderate to large earthquakes on strike-slip faults in southern California. Southern California offers a dense network of active strike-slip faults and high seismic activity. It is a very well instrumented area. Catalogs of seismicity provide a large observational time interval of seismicity records. We plan to examine the pattern of seismicity on different strike-slip fault segments to determine either spatially stable pattern (long-lived seismic structures) or systematic temporal varia-

tions related to recent earthquakes.

We use the 69-year catalog of the Southern California Seismic Network (SCSN) to identify target events. We use the catalog of relocated 1975-1998 earthquakes using the source specific station term method of *Richards-Dinger and Shearer* (2000), and the catalog of relocated events using a three-dimensional velocity model based on a joint-hypocenter-velocity (JHV) from 1981 to 2000 of *Hauksson* (2000) to do preliminary studies of aftershocks sequences.

Recently developed relative relocation techniques improve relative hypocenter locations (in favorable cases relative errors can be typically less than 20 m (*Waldhauser et al.*, 1999; *Waldhauser and Ellsworth*, 2000) and reveal greater details of the patterns of deformation during an earthquake cycle. We apply cross-correlation techniques and the double difference method of *Waldhauser and Ellsworth* (2000) to relocate earthquakes in the areas of interest (with the HypoDD relocation code).

#### 3.3 Preliminary results

We begin this study analysing the seismicity around the 1987 Superstition Hills earthquake ( $M_s=6.6$ ) as a first test case. Figure 15.7 shows a map view of the seismicity relocated using HypoDD around Superstition Hills for the time period 1983-2000. The inside box shows the zone of our study along the surface rupture of the earthquake.

We compare the time-dependent depth distribution of seismicity given by the different published catalogs (Figure 15.8). Figure 15.9 shows our relocated earthquake catalog for different velocity models. The different catalogs and our own relocation results show large variations of hypocentral depths. These variations seem mainly related to the choice of the velocity model for the upper crust. However, a persistent feature of the depth distribution of aftershocks is that in the immediate post-seismic period the aftershocks are deeper than the background seismicity and these deepest aftershocks become shallower with time following the mainshock. Preliminary analysis of other historic ruptures in the Mojave Desert show a similar pattern. In order to quantify these variations, we are working on obtaining a sharper picture of the time-dependent depth variation of the seismicity.

#### 3.4 Future work

Temporal changes in depth of seismicity may serve to increase our knowledge of (1) the depth to which upper crustal deformation is coupled to deformation within the

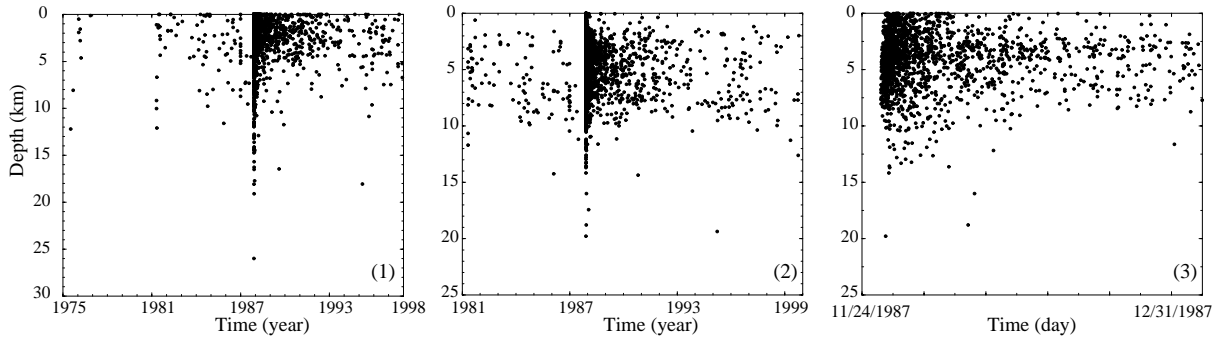


Figure 15.8: Time-dependent depth distribution of the seismicity from (1) the *Richards-Dinger and Shearer* catalog (2000), and from (2) the Hauksson catalog. (3) Detail of the distribution of seismicity from the Hauksson catalog from November 24 1987 to the end of 1987.

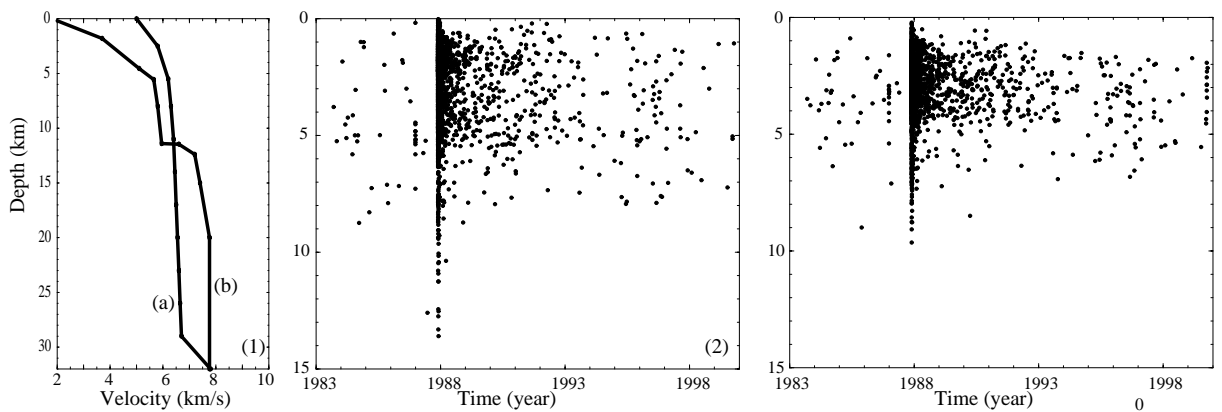


Figure 15.9: (1) Velocity structures used for relocation with HypoDD: (a) derived from *Shearer* (1997), (b) derived from *Fuis et al.* (1982). (2) Our relocation results obtained for velocity model (a), and (3) for velocity model (b). Note the difference in the depth scale with Figure 15.8.

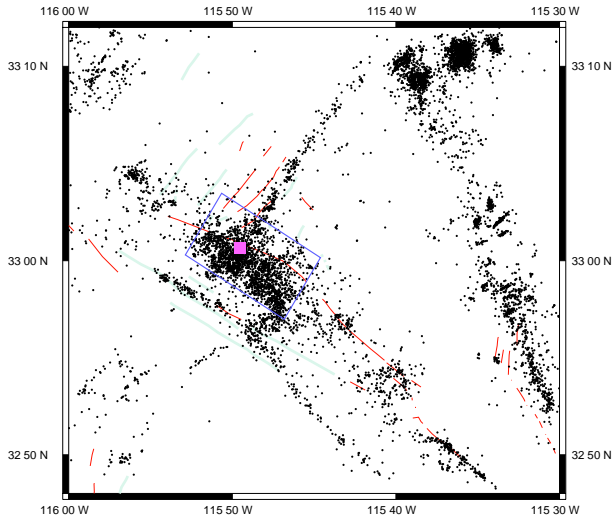


Figure 15.7: Seismicity (dots) around Superstition Hills from 1983 to 2000 relocated with HypoDD. The box indicates the seismicity used in this study around the surface rupture of the 1987 Superstition Hills earthquake (square). Active faults are shown.

lower crust, (2) the mechanics of fault zones near the base of the seismogenic zone where large earthquakes tend to nucleate and (3) of the transient deformation processes and their rheological parameters that are active during the postseismic period.

We are working on developing numerical finite-element models to compare these observations and the mechanical evolution of strike-slip faults and to infer fault slip and rheologic stratification. Our objective is to relate the depth distribution of hypocenters during an earthquake cycle to the evolution of the brittle-ductile transition to place constraints on strain rate at depth and on the partitioning of deformation between brittle faulting and distributed deformation.

### 3.5 References

Chery, J., M.D. Zoback, and R. Hassani, An integrated mechanical model of the San Andreas Fault in central and northern California, *J. Geophys. Res.*, *106*, 22,051-22,066, 2001.

Hauksson E., Crustal structure and seismicity distribution adjacent to the Pacific and North America plate boundary in southern California, *J. Geophys. Res.*, *105*, 13,875-13,903, 2000.

Magistrale, H. and H. Zhou, Lithologic control of the depth of earthquakes in southern California, *Science*, *273*, 639-642, 1996.

Meissner, R. and J. Strehlau, Limits of stresses in continental crusts and their relation to the depth-frequency distribution of shallow earthquakes, *Tectonics*, *1*, 73-79,

1982.

Richards-Dinger, K.B. and P. Shearer, Earthquake locations in southern California obtained using source-specific station terms, *J. Geophys. Res.*, *105*, 10,939-10,960, 2000.

Rolandone F. and C. Jaupart, The distribution of slip rate and ductile deformation in a strike-slip shear zone, *Geophys. J. Int.*, *148*, 179-192, 2002.

Scholz, C.H., The mechanics of earthquakes and faulting, pp. 439, *Cambridge University Press*, 1990.

Sibson, R.H., Fault zone models, heat flow, and the depth distribution of earthquakes in the continental crust of the United States, *Bull. Seismol. Soc. Am.*, *68*, 1421-1448, 1982.

Sibson, R.H., Roughness at the base of the seismogenic zone: contributing factors, *J. Geophys. Res.*, *89*, 5791-5799, 1984.

Tse, S.T. and J.R. Rice, Crustal earthquake instability in relation to the depth variation of frictional slip properties, *J. Geophys. Res.*, *91*, 9452-9472, 1986.

Waldhauser, F., W.L. Ellsworth, and A. Cole, Slip-parallel seismic lineations on the northern Hayward fault, California, *Geophys. Res. Lett.*, *26*, 3525-3528, 1999.

Waldhauser, F. and W. L. Ellsworth, A double-difference earthquake location algorithm: method and application to the northern Hayward fault, California, *Bull. Seismol. Soc. Am.*, *90*, 1353-1368, 2000.

Williams, C.F., L.A. Beyer, F.V. Grubb, S. Galanis, Heat Flow and the Seismotectonics of the Los Angeles and Ventura Basins of southern California, *Eos Trans. AGU*, *82(47)*, Fall Meet. Suppl., Abstract S11A-0534, 2001.

## 4. Moment-Length Scaling of Large Strike-Slip Earthquakes and the Strength of Faults

Barbara Romanowicz and Larry Ruff (University of Michigan)

### 4.1 Introduction

There has been a long lasting controversy in the literature as to whether earthquake moment ( $M_0$ ) scales with  $L^2$  or  $L$  for large earthquakes, where  $L$  is the length of the fault. In simple terms, the issue hinges on whether the average slip  $d$  during an earthquake grows with  $L$  or the width  $W$  of the fault. The issue of scaling is particularly important for seismic hazard estimation based on lengths of fault segments, since significantly different estimates of maximum possible earthquake size can be obtained for a given region, depending on the scaling law.

Several large strike slip earthquakes have occurred in various tectonic settings in the past 5 years, adding well documented data to the global collection of moment and length estimates for such earthquakes. Based on this augmented dataset, we have reexamined the controversial issue of scaling of seismic moment with length of rupture (Romanowicz and Ruff, 2002).

### 4.2 Background

Dislocation theory predicts that stress drop  $\Delta\sigma$  is proportional to  $d/W$ , hence slip scales with  $W$  for constant  $\Delta\sigma$ . This implies scaling of  $M_0$  with  $L^n$ , where  $n = 3$  for small earthquakes and  $n = 1$  for large earthquakes with  $W = W_0$ . Scholz (1982) proposed an alternative model, in which the slip scales with  $L$ . This model was motivated by inspection of slip versus length data that were available at that time. It implied that  $n = 2$  for large earthquakes. On the other hand, Romanowicz (1992) compiled the existing dataset for large strike-slip earthquakes on quasi-vertical transcurrent faults. She concluded that moment scales with  $n = 3$  for moments smaller than  $\sim 0.6 - 0.8 \times 10^{20} Nm$ , as known previously, while for larger moments, the data favored a scaling with  $n = 1$ , compatible with dislocation theory. Romanowicz and Rundle (1993) then showed, based on scale invariance arguments (e.g. Rundle, 1989), that the  $n = 1$  and  $n = 2$  scalings could also be differentiated on the basis of frequency-moment statistics, favoring of the "W-model".

Since then, the controversy has continued, using theoretical (e.g. Sornette and Sornette, 1994) as well as observational arguments (e.g. Pegler and Das, 1996; Mai and Beroza, 2000). On the other hand, new compilations of slip versus length data indicate that the increase of slip with  $L$  tapers off at large  $L$  (e.g. Bodin and Brune, 1996). This view has recently received further support from numerical modelling (Shaw and Scholz, 2001).

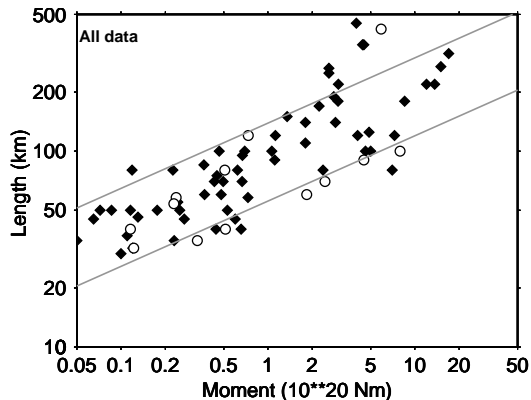


Figure 15.10: Moment-length plot for the dataset described. Lines corresponding to  $n = 3$  bracketing most of the data have been drawn for reference. Circles correspond to recent data for which length was estimated from the NEIC catalog.

### 4.3 Dataset used

We considered the catalog of Pegler and Das (1996) (PD96 in what follows), who have combined  $M_0$  estimates from the Harvard CMT catalog, with  $L$  for large earthquakes from 1977 to 1992 based on relocated 30-day aftershock zones. We add to this dataset the standard collection of reliable  $M_0/L$  data for large strike-slip earthquakes since 1900 (e.g. Romanowicz, 1992), data for great central Asian events since the 1920's (Molnar and Deng, 1984), as well as data for recent large strike-slip events (e.g. Balleny Islands '98; Izmit, Turkey '99 and Hector Mines, CA, '99) that have been studied using a combination of modern techniques (i.e. field observations, waveform modelling, aftershock relocation).

We also considered 15 other strike-slip events of moment  $M_0 > 0.05 \times 10^{20} Nm$  that occurred in the period 1993-2001. Three of these events were recently studied by Henry and Das (2001), and we used their length estimates. For the other 12, we obtained estimates of length based on the distribution of aftershocks of  $M > 4$  in the month following the event, as given in the NEIC contribution to the Council of National Seismic Systems (CNSS) catalog. We only kept those events with a clearly delineated aftershock zone.

### 4.4 Results and Conclusions

Most of the data follow the  $n = 3$  trend, albeit with significant dispersion, except for the largest events (Fig-

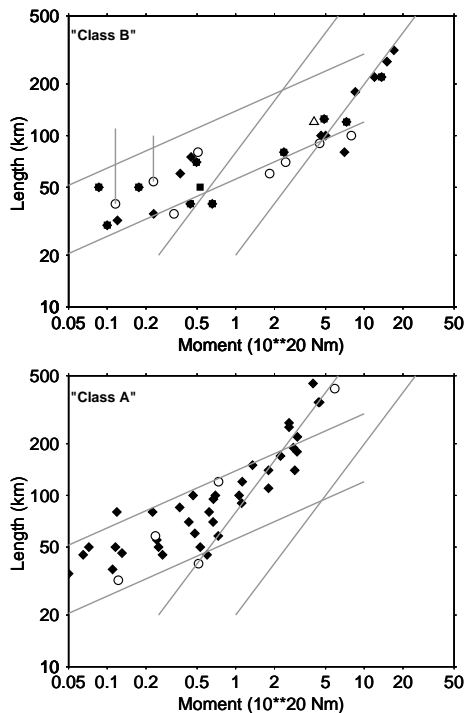


Figure 15.11: Moment-length plots for A (bottom) and B (top) events. Best fitting  $n = 1$  trends are indicated for each subset of data. Circles as in Figure 1, diamonds from other sources. Triangle is Luzon'90 event. Vertical lines point to the length estimates of PD96 for Aegean Sea events

ure 15.10). We separated our dataset into two subsets: subset A comprises mostly events that occurred in a continental setting, and/or which, if their moment is larger than  $1 \times 10^{20} Nm$ , follow the trend of events on the San Andreas and Anatolian faults, on which the analysis of Romanowicz (1992) was based. The second subset ("B") comprises the 12 large "anomalous" events mentioned above, four great earthquakes in central Asia, as well as smaller events occurring in an oceanic setting. The resulting separate  $M_0/L$  plots are shown in Figure 15.11.

We infer that each data subset can be fit rather tightly with an  $n = 1$  trend for the largest events. The change of scaling simply corresponds to a larger moment for events in subset B ( $M_0 \sim 5 \times 10^{20} Nm$ ) than for those in subset A ( $M_0 \sim 0.8 - 1 \times 10^{20} Nm$ ). For both subsets, the change in scaling occurs for  $L \sim 80 km$ . For smaller events, the dispersion is large, but, on average, the best fitting  $n = 3$  trend plots lower for subset B.

This difference in the position of the break in scaling in each subset can originate either from a difference in  $W_o$ , or from a difference in  $\Delta\sigma$ . If we assume that  $W_o$  cannot be much larger for events that occur in oceanic versus continental crust (at most a factor of 2 difference), Figure 15.11 implies that subset B has larger  $\Delta\sigma$  than subset A. In other words, in the latter case, the corresponding

faults are weaker. This result is consistent with studies that have compared intra-plate and inter-plate events (e.g. Kanamori and Anderson, 1975; Scholz et al., 1986), or determined that a continental inter-plate fault such as the San Andreas Fault in California is "weak" (e.g. Zoback and Zoback, 1987).

## 4.5 References

Bodin, P. and J. N. Brune, On the scaling of slip with rupture length for shallow strike-slip earthquakes: Quasi-static models and dynamic rupture propagation, *Bull. Seismol. Soc. Am.*, **86**, 1292-1299, 1996.

Henry, C. and S. Das, Aftershock zones of large shallow earthquakes: fault dimensions, aftershock area expansion and scaling relations, *Geophys. J. Int.*, **147**, 272-293.

Kanamori, H. and D. L. Anderson, Theoretical basis of some empirical relations in seismology, *Bull. Seism. Soc. Am.*, **65**, 1073-1095, 1975.

Mai, P. and C. Beroza, Source scaling properties from finite fault rupture models, *Bull. Seism. Soc. Am.*, **90**, 605-615, 2000.

Molnar, P. and Q. Denq, Faulting associated with large earthquakes and the average rate of deformation in central and eastern Asia, *J. Geophys. Res.*, **89**, 6203-6227, 1984.

Pegler, G. and S. Das, Analysis of the relationship between seismic moment and fault length for large crustal strike-slip earthquakes between 1977-92, *Geophys. Res. Lett.*, **23**, 905-908, 1996.

Romanowicz, B. Strike-slip earthquakes on quasi-vertical transcurrent faults: inferences for general scaling relations, *Geophys. Res. Lett.*, **19**, 481-484, 1992.

Romanowicz, B.; Ruff, L. J., On moment-length scaling of large strike slip earthquakes and the strength of faults, 10.1029/2001GL014479, 2002.

Romanowicz, B. and J. B. Rundle, On scaling relations for large earthquakes, *Bull. Seism. Soc. Am.*, **83**, 1294-1297, 1993.

Scholz, C. H., C. A. Aviles and S. G. Wesnousky, Scaling differences between large interplate and large intraplate earthquakes, *Bull. Seism. Soc. Am.*, **76**, 65-70, 1986.

Shaw, B. E. and C. H. Scholz, Slip-length scaling in large earthquakes: observations and theory and implications for earthquake physics, *Geophys. Res. Lett.*, **28**, 2995-2998, 2001.

Sornette, D. and A. Sornette, Theoretical implications of a recent non-linear diffusion equation linking short-time deformation to long-time tectonics, *Bull. Seism. Soc. Am.*, **84**, 1679-1983, 1994.

## 5. Historical Earthquake Re-analysis Project

R. A. Uhrhammer

### 5.1 Introduction

The objective of this USGS NEHRP funded two-year project, that commenced in March, 2000, is to characterize the spatial and temporal evolution of the San Francisco Bay Region (SFBR) seismicity during the initial part of the earthquake cycle as the region emerges from the stress shadow of the great 1906 San Francisco earthquake. The problem is that the existing BSL seismicity catalog for the SFBR, which spans most of the past century (1910-present), is inherently inhomogeneous because the location and magnitude determination methodologies have changed, as seismic instrumentation and computational capabilities have improved over time. As a result, the SFBR seismicity since 1906 is poorly understood.

Creation of a SFBR catalog of seismicity that is homogeneous, that spans as many years as possible, and that includes formal estimates of the parameters and their uncertainty is a fundamental prerequisite for probabilistic studies of the SFBR seismicity. The existence of the invaluable BSL seismological archive, containing the original seismograms as well as the original reading/analysis sheets, coupled with the recently acquired BSL capability to scan and digitize historical seismograms at high resolution allows the application of modern analytical algorithms towards the problem of determining the source parameters of the historical SFBR earthquakes.

Our approach is to systematically re-analyze the data acquired from the archive to develop a homogeneous SFBR catalog of earthquake location, local magnitude ( $M_L$ ), moment magnitude ( $M_w$ ), and seismic moment tensor (mechanism), including formal uncertainties on all parameters which extends as far back in time as the instrumental records allow and which is complete above appropriate threshold magnitudes. We anticipate being able to compile a new SFBR catalog of location and  $M_L$  which spans 1927 to the present and is complete at the  $M_L \sim 3$  threshold, and of  $M_w$  which spans 1911 to the present and which is complete at the  $M_w \sim 4.5$  threshold.

In addition to the above analysis, we will also search for sequences of repeating earthquakes. Identification of repeating earthquakes, which are nearly identical in all source properties, provides an internal consistency check on the location and magnitude homogeneity in the catalog over time.

### 5.2 Background and Motivation

Although the 1910 to present BSL catalog of earthquakes for the SFBR appears to be a simple list of events, one must remember that it really is a very complex

data set. It is easy to misinterpret observed variations in seismicity if we do not understand the limitations of this catalog. The existing 1910 to present BSL catalog of earthquakes for the SFBR is inhomogeneous in that it suffers from the three types of man-made seismicity changes identified by *Habermann*, 1987, namely detection changes, reporting changes, and magnitude shifts. The largest change in the detection capability of the BSL seismic station network occurred circa 1927-1931 with the installation of the Wood-Anderson and Benioff seismometers at four seismic stations (BRK, MHC, PAC, and SFB as shown in Figure 15.12) in the SFBR and the resulting increase in sensitivity lowered the threshold for detection of SFBR earthquakes by about 2  $M_L$  units. The most significant reporting change occurred circa 1942 when the BSL began determining  $M_L$  for some earthquakes and by 1948  $M_L$  was routinely determined and reported for all SFBR earthquakes listed in the BSL Bulletin (*Romney and Meeker*, 1949). A magnitude shift occurred in 1954 when the response of the Wood-Anderson seismographs changed (owing to changing the free period from 1.0 to 0.8 seconds) (*Bolt and Miller*, 1975).

The lack of a homogeneous catalog of earthquake for the SFBR which spans most of the past century, the availability of the invaluable BSL seismological archive, the interest in the Working Group on California Earthquake Probabilities (WGCEP, 1999), the funding of an initial effort with support from the USGS-PG&E CRADA, and the purchase and loan of a high-resolution wide-format digitizer by the USGS, combine to provide both an incentive and a unique opportunity to systematically re-process, using modern algorithms, the BSL seismographic records and data for SFBR earthquakes and to produce a homogeneous catalog of earthquakes for the region.

### 5.3 Initial Effort

During the summer of 1998, the USGS funded two students, via a USGS-PG&E CRADA, to transcribe the data from the original BSL reading/analysis sheets to computer readable form. With this funding, they were able to transcribe the reading/analysis sheets for SFBR earthquakes, working back in time from 1983 through 1944 (1984 onward was already in a computer database). The newly transcribed data along with the data already in the database were used to determine systematically the location,  $M_L$ , and corresponding uncertainties of earthquakes which have occurred in the SFBR. An interim catalog of SFBR earthquakes was subsequently developed

which includes hypocenter,  $M_L$ , and their uncertainties, and which spans from 1951 through 1998. The catalog starts in 1951 because amplitude data, used in the determination of  $M_L$ , were not registered on the reading/analysis sheets prior to that time. The interim catalog events are plotted in Figure 15.12 and available at <http://www.seismo.berkeley.edu/seismo/herp/>.

The rate of SFBR seismicity (see Figure 15.13) inferred from the 1951-1998 Interim Catalog is:  $\log N = 4.105 - 0.890 M_L$ . Assuming that the annual rate of SFBR seismicity ( $M_L \geq 3$ ) is stationary, we expect to observe an average of 27 earthquakes per year.

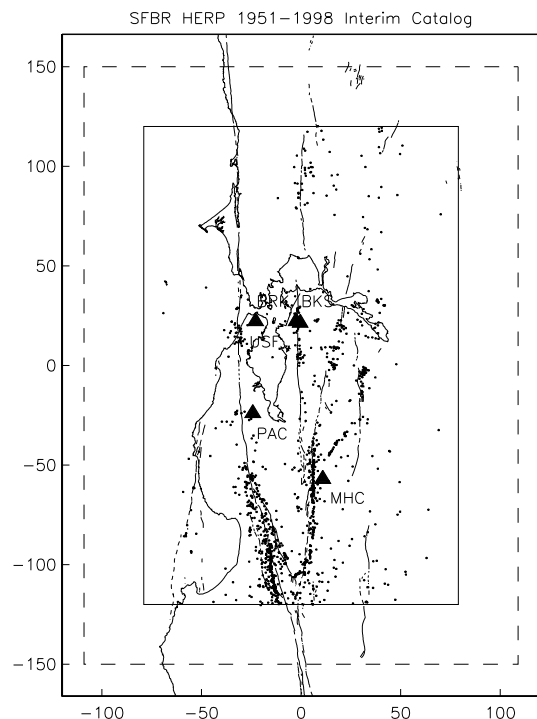


Figure 15.12: Map of the San Francisco Bay Region showing the Interim 1951-1998 Seismicity and the Stations which have housed Wood-Anderson seismographs. The solid inner box defines the SFBR (as given in the WGCEP 99 Report) and the dashed box is a 30 km buffer zone in which candidate SFBR events are also analyzed.

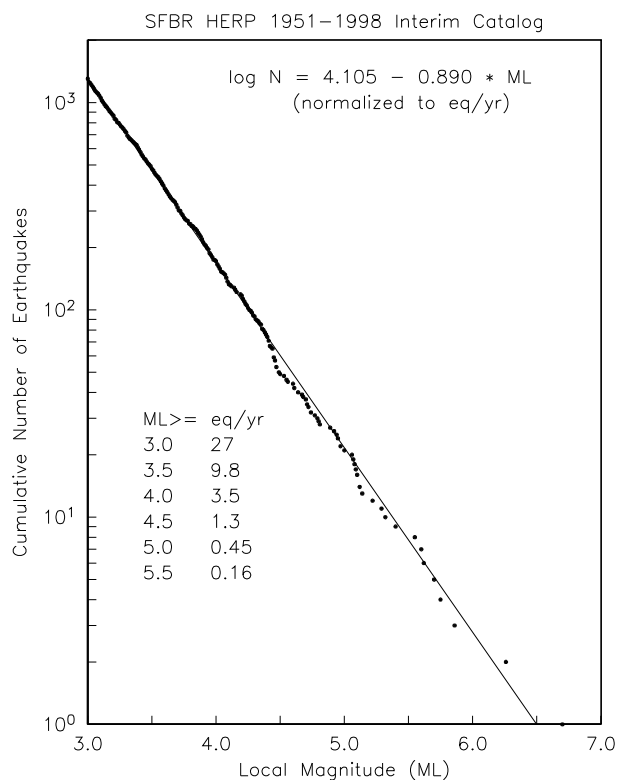


Figure 15.13: SFBR rate of seismicity inferred from the 1951-1998 catalog.

#### 5.4 Progress During the First Year

Since the Wood-Anderson maximum trace amplitude data used in the determination of  $M_L$  were not registered on the original reading/analysis sheets kept in the BSL archive, we read the maximum trace amplitudes recorded by the Wood-Anderson seismographs in order to calculate  $M_L$  and its uncertainty. The manpower intensive task of reading the maximum trace amplitudes registered by the Wood-Anderson seismographs for Berkeley (BRK), Mt. Hamilton (Lick Observatory; MHC), Palo Alto (Banner Station; PAC), and San Francisco (USF) that are kept on store in the BSL seismogram archive in Edwards Sta-

dium was completed by June 2001. We began with the 1950 records and worked backward in time and finished reading the earliest Wood-Anderson records (circa 1927) in June 2001.

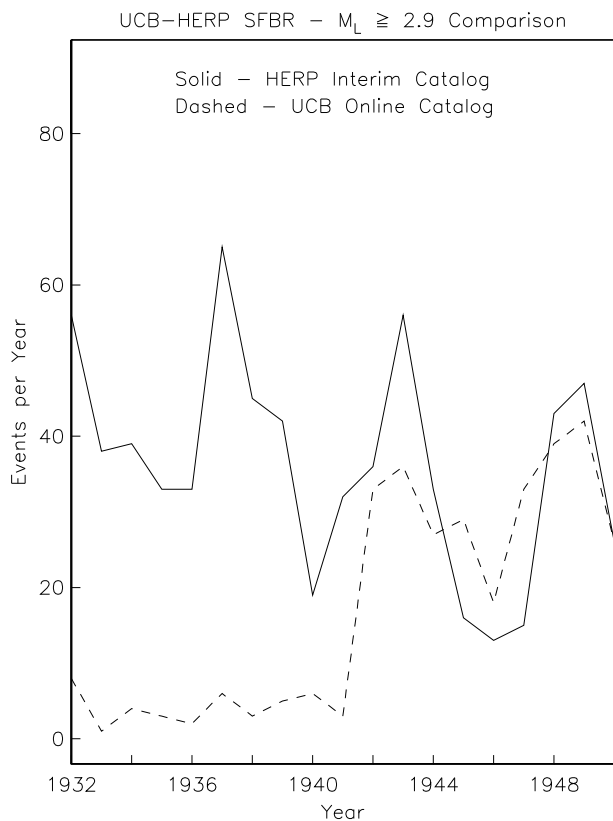


Figure 15.14: Number of 1932-1951 SFBR events analyzed (solid line) compared to the number of events listed in the BSL on-line catalog. Note that prior to 1942, the BSL on-line catalog does not list a large number of the events occurring in the SFBR owing to the fact that, since they had only a descriptive location rather than geographical coordinate location listed in the Bulletin, they were not transcribed when the computer readable database was initially compiled in the mid-1960's.

A list of candidate SFBR events, which included all events in the UCB catalog of earthquakes and also all events in the BSL Bulletins that were within the SFBR (including the 30 km buffer zone) and which either had a  $M_L$  of 2.8 or larger or else no  $M_L$  assigned, was compiled. The UCB catalog for the pre-1951 era is a composite based on the analysis of instrumental recordings and felt reports (*Bolt and Miller, 1975*). As we progressed back in time prior to 1951, the proportion of events with no  $M_L$  assigned increases and prior to 1942 it is virtually 100 percent. The number of 1932-1951 events analyzed is shown in Figure 15.14. To expedite the processing, we read the microfilm copies of the MHC Wood-Anderson

seismograms (*Uhrhammer, 1983*) to cull out events which are below the  $M_L$  2.8 threshold and thus minimized the number of records that we had to deal with in the BSL seismogram archive.

Originally, we did all the seismogram reading in the seismogram archive in Edwards Track Stadium and the students spent a significant amount of time shuttling between the BSL facilities in McCone Hall and Edwards Track Stadium. To expedite the processing, we transferred the seismogram bundles for the years that were being read to McCone Hall and this proved to be much more efficient.

## 5.5 Progress During the Past Year

We discovered a significant number of instances where the phases and maximum trace amplitudes were easily readable on the Wood-Anderson seismograms but there were no corresponding phase entries on the original reading/analysis sheets. Consequently we had to read the phase onset times for a numerous events that occurred prior to 1951. This process was quite tedious and time consuming owing primarily to the necessity of determining the clock corrections that convert the time on the record to Universal Time (UT). Clock corrections relative to a radio time standard were tabulated daily and linearly interpolated to determine the clock correction for a given event. The time corrections were occasionally unreliable (particularly so at USF) so we had to use relative times (the time difference between the P-wave and S-wave onsets) in place of absolute times when using the data to locate an event. The photographic paper was occasionally placed on the recording drums emulsion side down which resulted in faint and unreadable traces. Seismograms were occasionally fogged (inadvertently exposed to light) which also rendered them generally unreadable. Some seismograms are also difficult or impossible to read owing to the trace being out of focus due to misaligned optics.

We have finished transcribing the 1910-1927 data (pre-Wood-Anderson instrument) data. Prior to the advent of the Wood-Anderson seismographs, there were only two seismic stations operating in the Berkeley network, namely at the Student Observatory on the Berkeley Campus (BRK) and at the Lick Observatory at Mt. Hamilton (MHC). It should be noted that the earliest stations were operated at astronomical observatories primarily because these observatories had the means to routinely determine accurate clock corrections required for interpretation of data recorded on the seismograms. During the pre-1927 era, the primary seismic instrumentation at BKS and MHC consisted of Bosch-Omori and Wiechert seismographs which operated at low magnification (100x) and recorded on smoked paper.

We are also scanning and digitizing selected pre-1934 events recorded by Weichert and Bosch-Omori seismo-

graphs and the corresponding Wood-Anderson seismograms for those cases where the event was also recorded by Wood-Anderson seismographs. The primary objectives are to calibrate the determination of magnitude from the pre-Wood-Anderson recorded events and to begin the process of acquiring digital representations of the pre-1932 smoked paper seismograms. Obtaining digital representations of the Bosch-Omori and Weichert smoked paper seismograms is crucial particularly because the earliest smoked paper records, kept on store in the Berkeley Seismogram Archive, are becoming quite brittle and difficult to handle. We have been scanning these seismograms mostly on a flat bed scanner because some of the records could be damaged if they are passed through the rollers in the large format scanner.

## 5.6 Fuzzy-Logic-Based Location Algorithm

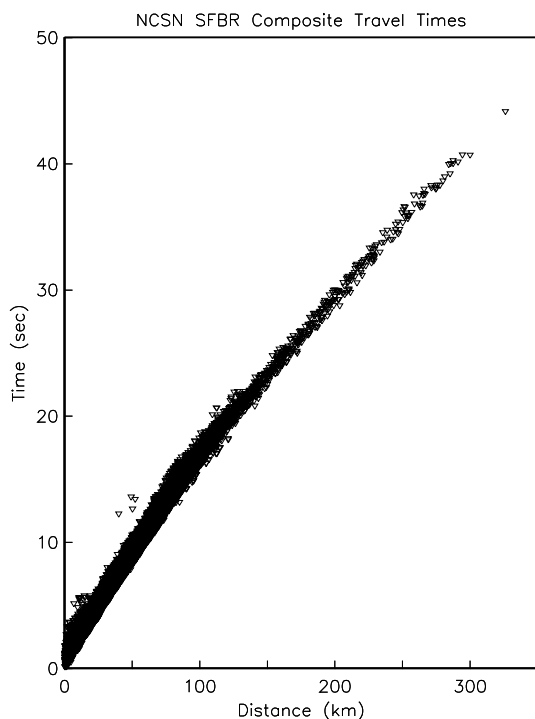


Figure 15.15: Observed travel times from SFBR earthquakes to NCSN SFBR stations. Plotted are travel time data from 1984-2000 for which the original waveforms are available on the NCEDC.

The end goal of HERP is to develop a uniform and internally consistent catalog of SFBR seismicity for instrumentally recorded earthquakes which have occurred during the past century in the region. As a part of this goal, we need to develop and calibrate a procedure for obtaining robust earthquake locations throughout a time when the number of SFBR seismic stations

evolved from the initial two stations (BRK and MHC) at the turn of the last century to the more than 100 seismic stations at present. The complex geology and faulting observed in the SFBR results in seismic wave propagation times which scatter significantly over differing propagation paths in the region as shown in Figure 15.15. Initially, the events are being located using a one-dimensional velocity model with appropriate station adjustments. Ultimately, however, a three-dimensional velocity model will be preferable for locating SFBR earthquakes.

We found that the existing earthquake location algorithms do not provide robust solutions when using the potentially imprecise data available from the sparse four-station pre-1960 SFBR seismic network. The distribution of observed P-wave travel times for the SFBR is shown in Figure 15.15. Consequently, a fuzzy logic based algorithm was developed to facilitate the determination of robust earthquake locations (Uhrhammer, 2001). The algorithm inherently has a high tolerance for imprecision in the observed data and it can yield robust sparse network solutions without requiring that the problematic observed data be either identified, down-weighted, or removed. This characteristic also renders the algorithm ideally suited for use in automated systems, such as the REDI Project, which provide rapid earthquake information.

## 5.7 Acknowledgements

We thank William Bakun of the USGS who encouraged us to pursue this project. UC Berkeley students Tom Fournier, Karin Spiller, Gabe Trevis, and Sierra Boyd participated in this project and we thank them for their efforts.

This project was supported by the USGS, through the NEHRP External Grants Program.

## 5.8 References

- Bolt, B. A. and R. D. Miller, Catalog of Earthquakes in Northern California and Adjoining Areas: 1 January 1910 - 31 December 1972, *Seismographic Stations, University of California, Berkeley*, iv + 567 pp., 1975.
- Habermann, R. E., Man-made changes of seismicity rates, *Bull. Seism. Soc. Am.*, 77, 141-159, 1987.
- Romney, C. F. and J. E. Meeker, Bulletin of the Seismographic Stations, *University of California Press*, 18, pp. 89, 1949.
- Uhrhammer, R. A., Microfilming of historical seismograms from the Mount Hamilton (Lick) seismographic station. *Bull. Seismo. Soc. Am.*, 73, 1197-1202, 1983.
- Uhrhammer, R. A., The San Francisco Bay Region Historical Earthquake Re-analysis Project: A progress report and locating pre-1960 instrumentally recorded earthquakes using a fuzzy-logic-based algorithm, *Seism. Res. Lett.*, 72, 245, 2001.

## 6. Northern California Seismicity Project

R. A. Uhrhammer

### 6.1 Introduction

The Northern California Seismicity Project (NCSP) is a counterpart to the San Francisco Bay Region (SFBR) - Historical Earthquake Re-analysis Project (HERP) reported in the research chapter on HERP. The initial objective of this project which commenced in August, 2000, is to transcribe the pre-1984 data for  $M_L \geq 2.8$  earthquakes which have occurred in Northern and Central California (NCC) (outside of the SFBR covered by HERP), from the original reading/analysis sheets, kept on store in the Berkeley Seismological Archives, to a computer readable format.

As is the case with HERP, characterization of the spatial and temporal evolution of NCSP seismicity during the initial part of the earthquake cycle as the region emerges from the stress shadow of the great 1906 San Francisco earthquake is the long term goal. The problem is that the existing BSL seismicity catalog for the SFBR, which spans most of the past century (1910-present), is inherently inhomogeneous because the location and magnitude determination methodologies have changed, as seismic instrumentation and computational capabilities have improved over time. As a result, NCC seismicity since 1906 is poorly understood.

Creation of a NCC seismicity catalog that is homogeneous, that spans as many years as possible, and that includes formal estimates of the parameters and their uncertainty is a fundamental prerequisite for probabilistic studies of the NCC seismicity. The existence of the invaluable BSL seismological archive, containing the original seismograms as well as the original reading/analysis sheets, coupled with the recently acquired BSL capability to scan and digitize historical seismograms at high resolution allows the application of modern analytical algorithms towards the problem of determining the source parameters of the historical SFBR earthquakes.

### 6.2 Background and Motivation

Although the 1910 to present BSL catalog of earthquakes for NCC appears to be a simple list of events, one must remember that it really is a very complex data set. It is easy to misinterpret observed variations in seismicity if we do not understand the limitations of this catalog. The existing 1910 to present BSL catalog of earthquakes for NCC is inhomogeneous in that it suffers from the three types of man-made seismicity changes identified by *Habermann, 1987*, namely detection changes, reporting changes, and magnitude shifts. The largest change in the detection capability of the BSL seismic station net-

work occurred starting circa 1927 with the installation of the Wood-Anderson and Benioff seismometers at several sites in NCC (see Figure 15.16) and the resulting increase in sensitivity lowered the threshold for detection of NCC earthquakes by about 2  $M_L$  units. The most significant reporting change occurred circa 1942 when the BSL began determining  $M_L$  for some earthquakes and by 1948  $M_L$  was routinely determined and reported for all SFBR earthquakes listed in the BSL Bulletin (*Romney and Meeker, 1949*). A magnitude shift occurred in 1954 when the response of the Wood-Anderson seismographs changed (owing to changing the free period from 1.0 to 0.8 seconds) (*Bolt and Miller, 1975*).

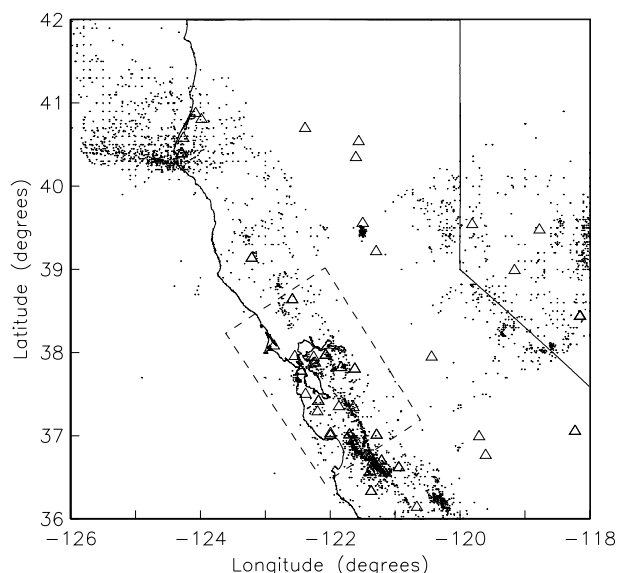


Figure 15.16: Map of the NCC Region showing the 1951-1983  $M_L \geq 2.9$  seismicity (small dots). The triangles are the seismic stations, operated by Berkeley and adjacent networks between 1951 and 1983, for which data are available. Events occurring in the dashed inset box are being transcribed and analyzed via HERP (see the HERP research chapter).

The lack of a homogeneous catalog of earthquake for the SFBR which spans most of the past century, the availability of the invaluable BSL seismological archive, the interest in the Working Group on California Earthquake Probabilities (WGCEP, 1999), the funding of an initial effort with support from the USGS-PG&E CRADA, and the purchase and loan of a high-resolution wide-format digitizer by the USGS, combine to provide both

an incentive and an unique opportunity to systematically re-process, using modern algorithms, the BSL seismographic records and data for SFBR earthquakes and to produce a homogeneous catalog of earthquakes for the region.

```

NEIS 1977/01/09 23:24:39 39.50N 121.64W 2          14 Northern
                                         California
NEIS M~L3.3(BRK), AFTER BRK.
NEIS IO=V MM AT DOBBINS. ALSO FELT AT GRIDLEY, GOLD RUN, RACKERBY,
MARYSVILLE, BROWNSVILLE AND OROVILLE.
BRK 1977/01/09 23:24:39 39.50N 121.64W 2 3.4L      Northern
                                         California
ISC *1977/01/09 23:24:37 39.55N 121.53W 2          15 Northern
                                         California
ORV 0.02 84 -iP Pn 23:24:42.00 -2.6
KPK 0.17 80 iP/PN Pn 23:24:44.10 -2.7
MIN 0.79 356 +iP/PKP Pn 23:24:56.00 0.4
WDC 1.29 323 +iP/PKP Pn 23:25:02.60 -0.1
WCN 1.39 99 iP/PN Pn 23:25:05.10 0.9
BKS 1.76 198 +iP/PKP Pn 23:25:09.00 -0.5
BKS S/(SKS) 23:25:30.00 -2.9
JAS 1.82 152 +iP/PKP Pn 23:25:10.20 -0.1
ARN 2.20 181 ePN Pn 23:25:15.60 -0.2
MHC 2.21 183 iP/PKP Pn 23:25:16.00 0.1
SAO 2.78 178 P/PKP Pn 23:25:24.00 -0.1
MNV 2.86 112 eP/PKP Pn 23:25:26.00 0.9
FRI 2.93 150 +iP/PKP Pn 23:25:26.90 0.7
BMN 3.42 74 ePN Pn 23:25:34.30 1.1
TNP 3.67 112 ePN Pn 23:25:37.40 0.7
EUR 4.30 89 iP Pn 23:25:46.00 0.4 Al.56E01 T 0.4
EUR i 23:26:53.80

```

Figure 15.17: Example of printer file of data for Berkeley network data extracted from ISC CDROM.

### 6.3 Current Effort

To expedite the transcription process, we converted all relevant available data from the online NCEDC event catalogs and the in-house phase data to the flat transcription file format as shown in Figure 15.17 for the years 1978 through 1983. We also acquired a copy of the International Data Center (ISC) CDROM which contains events and associated station data published in the ISC Bulletins from January 1964 through December 1977 (Version 1.2). This ISC data set includes event and station data contributed by Berkeley and the CDROM also contains a algorithm to search the database and extract and translate the ISC coded phase Berkeley data to a readable print format for years 1963 through 1977. This enabled us to start with transcription files that contained approximately half of the data that is on the original reading/analysis sheets for the years 1964 through 1983. The primary data from the original reading/analysis sheets, that was not included in this process, was the Wood-Anderson maximum trace amplitude data that is crucial for the determination of local magnitude.

During the past year five students worked on the process of transcribing the data from the original BSL reading/analysis sheets to computer readable form. They started by transcribing the original reading/analysis sheets from 1983 and they have been working back in time. The data from 1964 through 1983 has now been transcribed.

We are currently transcribing reading/analysis sheet

data from 1963. Since none of the data on the pre-1964 reading/analysis sheets exists in a computer readable form, all data has to be transcribed and consequently it takes more time to transcribe each event.

```

E 010977 232439.5 39-30.1 121-38.6 2.0 3.4
C 5KM SOUTHWEST OF OROVILLE, CALIFORNIA
F MMI V at Oroville
F Also felt at Gridley, Gold Run, Rackerby, Marysville and
F Brownsville
P BKS Ben Z e P c 232509.0
P BKS Ben E e S - 232529.5
A BKS WA - 0.65 0.7
P MIN Ben Z i P c 232456.0
A MIN WA - 5.2 6.0
P PCC Ben Z e (P) - 232515
A PCC Ben 11 - -
P MNV Ben Z e P - 232526.-
P PRI Ben Z e - - 232538
P ORV Ben Z i P d 232442.0
P JAS Ben Z e P c 232510.2
P WDC Ben Z i P c 232502.6
A BRK Ben Z e (P) - 232510
A BRK Ben 6 - -
P SAO Ben Z e (P) - 232524.2
P FRI Ben Z e P c 232526.9
P MHC Ben Z e P (c) 232516.0
A MHC WA - 0.35 0.25
P GCC Ben Z e - - 232520
P PRS Ben Z e (P) - 232530.8
P LLA Ben Z e - - 232527
A LLA Ben 19 - -
P FHC Ben Z e - - 232518
X

```

Figure 15.18: Example of completed transcription file format for the event shown in Figure 15.17.

### 6.4 Acknowledgements

UC Berkeley students Tom Fournier, Karin Spiller, Gabe Trevis, Maxwell Wilmarth, and Jennifer Epstein participated in this project and we thank them for their efforts.

This project was partially supported by the USGS funding of the Northern California Earthquake Data Center.

### 6.5 References

Bolt, B. A. and R. D. Miller, Catalog of Earthquakes in Northern California and Adjoining Areas: 1 January 1910 - 31 December 1972, *Seismographic Stations, University of California, Berkeley*, iv + 567 pp., 1975.

Habermann, R. E., Man-made changes of seismicity rates, *Bull. Seism. Soc. Am.*, 77, 141-159, 1987.

Romney, C. F. and J. E. Meeker, Bulletin of the Seismographic Stations, *University of California Press*, 18, pp. 89, 1949.

## 7. Accelerated Stress Buildup on the Southern San Andreas Fault and Surrounding Regions Caused by Mojave Desert Earthquakes

Andrew M. Freed and Jian Lin (Woods Hole Oceanographic Institution)

### 7.1 Summary

Scientists have hypothesized for decades that one major earthquake can trigger another earthquake on a nearby fault through stress interaction. More recent studies have further suggested that this interaction may be delayed by the slow viscous creeping of rocks in the Earth's lower crust and upper mantle. This is best illustrated by the 1999 magnitude 7.1 Hector Mine earthquake, which occurred only 30 km away from the 1992 magnitude 7.3 Landers quake, but seven and half years later. The delay between these events can be explained by viscous flow consistent with observations of continuous ground deformation following the Landers quake (Freed and Lin, 2001). In our more recent study (Freed and Lin, 2002), we further calculated how the Landers, Hector Mine, and two other earthquakes in the Mojave Desert have changed stresses on the nearby southern San Andreas and adjacent fault systems. We calculated that these earthquakes and continuous viscous creeping at depth are causing a rapid increase of stresses on a section of the San Andreas Fault, called the San Bernardino Mountain segment, that is located only 80 km from Los Angeles (Figure 15.19). The San Bernardino Mountain segment is worthy of special attention because it is capable of producing major earthquakes with magnitude greater than 7. Since the last major earthquake on this segment was over 190 years ago, the fault may be late in its earthquake cycle, and thus the calculated ongoing stress increase on the fault is of added significance. In addition, we calculated that parts of the San Jacinto, Elsinore, and Calico faults are also experiencing accelerated stress buildup. In particular, the Calico fault, which lies just north of the Landers rupture (near Barstow), appears to have the calculated stress patterns and the observed post- Landers aftershock clustering quite similar to the Hector Mine region before the 1999 quake. This makes the Calico fault another candidate for a potential earthquake in the future, where seismic activity should be watched closely.

### 7.2 References

Freed, A.M., and J. Lin, Delayed triggering of the 1999 Hector Mine earthquake by viscoelastic stress transfer, *Nature*, 411, 180-183, 2001.

Freed, A.M., and J. Lin, Accelerated stress buildup on the southern San Andreas fault and surrounding regions caused by Mojave Desert earthquakes, *Geology*, 30, 571-574, 2002.

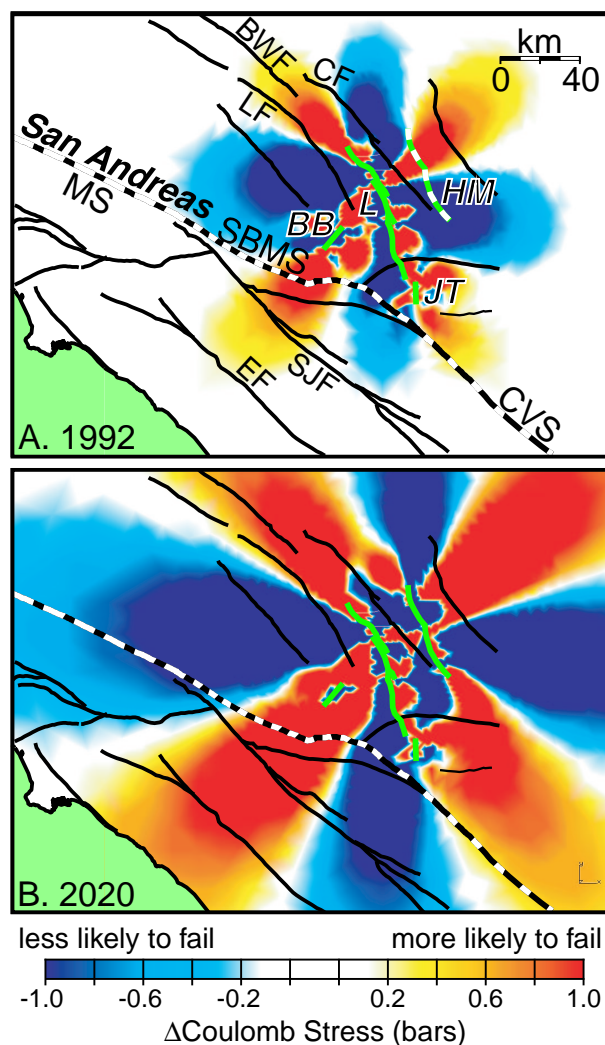


Figure 15.19: A. Calculated coseismic Coulomb stress changes caused by fault slip associated with the 1992 Joshua Tree (JT), Landers (L), and Big Bear (BB) earthquakes (green lines). Other faults: MS - Mojave segment, SBMS - San Bernardino Mountain segment, and CVS - Coachella Valley segment of San Andreas fault; SJF - San Jacinto fault, EF - Elsinore fault, CF - Calico fault, LF - Lenwood, and BWF - Blackwater fault. Location of future 1999 Hector Mine (HM) earthquake (green dashed line) is also shown. B. Same as A but with addition of stresses associated with 1999 Hector Mine earthquake and postseismic relaxation to the year 2020.

## 8. Land Uplift and Subsidence in the Santa Clara Valley

David Schmidt and Roland Bürgmann

### 8.1 Introduction

The Santa Clara Valley is a sedimentary basin whose stratigraphy forms a series of interbedded aquifers and aquitards (Clark, 1924). Land uplift and subsidence in the valley due to the recharge and withdrawal of fluids is well documented by several public agencies such as the Santa Clara Valley Water District (SCVWD) and the USGS (see Poland and Ireland, 1988). An increase in the withdrawal of water from the aquifer and a decrease in rainfall for the first half of the twentieth century resulted in a substantial drop in well levels and a corresponding land subsidence of  $\sim 4$  m. Recovery efforts over the past quarter century, such as the import of water from outside sources and the construction of percolation ponds, have allowed water levels to partially recover. Preservation of the aquifer requires the continual monitoring through extensometers, well water levels, and level line observations.

InSAR is an attractive method for monitoring land subsidence because of its spatial coverage and precision (e.g., Galloway et al., 1998; Hoffmann et al., 2001). However, individual interferograms are often difficult to interpret because the amount of deformation that is observed is highly dependent on the time of the season that the first and second SAR scenes are acquired. A time-series analysis has the potential to overcome this limitation by resolving the temporal variability of the surface deformation. We perform an InSAR time-series analysis using 115 interferograms spanning the time period from April of 1992 to June of 2000. The time-series analysis inverts for the incremental range-change between SAR scene acquisitions, producing a time-dependent signal of land uplift and subsidence.

### 8.2 Time-Series Result

The InSAR time series reveals an overall pattern of uplift since 1992 (Figure 15.20). The uplift is attributed to an increase in the ground water levels. The increase in pore pressure reduces the vertical effective stress on the skeletal matrix resulting in regional uplift. We observe as much as  $41 \pm 18$  mm of uplift centered north of Sunnyvale. Most of this uplift took place between 1992 and 1998 with a mean uplift rate of  $6.4 \pm 2.2$  mm/yr. Uplift is also observed in the Evergreen Basin located in the eastern portion of the Santa Clara valley. Significant subsidence relative to Oak Hill is also observed along the western margin of the valley. The southwestern portion of the valley shows insignificant uplift with no distinctive pattern. Continual uplift extends along several ma-

ior tributaries, especially along Garabazas and Saratoga creeks.

The time series also resolves a seasonal uplift pattern with the largest magnitude centered near San Jose (Figure 15.20b). The seasonal signal is sharply bounded on the east by a structure that aligns with the northward extension of the Silver Creek fault. Both ascending and descending interferograms show consistent deformation across this fault suggesting that the relative motion is vertical and not related to strike-slip fault motion. The fault appears as a sharp discontinuity in the deformation field of several interferograms that can be explained by differential subsidence across the structure. A seasonal subsidence pattern is also observed in the northwest portion of the region, however this signal is more complex and difficult to characterize.

### 8.3 Interpretation of Subsidence Pattern

The InSAR time-series results suggest that the aquifer can be further subdivided into three domains based on the deformation pattern: two regions experiencing net uplift (1992-2000) centered in Sunnyvale and the Evergreen basin, and a central region dominated by seasonal deformation. The seasonal uplift is bounded on the west where the thickness of unconsolidated sediments decreases along the northwesterly-striking basement high extending from Edenvale Ridge and Oak Hill.

The magnitude of elastic rebound is expected to correlate with the thickness of unconsolidated alluvium, or the depth to basement assuming that a change in pore pressure is translated to the full thickness. Unfortunately, the depth to basement is unconstrained for much of the valley; few of the wells reach consolidated bedrock. At several localities, such as in San Jose and north of Sunnyvale, the depth to basement is believed to be in excess of 420 m (Meade, 1967; California Department of Water Resources (CDWR), 1967). Well data suggests that the depth to basement is highly variable throughout the San Francisco Bay region where faulting and erosion during periods of low sea level have created an irregular bedrock surface.

The thickness of the alluvium is not the only property of the aquifer that may control the elastic response. The heterogeneity of sediment type and the connectivity of permeable beds may also play a significant role. The effective time constants of flow depend on the thickness of interbeds and the vertical hydraulic diffusivity of aquitards. The petrology and grain size of sediments from well cores were cataloged in an effort to character-

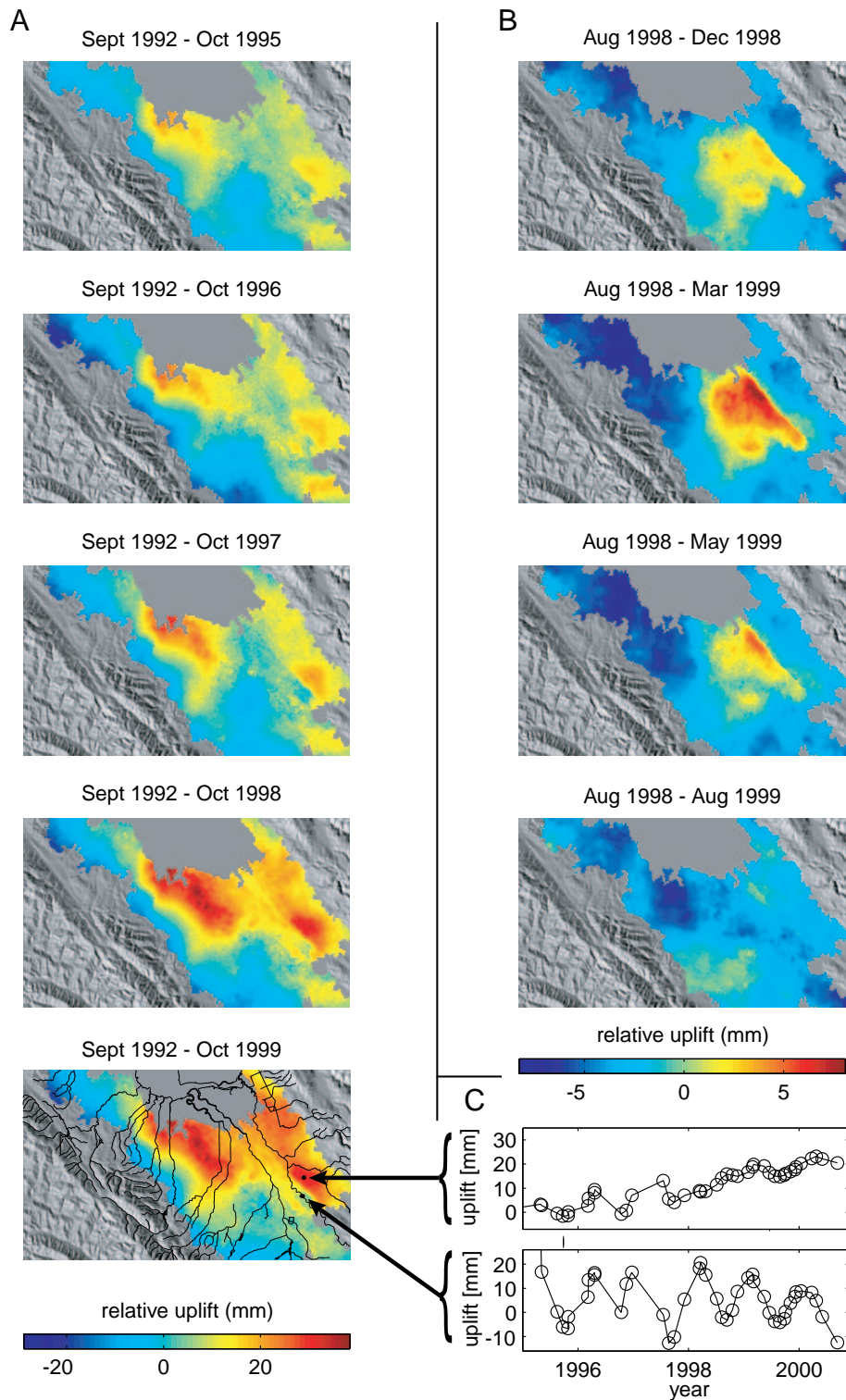


Figure 15.20: (A) Five frames from the InSAR time series show the pattern of net uplift since September of 1992. Uplift is centered north of Sunnyvale and east of the Silver Creek fault in the Evergreen Basin. Uplift is relative to Oak Hill (open square in final frame). The drainage network for the Santa Clara valley is also shown in the final frame. (B) The seasonal uplift pattern during a period from August of 1998 through August of 1999. (C) Time series at two points (dots in final frame of A) are compared to illustrate the seasonal versus long term deformation pattern. The points are separated by the Silver Creek fault which partitions the aquifer.

ize the constituents of the aquifer system. Meade (1967) and Johnson *et al.* (1968) analyzed core samples from the Sunnyvale and San Jose extensometer sites. Fine sands and clays dominate the sediment found at the Sunnyvale site with grain sizes ranging from 0.001 to 0.2 mm. In San Jose, grain sizes were generally larger ranging from 0.004 to 1.5 mm with often abrupt transitions between fine and coarse deposits. Developing geologic cross sections from well logs can be difficult because stratigraphic units may not correlate, especially if the units have an appreciable dip. Johnson (1995) used statistical correlations between well-perforation indicators to determine the lateral extent of water-bearing units. Coarse-grained units were found to be correlated over a wider area near San Jose than in Sunnyvale with an average bed thickness of 2.5 versus 1.3 m, respectively.

Despite the difficulty in correlating units from one well to the next, well log data and hydraulic head levels at different depths identified a sequence of productive water-bearing units identified as the Agnew aquifer (CDWR, 1967; Johnson, 1995). The deposition of these units is associated with the ancestral drainage of the Coyote creek and the Guadalupe river, both of which transport sediment down the valley axis on the way to the bay (Meade, 1967; CDWR, 1967). Seasonal uplift and subsidence shown in Figure 15.20b outlines a tabular region that broadens towards the north and may reflect the seasonal recharge of the Agnew aquifer. The InSAR data is not sufficient to resolve whether recharge has occurred in the shallow or deep sequence of the Agnew aquifer. The southern end of the seasonal uplift signal is co-located with the southernmost limit of the confined zone. Recharge of the basin is accommodated through the flow of subsurface water from the Coyote valley located to the south of the Santa Clara valley. Subsurface water flows through a narrow alluvial channel between Oak Hill and the Edenvale Ridge before cascading into the deeper aquifer (CDWR, 1967).

The long term uplift pattern also suggests that the permeable beds extend along stream channels to the west; however, these regions do not exhibit much seasonal deformation. The subsidence along the west side of the valley observed in Figure 4a outlines the Santa Clara formation which is traditionally characterized as the recharge zone. The coarser sediment found in the San Jose well log implies higher hydraulic conductivities. The large seasonal uplift pattern in San Jose may be explained by a system where the seasonal influx of groundwater is redistributed over short periods of time. In contrast, the aquifer north of Sunnyvale and in the Evergreen basin may be characterized by lower hydraulic conductivities because of a greater percentage of fine sediment and clay layers resulting in the slow influx of groundwater into these parts of the aquifer.

The uplift pattern observed using the InSAR time se-

ries highlights the spatial complexity of the aquifer system in the Santa Clara valley. The temporal and spatial pattern of uplift and subsidence afforded by InSAR provides important constraints on the lateral distribution of water bearing units and the time scales over which the groundwater is exchanged. Ultimately, knowing the lateral extent and connectivity of water bearing units will improve numerical studies which attempt to model the mechanics of the aquifer system.

## 8.4 Acknowledgements

SAR data was provided to the WInSAR Consortium by the European Space Agency (ESA) through their North American distributor, Eurimage. Original SAR data ©ESA (1992-2000). Additional data provided by an ESA (ENVISAT) data grant.

## 8.5 References

- California Department of Water Resources, Evaluation of groundwater resources, South San Francisco Bay, appendix A: Geology, Bulletin 118-1, 153 pp., 1967.
- Clark, W. O., Ground water in Santa Clara valley, California, *U. S. Geol. Surv. Water-Supply Pap.*, 519, 209 pp., 1924.
- Galloway, D.L., Hudnut, K.W., Ingebritsen, S.E., Phillips, S.P., Peltzer, G., Rogez, F., and P. A. Rosen, Detection of aquifer system compaction and land subsidence using interferometric synthetic aperture radar, Antelope valley, Mojave Desert, California, *Water Resour. Res.*, 34, 2573-2585, 1998.
- Hoffmann, J., Zebker, H., Galloway, D., and F. Amelung, Seasonal subsidence and rebound in Las Vegas valley, Nevada, observed by synthetic aperture radar interferometry, *Water Resour. Res.*, 37, 1551-1566, 2001.
- Johnson, A. I., Moston, R. P., and D. A. Morris, Physical and hydrologic properties of water-bearing deposits in subsiding area in central California, *U. S. Geol. Surv. Prof. Pap.*, 497-A, 71 pp., 1968.
- Johnson, N. M., Deterministic and stochastic approaches for evaluating multiple scales of Santa Clara valley hydrostratigraphy, in Sangines, E. S., Anderson, D. A., and A. V. Busing, Recent Geologic Studies in the San Francisco Bay Area, Pacific Section of the Society of Economic Paleontologists and Mineralogists, 76, 193-208, 1995.
- Meade, R. H., Petrology of sediments underlying areas of land subsidence in central California, *U. S. Geol. Surv. Prof. Pap.*, 497-C, 83 pp., 1967.
- Poland, J. F., and R. L. Ireland, Land Subsidence in the Santa Clara valley, California, as of 1982, *Mechanics of Aquifer Systems, U. S. Geol. Surv. Prof. Pap.*, 497-F, 61 pp., 1988.

## 9. Application of Point Measurements from InSAR to Study Slow Earthquakes on the Central San Andreas Fault

Ingrid A. Johanson and Roland Bürgmann

### 9.1 Introduction

In 1992, 1996 and 1998, creepmeters and strainmeters on the San Andreas fault (SAF) near San Juan Bautista recorded slip transients identified as slow earthquakes (SEQs) (Linde *et al.*, 1996; Gwyther *et al.*, 2000). These authors determined that SEQs in this area had moment magnitudes equivalent to the largest seismic quakes ( $M_w$  4.8-5.1) in this region. Their size and frequency suggest that SEQs are an important contributor to strain release. Additionally, SEQs primarily occur in areas of transition between locked and stably sliding faults, and may offer clues as to why and how these transitions take place. However, the low density of creep- and strainmeters makes it difficult to determine basic rupture parameters, such as the area or depth of the slip patch, with much certainty. In fact, the instrument density is so low that the network may fail to record many slow earthquakes. We are using high resolution geodetic measurements adjacent to the fault in an attempt to significantly improve our observations of SEQs and to possibly identify unrecorded SEQs. In particular, we would like to know: how common slow earthquakes are, how much of the fault's total slip they accommodate, whether they consistently rupture the same fault patch and how their occurrence depends on depth. Ultimately, our results should give us a better understanding of how episodic, aseismic slip events fit into the overall mechanics of fault systems.

### 9.2 InSAR

The extensive spatial coverage, good resolution and sub-centimeter precision of Interferometric Synthetic Aperture Radar (InSAR) makes it an ideal tool for measuring surface deformation due to slow earthquakes. However, the ground cover for this section of the SAF is largely vegetation and many interferograms are reduced to random scatter as a result of decorrelation noise (Figure 15.22). We must remove any decorrelation noise before we can identify a geophysically based signal. Our observations of InSAR amplitudes and air photos reveal that small buildings and rock outcrops exist within the vegetated areas that could provide stable and accurate measurements (Figure 15.21). These isolated stable patches ('stable scatterers'), ranging in size from a small town to a single pixel, can be extracted from the sea of decorrelation noise and pieced together to increase the useful area of an interferogram.



Figure 15.21: InSAR amplitude image of the San Juan Valley showing the locations of 'stable scatterers' (black circles). The dotted line delimits the swath box from which the profile in Figure 3 is extracted. Also shown is the San Andreas Fault (solid line).

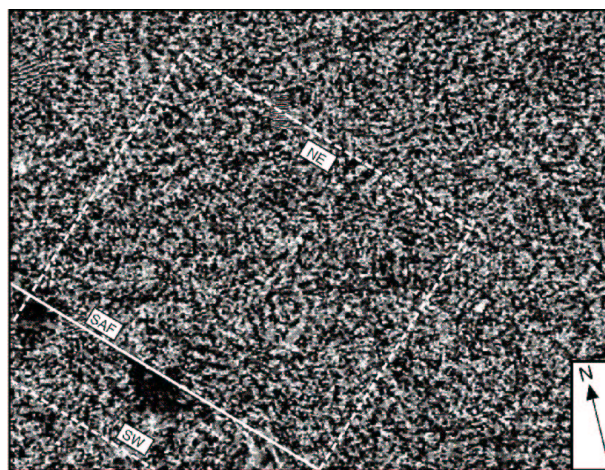


Figure 15.22: Wrapped interferogram corresponding to the area covered in Figure 1 and spanning from May 19, 1996 to August 8, 1998; with a perpendicular baseline of 7 meters. Although the image has been spatially filtered to enhance any signal, random noise still dominates.

### 9.3 Stable Scatterers

Ferretti et al. (2001) proposed, as a part of their Permanent Scatterer Method, that the stability of individual amplitude and phase measurements across many interferograms be used to identify stable pixels. Buildings (which are often picked as ‘Permanent Scatterers’ because of their good stability) have corner reflecting walls that reflect much more brightly than any surrounding vegetation. ‘Stable scatterers’ can therefore also be identified as points with consistently high amplitudes (Johanson and Bürgmann, 2001). We are implementing this adaptation of the Permanent Scatterer Method to accurately measure surface deformation due to slow earthquakes on the central SAF. InSAR amplitude suggests that there is a sufficient number of potential ‘stable scatterers’ to make this approach viable (Figure 15.21). Across-fault profiles of stable scatterers from our preliminary results are more coherent than randomly chosen points and exhibit geophysically reasonable motions (Figure 15.23). However patches of high scatter in the profile show that additional refinement of our ‘stable scatterer’ definition may be necessary.

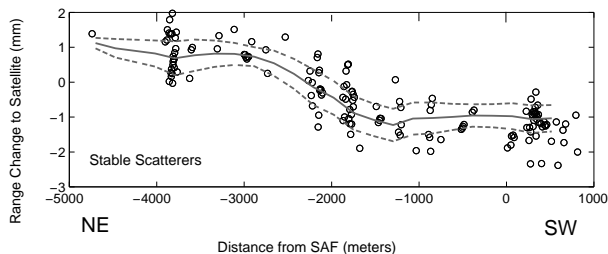


Figure 15.23: Unwrapped profile across the San Andreas Fault of ‘stable scatterers’ contained within the swath box as shown in Figure 1, extracted from an unfiltered version of Figure 2. Wrapped range change values can vary between 1.4 & -1.4 cm. This profile represents a 26% reduction in angular deviation as compared with randomly selected points.

### 9.4 Future Work

With nearly 100 available interferograms of the central SAF, we plan to construct a time series that can be analyzed together with a campaign GPS data set spanning 1989-2002. Yearly observations of a GPS network covering the Santa Cruz, Hollister, and Salinas areas, have yielded precise measurements of the post-seismic deformation from the 1989 Loma Prieta earthquake and of the regional interseismic deformation. The pattern of ground movement from these processes overprints the deformation pattern from SEQs and should be removed from the InSAR analysis. Another benefit of GPS data is that it measures ground movement in three components and can

provide a basis for differentiating between horizontal and vertical ground movement in the interferograms.

### 9.5 References

- Ferretti, A., C. Prati, and F. Rocca, Permanent scatterers in SAR interferometry, *IEEE Transactions on Geoscience and Remote Sensing*, 39 (1), 8-20, 2001.
- Gwyther, R.L., C.H. Thurber, M.T. Gladwin, and M. Mee, Seismic and aseismic observations of the 12th august 1998 San Juan Bautista, California m5.3 earthquake, in *3rd San Andreas Fault Conference*, pp. 209-213, Stanford University, 2000.
- Johanson, I.A., and R. Bürgmann, Using point measurements from InSAR to detect transient deformation (abstract), *EOS Transactions, AGU*, 82 (47), 266, 2001.
- Linde, A.T., M.T. Gladwin, M.J.S. Johnston, R.L. Gwyther, and R.G. Bilham, A slow earthquake sequence on the San Andreas Fault, *Nature*, 383 (6595), 65-8, 1996.

# 10. Crustal Deformation Along the Northern San Andreas Fault System

M. H. Murray

## 10.1 Introduction

The 100-km wide San Andreas fault system in northern California is composed of three sub-parallel right-lateral faults: the San Andreas, Ma'acama, and Bartlett Springs faults. The San Andreas fault has been essentially aseismic since it last ruptured from San Juan Bautista to Cape Mendocino in the great 1906 San Francisco earthquake. No major earthquakes have occurred during the historical record on the more seismically active Ma'acama, and Bartlett Springs faults, northern extensions of the Hayward-Rodgers Creek and Calaveras-Concord-Green Valley faults in the San Francisco Bay area, but the slip deficit on the Ma'acama fault, based on a high slip rate found by previous geodetic studies, may now be large enough to generate a magnitude 7 earthquake, posing a significant seismic hazard.

In Fall 2002 we will resurvey about 40 monuments that form 4 profiles across the northern San Andreas fault system (Figure 15.24). Most of the monuments were last observed in 1993 or 1995, so the new observations will significantly improve estimates of their relative motion and models of average interseismic strain accumulation, including possible spatial variations along the fault system, and will form the basis for future observations to detect temporal variations in deformation. The monitoring network will provide roughly 10-station profiles every 50 km from Pt. Reyes to Cape Mendocino. We will reprocess the GPS observations using more modern techniques and apply recently developed modeling techniques to provide a more self-consistent description of deformation across northern California and strain accumulation on the northern San Andreas fault system.

## 10.2 Geodetic Measurements

The northern segment is the youngest portion of the San Andreas fault system, forming in the wake of the northward propagation of the Mendocino triple junction (MTJ) where the Pacific, North America, and Gorda (southern Juan de Fuca) plates meet. The Pacific plate moves northwestward about 35-40 mm/yr relative to central California across a broad 100 km zone in northern California, with the additional motion accommodated in eastern California and the Basin and Range province making up the total relative Pacific-North America, about 50 mm/yr predicted by NUVEL-1A.

Geodetic measurements, which are particularly useful for detecting deformation and strain on deep structures throughout the seismic cycle, currently provide only weak constraints on average strain accumulation for much of

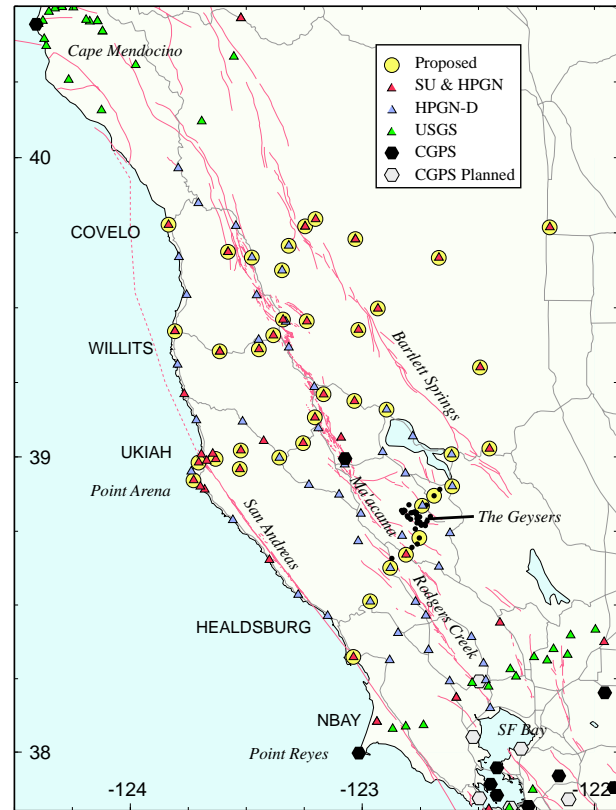


Figure 15.24: GPS sites (circled) to be resurveyed along the northern San Andreas fault system in Fall 2002. Profile names are capitalized. USGS survey-mode sites are observed annually along the NBAY profile and their network near Cape Mendocino were observed in Summer 2001. Only one continuous GPS station (HOPB) at a BSL broadband seismic site near Hopland currently operates in this region.

this region. This is particularly true north of Point Arena, where the San Andreas fault lies offshore and bends 20 clockwise as it comes onshore at Point Delgada before terminating at the Mendocino triple junction near Cape Mendocino. The Ma'acama and Bartlett Springs faults also undergo clockwise rotation to a lesser degree and appear to reactivate older subduction structures as the triple junction migrates northwestward. This complex geometry and other features, such as surface creep on the Ma'acama fault, suggest the deformation may be spatio-temporally variable, similar to deformation that has been observed, and is now being monitored by continuous, frequent survey-mode GPS, and other geodetic

observations, on the southern extensions of these faults in the Bay Area that share many of the same characteristics. Understanding how this spatio-temporal variability affects strain accumulation on the faults is critical for assessment of the timing and hazards posed by future earthquakes.

In *Freymueller et al.* (1999) we reported on data collected in 1991-1995, primarily from the Ukiah and Willits profiles (Figure 15.24). GPS velocities from this network place some constraints on the total slip rate on the San Andreas fault system, which we estimate to be  $39.6 \pm 1.5 - 0.6$  mm/yr (68.6% upper and lower confidence intervals from a nonlinear inversion are indicated by subscripts and superscripts). Slip rates on the individual faults are determined less precisely due to the high correlations between estimated slip rates and locking depths, and between slip rates on adjacent faults. Our estimated slip rate on the San Andreas fault is lower than all geologic estimates, although the 95% confidence interval overlaps the range of geologic estimates. Our estimate of the Ma'acama fault slip rate is greater than slip rate estimates for the Hayward or Rodgers Creek faults, its continuation to the south. The Ma'acama fault most likely poses a significant seismic hazard, as it has a high slip rate and a slip deficit large enough to generate a magnitude 7 earthquake today since there have been no significant earthquakes on the fault in the historical record.

### 10.3 Deformation Modeling

In our *Freymueller et al.* (1999) study, we used a single station constrained to a VLBI-derived velocity to define the velocity reference frame, and were unable to properly account for the far-field motions in terms of angular velocities. We will reanalyze the observations using a more robust, globally defined reference frame that will facilitate application of the angular velocity-fault backslip model (*Murray and Segall, 2001*), and provide a more self-consistent description of northern California deformation. The method can accommodate the observed creep on the faults, and we will also extend the technique to 3D models using backslip on shallow rectangular dislocations in order to investigate the effects of the fault orientations rotating more clockwise at the northernmost segment.

We will investigate the uncertainties of our strain accumulation models using the bootstrap techniques, which provide realistic uncertainties for nonlinear optimization problems. The correlations between slip-rates and locking depths are highly correlated, so that higher slip rates on the San Andreas fault, for example, can tradeoff with lower slip-rates on the Ma'acama fault with almost equal misfit. We will test methods for adding geologic and other information, using Bayesian techniques, to test whether the additional information can reduce the correlations and provide better resolution on other param-

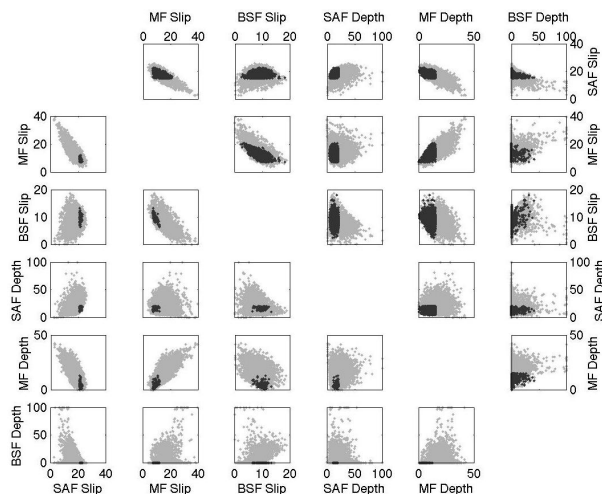


Figure 15.25: Full slip-rate and locking depth covariance for the *Freymueller et al.* (1999) study of the San Andreas (SAF), Ma'acama (MF), and Bartlett Springs (BSF) faults. Shaded areas, the best 95% of the original 10,000 bootstrap trials. Dark shaded areas only, resolution improved by applying Bayesian constraints based on seismic, geodetic, and paleoseismic observations, including maximum locking depths on SAF and MF faults, and minimum slip-rate on the MF. SAF slip-rate constrained to estimates from two recent studies: 21-27 mm/yr (bottom triangle), and 15-23 mm/yr (top triangle).

eters. For example, the previously determined slip-rate on the San Andreas fault ranged from 10.5-22.6 mm/yr at 95% confidence with locking depths ranging 4.7-44.6 km. By applying constraints derived from other seismic, geodetic, and paleoseismic observations, the estimated parameters can be much better resolved (Figure 15.25).

### 10.4 Acknowledgments

This project is supported by the USGS, through the NEHRP External Grants Program.

### 10.5 References

- Freymueller, J. T., M. H. Murray, P. Segall, and D. Castillo, Kinematics of the Pacific-North America plate boundary zone, northern California, *J. Geophys. Res.*, *104*, 7419-7442, 1999.
- Murray, M. H., and P. Segall, Modeling broadscale deformation in northern California and Nevada from plate motions and elastic strain accumulation, *Geophys. Res. Lett.*, *28*, 4315-4318, 2001.

# 11. Urban Geodesy: Monitoring Active Deformation near the Hayward fault

Matthew A. d'Alessio, David Schmidt, Roland Bürgmann, and the UC Berkeley Active Tectonics Group

If you need to take measurements in the middle of a busy intersection, or in a stadium that houses thousands of voracious football fans, or even at a freeway offramp in the middle of rush-hour, you need an urban geodesist. And the Hayward fault, which passes through one of the most densely populated strips in California, is a place where urban geodesy is king.

Geodesy, the science of surveying and measuring the earth's surface, is one of the many tools used by earthquake scientists to understand the behavior of faults. This paper describes the Berkeley Seismological Laboratory's ongoing effort to use geodesy to monitor the movement of the Hayward fault, as well as some of the challenges introduced by doing science in a densely populated urban region.

## 11.1 Hayward Fault GPS Campaign

The Hayward fault is unique because it not only produces large earthquakes like the estimated M7 1868 earthquake, but it also slowly slips along in a process called aseismic creep. In recent years, the Berkeley Seismological Laboratory has begun utilizing measurements with the Global Positioning System (GPS) to monitor creep along the Hayward fault. This work will provide an unprecedented spatial resolution of GPS measurements about a creeping fault and should allow us to determine where the fault is creeping, how fast it is creeping, and most importantly, how deep the creep extends. Since aseismic creep relieves stress along the fault, identifying locked patches at depth can give us clues to determine where large earthquakes might eventually nucleate and how big they could be.

In a GPS "campaign", we use research-grade GPS equipment to determine the location of a point on the ground to a precision of less than 5 mm. In other words, we can determine locations on earth to within an area half the size of a dime. The next year, we repeat the campaign and return to the exact same location to determine the position again. Because the Hayward fault is slowly creeping along, the spot will have moved; with our high precision positioning, we hope to determine exactly where and how fast. The precision and reliability of our measurements depend on several factors that are all more difficult in the urban setting. See the table on the following page for more details.

As part of the Berkeley Seismological Laboratory's ongoing effort to monitor active deformation along the Hayward fault, we determine positions of over fifty bench-

marks within ten kilometers of the fault (Figure 15.26). Of these fifty monuments, about two thirds of them are in logistically difficult urban settings while the remainder are in the scenic rolling hills that flank the fault. The first surveys of most benchmarks were made in 1998, and our group has been returning each summer to take new measurements.

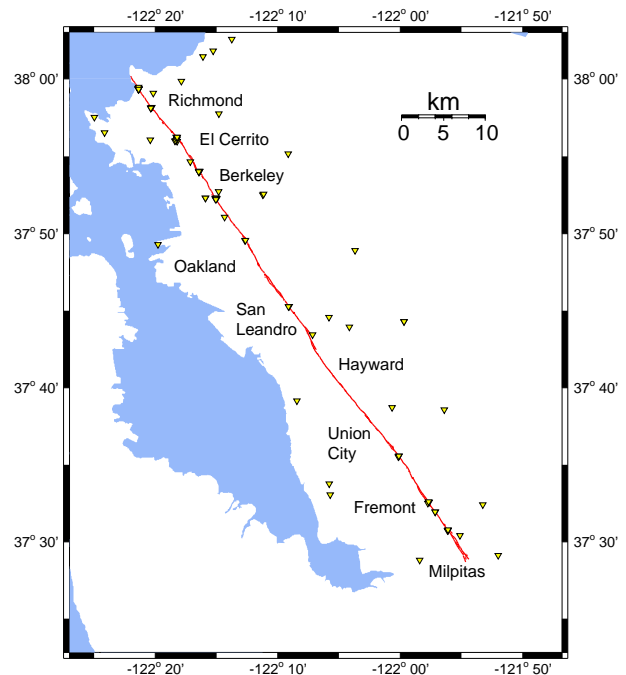


Figure 15.26: The Hayward fault and urban areas of the East Bay. Each triangle shows the location of a benchmark surveyed annually since 1998

## 11.2 Current Progress

In the last year, the Active Tectonics group purchased seven new, state of the art, geodetic grade GPS receivers. The Trimble 5700 receivers are smaller, lighter, and draw less power than receivers used in the past, making them ideal for both urban geodesy and more remote GPS sites that can only be accessed by hiking. Initial trials using the new receivers show that they produce good quality data that is consistent with the receivers used in past campaigns. The 2002 campaign, which is currently underway, promises to yield excellent estimates of the velocities over the last four years.

Results from our test site at UC Berkeley’s Memorial Stadium appear in Figure 15.27. We should note that in order to take measurements at this site, three of the stations must be set up on staircases inside the stadium, meaning that the operator must make sure that the tripod is perfectly level even though the legs are on a completely uneven surface. Further, the tripod at station STAA must carefully straddle a railing along one stairway. Despite these difficult conditions, our calculations of the fault-parallel velocity across the stadium from these observations is  $4.2 \pm 0.3 \text{ mm} \cdot \text{yr}^{-1}$  – in very close agreement with the creep rate determined from off-set curbs along nearby Dwight Way of  $3.9 \pm 0.1$  and  $4.1 \pm 0.1 \text{ mm} \cdot \text{yr}^{-1}$ . We expect results from the rest of our 2002 campaign (currently underway) to yield equally reliable velocities.

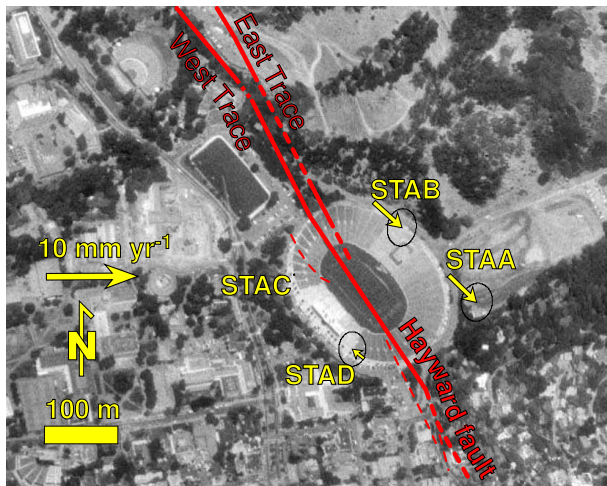


Figure 15.27: Velocities for 1998 - 2002 of four benchmark in UC Berkeley’s Memorial Stadium, shown relative to station STAC. The Hayward fault cuts down the middle of the stadium. These observations show that the Hayward fault creeps at a rate of about  $4.2 \pm 0.2 \text{ mm} \cdot \text{yr}^{-1}$ . The locations of faults are from a recent paleoseismological report by Geomatrix Consultants, 2001.

### 11.3 The Challenge

The more densely populated the region, the more valuable seismic hazard assessment becomes. Unfortunately, the more densely populated the region, the more difficult it is to collect reliable data. This is the challenge to the urban geodesist.

## 11.4 Recipe for High Precision

The following table describes conditions that contribute to high quality estimates of position during a GPS campaign, and why it is challenging to achieve these conditions in the urban environment:

<b>Benchmark Stability</b>	
<i>Explanation</i>	If the location we survey is on unstable ground, the movement we record may not be related to fault motion at all.
<i>Urban Challenges</i>	Near-surface rocks in urban areas are often artificial fill which can be less stable.
<b>Consistent Setup</b>	
<i>Explanation</i>	We must position our instruments in exactly the same location each time with less than a millimeter of tolerance – a job that requires a fair amount of patience, skill, and experience.
<i>Urban Challenges</i>	Even with proper safety gear, try achieving millimeter-level precision in the middle of a busy intersection!
<b>Unobstructed Sky View</b>	
<i>Explanation</i>	GPS receivers determine position by recording broadcasts from satellites orbiting overhead. Overhead obstructions can therefore block or distort the signal.
<i>Urban Challenges</i>	Tall buildings, fences, trees, buses, etc.
<b>Long Duration Measurements</b>	
<i>Explanation</i>	We must collect data for at least 6 to 72 hours continuously. During that time, the instrument must not be disturbed and cannot move even a millimeter.
<i>Urban Challenges</i>	An operator must guard the instrument from both theft and disturbance during the entire time. In busy settings with passing cars, the vibrations can often move the instrument slightly. When placed on asphalt, the instrument can sink into the pavement on hot days.

## 12. Active Tectonics of the Adriatic Region (Central Mediterranean)

M. Battaglia, M. H. Murray, R. Bürgmann  
D. Zuliani, A. Michelini, CRS (Italy)

### 12.1 Introduction

The Adriatic region can be considered an ideal natural laboratory for studying the kinematics and dynamics of micro-plate tectonics because of the wide variety of tectonic processes encompassed. These include continental collision, subduction of continental and oceanic lithosphere, major continental faults such as the Periadriatic Line, and a variety of smaller scale processes associated with African-Eurasian plate interaction. It is widely accepted that the Adriatic block was originally an African promontory that was indented into the European lithosphere by the convergence of the African and Eurasian plates. However, the present-day kinematics of the Adriatic block are more uncertain: is it still closely connected with the African continent or does it behave as an independent microplate? The distribution of seismicity in the Adriatic region is distinguished by very low seismicity in the plate interior compared to intense activity in the high topographic belts that border the region in the SW, NW and NE. One of the strongest clusters of seismic activity is in the greater Friuli region, located at the convergent NE edge of the Adriatic region, where the  $M_s=6.5$  1976 Friuli earthquake caused widespread damage.

### 12.2 Geodetic monitoring in the Friuli Seismic Zone

The Friuli Regional Deformation network (FReDNet) of continuously operating Global Positioning System (GPS) receivers monitors crustal deformation along northeast boundary of the Adriatic microplate, which in the Friuli region is thought to be on the order of 5 mm/yr north-south convergence. FReDNet is operated by the Centro Ricerche Sismologiche (CRS) of the Istituto Nazionale di Oceanografia e di Geofisica Sperimentale (OGS). The principal goals of the FReDNet program are to determine the distribution of deformation in this region, to estimate interseismic strain accumulation on its active faults to better assess seismic hazards, to monitor hazardous faults for emergency response management, and to provide infrastructure for geodetic data management and processing. FReDNet will also be part of a proposed larger program of geodetic monitoring of the Adriatic microplate that includes repeating episodic measurements of geodetic points (e.g., points of the IGM95 geodetic network).

In June 2002, Maurizio Battaglia and Mark Murray visited the CRS in Udine, located in the central Friuli region, to assist in site reconnaissance, permitting, and

installation of the first FReDNet stations, and to initiate data acquisition, quality checking, archiving, and analysis. Most of the stations will be collocated with broadband seismometers maintained by the OGS, allowing us to employ some of the procedures developed at the BSL to integrate geodetic and seismic data from the BARD and BDSN networks. In April 2002, David Zuliani of the CRS visited the BSL to better study these procedures.

The CRS purchased 6 Ashtech Micro-Z GPS receivers with chokering antennas for the initial deployment of the new continuous stations. We inspected 5 sites with acceptable sky visibility for GPS observations. Four of the sites are collocated with existing seismic stations (ZOU, LSR, CAE, and MPRI, Figure 15.28), all within the southern Alpine foothills in north Friuli. The southern Friuli region is overlain by Quaternary sediment deposits that are not suitable for GPS monuments needing long-term stability. However, at the Medea site a block of Jurassic sandstones has been uplifted, providing a more tectonically stable setting for the GPS monument. Except for ZOU, additional permitting was required at all the sites. Currently, we have obtained permits for all the sites except LSR, although the fees requested for the CAE site were deemed to prohibitive. We are now pursuing an alternative site at Faloria (AFL), collocated with a seismic station in the Dolomites to the west of Friuli. A sixth station will be located near the main OGS campus in Trieste for demonstration purposes.

In June 2002, we installed the GPS station ZOUF at Zouf Plan, collocated with the ZOU seismic station (Figure 15.29). A 1-m concrete pier was attached to surface bedrock using epoxied metal rods, and the chokering antenna was attached to the monument using a SCIGN antenna adapter and covered with a SCIGN dome. The antenna cable was trenched to a nearby building housing the seismic data loggers and GPS receiver. Cellular modems are used to telemeter the data once per day, using SHARC/EGADS to control the data retrieval. A second station (UDIN) was installed on the roof of a CRS building in Udine for testing purposes. In July 2002, the monument at Monte Prat (MPRI) was installed (Figure 15.30). The CRS is currently resolving problems telemetering the data from this station.

We installed the GAMIT/GLOBK GPS analysis package on a Linux computer at CRS, and initiated automatic processing of the data from ZOUF and UDIN, in combination with other EUREF continuous stations. Preliminary analysis shows short-term repeatabilities in the horizontal components of 2 mm in the north and 4 mm

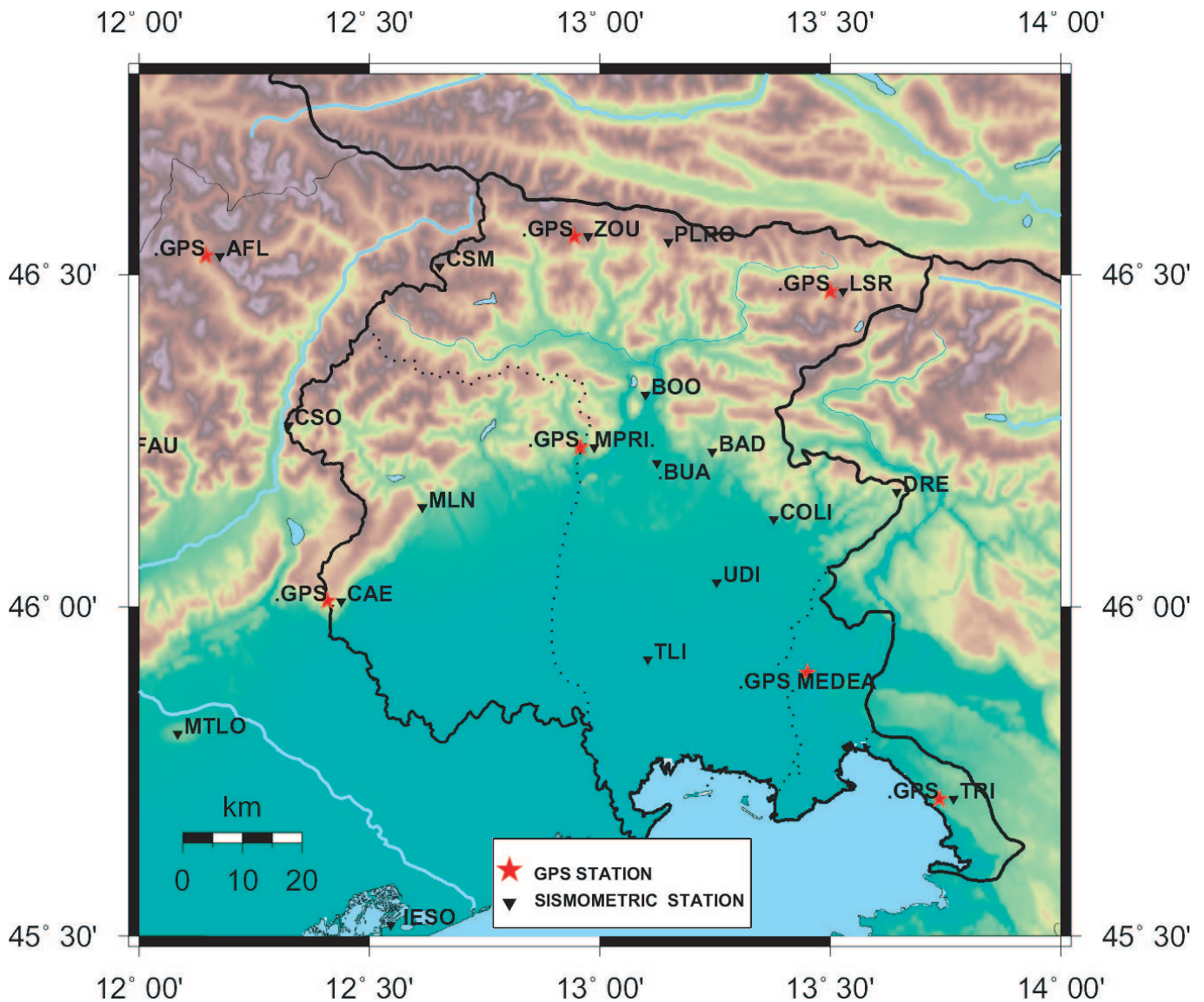


Figure 15.28: Existing and planned GPS continuous stations of the FReDNet in the Friuli region, northeastern Italy. Stations IESO is near Venice, TRI is near Trieste and the border with Slovenia, and ZOU is near the Austrian border. Red stars, GPS stations. Triangles, CRS seismic stations monitoring the Friuli seismic zone. Epicenter of the Ms=6.5 1976 Friuli earthquake is near the station BOO.

in the east. The higher east repeatabilities are mostly likely due to poor phase ambiguity resolution between the FReDNet and EUREF sites, which are over 100 km distant. These results should improve as the other FReDNet stations are installed, providing short distances that can be more easily resolved.

In the coming year, the CRS plans to finish the installation of the 6 initial stations and make the data publicly available, and we will continue to assist them in processing the observations in combination with other European stations in order to obtain initial estimates of the rate of convergence across the Friuli Seismic Zone.

### 12.3 Acknowledgements

We thank the staff of the CRS/OGS for their abundant assistance and hospitality during the station installations, particularly Alberto Michelini, David Zuliani, Giorgio Duri, Fausto Ponton, Paolo Di Bartolomeo, Gianni Bressan, Aladino Govoni, and Pier Luigi Bragato. This project is partially supported by the Centro Ricerche Sismologiche (CRS) of the Istituto Nazionale di Oceanografia e di Geofisica Sperimentale (OGS), Trieste, Italy.



Figure 15.29: GPS station at Zouf Plan (ZOUF), collocated with seismic station ZOU. The 1-m high concrete pier with GPS antenna and dome mounted on top are on the right. Solar panels and radio antenna mast for the seismic station are on the left.



Figure 15.30: Installation of the GPS monument at MPRI. Concrete pier is tied to near surface bedrock using epoxied steel bars. A compass attached to a wooden rod is here being used to orient the antenna adapter to north.

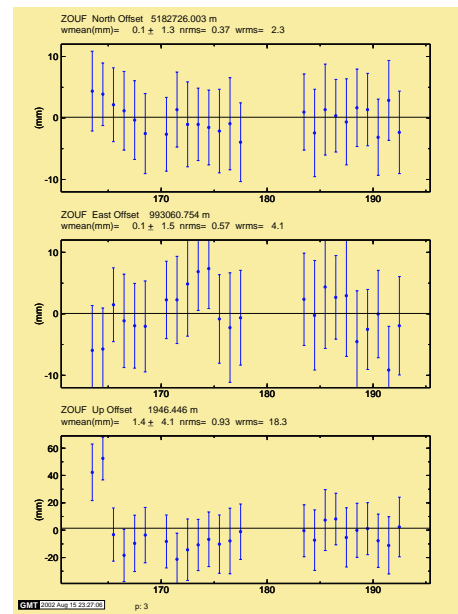


Figure 15.31: Preliminary position estimates of ZOUF relative to a European fixed reference frame defined by several IGS stations. Short-term repeatabilities are typical for unresolved phase ambiguity solutions.

## 13. Fluid Influenced Faulting in Long Valley Caldera

Dennise Templeton and Douglas Dreger

### 13.1 Introduction

The most recent episode of unrest in the Long Valley Caldera (LVC) manifested itself in 1997 as an increase in the rate of inflation of the resurgent dome and an increase in seismic activity in the south moat. Ground deformation in the LVC reached a peak in November 1997 and was accompanied by three M4 earthquakes with significant volumetric components, indicating that fluids were involved in the source process of these earthquakes (Dreger *et al.*, 2000). This project seeks to ascertain the extent of fluid influenced faulting triggered by the hydrothermal or magmatic system under LVC.

### 13.2 Moment Tensor Inversion

We inverted regional broadband data to compute deviatoric and full moment tensor (FMT) solutions for events greater than M4.0 since 1993. We solve for the FMT to determine the coseismic volume changes in the source region and compare it to the deviatoric solution which assumes no volume change. We performed a time domain inversion of complete three-component displacement seismograms. Seven stations were chosen within the Berkeley Digital Seismic Network (BDSN) that provided the best azimuthal coverage and data quality. Green's functions were computed using the SoCal velocity model which is appropriate for the eastern California and Sierra Nevada regions. Both the data and the Green's functions were bandpass filtered between 0.02 to 0.05 Hz using a causal Butterworth filter.

The F-test was used to determine if the improvement in fit between the deviatoric and FMT solutions is significant. The volumetric components of FMT solutions which exceed the 90% confidence level are taken to be statistically significant. To determine the stability of our solution, we use a Jackknife test to iterate over all possible subsets of data. Solutions from different station combinations can be compared to determine if solutions are stable or are influenced by path effects. The results from this test indicate that our solutions are stable for sub-station combinations of two or more.

In the original study of the 1997 swarm, four earthquakes were found to have significant volumetric components including one which had waveforms similar to nearby tectonic events. In this more detailed study, the volumetric component of that earthquake was determined not to be statistically significant. In addition to the three 1997 earthquakes that were previously discovered, two other events were found south of the caldera wall with statistically significant volumetric components

(Figure 15.32). These new events were not located near the 1997 events. Instead, they formed part of a 1998 earthquake swarm within the Sierra Nevada block. Interestingly, this sequence had hints of magmatic involvement that suggested some degree of magma or fluid movement (Hough *et al.*, 2000).

The majority of the events in the LVC area do not have significant isotropic components. Out of the 32 events studied with M4.0 or greater, only five earthquakes had a significant volumetric component in their source region. All of the five earthquakes occurred in areas which had evidence suggesting active magmatic activity.

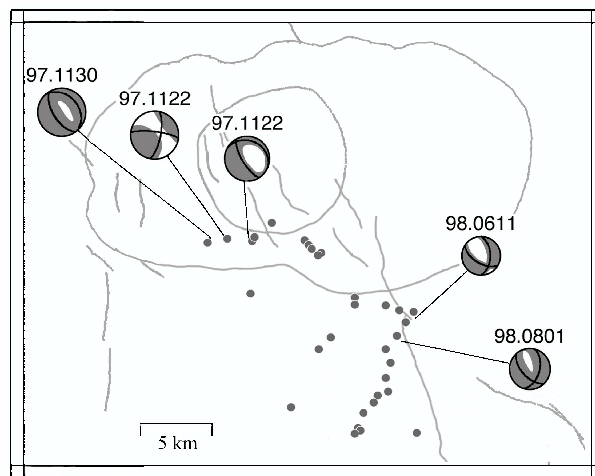


Figure 15.32: Map of LVC, the resurgent dome, and major faults. Seismicity above M4.0 is plotted as circles. FMT solutions are plotted for the five events with significant volumetric components. Event dates, in the form of YY.MMDD, are plotted above the solutions.

### 13.3 Acknowledgements

We appreciate support for this project by NSF through contract EAR-0087147.

### 13.4 References

- Dreger, D. S., H. Tkalčić, and M. Johnston, Dilational Processes Accompanying Earthquakes in the Long Valley Caldera, *Science*, 288, 122-125, 2000.
- Hough, S. E., R. S. Dollar, and P. Johnson, The 1998 Earthquake Sequence South of Long Valley Caldera, California: Hints of Magmatic Involvement, *Bull. Seism. Soc. Am.*, 90, 752-763, 2000.

# 14. Finite Fault Inversion of the September 25, 1999 ( $M_w=6.4$ ) Taiwan Earthquake

Wu-Cheng Chi and Douglas Dreger

## 14.1 Introduction

More than six  $M_w$  6 and greater aftershocks of the 1999, Chi-Chi, Taiwan earthquake ( $M_w=7.6$ ) were well-recorded. In this study we invert for the finite source rupture process for one of the largest aftershocks (23.86N, 121.01E) that occurred on 1999/9/25 at 23:52:49.5 UTC, 5 days after the mainshock. Through inversions we hope to discriminate the causative fault plane from the auxiliary plane. There are 3 scenarios for the ruptured plane: down-dip extension of the mainshock on the detachment, backthrust above the detachment, and a basement-involved fault below the detachment (Figure 15.33). Although the hypocenter is located in the vicinity of the proposed major shallow east-dipping fault, previous data could not exclude the possibility of a high-angle, west-dipping conjugate fault (backthrust). If true, a backthrust scenario will give us an important constraint on the deep crustal geometry under Taiwan. In addition, recent seismicity studies (e.g. *Carena et. al.*, EOS 82(47), p1176, 2001) show a steep, west-dipping fault below the detachment and the aftershock might have occurred on this fault, if the aftershock focal depth is actually deeper than reported. This scenario implies that large seismic strains can be stored in the footwall of the detachment and future geodynamic studies might need to consider a deformable footwall block that can generate  $M_w > 6$  earthquakes. If the rupture was on the proposed detachment, we can delineate its attitude and slip distribution, which can be compared to the mainshock.

## 14.2 Method and Results

We used strong motion data from the Central Weather Bureau of Taiwan (*Lee at al.*, 2001) to invert the representation theorem for finite source parameters by using the method of *Hartzell and Heaton* (1983). We used a linear least-squares inversion of observed velocity seismograms to compute the spatio-temporal slip distribution. To improve inversion stability, we have applied the following additional constraints: slip-positivity, Laplacian smoothing, and moment minimization. We have performed a grid-search over a range of focal parameters to find the optimal orientation using the variance reduction measure. In total, 1036 inversions were performed and we chose 5/30/100 (variance reduction 73 percent) as our preferred model.

## 14.3 Interpretation and Conclusion

One surprising outcome from this study is that the strike of our preferred focal mechanism (5) is different from that of teleseismic results (28). An initial teleseismic moment tensor inversion for the Chi-Chi mainshock also gave a strike of 26, compared with the strike of 5 derived from the mainshock surface rupture, thus this discrepancy could be systematic and relate to complex crustal velocity structures underneath Taiwan. The dip is 30 to the east.

The relatively large moment release from this aftershock indicates that its effects should be incorporated into the ongoing aftershock/afterslip studies. Our results might help recalibrate the coseismic/postseismic GPS data. Here we forward modeled the GPS displacements using our slip model in an elastic half space (c.f. *Okada*, 1992). For stations near the aftershock epicenter, most of the horizontal surface displacements are about 1/500 of the observed GPS data from the mainshock. The small displacements are due to the greater depth of this aftershock. However, the displacements can still be up to 3.3 cm at some GPS stations, and thus need to be taken into account in afterslip studies.

## 14.4 Acknowledgements

We thank Roland Burgmann and David Schmidt for their constructive discussions. This research is partially funded by NSF Grant EAR-0105998.

## 14.5 References

- Chi, Wu-Cheng, D. Dreger, and A. Kaverina, Finite-source modeling of the 1999 Taiwan (Chi-Chi) Earthquake derived from a dense strong-motion network, *Bull. Seism. Soc. Am.*, 91, 1144-1157, 2001.
- Hartzell, S.H., and T.H. Heaton, Inversion of strong ground motion and teleseismic waveform data for the fault rupture history of the 1979 Imperial Valley, California, Earthquake, *Bull. Seism. Soc. Am.*, 73, 1553-1583, 1983.
- Lee, W. H.K., T.C. Shin, K.W. Kuo, and K.C. Chen, CWB free-field strong-motion data from the 921 Chi-Chi Earthquake: Volume 1. digital acceleration files on CD-ROM, *pre-publication Version (December 6, 1999)*, *Seismology Center, CWB, Taipei, Taiwan*, 1999.
- Okada, Y., Internal deformation due to shear and tensile faults in a half-space, *Bull. Seism. Soc. Am.*, 82, 1018-1040, 1992.

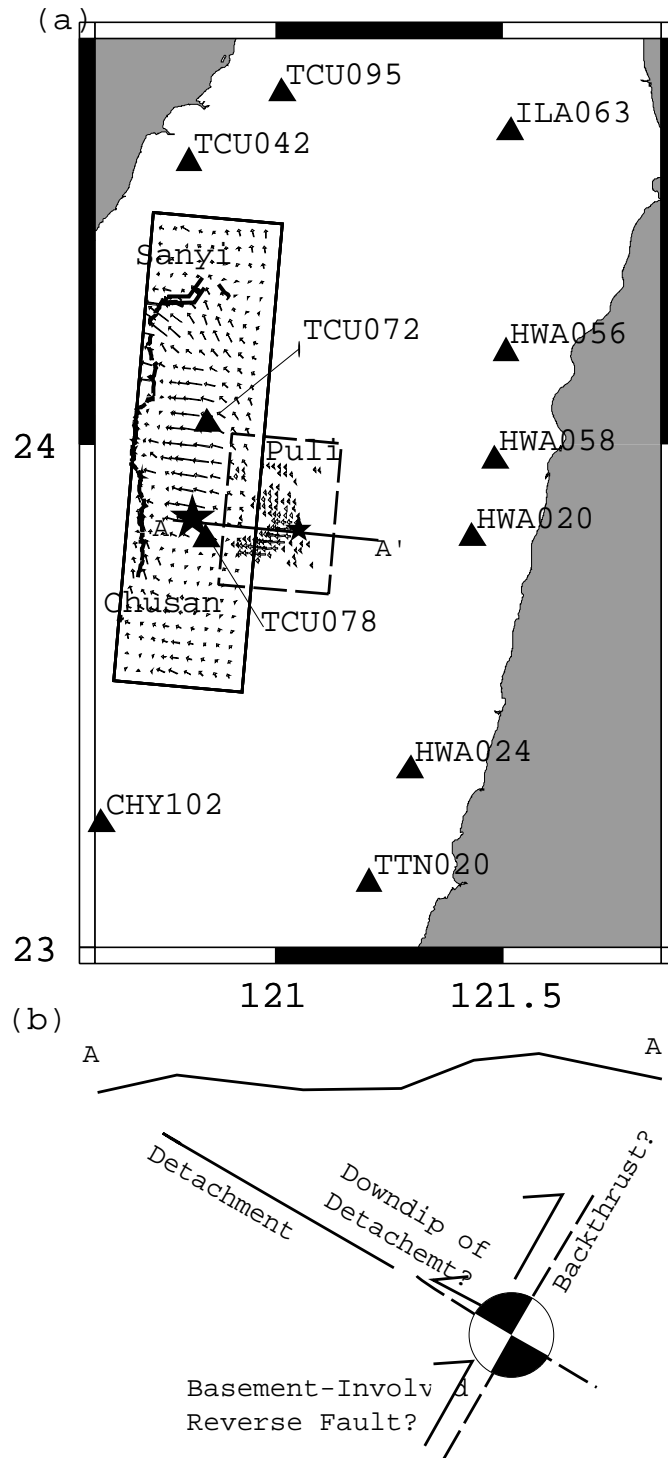


Figure 15.33: (a) Location map. The large star shows the epicenter of the Chi-Chi mainshock and its surface rupture is shown as the thick solid lines. The small star is the epicenter of the 9/25 event from this study. The 11 stations we used to invert the 9/25 event are plotted as triangles. The dense vectors show the 9/25 slip derived from this study. The maximum slip is 1.8 m. The sparse vectors show the mainshock model (*Chi et al.*, 2001), where the maximum slip is 10 m. (b) A schematic cross section along AA', showing 3 possible 9/25 rupture scenarios as discussed in the text.

## 15. Automated Moment Tensor Software for Monitoring the Comprehensive Test Ban Treaty

Margaret Hellweg, Douglas Dreger, Barbara Romanowicz, Jeffrey Stevens (SAIC)

### 15.1 Introduction

Seismology makes an important contribution toward monitoring compliance with the Comprehensive Test Ban Treaty (CTBT). One task at the testbed of the Center for Monitoring Research (CMR, Washington DC, USA) and the International Data Center (IDC) of the Comprehensive Test Ban Treaty Organization (CTBTO, Vienna, Austria) is the detection, location and characterization of seismic events in order to distinguish between possible nuclear tests and earthquakes or other natural sources of seismic signals. While this is not particularly difficult for large events, whether natural or man-made, small events present a greater challenge. Although their epicenters and magnitudes can be determined fairly precisely, seismic moment tensor analysis can help in two ways. It not only gives information about the size and mechanism of a source in terms of its seismic moment and the moment tensor components. It provides, in addition, an estimate of the source's depth, which cannot always be reliably determined using normal location techniques. Thus, a large non double-couple component ( $> 50\%$ ) may be an indication for a nuclear explosion, as compared to the typically more than 70-80% double couple for an earthquake (Dreger and Woods, 2002). The source depth determined from moment tensor analysis may also help to weed out tectonic events from among the more than 100000 events of magnitude 4 and greater that occur annually. Only events at shallow depths need be scrutinized by the monitoring process of the Comprehensive Test Ban Treaty (CTBT).

This project's goal is to implement the process for automatic determination of seismic moment tensors routinely used in real-time at the University of California at Berkeley (UCB, Romanowicz *et al.*, 1993; Dreger and Romanowicz, 1994; Pasyanos *et al.*, 1996) on the testbed at CMR. Although the moment tensor process will not be running in real-time on the testbed, in its final implementation it will run automatically, triggered from the Reviewed Event Bulletin (REB). Thus, it will be an additional, potentially powerful event screening procedure (Pechmann *et al.*, 1995; Dreger and Woods, 2002), providing estimates of: (1) the moment magnitude,  $M_w$ , a very accurate measure of event size; (2) the source depth, which will help distinguish natural events with typical depths greater than than 1 km from nuclear explosions and (3) radiation characteristics, such as deviations from the typically double-couple radiation of earthquakes.

### 15.2 Progress and Results

The automated procedure developed at UCB and implemented at CMR uses two methods for determining the moment tensor. One is a time domain, waveform fitting procedure that utilizes the complete, long-period recordings (CW, Dreger and Romanowicz, 1994; Pasyanos *et al.*, 1996; Fukuyama *et al.*, 1998; Fukuyama and Dreger, 2000). The other tensor method fits the surface waves in the frequency domain (SW). It is adapted from the two-step method of Romanowicz (1982).

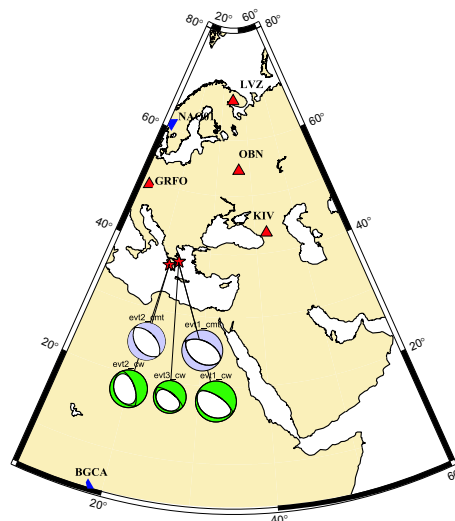


Figure 15.34: Moment tensors solutions (dark, colored) determined using the CW method for events in Greece (Mainshock (evt1): Sep. 07, 1999,  $M_w$  6.0; evt2  $M_w$  5.6 evt3  $M_w$  4.8). Inverted triangles denote IMS primary stations, while triangles are auxiliary stations. The light gray solutions for evt1 and evt2 are taken from the Harvard CMT catalog

During the past year, we have completed the installation of the moment tensor codes on the testbed at CMR. The software package now automatically extracts event information and waveform data from the database there, performs basic quality control and preprocesses the waveforms before running the two inversions to produce independent solutions. As testing has proceeded, we have improved the Greens functions produced for the CW method by applying a flattening algorithm to the radially symmetric velocity structures (Müller, 1973, Müller, 1977). We have also adapted the set of periods used for

the SW inversion from those used for the regional application in California to for application world-wide on intermediate-sized events.

We have applied the procedure to events shallower than 200 km with  $m_b > 5.4$  in a test dataset, the 90 day interval between from July 19, to October 17, 1999. For the event in Greece on September 7, we have investigated the use of data from auxiliary stations of the IMS network in addition to the primary stations. Figure 15.34 shows results for the mainshock ( $M_w$  6.0) as well as two aftershocks (evt2  $M_w$  5.6 and evt3  $M_w$  4.8). Clearly, the method is effective in this region, even for the small aftershock.

For events in the test dataset we have run inversions using two different velocity models. The maps in Figure 15.35 show the IMS stations used for the inversions, as well as the moment tensor solutions determined by the complete waveform inversion and the surface wave method, respectively. In both Figure 15.35 A and B, the solutions derived using two different velocity models are compared with the moment tensors given in the Harvard CMT and USGS catalogs.

While the match between catalog source mechanisms and those calculated using the two automated moment tensor methods is good for some events, for others the process is not so successful. One typical problem is that for this interval, data is not always available from many of the primary stations of the seismic network of the International Monitoring Systems (IMS), the data source for the automatic process. For the CW method, for example, the moment tensors derived for events east and northeast of Australia differ from those given by both the Harvard and USGS catalogs. However, for each of these events, data were only available from one primary station less than 5000 km from the epicenter, STKA. The solutions calculated by the CW method are consistent with the waveforms from this station. The dearth of data is apparent for the SW method in in Figure 15.35 B which shows solutions for only 13 of the 19 events shown in Figure 15.35 A.

### 15.3 Perspectives

Currently, we are directing our efforts toward three fronts. First, we will attempt to improve the automated procedure by incorporating data from additional stations. Since 1999, the primary stations of the IMS network have been improved, both in their equipment and in their reliability. In addition, many of the auxiliary stations of the IMS network satisfy the need for the broadband, high dynamic range data which is necessary for the methods to work well. We will factor in data from these stations to improve the solutions. Secondly, we are working to develop and apply quantitative comparisons of the moment tensor solutions from various sources, CW or SW methods, as well as Harvard CMT and USGS. Finally,

we are developing a regionalized calibration for the Far East. As part of an advanced concept demonstration, the CMR has collected event information and seismograms, as well as information about the Earth's structure in the region around Lop Nor. We will use this data to generate Greens functions and path information, so that we can calculate moment tensors for events, man-made or natural, occurring in this area.

### 15.4 Acknowledgements

This project is funded under the Defense Threat Reduction Agency contract DTRA01-00-C-0038.

### 15.5 References

- Dreger, D. and B. Romanowicz, Source characteristics of events in the San Francisco Bay Region, *USGS Open-file report, 94-176*, 301-309, 1994.
- Dreger D. and B. Woods, Regional Distance Seismic Moment Tensors of Nuclear Explosions, *Tectonophysics*, in press, 2002.
- Fukuyama, E., M. Ishida, D. Dreger, and H. Kawai, Automated seismic moment tensor determination by using on-line broadband seismic waveforms, *Jishin*, 51, 149-156, 1998.
- Fukuyama, E. and D. Dreger, Performance test of an automated moment tensor determination system, *Earth Planets Space*, 52, 383-392, 2000.
- Müller, G., Theoretical Body Wave Seismograms for Media with Spherical symmetry; Discussion and Comparison of Approximate Methods, *J. Geophysics*, 39, 229-246, 1973.
- Müller, G., Earth-Flattening Approximation for Body waves Derived from Geometric Ray Theory; Improvements, Corrections and Range of Applicability, *J. Geophysics*, 42, 429-436, 1977.
- Pasyanos, M., D. Dreger, and B. Romanowicz, Toward real-time estimation of regional moment tensors, *Bull. Seism. Soc. Am.*, 86, 1255-1269, 1996.
- Pechmann, J.C., W.R. Walter, S.J. Nava, and W.J. Arabasz, The February 3, 1995,  $M_L$  5.1 seismic event in the Trona mining district of southwestern Wyoming, *Seis. Res. Lett.*, 66, 25-34, 1995.
- Romanowicz, B., Moment tensor inversion of long period Rayleigh waves: a new approach, *J. Geophys. Res.*, 87, 5395-5407, 1982.
- Romanowicz, B., M. Pasyanos, D. Dreger, and R. Uhrhammer, Monitoring of strain release in central and northern California using broadband data, *Geophys. Res. Lett.*, 20, 1643-1646, 1993.

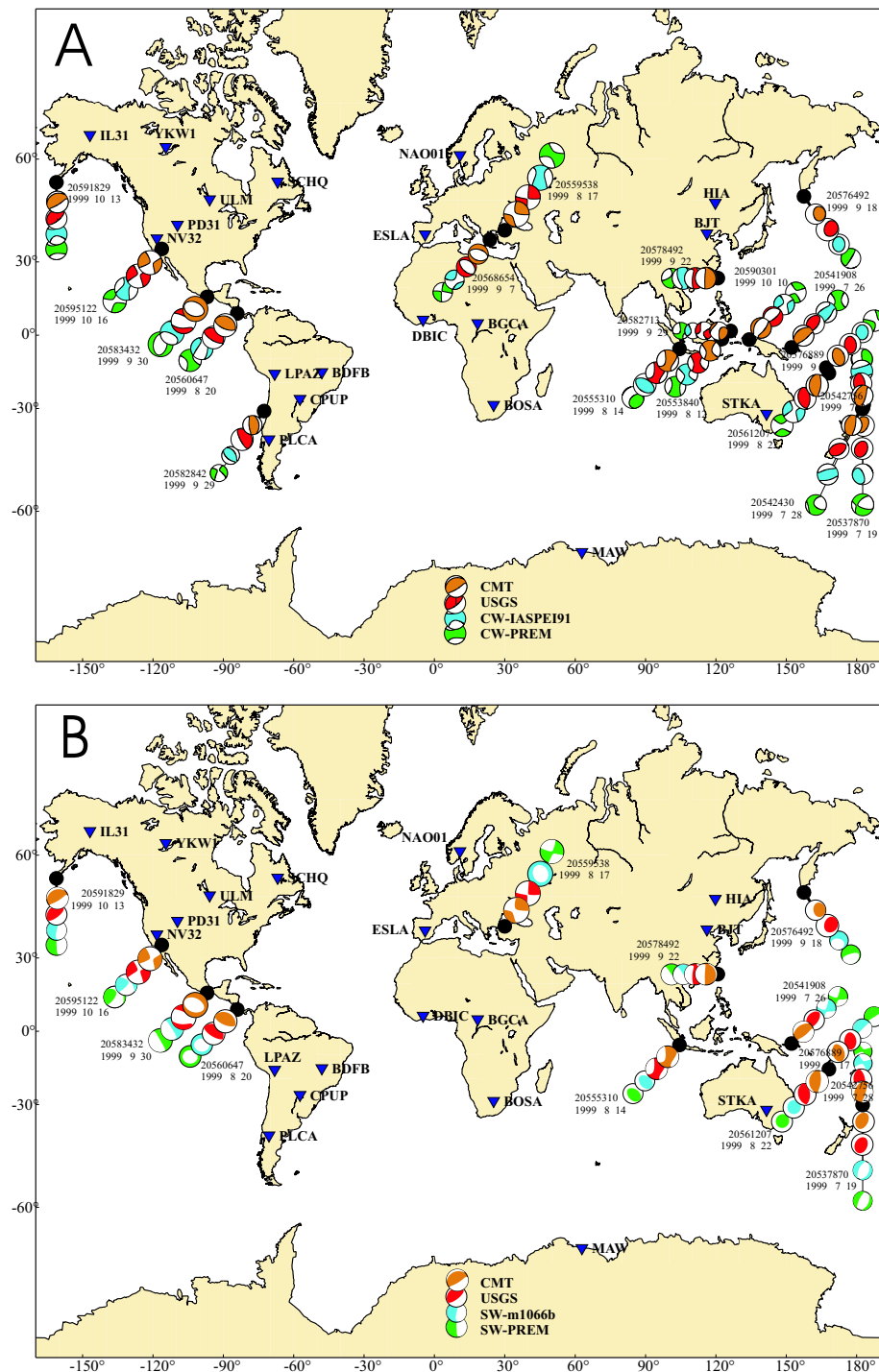
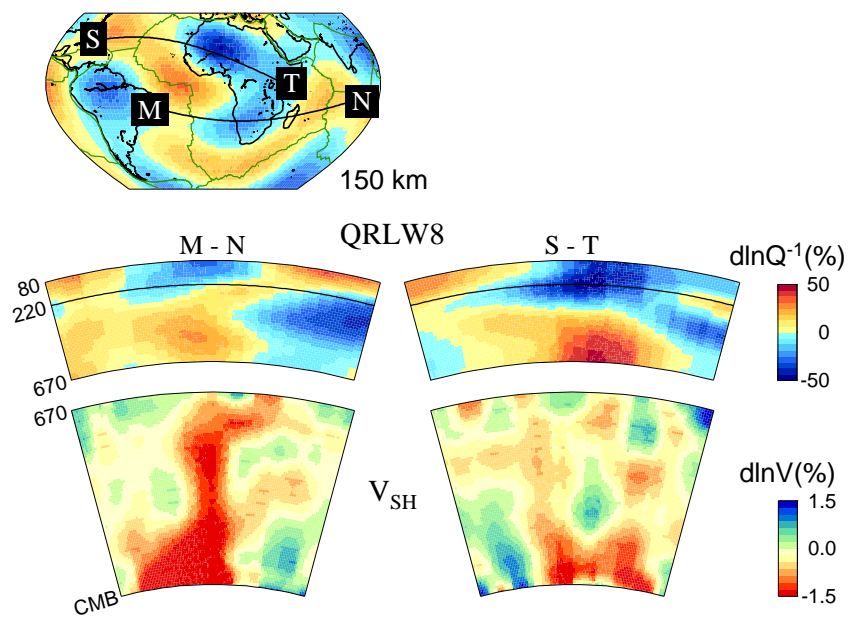


Figure 15.35: (A) Map showing stations (triangles) and inversion results for the complete waveform method. Taken in order from the event hypocenter (dot), focal mechanisms are from the Harvard CMT catalog, USGS catalog, CW method using iasp91 velocity model and CW method using PREM. (B) Map showing stations (triangles) and inversion results for the surface wave method. Taken in order from the event hypocenter (dot), focal mechanisms are from the Harvard CMT catalog, USGS catalog, SW method using m1066b velocity model and SW method using PREM.

# Chapter 16

## Regional and Global Structure Studies



# 1. Waveform Constrained Seismic Velocity Structure in Northern California

Junkee Rhie and Douglas S. Dreger

## 1.1 Introduction

1D and 2D shear wave velocity structure from Mammoth Lakes to Yreka is determined by SH waveform modeling and receiver-function analysis. Three local events are selected by considering epicentral distances from stations and the availability of reliable source parameters (e.g. Dreger *et al.*, 1995). The six teleseismic events are also selected by considering preferred back azimuth and S/N ratio (Figure 16.1). Regional broadband waveforms from the 21 September 1993 Klamath Falls ( $M_w$  6.0), the 15 May 1999 Mammoth Lakes ( $M_w$  6.0), and the 10 August 2001 Portola ( $M_w$  5.2) events were well recorded by 4 to 5 BDSN stations that are also located nearly on the same NNW line (Figure 16.1). This naturally aligned configuration of three local earthquakes and stations provides an excellent opportunity to determine a waveform constrained velocity model along the profile. Before performing the waveform modeling, a receiver function technique is applied to constrain the depth of major discontinuities, especially Moho, at each station. 1D and 2D models are estimated by forward modeling of the broadband waveforms and the receiver-functions.

## 1.2 Method

Receiver-function analysis is a very appropriate method to look at the discontinuities in the crust and upper-mantle. However, the velocity structure obtained from receiver-function analysis is not unique since receiver-functions, especially the radial components, are mostly sensitive to P to S velocity ratio rather than the absolute velocity at each depth (Ammon *et al.*, 1990). Three component broadband waveforms from regional events are relatively more sensitive to the absolute velocity at each depth. These complementary properties give us a chance to obtain more constrained velocity structure than those obtained by only one or the other of the two methods. Langston (1994) showed that regional broadband waveform modeling based on an initial 1D model obtained by teleseismic receiver function inversion is very promising for the determination of source parameters and to infer details of crustal and upper mantle structure. But he also mentioned that lateral heterogeneity in velocity structure is still an obstacle to overcome. The basic idea of this work is the same as his, but the final goal is to determine 2D or 3D model, which can include the effect of lateral heterogeneities. Many 1D models obtained by waveform modeling of receiver functions and regional broadband waveforms can be used as a basis for

more complex 2D and 3D models. The detailed process of waveform modeling scheme for 1D modeling is as follows; 1) The depth of major discontinuities, especially Moho, is constrained by receiver function inversion. 2) S-wave velocities in each layer are modified to fit the observed SH regional waveform. 3) P-wave velocity is obtained by perturbing P velocity to explain P-SV regional waveforms. 4) The P model can provide more constraint on the depths of major discontinuities identified by the receiver function analysis and then the above process is repeated to obtain a reliable 1D model, which can explain receiver function and regional waveforms simultaneously. The more complex 2D or 3D model will be estimated based on many 1D models.

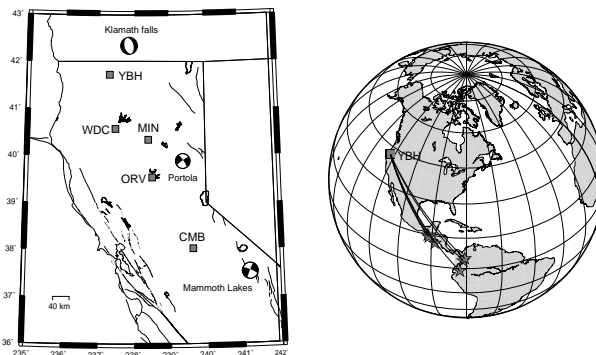


Figure 16.1: Location map of stations and events for regional (left) and teleseismic (right) cases. The regional events and broad band stations are located on the NNW line. The teleseismic events of which back azimuth from BDSN is similar to the trend of NNW line was selected for receiver function analysis

## 1.3 Discussion and Results

A preliminary 2D shear wave velocity model for NNW profile in northern California was estimated. Three 1D models for the S structure under YBH, ORV and CMB stations are interpolated to get the 2D result. Stacked waveforms from teleseismic events are used as input waveforms for receiver function calculation. Tangential component of regional waveforms recorded at the three BDSN stations are modeled by forward waveform modeling approach with fixed depths of major discontinuities that were obtained from receiver function inversion. The variance reductions of each waveform fit are all about

60 % or larger, even for frequencies up to 0.5 Hz (Figure 16.2). Although we did not give more constraint on depths of major discontinuities by P-SV waveform modeling, the obtained 1D models seem to be able to explain regional tangential waveforms well. However, this 1D model cannot explain receiver functions simultaneously (Figure 16.2). The preliminary 2D model based on an interpolation of given 1D models from waveform modeling cannot explain the waveforms which propagated along the NNW line. However, this model roughly shows the reasonable variation of the velocity structure along the NNW line; deeper Moho and higher velocity layer under Sierra Nevada and shallower Moho and lower velocity layer under Klamath Mountains (Figure 16.3). The further direction of this study will be to estimate 1D models which can explain waveform of regional events and receiver functions simultaneously. P-SV waveforms will be incorporated and the results of the 1D analyses will be used to construct a 2D model for the path. In addition, other source-receiver pairs and receiver functions with wide variety of back azimuth will be used to estimate 3D velocity structure model.

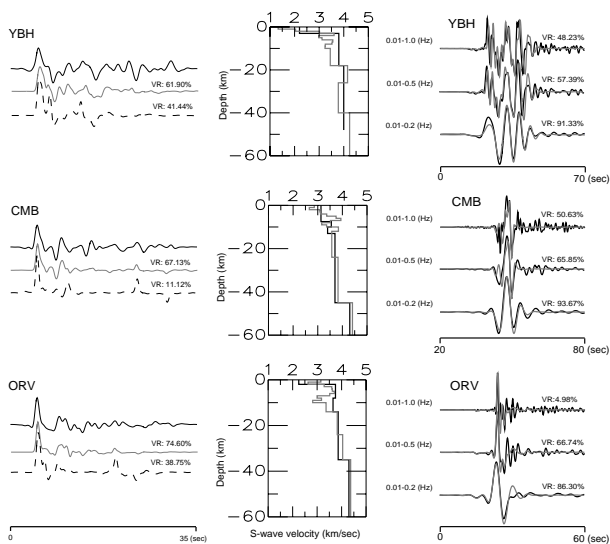


Figure 16.2: Preferred receiver function models (grey) and refined models (black). The refined models were obtained by forward waveform modeling. Left: Radial component receiver function based on receiver function model (grey) and refined model (dotted). Right: Comparison between observed (black) and synthetic tangential waveforms (grey) for refined model

### 1.4 Acknowledgements

We thank C. Ammon for letting us apply his RFTN software package to all receiver-function related calculations.

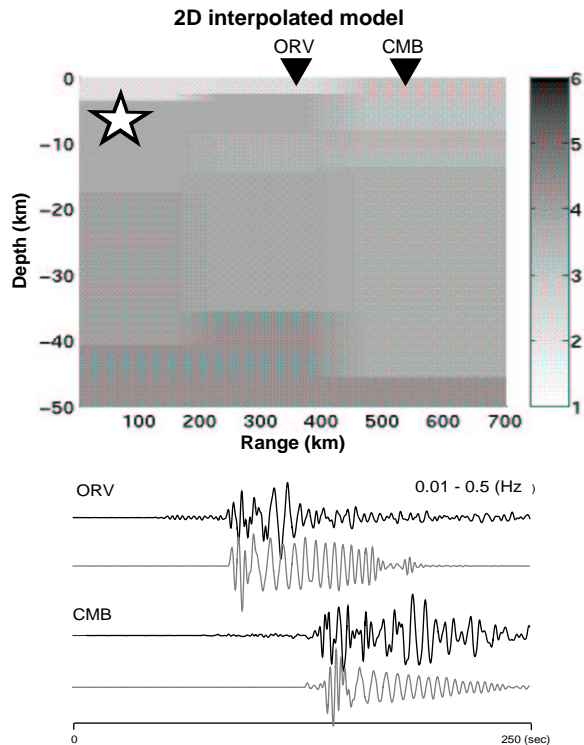


Figure 16.3: The preliminary 2D shear wave velocity model is constrained using three 1D models obtained from regional waveform modeling. Comparison between observed (black) and synthetic tangential waveforms (grey) for interpolated model

### 1.5 References

Ammon, C. J., G. E. Randall, and G. Zandt, On the non-uniqueness of receiver function inversions, *J. Geophys. Res.*, *95*, 15,303-15,318, 1990.  
 Dreger, D., J. Ritsema, and M. Pasyanos, Broadband analysis of the 21 September, 1993 Klamath Falls earthquake sequence, *Geophys. Res. Lett.*, *22*, 997-1000, 1995.  
 Langston, C., An integrated study of crustal structure and regional wave propagation for southeastern Missouri, *Bull. Seism. Soc. Am.*, *84*, 105-118, 1994.

## 2. Detection and Location of Potential Sources of Background Low Frequency Surface Wave Energy

Junkee Rhie and Barbara Romanowicz

### 2.1 Introduction

Earth's background free oscillations were reported recently by *Nawa et al.* (1998). They observed the excitation of the peaks of fundamental spheroidal modes on superconducting gravimeter data in the frequency range between 0.3 to 5 mHz even during periods of no significant earthquakes. Numerous observations and studies strongly suggest that this phenomenon is real and the coupling of the solid earth with the atmosphere/ocean system is likely involved in source mechanism (*Suda, et al.*, 1998; *Tanimoto et al.*, 1998; *Kobayashi and Nishida*, 1998; *Ekström*, 2001). However, the spatial distribution of the sources remains unknown. Previous studies use stacking of power spectral density and correlating multi-orbit surface waves but provide no spatial resolution of the sources. To locate the sources and better understand the source, an array-based method, a modification of the autogram method (*Ekström*, 2001), can be a useful tool.

### 2.2 Array-based method

There are two basic assumptions of an array-based method: one is that we can approximately map a long-period surface wave field recorded at given station onto any reference point with same back azimuth by introducing some parameters obtained from the spherically symmetric reference earth model (e.g. PREM). We also assume that the surface wave energy propagates as a plane wave if the source is far from the array (Figure 16.4).

We use vertical component recordings at BDSN array. Instrument response is removed and band-pass filter (100-500 sec) is applied. We first map the surface wave field at a given station onto a reference point which is inside the array. The mapping is performed by deconvolving transfer function  $T(\omega, \delta X)$ , which represents the propagation effects of surface wave between a given station and reference point. The second step is to break up the deconvolved records into successive time intervals with duration of 500 sec and lagged by 100 sec. The records in each time interval are divided into two subsets, "far" and "near" stations, with respect to the chosen back azimuth. We then stack the records in each subset and each time interval separately. The final step is to compare these two stacked records corresponding to "far" and "near" stations by calculating variance reduction. The above processes are repeated for all possible back azimuths. Final output of the given process is variance reduction as a function of time and back azimuth. Our preliminary results for several known teleseismic events

show that the lower threshold of detection can be down to  $M_w$  5.5. And we can get a rough estimate of back azimuth for the source and arrival time of surface wave energy. To locate the sources of the long period surface wave energy, we need other dense arrays, such as arrays in Japan and Germany. Three different estimates of back azimuths and absolute arrival times will better constrain the source location.

Scanning available records from the past 5 years to search for the sources of long period surface wave energy not related to known events is further direction of this work.

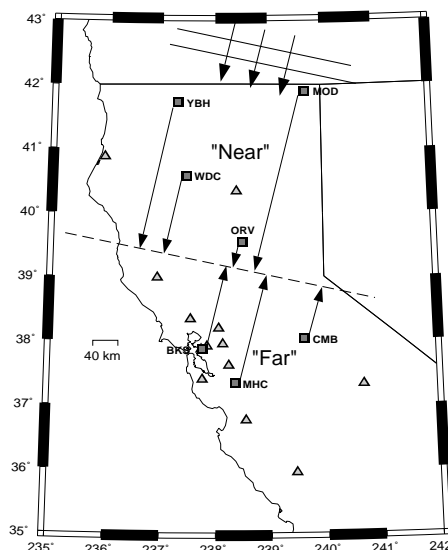


Figure 16.4: Map of northern California showing the incidence of a surface wave as a plane wave (solid lines and arrows) on BDSN. Squares: quietest BDSN stations. These were used in example plot, except MOD which was installed in 2001. Triangles: other BDSN stations. The broken line indicates the reference line onto which the waveforms are back (or forward) projected before stacking

### 2.3 Discussion

The current goal of this work is to estimate the spatial distribution of the sources of background free oscillations. As we mentioned before, our preliminary result shows that the detection limit of this method is at least  $M_w$  5.5 (Figure 16.5). This magnitude is less than the doc-

umented level of equivalent magnitudes of excitation of background free oscillation, which are 6.0 or 5.75 based on different approaches (Tanimoto and Um, 1999; Ekström, 2001). It implies that we can detect the long period surface wave energy when only one localized source produces equivalent moment. However, it is also possi-

mal stacking scheme and grouping of stations, as well as the choice of traces. Even if we cannot locate the source associated with background free oscillations due to very broad distribution of sources in time and space (Nishida and Kobayashi, 1999), this methodology will still be useful in searching for the silent/slow earthquakes or automatic identification and preliminary location of teleseismic events using a small number of local arrays.

## 2.4 References

Ekström, G., Time domain analysis of Earth's long-period background seismic radiation, *J. Geophys. Res.*, *106*, 26483-26493, 2001.

Kobayashi, N., and K. Nishida, Continuous excitation of planetary free oscillations by atmospheric disturbances, *Nature*, *395*, 357-360, 1998.

Nawa, K., N. Suda, Y. Fukao, T. Sato, Y. Aoyama, and K. Shibuya, Incessant excitation of the Earth's free oscillations, *Earth Planets Space*, *50*, 3-8, 1998.

Nishida, K. and N. Kobayashi, Statistical features of Earth's continuous free oscillations, *J. Geophys. Res.*, *104*, 28741-28750, 1999.

Suda, N., K. Nawa, and Y. Fukao, Earth's background free oscillations, *Science*, *279*, 2089-2091, 1998.

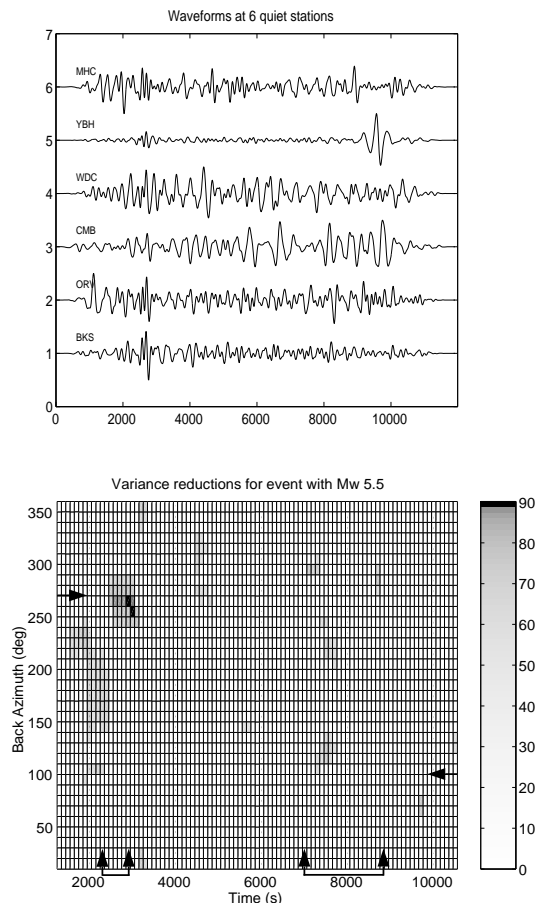


Figure 16.5: Examples of analysis for an event of  $M_w$  5.5 in new Ireland region (10/12/1999), depth = 15km, distance = 89.5 deg, backazimuth = 265.5 deg). Top: waveforms at 6 quiet stations, bandpass filtered between 100 and 500 sec. Time starts from origin time of the event. Bottom: detection result: maximum variance reduction (scale shown on the right) corresponds to the arrival of R1. Arrows indicate expected back azimuths and arrival intervals for R1 and R2 corresponding to group velocities between 4.3 and 3.4 km/s. Station YBH exhibits a glitch around 9000 sec. For this smaller magnitude event, and the period range considered, only R1 is clearly detected

ble that the previous estimates of equivalent moments are due to numerous localized or broadly distributed sources. In this case, we need a more robust method. We are trying to optimize the method to increase the detection limit by fine tuning optimal duration of interval, opti-

### 3. Global Anisotropy beneath Continental Roots

Yuancheng Gung, Mark Panning and Barbara Romanowicz

#### 3.1 Introduction

The spatial distribution of seismic velocity revealed by global tomography has been a powerful tool in understanding the internal structure of the Earth. In the uppermost mantle, the higher than average velocity under continents is commonly interpreted as the signature of continental roots, as they are presumably colder than their surrounding. In general, the extension of this signature in depth correlates to the lithospheric thickness. However, this seismically defined thickness of continental roots shows diverse features among the recent global tomographic models. Unlike the well documented anisotropic feature under Centre Pacific (e.g. *Montagner and Tanimoto, 1991; Ekström and Dziewonski, 1998*), these dissimilar features below lithospheric depth are less explored, and are generally accepted as a result of various data coverage and different methodology.

Here we present results from a global tomographic model derived by using joint anisotropic inversion of  $V_{SV}$  and  $V_{SH}$ . Our results demonstrate that these diverse characteristics can be explained by the ubiquitous existence of transverse anisotropy beneath major continental shields.

#### 3.2 Methodology

Separate isotropic inversion of Love and Rayleigh waves is a convenient approach to measure the anisotropy in the uppermost mantle based on the fact that the fundamental modes of Love/Rayleigh waves are mainly sensitive to  $V_{SH}/V_{SV}$ . However, the condition is not generally true for overtone phases (Figure 16.6), and it limits the resolution of the anisotropic features derived from the pseudo-isotropic inversion (e.g. *Regan and Anderson, 1984*).

In this study, we implement a joint inversion on three component seismic waveform data. The sensitivity kernels of  $V_{SV}$ ,  $V_{SH}$ ,  $\eta$ ,  $V_{P_{iso}}$  (isotropic  $V_P$ ),  $\phi$ , and  $\rho$  are calculated based on the assumption of weak transverse anisotropy. Starting from our most recent tomographic models, SAW24B16 (*Mégnin and Romanowicz, 2001*) for  $V_{SH}$  and SAW16BV (*Gung and Romanowicz, 2002; Romanowicz and Gung, 2002*) for  $V_{SV}$ , we invert for  $V_{SH}$  and  $V_{SV}$  up to degree 16. The scaling relations among anisotropic parameters  $\phi$ ,  $\xi$  and  $\eta$  based on *Montagner and Anderson (1989)* are applied. This allows us to incorporate the effects of  $V_{SV}$  on Love waves,  $V_{SH}$  on Rayleigh waves and the effects of  $P$  anisotropy. Since  $SV$  component data have less sensitivity in the lowermost mantle than  $SH$  component data, to avoid the bias from

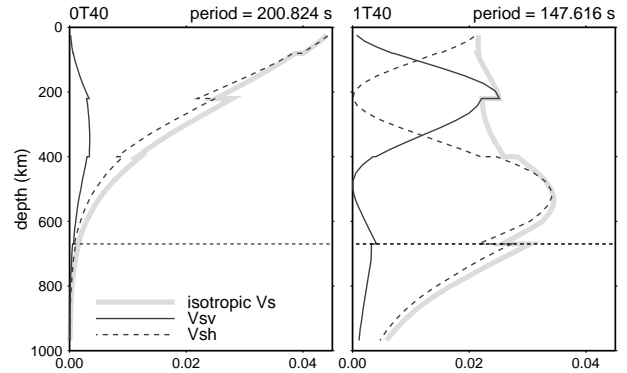


Figure 16.6: Sensitivity kernels of isotropic  $V_S$  and anisotropic  $V_{SV}$  and  $V_{SH}$  for fundamental mode  ${}_0T_{40}$  and overtone  ${}_1T_{40}$ .

anisotropic features from the deep mantle, we have restricted our inversion to the top 1500km of the mantle in this study.

#### 3.3 Data

Three component waveform data composed of surface waves ( $\approx 85,000$  wavepackets) and body waves ( $\approx 60,000$  wavepackets) are used in this study. In addition to fundamental surface waves, we also include overtone phases, which greatly enhance the resolution in the upper mantle transition zone.

#### 3.4 Preliminary results and discussion

Figure 16.7 shows our preliminary results of depths 175km and 250km. It is observed that the major features in  $V_{SV}$  and  $V_{SH}$  from the separate inversions are preserved in this depth range. Probably because it is mainly constrained by fundamental surface waves.

At the depth of 175km, the Pacific region shows similar anisotropic features as previous studies (e.g. *Montagner and Tanimoto, 1991; Ekström and Dziewonski, 1998*) most areas at this depth are characterized by  $V_{SH} > V_{SV}$ . There are two prominent exceptions in our model: East Pacific Rise and regions around Hawaii islands, where we observe strong signal of  $V_{SV} > V_{SH}$ , presumably due to vertical flow.

The anisotropy under oceanic regions at larger depth (250km) becomes weaker, and the contrast between  $V_{SV}$  and  $V_{SH}$  is highlighted in the continental regions. We observe that most continental shields are characterized by  $V_{SH} > V_{SV}$ , such as Canadian shield, Siberia platform,

Baltic shields, West Africa, Amazonian and Australian craton.

We propose that this anisotropy, characterized by  $V_{SH} > V_{SV}$ , is due to asthenospheric horizontal flow underneath the continental lithosphere. Similar to what happens under the Pacific plate, albeit at shallower depth (because the lithosphere is thinner). We also propose that this strong anisotropy under continents marks the Lehmann discontinuity, and the anisotropy under oceanic plates marks the G discontinuity. This explains the geographic preferential detections of these two discontinuities. (Gu, Dziewonski and Ekström, 2001; Revenaugh J. and T. H. Jordan, 1996)

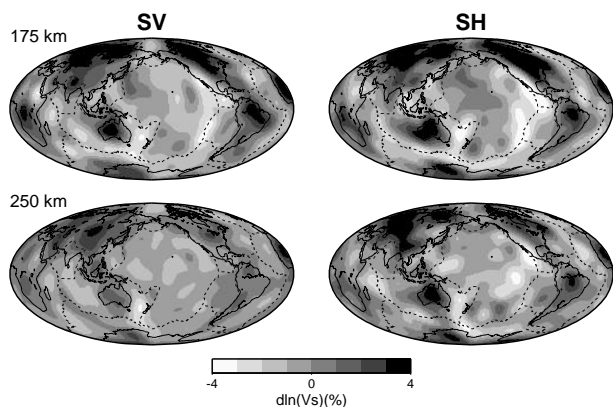


Figure 16.7: Lateral variations in  $V_{SV}$  and  $V_{SH}$  at the depth 175km and 250km.

### 3.5 Acknowledgements

We thank the National Science Foundation for support of this research.

### 3.6 References

Ekström, G. and A. M. Dziewonski, The unique anisotropy of the Pacific upper mantle, *Nature*, 394, 168-171, 1998.

Gu, Yu. J., Dziewonski Adam, and Ekström G., Preferential detection of Lehmann discontinuity beneath continents, *Geophys. Res. Lett.* 28, 4655-4658, 2001

Gung, Y., and B. Romanowicz,  $Q$  tomography of the upper mantle using three component long period waveforms, submitted to *Geophys. J. Res.*, 2002

Li, X.D. and B. Romanowicz, Global mantle shear-velocity model developed using nonlinear asymptotic coupling theory, *Geophys. J. R. Astr. Soc.*, 101, 22,245-22,272, 1996.

Mégnin, C., and B. Romanowicz, The 3-D shear velocity structure of the mantle from the inversion of body, surface, and higher mode waveforms, *Geophys. J. Inter.*, 143 709-728, 2001.

Montagner J. P. and Don L. Anderson, Petrological constraints on seismic anisotropy, *Phys. Earth and Plan. Int.*, 54, 82-105, 1989.

Montagner J. P. and T. Tanimoto, Global upper mantle tomography of seismic velocities and anisotropies, *Geophys. J. Res.* 96,, 20,337-20,351, 1991.

Regan, Janice and Don L. Anderson, Anisotropic model of the upper mantle, *Phys. Earth and Plan. Int.*, 35, 227-263, 1984.

Revenaugh J. and T. H. Jordan, Mantle layering from  $ScS$  reverberations 3. the upper mantle *Geophys. J. Res.* 96,, 19,781-19,810, 1991.

Romanowicz, B., and Y. Gung, Superplumes from the core-mantle boundary to the lithosphere: implications for heat flux, *Science*, 296, 513-516, 2002.

## 4. Superplumes from the core-mantle boundary to the base of the lithosphere: evidence from Q tomography

Yuancheng Gung and Barbara Romanowicz

### 4.1 Introduction

Global seismic tomography aims at improving our understanding of mantle dynamics by providing constraints on three-dimensional (3D) temperature and composition, using elastic velocities as proxies. Much progress has been made in recent years in resolving increasingly finer details in the 3D distribution of elastic velocities from the inversion of seismic phase and travel time data. However, the detailed morphology and role of upwellings, as manifested by two prominent zones of lower than average velocity, commonly referred to as superplumes, in the lowermost mantle, is not yet clear. Their location, under the south-central Pacific and under Africa, correlates with the global distribution of hotspots, as well as two major geoid highs. Recent tomographic S wave velocity models suggest that the superplumes rise high above the core-mantle boundary (CMB) *Mégnin and Romanowicz, 2000; Ritsema et al., 1999*, and joint seismic/geodynamic studies imply that they may be active upwellings (*Forte and Mitrovica, 2001*). However, finer scale resolution is still lacking.

To obtain additional constraints on hotter than average features, we consider amplitudes of seismic waves, which are sensitive to 3D anelastic structure. Owing to the exponential dependence on temperature of attenuation, which we shall express in terms of  $Q^{-1}$ , where  $Q$  is the quality factor, we expect anelastic tomography to highlight hotter than average regions better than standard elastic tomographic approaches.

### 4.2 Data and Inversion results

We have developed a waveform tomographic inversion method, originally aimed at constructing global 3D elastic models of the whole mantle (*Li and Romanowicz, 1996*), which now has been extended to iteratively solve for elastic and anelastic structure in the upper mantle, using three-component waveform data of fundamental and higher mode surface waves (*Gung and Romanowicz, 2002*). While we do not directly account for elastic effects in the amplitudes, strict data selection criteria are designed to reject data most strongly contaminated by focusing. The first step (elastic inversion) allows us to align the phases in our waveforms, and we do so separately for SV sensitive (vertical and longitudinal S wave component) and SH sensitive (transverse S wave component) data, to account for anisotropy in the uppermost mantle. In the second step, the  $Q^{-1}$  model, *QRLW8*, is derived using all three component data.

In the top 250 km of the mantle, correlation of high Q regions with shields is seen systematically in North and South America, Eurasia, Australia and Antarctica, whereas mid-ocean ridges in the Pacific, Atlantic and Indian Ocean exhibit generally low Q values, as do western Pacific back-arc regions (Figure 16.8). This is similar to what is observed in elastic velocity models, with regions of high/low velocity correlated with regions of high/low Q. A notable exception is an elongated zone of high attenuation in the central Pacific, extending from south of the equator to Hawaii, not seen in *SH* velocity models at these depths. Below 250 km, this tectonics-related Q distribution is gradually replaced by a simpler pattern, with two strong attenuation maxima centered in the southern Pacific and under Africa, throughout the upper mantle transition-zone. At depths greater than 400 km, a majority of hotspots are located above regions of high attenuation.

In model *QRLW8*, the high attenuation regions in the transition zone coincide in location with the minima in elastic velocity associated with the two superplumes in the lowermost mantle. Correlation between Q in the transition zone and velocity in the last 500 km of the mantle is particularly strong at degree 2 (Figure 16.9), but persist at shorter wavelengths. Cross-sections in the Pacific and under Africa (Figure 16.10) comparing upper mantle  $Q^{-1}$  with lower mantle velocity distributions, emphasize the vertical correspondence of the lowermost mantle superplumes with transition zone low Q zones. Because our  $Q^{-1}$  model does not extend to the lower mantle, and the low velocity zones are only expressed faintly in the upper half of the lower mantle, where they appear to be narrower and have a contorted shape, it is not possible to determine whether the superplumes are simply continuous across the 670 km discontinuity, or whether they induce rising hot currents in the upper mantle through thermal coupling processes. However, our results show that the superplumes must carry enough energy across the lower mantle to create coherent upwelling flow in the upper mantle transition zone, in agreement with mantle flow models. In contrast, ridges are shallow high attenuation features, mostly confined to the upper 200 km of the mantle.

The low Q zones in the transition zone connect with shallower ones whose positions are shifted horizontally, suggesting that the upwelling, plume related flow is deflected horizontally below the cold lithosphere, towards the Indian and Atlantic mid-ocean ridges under Africa,

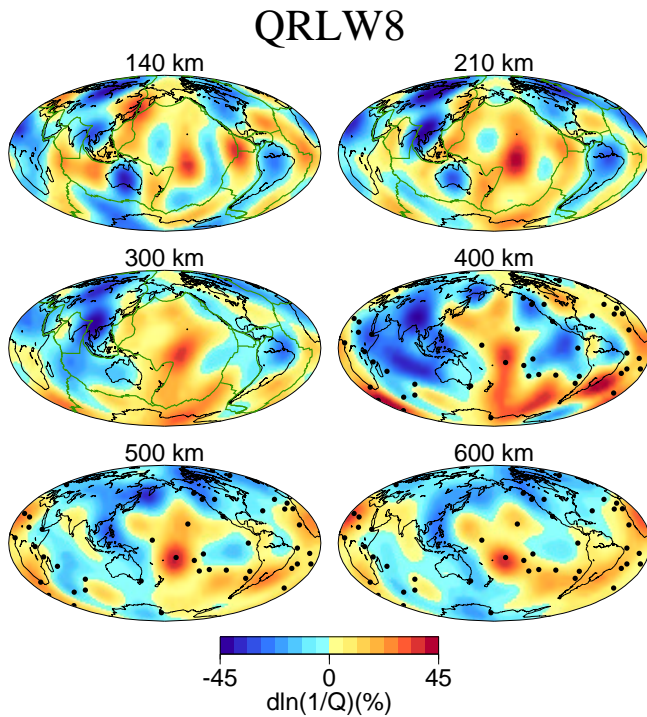


Figure 16.8: Images of model QRLW8 at six different depths. The lateral variations are expressed in terms of relative variations in  $1/Q$  with respect to QL6: red and blue indicates regions of high and low attenuation, respectively. The distribution of hotspots is also shown, indicating its correlation with low  $Q$

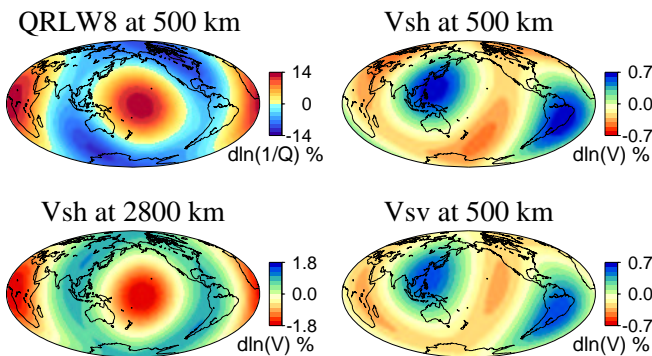


Figure 16.9: Comparison of the degree 2 distribution in  $Q$  in the upper mantle transition zone (depth of 500 km), for model QRLW8, with the corresponding distribution in  $SH$  and  $SV$  velocity as well as  $SH$  velocity at 2600 km in model SAW24B16

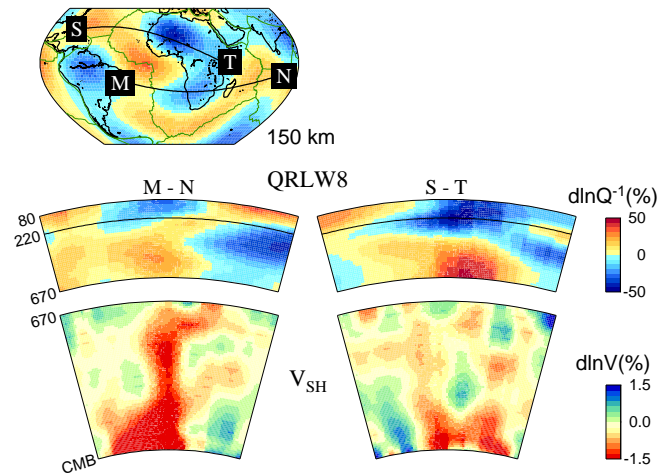


Figure 16.10: Depth cross-sections under Africa along profiles indicated in the top panel showing, for each profile (top to bottom),  $Q$  distribution in the upper mantle (to degree 8), and  $V_{SH}$  distribution in the lower mantle (to degree 24).

and in the Pacific, towards the East Pacific rise and the center of the Pacific plate. In the latter case, the flow is impeded on the west side by the presence of the Fiji-Tonga subduction zone. This deflection occurs at greater depths under the thicker continental lithosphere ( $\sim 350\text{km}$ , Fig. 3 b) than under the oceanic one ( $\sim 200\text{km}$ , Fig. 3a).

### 4.3 Acknowledgements

We thank the National Science Foundation for support of this research.

### 4.4 References

- Forte, A. M. and J. X. Mitrovica, *Nature*, **410**, 1049 (2001)
- Gung, Y.C. and B. Romanowicz,  $Q$  tomography of the upper mantle using three component long period waveforms, submitted to *J. Geophys. Res.*
- Li, X.D. and B. Romanowicz, Global mantle shear velocity model developed using nonlinear asymptotic coupling theory, *J. Geophys. Res.* **101** 22,245 (1996).
- Mégnin, C., and B. Romanowicz, The 3-D shear velocity structure of the mantle from the inversion of body, surface, and higher mode waveforms, *Geophys. J. Inter.*, **143** 709-728, 2001
- Ritsema, J. , H. van Heijst and J. Woodhouse, Complex shear wave velocity structure imaged beneath Africa and Iceland, *Science* **286**, 1925-1928, 1999.
- Romanowicz, B. and Y. C. Gung, Superplumes from the core-mantle boundary to the base of the lithosphere, *Science*, **296**, 513-516, 2002.

## 5. Progress in modeling deep mantle isotropic shear and compressional velocity structure using waveform inversion

Mark Panning and Barbara Romanowicz

### 5.1 Introduction

Seismic tomography is an important tool for determining the structure and dynamics of the Earth's mantle. It is a technique which utilizes geophysical inverse theory to use large amounts of seismic data (both travel times and waveforms) to model the elastic structure of the Earth. With the use of nonlinear asymptotic mode coupling theory (NACT) (*Li and Romanowicz, 1996*) and three component body and surface waveform data, we are able to model 3D isotropic shear and compressional velocity structure throughout the mantle.

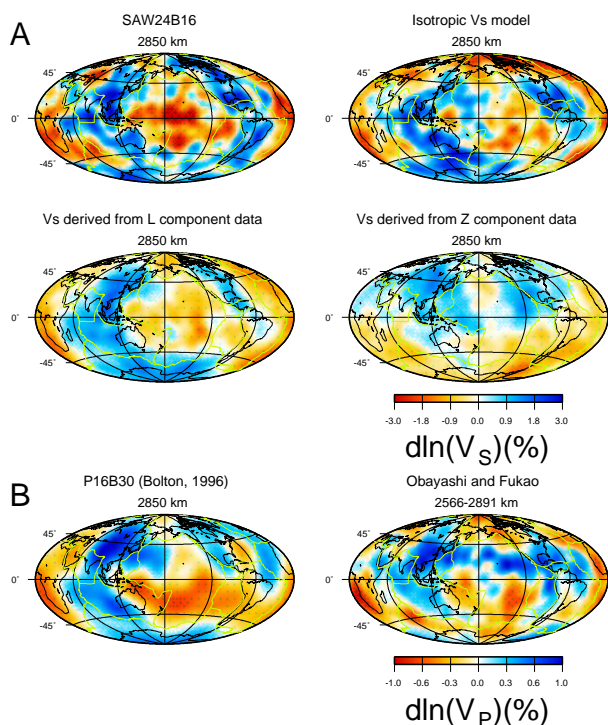


Figure 16.11: (A) Comparison of SAW24B16 and the isotropic S velocity model in the core-mantle boundary region. Inversions are also shown for only the L component data and only the Z component data. (B) P velocity models P16B30 (*Bolton, 1996*) and WEPP2 (*Fukao et al., 2001*) are shown for comparison.

While simultaneous models of shear and compressional velocity (or alternatively shear and bulk sound velocity) with P sensitivity based primarily on travel times (i.e. *Masters et al., 1999*) have been developed, very little

work has been done to explore  $V_P$  modeling using waveforms due to the higher dominant frequency of  $V_P$  data.

### 5.2 Degree 24 Isotropic S Velocity Model

We inverted 3 component body and surface wavepackets for mantle S velocity. We used SAW24B16 (*Mégnin and Romanowicz, 2000*), an SH velocity model based only on T component data, as a starting point. However, since our new model uses all three components of data, it is a model of isotropic  $V_S$  perturbations. The model obtained has similar T component variance reduction to SAW24B16, while performing significantly better for L and Z component data. Features in the uppermost mantle are what we would expect due to SV/SH anisotropy observed in other upper mantle models (e.g. *Ekström and Dziewonski, 1998; Montagner and Tanimoto, 1991*). An interesting difference can be seen between the two models in the western Pacific in the core-mantle boundary region (figure 16.11). The isotropic model has a pronounced fast anomaly in this area, while it is slow in the SH model. Resolution tests indicate this feature to be robust. Since this model differs from the SH model by including L and Z component data, we inverted only the latter datasets to see where the signal originates. While L component data produces a model similar to the SH model, the model from Z component data is quite different. Since most S sensitivity in the core-mantle boundary region is from vertically arriving phases such as SKS and Sdiff, which will primarily show up on the L component, this provides a hint that the signal may originate from  $V_P$  energy. This enters our model through an assumed  $d(\ln V_S)/d(\ln V_P)$  scaling relationship. Figure 16.11 also shows two  $V_P$  mantle models. While the models differ, both show a fast anomaly in the western Pacific.

### 5.3 Waveform Inversion for P Velocity Structure

Due to the apparent  $V_P$  contamination in the isotropic  $V_S$  model, we tested whether we could perform a direct waveform inversion for  $V_P$  structure. Coverage tests indicate that there is some coverage throughout the mantle, although significantly less than  $V_S$  sensitivity. For the inversion, the S velocity was fixed to that of SAW24B16 truncated to degree 12, and the P velocity was perturbed from the PREM velocities. The degree 8  $V_P$  model in figure 16.12 gives a variance reduction of 45% compared to 39% for truncated SAW24B16 with no P model. For long wavelengths, it is quite similar to P16B30 (*Bolton,*

1996), indicating the method has potential. With a more

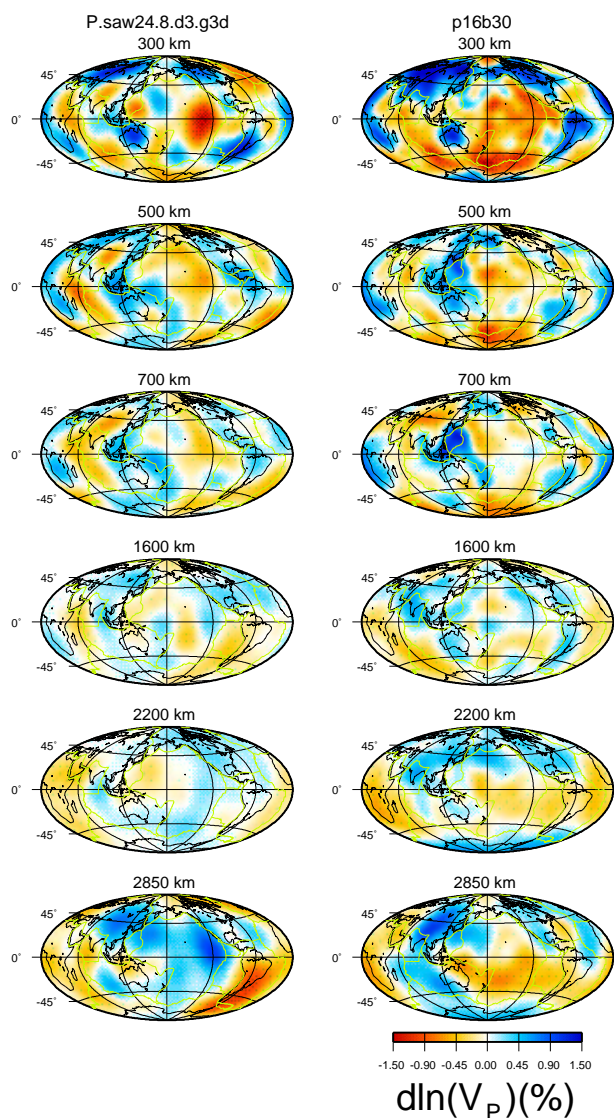


Figure 16.12: Comparison of P velocity models up to degree 8 for this study (left) and P16B30 (right).

optimal dataset (with periods shorter than 32s cutoff here and wavepackets better defined for P phases), a waveform inversion for  $V_P$  mantle structure appears to be feasible.

## 5.4 Conclusions

The degree 24 isotropic  $V_S$  model differs from SAW24B16 in several areas of the mantle. While these changes can be due to SV/SH anisotropy or other causes, the differences in the models in the core-mantle boundary region appear to be caused by  $V_P$  signal, indicating a potential breakdown in  $d(\ln V_S)/d(\ln V_P)$  scaling relationships. Although more data coverage is needed, preliminary tests indicate modeling  $V_P$  structure using

waveform inversion is possible.

## 5.5 Acknowledgements

We thank the National Science Foundation for support of this research.

## 5.6 References

- Bolton, H., Long period travel times and the structure of the mantle. Ph.D. Thesis, La Jolla, 204 pages, 1996.
- Ekström, G. and A.M. Dziewonski, The unique anisotropy of the Pacific upper mantle, *Nature*, 394, 168-172, 1998.
- Fukao, Y., S. Widiyantoro and M. Obayashi, Stagnant slabs in the upper and lower mantle transition region, *Rev. of Geophys.*, 2001.
- Li, X.D., and B. Romanowicz, Global shear velocity model developed using nonlinear asymptotic coupling theory, *Jour. Geophys. Res.*, 101, 22,245-22,272, 1996.
- Masters, G., H. Bolton, and G. Laske, Joint seismic tomography for P and S velocities: How pervasive are chemical anomalies in the mantle? *EOS Trans. AGU*, 80 S14, 1999.
- Mégnin, C., and B. Romanowicz, The 3D shear velocity of the mantle from the inversion of body, surface, and higher mode waveforms, *Geophys. Jour. Intl.*, 143, 709-728, 2000.
- Montagner, J.P., and T. Tanimoto, Global anisotropy in the upper mantle inferred from the regionalization of phase velocities. *Jour. Geophys. Res.*, 95, 4797-4819, 1990.

# 6. Investigating Mantle’s density resolution using the Neighborhood Algorithm

Sébastien Rousset and Barbara Romanowicz

## 6.1 Introduction

Unlike travel times or waveform data, normal mode data are directly sensitive to density. However, the sensitivity kernels for density are much smaller than those for velocities, so the controversy about the possibility of resolution of the mantle’s density is still vivid, especially since the publication of model SPRD6 (*Ishii and Tromp, 1999*). Several authors (*Resovsky and Ritzwoller, 1999, Romanowicz, 2001, Kuo and Romanowicz, 2002*) objected that density cannot yet be constrained and the controversy is still going.

However the inversion processes used by previous studies all rely on least-square inversions and require the use of a starting model, the choice of which is critical for the reliability of the results. Unlike this simple inversion scheme whose result is one "best" model, stochastic methods sample the parameter space, and their result is a set of models whose statistical properties reflect the likelihood function. In this study, in order to investigate the resolution, we use the Neighbourhood Algorithm (*Sambridge 1999a,b*) which uses forward modeling to sample the parameter space preferentially where the fit is better. A second part of the algorithm can use this sampling set to retrieve quantitative information on the distribution of models.

## 6.2 Dataset and Model Parameterization

### Theoretical background and dataset

We use a 2 steps inversion, as was done by *Ishii and Tromp* ; this method is simpler, but the coefficients measured may not correspond to a unique Earth model. Some studies (*Kuo and Romanowicz, 2002*) prefer a 1-step inversion, but this method is not practicable with the neighbourhood algorithm since the forward modeling of synthetic seismograms for each model would require too much computation.

During the first step, splitting coefficients (*Giardini and al., 1988*) of normal mode were obtained by non-linear inversion. Our dataset consist in splitting coefficients of 63 modes (*He and Tromp, 1996* and *Resovsky and Ritwoller, 1998*), corrected for the crust contribution and the effects of rotation. We have excluded a few modes for which 2 measurements were available but incompatible.

These coefficients are linearly related to the aspherical structure of the Earth considered as a perturbation  $\delta x$  of the elastic parameter  $x$  of our reference model PREM,

integrated over depth :

$$C_{st} = \int_0^a \left(\frac{\delta x}{x}\right)_{st}(z) K_s^x(z).dz \quad (16.1)$$

where  $s, t$  are degree and order in spherical harmonic expansion and  $a$  the Earth’s radius. The sensitivity kernel  $K_s^x$  is calculated for the reference model and depends only on the degree  $s$  of the expansion.

In this study, we limit ourselves to degree 2 perturbations and invert the 5 degree 2 splitting coefficients  $C_{20}, C_{21}, S_{21}, C_{22}$  and  $S_{22}$  of the selected modes for the corresponding degree 2 structure of  $V_p, V_s$  and  $\rho$  in the mantle.

### Inversion settings

The neighbourhood algorithm (NA) is a stochastic method comparable to Monte-Carlo method, genetic algorithm or simulated annealing (*Moosegard and Sambridge, 2002*). We are using the first part (*Sambridge 1999a*) of the algorithm to sample the parameter space preferentially in good fitting areas, using the geometrical construction of Voronoi cells (closest neighbourhood) to fill the space. At each iteration,  $n_s$  new models are randomly generated in the  $n_r$  best fitting cells, the cells being defined by all previously generated models. After a sufficient number of iterations, we obtain a large (about 150 000 for our problem) set of models with more models in good fitting areas. The parameters  $n_s$  and  $n_r$  must be tuned for each problem ; an important value is the parameter space dimension which largely governs the choice of  $n_s$  and  $n_r$  and seems to be the main limitation of the use of the algorithm : the concentration of models in good fitting areas failed for high dimension, at least in reasonable computation time.

### Model parameterization

The model is naturally laterally parameterized by spherical harmonics, but we have the choice of the radial parameterization : layered models (equivalent to gate functions), splines functions, polynomials... Several trials show that 6 to 8 functions are a sufficient number to retrieve feature while keeping the total number of parameters low enough for use with the NA. Layered models oscillate and forcing them to be smooth causes instability and introduces arbitrary constraints that we would like to avoid. The splines-based parameterization that we selected allow smoother models.

### 6.3 Results

The most acceptable models are obtained when adding a spline-based model to the contribution of tomographic input models (Figure 16.13). The  $V_s$  perturbation is well retrieved while the  $V_p$  perturbation doesn't agree well with the input. The  $\rho$  perturbation is still oscillating, although smoother acceptable models exist.

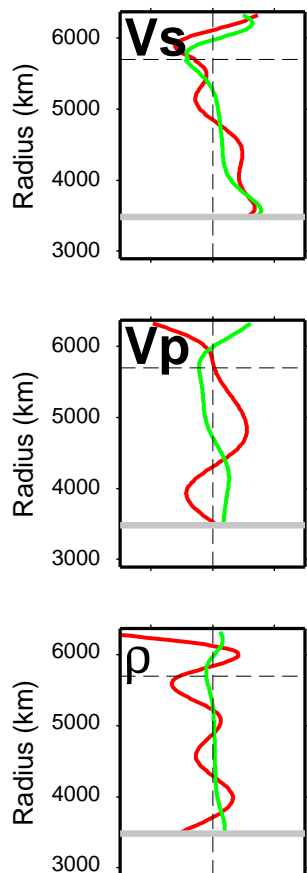


Figure 16.13: Best  $V_s$  model (black) obtained when using the tomographic (grey) model as input and 7 splines, for spherical harmonic coefficient  $C_{20}$

One noteworthy feature of all parameterizations is the good fit between the  $V_s$  model obtained in our inversion of splitting coefficients and the  $V_s$  tomographic model, even when this model is not used as input, the difference residing mostly in the uppermost mantle where simple parameterization like ours is more likely to fail.

Figure 16.14 show the distribution of models for the  $C_{20}$  contribution of the shear velocity perturbation. This distribution is stable and satisfactory, giving good confidence in the uniqueness of the  $V_s$  solution, but is obtained using tomographic models as input and the stability if the result with respect to the choice of the input model remains to be tested.

Further work will make use of the second part of the

algorithm (Sambridge, 1999b) which use Bayesian integrals to analyze quantitatively the set of model obtained during the first part (or any other method generating a large set of models).

### 6.4 Acknowledgements

Special thanks to Malcolm Sambridge for making the NA software package available. This package, its very helpful online help and a short description of the algorithm can be found at <http://rses.anu.edu.au/~malcolm/na/na/html>

We thank the National Science Foundation for support of this research.

### 6.5 References

- Giardini, D., X.D. Li and J. Woodhouse, Splitting functions of long-period normal modes of the Earth, *J. Geophys. Res.*, *93* B11, 1988.
- He, X. and J. Tromp, Normal-mode constraints on the structure of the Earth, *J. Geophys. Res.*, *102*, 17981-17994, 1996.
- Ishii, M. and J. Tromp, Normal-Mode and Free-Air Gravity Constraints on Lateral Variations in Velocity and Density of Earth's Mantle, *Science*, *285*, 1231-1236, 1999.
- Kuo, C. and B. Romanowicz, On the resolution of density anomalies in the Earth's mantle using spectral fitting of normal mode data, *Geophys. J. Inter.*, in press
- Li, X.D., D. Giardini and J.H. Woodhouse, Large-Scale Three-Dimensional Even-Degree Structure of the Earth from Splitting of Long Period Normal Modes, *J. Geophys. Res.*, *91* B1, 551-577, 1991.
- Moosegard, K. and M. Sambridge, Monte Carlo Analysis of inverse problems, *Inverse Problem*, *18* R29-R54, 2002.
- Romanowicz, B, Can we resolve 3D density heterogeneity in the lower mantle ?, *Geophys. Res. Lett.*, *28*, 15, 1107-1110, 2001.
- Resovsky, J. and M. Ritzwoller, Regularisation uncertainty in density model estimated from normal mode data, *Geophys. Res. Lett.*, *26*, 15, 2319-2322, 1999.
- Resovsky, J. and M. Ritzwoller, New and refined constraints on 3D Earth structure from normal modes below 3mHz., *J. Geophys. Res.*, *103*, 783-810, 1998.
- Sambridge, M., Geophysical inversion with a neighbourhood algorithm I - Searching a parameter space, *Geophys. J. Int.*, *138*, 479-494, 1999.
- Sambridge M., Geophysical inversion with a neighbourhood algorithm II - Appraising the ensemble, *Geophys. J. Int.*, *138*, 727-746, 1999.

# Results for Saw\_spl3 Vs c20

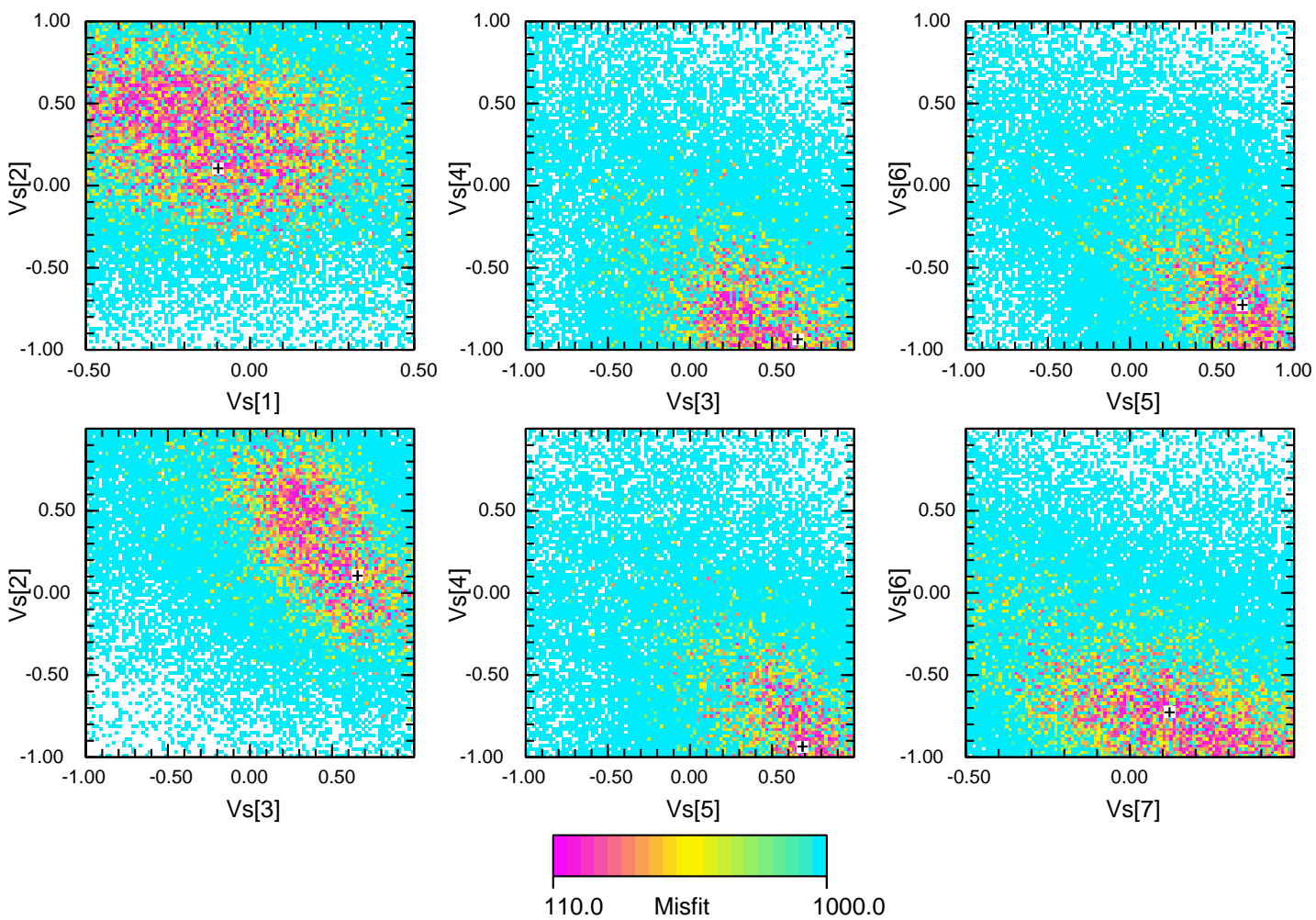


Figure 16.14: Projections of the set of  $V_s$  models obtained as output of the NA program ;  $Vs[x]$  is the value of the coefficient for the  $x^{th}$  spline, 1 being the deepest and 7 the most shallow spline.

## 7. Towards Forward Modeling of 3D Heterogeneity at the Base of the Mantle

Akiko To, Yann Capdeville and Barbara Romanowicz

### 7.1 Introduction

At the base of the mantle, strong lateral variations in S velocity structure and anisotropy have been documented, in recent years, at the borders of the two large superplumes in the central Pacific and under Africa. These features undoubtedly hold important clues for understanding the dynamics of the earth's mantle. Current tomographic models of S velocity represents good starting models to fit travel times and some aspects of S and ScS waveforms along selected profiles sampling these regions (e.g. Bréger and Romanowicz, 1998; Breger et al., 2001). Increasing the strength of heterogeneity while keeping the original distribution of velocity highs and lows goes a long way towards explaining the observed trends.

However, these results point to the complex 3D nature of this heterogeneity, appropriate forward modeling tools need to be developed to handle strong 3D heterogeneity in this region, at relatively short periods and including diffracted waves. The coupled mode/spectral element method developed by Capdeville et al.(2001) and adapted to a heterogeneous layer (i.g. D'') between two spherically symmetric shells affords both numerical accuracy and the computational efficiency for this purpose.

Our goal is to extend the forward modeling approach of D'' structure ( Bréger and Romanowicz, 1998 ), so far limited to travel times, to also include waveforms, applying the hybrid spectral element method and further explore 3D structure and anisotropy at the base of the mantle.

### 7.2 Work plan and Preliminary result

First, we will collect the waveforms of core sensitive phases (Sdiff,SKS,SKKS,ScS) and measure differential travel times within them. Then, starting from the tomographic model, we will adjust the strength and boundaries of the velocity structure to match differential travel times between Sdiff -SKS,Sdiff-SKKS and ScS-S . The advantage of this approach is that while it uses an infinite frequency approximation and therefore inaccurate to model broadband S travel times, it is very expedient and allows to rapidly get closer to an adequate final model. Finally, we will refine the model by computing numerical synthetics in 3D.

Fig 16.15 shows the preliminary result of the comparison between synthetics from 1D, 3D model and observations. 1D synthetics are calculated from PREM (Dziewonski and Anderson, 1981) by normal mode summation. 3D synthetics are calculated from the model

which has 3D structure of SAW24b16 (Megnin and Romanowicz, 2000) at the bottom 370 km of the mantle and sandwiched by PREM for the other part of the Earth. It is calculated by hybrid spectral element and modal summation method. Sdiff and sSdiff phase are shown. 3D model fits better to the observation especially for stations with longer distance (KBS,BOSA,LMN). For some stations, time shift for 3D is too strong (INK,YKW3) and sometimes both amplitude and time shift are poorly explained (CCM).

### 7.3 Acknowledgement

We thank the National Science Foundation for support of this research.

### 7.4 References

- Bréger, L. and B. Romanowicz, Thermal and Chemical 3D heterogeneity in D'', *Science*, 282, 718-720, 1998
- Bréger, L., B. Romanowicz and C. Ng, The Pacific plume as seen by S,ScS and SKS, *Geophys. Res. Lett.*, 28, 859-1862, 2001.
- Capdeville Y., E. Chaljub, J.P. Vilotte and J.P. Montagner, Coupling the Spectral Element Method with a modal solution for Elastic Wave Propagation in Global Earth Models, **accepted** in *Geophys. J. Int*, 2001
- Dziewonski A.M. And D.L. Anderson, Preliminary reference Earth model, *Phys. Earth Planet. Inter.*, 25, 297-356, 1981.
- Megnin, C. and B. Romanowicz, The shear velocity structure of the mantle from the inversion of of body, surface and higher modes waveforms, *Geophys. J. Int*, 143, 709-728, 2000

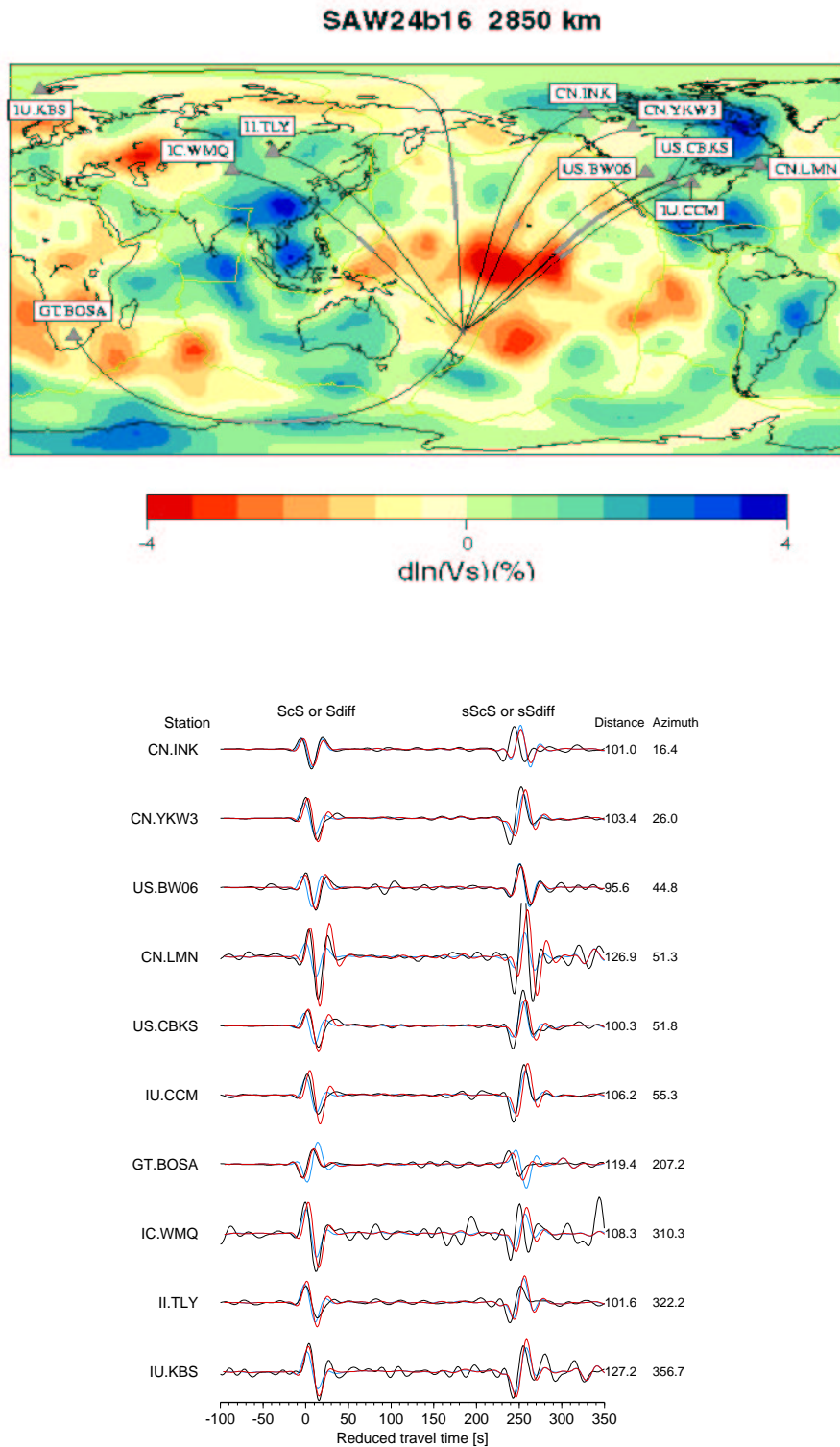


Figure 16.15: Top: The background model is the a velocity tomographic model SAW24b16 just above the CMB. Path between source and stations are plotted. The diffracting portions of Sdiff phase are plotted by bold gray. Bottom: Comparison between data (Black), synthetics for the PREM model (blue) and synthetics for SAW24B16+PREM (red).

## 8. Using the Coupled Method of Spectral Elements and Modal Solution to study the D'' layer.

Yann Capdeville, Barbara Romanowicz, Akiko To

### 8.1 Introduction and Research objectives

The D'' region, which encompasses the last 300 km or so of the deep mantle, is thought to be both a thermal and a chemical boundary and the site of vigorous dynamic processes. Its structure is believed to hold the key to many largely unanswered questions in deep Earth geodynamics, such as the ultimate fate of subducting slabs, the origin of hotspots, the amount of bottom heating driving global mantle circulation, electro-magnetic coupling between the core and the mantle, and the nature of chemical heterogeneity in the deep mantle. Strong lateral variations in D'' as well as the presence of topography on the fluid-solid core mantle boundary, has to be addressed by forward modeling approaches. However, present global waveform modeling can not handle wave propagation in this region of the Earth. Another difficulty is that the relevant frequency cutoff is high (0.1 Hz or higher) which leads to very high costs of numerical simulations. The coupled method of Spectral Elements and Modal Solution is very well adapted to such a problem by allowing to restrict the 3D model in the D'' layer and to use a spherically symmetric model is enough in the rest of the Earth. Until now, this method is the only one able to address 3D wave propagation in this region at realistic frequencies. By producing synthetic seismograms using the coupled method in different D'' layer models and confront them to real data, we hope to provide significant advances to our understanding of this region, especially using both amplitude and time shift informations of data.

### 8.2 Method

This work is based upon an extension to the coupling scheme of the Spectral Element Method (SEM) with a normal mode solution in spherical geometry. This extension allows us to consider a thin spherical shell of spectral elements between two modal solutions above and below. The SEM is based on a high order variational formulation in space and a second-order explicit scheme in time. It combines the geometrical flexibility of the classical finite element method with the exponential convergence rate associated with spectral techniques. In the inner sphere and outer shell, the solution is sought in terms of a modal solution in the frequency domain after expansion on the spherical harmonics basis. The SEM has been shown to obtain an excellent accuracy in solving the wave equation in complex media but is still numerically expen-

sive for the whole Earth for high frequency simulations. On the other hand, modal solutions are well known and numerically cheap in spherically symmetric models. By combining these two methods we take advantage of both, allowing high frequency simulations in global Earth models with 3D structure in a limited depth range. Within the spectral element method, the coupling is introduced via a dynamic interface operator, a Dirichlet-to-Neumann ( $DtN$ ) operator which can be explicitly constructed in the frequency and generalized spherical harmonics domain using modal solutions in the inner sphere and outer shell. The presence of the source and receivers in the top modal solution shell requires some special treatment. The accuracy of the method is checked against the mode summation method in simple spherically symmetric models and shows very good agreement for all type of waves, including diffracted waves traveling on the coupling boundary.

Simulations in a 3D D'' layer model based on the tomographic model SAW24B16 has been performed up to a corner frequency of 1/12 s. The mesh used is presented on Fig. 16.16. The comparison with data using deep

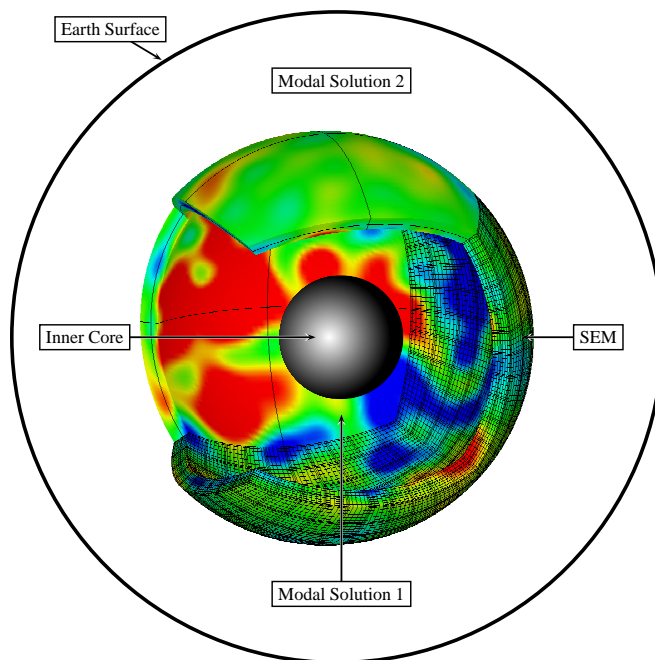


Figure 16.16: Sandwich of spectral elements between two modal solutions for D'' application with SAW24B16 model.

events shows surprisingly good results for the 3D model even when the observed waveform amplitudes differ significantly from the ones predicted in the spherically symmetric reference model (PREM). Some examples of synthetics are given on Fig. 16.17.

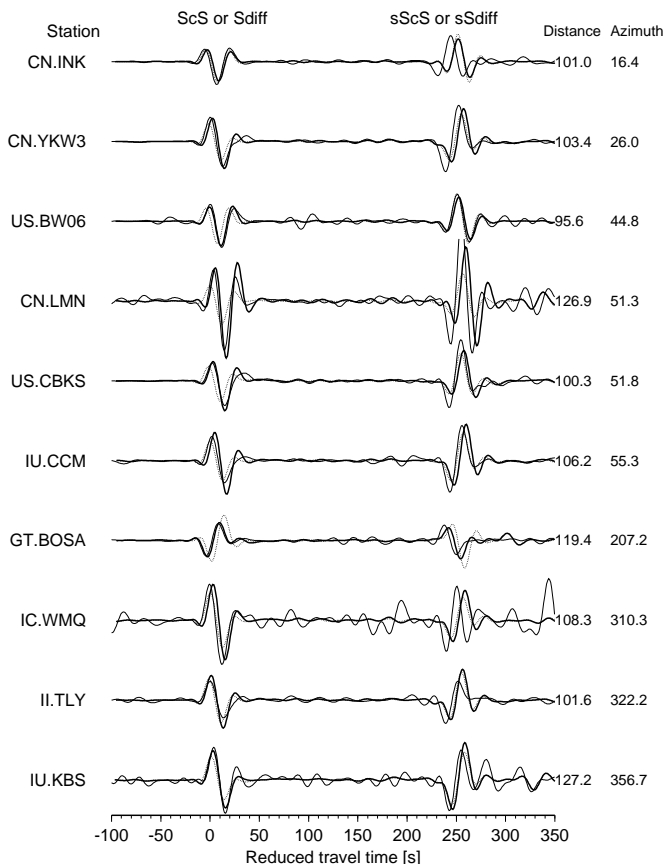


Figure 16.17: Comparison between data (thin line), synthetics in PREM (dotted line) and synthetics in SAW24B16 + PREM (bold line) for an event in the Fidji Island recorded at different stations around the world.

A description of the method with illustrations can be found on <http://www.seismo.berkeley.edu/~yann>

### 8.3 Accomplishments during 2001-2002

The accomplishments achieved during 2000-2001 include:

- Technical and practical developments and optimizations of the code on the IBM SP of the NERSC.
- Comparison of synthetics seismograms in the tomographic model SAW24B16 and data for several deep events. These comparisons will lead to an improved model of the D" layer.

### 8.4 Acknowledgements

The computation were made using the computational resources of the NERSC, especially the IBM SP, under repo mp342.

We thank the Miller Insitute for their support.

### 8.5 References

Y. Capdeville, B. Romanowicz and A. To, Coupling Spectral Elements and Modes in a spherical earth: an extension to the "sandwich" case. **Submitted** to *Geophys. J. Int.*, 2002.

Capdeville Y., C. Larmat, J.P. Vilotte and J.P. Montagner, Numerical simulation of the scattering induced by a localized plume-like anomaly using a coupled spectral element and modal solution method. **In press** in *Geoph. Res. Lett.*, 2001.

Capdeville Y., E. Chaljub, J.P. Vilotte and J.P. Montagner Coupling the Spectral Element Method with a modal solution for Elastic Wave Propagation in Global Earth Models. **accepted** in *Geophys. J. Int.*, 2001.

Chaljub, E. Capdeville, Y. and Vilotte, J.P., Solving elastodynamics in a solid heterogeneous 3D-sphere: a parallel spectral element approximation on non-conforming grids. **Submitted** to *J. Comp Phy.*, 2001.

## 9. Short scale heterogeneity in the lowermost mantle: insights from PcP-P and ScS-S data

Hrvoje Tkalčić and Barbara Romanowicz

### 9.1 Introduction and Motivation

An important question in global geodynamics is whether the 3D seismic velocity anomalies, as seen in tomographic models of the mantle, are of a thermal or a compositional nature, or a combination of both. While global tomographic S models consistently show predominance of long wavelength structure at the base of the mantle, and in particular two large slow domains in the central Pacific and under Africa, referred to as "superplumes", seismic evidence for shorter scale heterogeneity at these depths is growing. The existence of strong heterogeneity in the vicinity of the two superplumes has been documented through forward modeling of seismic travel times and waveforms. Recent studies have also found evidence for locally rapid variations in other areas such as middle America.

On the other hand, several studies have compared global variations in S and P velocities from tomographic inversions, and some of them found evidence for a strong increase in  $R = \partial \ln V_s / \partial \ln V_p$  near the bottom of the mantle, as well as a possible decorrelation between shear and acoustic velocity variations below 2000 km depth. Furthermore, while there is evidence for zones of strongly reduced P velocity at the base of the mantle, there is no evidence that these are accompanied with a comparable drop in S velocity.

Through an inversion of PcP-P and PKP(AB-DF) data, we recently obtained maps of D" with lateral P velocity variations that show much shorter wavelength features than seen in S tomographic models (Tkalčić *et al.*, 2002). Here, we consider PcP-P and ScS-S travel time residuals, and analyze their spatial relationship in several regions which are sampled both by PcP and ScS, in comparison to tomographic maps. We discuss implications of our results for the relative variations in P and S velocities in the lowermost mantle, in particular from the stand-point of  $\partial \ln V_s / \partial \ln V_p$  ratios and their interpretation.

### 9.2 Results

We compared the lateral variations observed in a global dataset of PcP-P differential travel times sensitive to structure in the bottom 500-1000 km of the mantle, to the predictions of global tomographic models, on the one hand, and ScS-S differential travel times, on the other.

This comparison has shown that the different datasets are in good agreement in some regions, in particular in eastern Asia, where fast anomalies over a broad domain

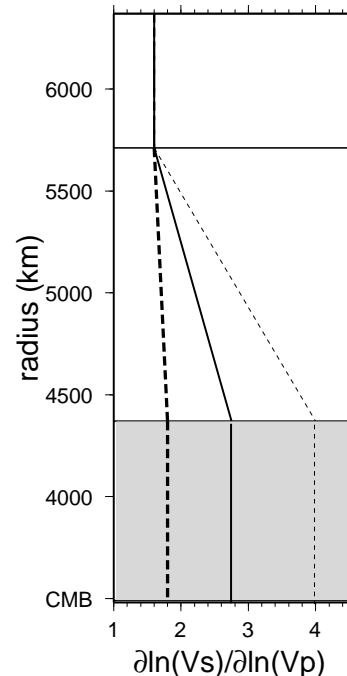


Figure 16.18: Best fitting depth profiles of  $R = \partial \ln V_s / \partial \ln V_p$  obtained by comparing PcP-P travel time data to S tomographic velocity models, using a parameter search for the thickness of the bottom layer and the value of  $R$  inside it. Comparison restricted to a subset of PcP-P residuals with PcP reflection points under eastern Eurasia with global S tomographic models *SAW24B16* (Méglin and Romanowicz, 2000) (solid line, variance reduction 57%), and models *SB4L18* (Gu and Dziewonski, 2001) and *S362D1* (Masters *et al.*, 2000) (thick dashed line, variance reduction 60% and 52%, respectively). The thin dashed line corresponds to the best fitting depth profile of  $R$  using the global PcP-P dataset and model *SAW24B16* (variance reduction 10%). Shaded area represents the uncertainty in the thickness of the lowermost layer for the parametrization used.

are inferred both from tomographic P and S models and from the core-reflected phase data, resulting in a value of  $R$  compatible with a thermal origin of heterogeneity at the base of the mantle in this region (solid and thick dashed lines in Figure 16.18). It is interesting to compare this regional result with that obtained by applying the same methodology to the global dataset. The best variance reduction is obtained for model *SAW24B16* (Mégnin and Romanowicz, 2000) and does not exceed 10%. Figure 16.18 also shows the best fitting  $R$  profile (thin dashed line) obtained with this model.

On the other hand, the PcP-P data indicate shorter scale lateral variations in many other regions. We studied in detail two such localized regions, under central America and south-east Africa, which correspond to downwelling and upwelling regions respectively, as seen in global tomographic models. In central America, lateral variations in P and S velocity appear to track each other. With only a few exceptions, the variations in PcP-P residuals are in good agreement with the slow (resp. fast) regions delineated by ScS-S from the study of Wyssession et al. (2001). Resulting estimates of the ratio  $R$  in the last 500 km of the lower mantle are not particularly high. Under Africa (Figure 16.19a), one profile (AB) shows similar results (Figure 16.19b), whereas a slightly more northerly neighboring path (profile CD) indicates fast P velocities in the heart of the low S velocity African "plume" (Figure 16.19c). A similar situation is found on the eastern edge of the Pacific plume, where the simultaneous availability of PcP-P and ScS-S data allows us to infer the existence of sharp lateral gradients across compositionally different domains.

Our study documents existence of strong lateral variations at the base of the mantle on scale lengths of several hundred kilometers, implying the existence of compositional variations in D". We note however that the computation of meaningful estimates of  $R$  at the base of the mantle, as an indicator of the nature of heterogeneity, remains a challenge. In order to do it correctly, better spatial sampling in both P and S data is needed, as different smoothing of short scale structures can lead to biased estimates.

Collecting more PcP-P and ScS-S data with a compatible sampling of the lowermost mantle on the one hand, and increasing the resolution and accuracy of tomographic models on the other is necessary to gain further insight regarding the nature of heterogeneity in the lowermost mantle.

### 9.3 Acknowledgements

Data were obtained from the IRIS Data Management Center. We thank Nicolas Houy, who measured most of the PcP-P travel times used in this study and Michael Wyssession for sharing his MOMA S-ScS dataset with us. Figures were made with the General Mapping Tools (P.

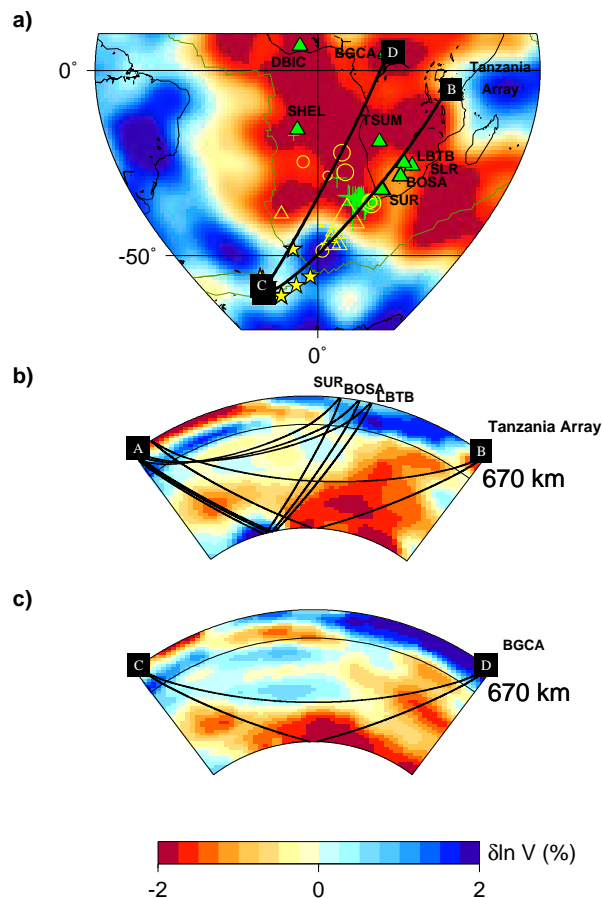


Figure 16.19: PcP-P travel time residuals plotted at the surface projections of PcP bouncing points for south Atlantic/south Africa region. The largest triangle and circle correspond to residuals of +3 s and -1.5 s, respectively. The background model is *SAW24B16*. Green crosses are ScS reflection points. (b) Cross-section through *SAW24B16* along profile AB, with P and PcP paths from a South Sandwich Islands region event to SUR, BOSA and LBTB stations and a south Atlantic ridge event to Tanzania network; (c) Cross-section through *SAW24B16* along profile CD, with P and PcP paths from a South Sandwich Islands region event to BGCA station.

Wessel and W. H. F. Smith, *EOS Trans. AGU* **76**, 329, 1995).

We thank the National Science Foundation for support of this research.

## 9.4 References

Gu, Y., A.M. Dziewonski, Shear velocity of the mantle and discontinuities in the pattern of lateral heterogeneities, *J. Geophys. Res* 106, 11169-11199, 2001.

Masters, G. , G. Laske, H. Bolton, and A.M. Dziewonski, Earth's Deep Interior: Mineral Physics and Tomography From the Atomic to the Global Scale. *Geophys. Monogr. Ser. (eds Karato. S.-I. et al.)* 117, AGU, Washington, DC, 63-87, 2000.

Mégnin, C., B. Romanowicz, The 3D shear velocity structure of the mantle from the inversion of body, surface, and higher mode waveforms, *Geophys. J. Int.*, 143, 709-728, 2000.

Tkalčić, H., B. Romanowicz, N. Houy, Constraints on D'' structure using PKP(AB-DF), PKP(BC-DF) and PcP-P travel time data from broadband records, *Geophys. J. Int.*, 148(3), 599-616, 2002.

Tkalčić, H., B. Romanowicz, Short scale heterogeneity in the lowermost mantle: insights from PcP-P and ScS-S data, *Earth Planet. Sci. Lett.*, 201(1), 57-68, 2002.

Wyssession, M.E., K.M. Fischer, G.I. Al-eqabi, P.J. Shore, Using MOMA broadband array, ScS-S data to image smaller-scale structures at the base of the mantle, *Geophys. Res. Lett.*, 190, 167-170, 2001.

Part IV  
Appendices

